Dynamics of Charge Movement in α-Al_2O_3:C,Mg using Thermoluminescence Phototransferred and Optically Stimulated Luminescence

Aaron Joel Lontsi Sob

A thesis submitted in fulfillment of the requirements
for the degree of
Doctor of Philosophy in Physics

Supervised by Professor Makaiko L. Chithambo
Department of Physics & Electronics
17th February 2022

Abstract

The dosimetric features of α-Al_2O_3:C,Mg have been investigated for unannealed and annealed samples. The unannealed sample is referred to as sample A whereas the samples annealed at 700, 900 and 1200°C for 15 minutes each are referred to as samples B, C and D respectively. A glow curve of unannealed α-Al_2O_3:C,Mg measured at 1°C/s after irradiation to 2.0 Gy consists of peaks at 43, 73, 164, 195, 246, 284, 336 and 374°C respectively. For sample B (annealed at 700°C), a glow curve measured at 1°C/s after irradiation to 3.0 Gy has peaks at 46, 76, 100, 170, 199, 290, 330 and 375°C whereas the glow curve of sample C (annealed at 900°C) recorded under the same conditions consists of peaks at 49, 80, 100, 174, 206, 235, 290, 335 and 375°C respectively. Sample D (annealed at 1200°C) is the most sensitive of the four samples. A glow curve of sample D measured at 1°C/s after irradiation to 0.2 Gy has peaks at 52, 82, 102, 174, 234, 288 and 384°C respectively. The peaks are labelled I-VIII in order of appearance. The 100°C peak, labelled IIa, is induced by annealing at or above 700°C. The dose response of these peaks was studied for doses within 0.1-8.2 Gy. The reported peaks follow first-order kinetics irrespective of annealing temperature. Peaks I-III of each sample are reproduced under phototransfer for preheating up to 400°C. For the unannealed sample, the reproduced peaks are labelled A1-A3 whereas for the annealed samples, they are labelled B1-B3, C1-C3 and D1-D3 respectively. The annealing-induced peak at 100°C is reproduced as B2a, C2a and D2a for samples B, C and D respectively. A PTTL peak labelled C2b or D2b is also observed near 140°C in samples C and D. In addition to these PTTL peaks, a PTTL peak corresponding to peak IV is also found for sample D and for the unannealed sample. As the corresponding conventional peaks, the PTTL peaks of each sample follow first-order kinetics. Peak I and its corresponding PTTL peak for each sample are unstable and fade to a minimal level after 300 s of storage time. On the other hand, peak II of each sample and its corresponding PTTL peak could still be observed with delay up to 5000 s. Peak III of the unannealed sample remains stable with storage time up to 48 hours. Irrespective of annealing, the trap corresponding to peak III is the most sensitive to optical stimulation. Time-dependent profiles of PTTL from unannealed and annealed α-Al_2O_3:C,Mg were also studied. The mathematical analysis of the PTTL time-response profiles is based on experimental results. The role of various electron traps in PTTL was determined by using pulse annealing and by monitoring the dependence of peak intensity on duration of illumination for peaks not removed by preheating. The presence and role of deep traps were further demonstrated with thermally assisted optically stimulated luminescence.For the unannealed sample, the activation energy for thermal assistance is 0.033 ± 0.001 eV and the activation energy for thermal

quenching is 1.043 ± 0.001 eV. For sample C, the activation energy for thermal assistance is 0.044 ± 0.003 eV whereas that for thermal quenching is 1.110 ± 0.006 eV. The values for the activation energy for thermal assistance are lower than those reported in literature. Only the values for the activation energy for thermal quenching are somewhat comparable to values reported elsewhere.

Acknowledgements

"Appreciation is a wonderful thing.
It makes what is excellent in others belong to us as well."
– Voltaire

First and foremost I would like to express my deepest gratitude to Prof. Makaiko L. Chithambo for supervising this work. It has been a great privilege to study, learn and work with you over the course of this project. I thank him for patiently going over my draft and for suggesting how it could be improved. I am also grateful to him for recommending me for funding opportunities at Rhodes University. I am grateful to Ulrich and the rest of the family for their support and encouragement during this period. I thank my fellow mates and the staff of the Physics department for creating a conducive environment in which to work. I thank Lexi and Cyndie for the good humour they bring to the office. Without them it will be a very boring place. My thanks also go my research fellows of the Luminescence Research Group. In particular, I would like to express my gratitude to Dr. Folley for her encouragement during the course of this work. I extend my sincere thanks to Rhodes University for the funding I received in the form of bursaries. Last but not least, I am grateful to my wife, Samanta for her encouragement and love.

Contents

Declaration

The work in this thesis is based on research carried out at the Luminescence Research Laboratory in the Department of Physics and Electronics at Rhodes University. No part of this thesis has been submitted elsewhere for any other degree or qualification, and it is the sole work of the author unless referenced to the contrary in the text.

Some of the work presented in this thesis has been published in journals as cited in the thesis. The relevant publications are listed in the appendix.

List of Figures

List of Tables

Chapter 1

Introduction

This chapter describes the process of luminescence emission. The aim of the thesis and its specific objectives are presented and to conclude, a synopsis of the remaining chapters is given.

1.1 Luminescence mechanisms

Luminescence, as a process, is the stimulated emission of light from a previously irradiated insulator or semiconductor (Chen and McKeever, 1997). Luminescence may however be observed without prior irradiation. This is the case with photoluminescence (Sykora and Akselrod, 2010). Due to their electronic structure, only insulators and semiconductors emit luminescence. These luminescent materials are also referred to as phosphors. The light emitted during the luminescence process should be distinguished from the spontaneous emission of light which is observed during incandescence (McKeever, 1985).

The two main steps of the luminescence process are excitation and stimulation (McKeever et al., 1995). During excitation, the material absorbs energy from an external source. Common sources of excitation are nuclear radiation such as γ-rays, beta-particles and X-rays. Ultra-violet light is also a common source of optical excitation (McKeever, 1985; McKeever et al., 1995). The purpose of excitation is to create electron-hole pairs which are essential to luminescence emission. After excitation, luminescence may be thermally or optically stimulated from the material. For thermal stimulation, the material is heated at a controlled rate from a temperature T_0 to a final temperature T. The final temperature T to which the sample is heated is limited by the experimental instrument to prevent damage to the photomultiplier tube and avoid incandescence. The ensuing luminescence is referred to

as thermally stimulated luminescence or thermoluminescence (Chen and McKeever, 1997). For optical stimulation, the irradiated sample is exposed to light of suitable wavelength (for example 470 nm blue light). Following optical stimulation, the resulting luminescence is termed optically stimulated luminescence (Bøtter-Jensen et al., 2003; Yukihara and McKeever, 2011; Chithambo, 2018).

Irrespective of the stimulation source, luminescence can be classified into fluorescence or phosphorescence depending on the mean-time, τ, between stimulation and emission. Fluorescence is observed if $\tau < 10^{-8}$ s. Figure 1.1 shows the basic process of fluorescence emission. The electron moves directly from the ground state g to the excited energy level e after absorption of energy. From e, the electron relaxes back to the ground state g with emission of light.

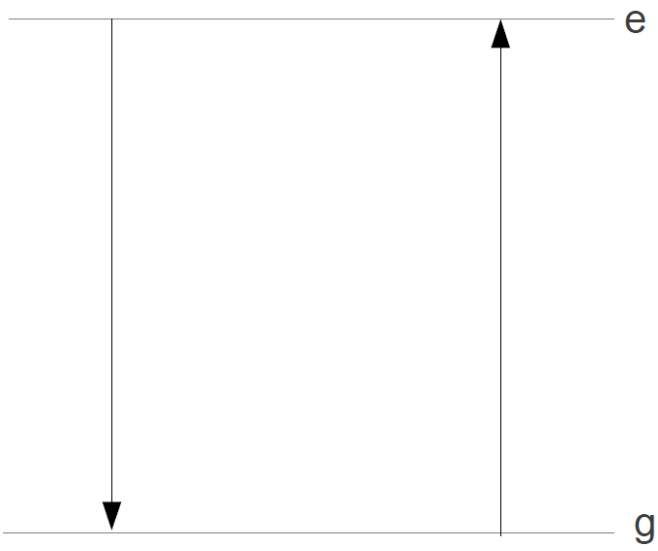

Figure 1.1: Energy level diagram depicting the fluorescence process. The up and down arrows each corresponds to absorption and emission of energy leading to fluorescence (reproduced from (McKeever, 1985)).

When the mean-time $\tau > 10^{-8}$ s, the luminescence is referred to as phosphorescence. Figure 1.2 shows the basic steps involved in phosphorescence. In addition to the ground state g and the excited state e, there is a metastable state m. After absorption of energy from the external source, electrons from the ground state g move to the excited state e. From level e, electrons transit into and out of level m before decaying to the ground state g. The time spent by electrons at level m accounts for most of the delay between stimulation and emission of light. Fluorescence is temperature independent whereas phosphorescence depends strongly on temperature (Chen and McKeever, 1997). Electrons from the metastable state m can be freed by heating.

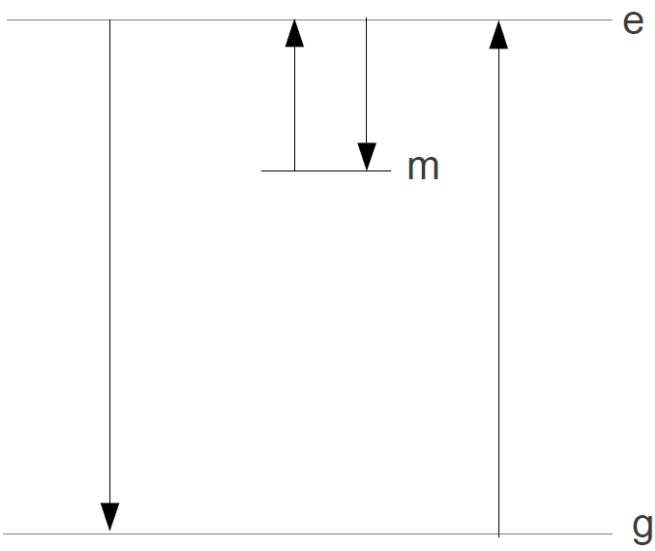

Figure 1.2: Energy level showing the phosphorescence process. The electron is trapped at level m before transiting to level e and then decaying to the ground state g. The up and down arrows corresponds to absorption and emission of energy respectively (reproduced from (McKeever, 1985)).

1.1.1 Thermally stimulated luminescence

Thermally stimulated luminescence, also referred to as thermoluminescence (TL), is the light emitted from a previously irradiated material when heated at a controlled rate (McKeever, 1985; Chen and McKeever, 1997). As stated before, only insulators and semiconductors are suitable as luminescent materials. According to the energy band model of solids, there are allowed energy bands which electrons can occupy. The valence band is the lowest energy band occupied by electrons. It is separated from the next allowed energy band namely; the conduction band by the forbidden gap (Kittel, 2005). Hence, in a perfect crystal there should not be localised energy levels within the forbidden gap. However, crystals are never ideal and contain defects or impurities within them (Agulló-López et al., 1988). These defects or impurities give rise to additional energy levels within the forbidden gap where electrons and holes may be trapped.

Figure 1.3 shows the process of stimulated luminescence with the aid of the one-trap-one-recombination centre (OTOR) model. Exposure to ionising radiation liberates electrons from the valence band. These electrons are then free to move within the crystal. Transition a depicts the movement of electrons into the conduction band. From the conduction band, some electrons are then trapped at localised energy levels; represented here as level T while holes are captured at the

recombination centre R. These two transitions are labelled b. The trap depth or activation energy E is the energy required to free electrons at trap T into the conduction band. Hence for trapped electrons to be evicted into the conduction band, the energy provided through thermal stimulation should be at least equal to E. The Fermi level is denoted by E_f. Transition c represents the eviction of trapped electrons into the conduction band. From the conduction band, some electrons recombine with holes at the luminescence centre R. The recombination process results in luminescence emission.

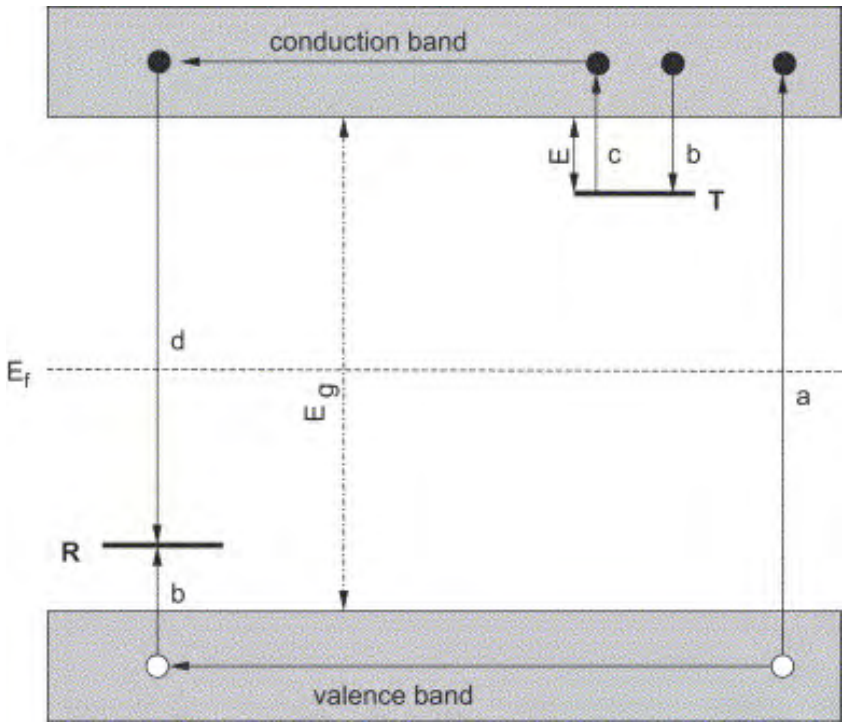

Figure 1.3: Energy band model showing electronic transitions during the TL process. (a) generation of electrons and holes; (b) electron and hole trapping; (c) electron release due to thermal stimulation; (d) electron-hole recombination. Solid circles represent electrons and open circles are holes. Level T is an electron trap, level R is a recombination centre, E_f is the Fermi level, E_g is the energy band gap. Diagram reproduced from (Bos, 2006).

1.1.1.1 Analysis of thermoluminescence

To explain the stimulation and emission of TL, we first consider the one-trap-one-recombination centre (OTOR) model shown in Figure 1.3.

Let n (m^{-3}) and n_c (m^{-3}) denote the instantaneous concentration of electrons at the electron trap T and in the conduction band respectively. Let m (m^{-3}) denote the instantaneous concentration of holes at the recombination centre R. The trap T

is progressively emptied as electrons move to the conduction band during thermal stimulation (transition c). The probability p (s^{-1}) per unit time of release of a trapped electron is given by

$$p = s \exp\left(-\frac{E}{kT}\right), \tag{1.1}$$

where s is the number of times a trapped electron attempts to detach from its binding potential (Chithambo et al., 2017b). For the OTOR model, s is considered to be independent of temperature. The value of s is expected to be of the order of the lattice vibration frequency namely 10^{12} - 10^{14} s^{-1} (Carter, 2000). In equation (1.1), E denotes the trap depth; k the Boltzmann constant and T the absolute temperature. Equation (1.1) shows that the probability p of release from the trap increases with temperature thereby enabling the release of trapped electrons into the conduction band. Luminescence results from the recombination of conduction electrons with holes at the recombination centre R. The luminescence intensity is proportional to the rate at which electrons and holes recombine and may be stated as

$$I(t) = -\frac{dm}{dt} = n_c m A_m, \tag{1.2}$$

where the negative sign indicates the loss of holes due to recombination and A_m (m^3s^{-1}) is the probability of recombination. For simplicity, equation (1.2) assumes that all recombinations are radiative. The rate of change in the concentration of trapped electrons with respect to time depends on the excitation rate (np) and the retrapping rate ($n_c(N-n)A_n$). The rate of change in the concentration of trapped electrons is then given by

$$\frac{dn}{dt} = -np + n_c(N-n)A_n, \tag{1.3}$$

where N is the concentration of electron traps and, A_n in m^3s^{-1} is the probability of retrapping. All the other terms are as previously defined. The rate of change in the concentration of holes at the recombination centre is expressed as

$$\frac{dm}{dt} = \frac{dn_c}{dt} + \frac{dn}{dt}, \tag{1.4}$$

where $\frac{dn}{dt}$ is as defined earlier and $\frac{dn_c}{dt}$ is the rate of change in the concentration of electrons in the conduction band. We assume that only trapped electrons are freed during thermal stimulation; that is, the change in concentration of holes, n_v in the valence band is zero. For charge to be conserved, the total concentration of

electrons at electron traps and in the conduction band should be equal to that of holes at the recombination centre that is,

$$n_c + n = m. \tag{1.5}$$

Equation (1.5) expresses charge conservation. Equations (1.2)-(1.4) are first-order coupled non-linear differential equations. They cannot be solved analytically. A solution can be generated by invoking certain assumptions. We first assume that electrons do no accumulate in the conduction band that is $n_c \approx 0$ (hence, $n \approx m$). This assumption is referred to as the quasi-equilibrium approximation (Chen and McKeever, 1997). From equations (1.2) - (1.4), we then obtain

$$I(t) = \frac{mA_m np}{(N-n)A_n + mA_m} = \frac{mA_m}{(N-n)A_n + mA_m} ns \exp\left(-\frac{E}{kT}\right). \tag{1.6}$$

Equation (1.6) is referred to as the general one trap (GOT) equation.

1.1.1.2 First-order kinetics

First-order kinetics can be derived by assuming that the probability of electron retrapping during thermal stimulation is negligible i.e., $mA_m \gg (N-n)A_n$ (Randall and Wilkins, 1945a,b). Under this assumption, equation (1.6) reduces to

$$I(t) = -\frac{dn}{dt} = s\,p = n\,s \exp\left(-\frac{E}{kT}\right). \tag{1.7}$$

Equation (1.7) is referred to as the first-order kinetics equation because the luminescence intensity, I, is directly proportional to n. If the measurement temperature is constant during the TL readout, the intensity decays exponentially and is given by

$$I(t) = I_0 \exp(-tp), \tag{1.8}$$

where I_0 is the initial intensity and t is the time. For a linear heating profile, the sample temperature at time t is

$$T(t) = T_0 + \beta t, \tag{1.9}$$

where T_0 is the initial temperature and β is the heating rate. Equation (1.7) can be rewritten implicitly as

$$\frac{dn}{dt} = \frac{dn}{dT}\frac{dT}{dt} = \beta\frac{dn}{dT} \tag{1.10}$$

where $\beta = \frac{dT}{dt}$. By integrating both sides of equation (1.10), we obtain the concentration of trapped electrons at temperature T as

$$n = n_0 \exp\left[-\int_{T_0}^{T}\left(\frac{s}{\beta}\right)\exp\left(-\frac{E}{kT'}\right)dT'\right], \tag{1.11}$$

where n_0 is the concentration of trapped electrons at time $t = 0$ i.e., prior to stimulation and T' is a dummy variable of integration. The TL intensity is then derived from equation (1.11) as

$$I(T) = n_0 s \exp\left(-\frac{E}{kT}\right)\exp\left[-\int_{T_0}^{T}\left(\frac{s}{\beta}\right)\exp\left(-\frac{E}{kT'}\right)dT'\right]. \tag{1.12}$$

A plot of the TL intensity against temperature is known as a glow curve. Figure 1.4 shows an example of glow curve of unannealed α-Al_2O_3:C,Mg measured at 1°C/s after irradiation to 2.0 Gy. This glow curves consists of various peaks at 43, 73, 165, 195°C, etc. Each peak reflects the emptying, by heating, of a specific electron trap.

The temperature T_m corresponding to the maximum intensity of the resulting glow peak is obtained by setting $\frac{dI}{dT} = 0$. This leads to

$$\frac{\beta E}{kT_m^2} = s\exp\left(-\frac{E}{kT_m}\right). \tag{1.13}$$

Equation (1.13) shows that the peak temperature, T_m, does not depend on n_0. This is a characteristic of first-order kinetics (Chen and McKeever, 1997; Pagonis et al., 2006).

1.1.1.3 Second-order kinetics

Garlick and Gibson (1948) derived the second-order kinetics expression by considering the case where retrapping dominates namely, $mA_m \ll (N-n)A_n$. By also assuming that the trap is far from saturation i.e., $N \gg n$ and $m = n$, equation (1.6) becomes

$$I(t) = -\frac{dn}{dt} = s\frac{A_m}{NA_n}n^2\exp\left(-\frac{E}{kT}\right). \tag{1.14}$$

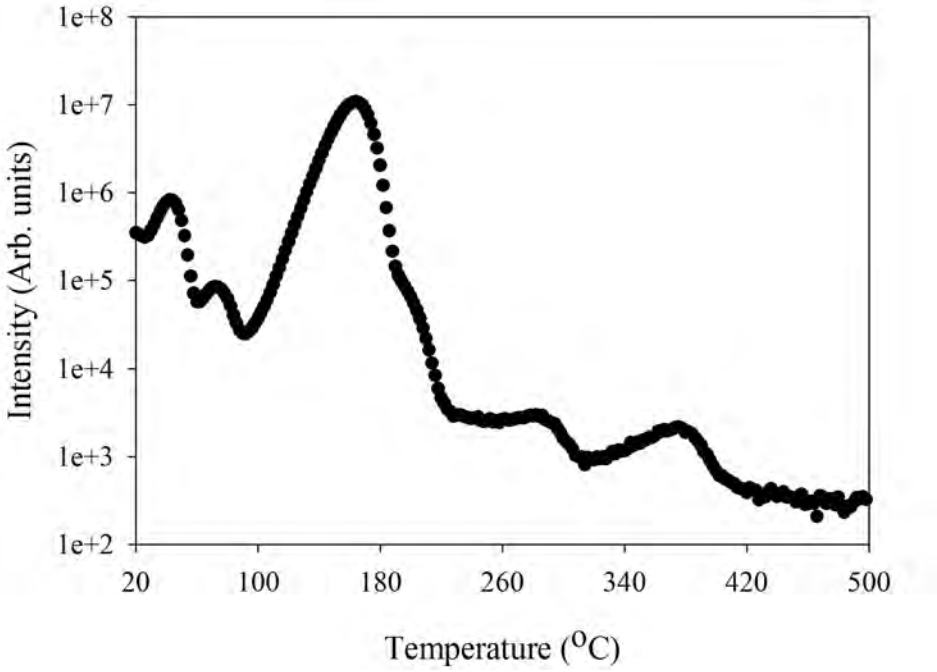

Figure 1.4: A glow curve of unannealed α-Al_2O_3:C,Mg measured at 1°C/s after irradiation to 2.0 Gy.

The intensity, $I(t)$, in equation (1.14) is proportional to n^2 and is the reason the equation is referred to as the second-order kinetics equation. Garlick and Gibson (1948) further assumed that $A_m = A_n$. Considering a linear heating profile and then integrating equation (1.14), the TL intensity can be obtained as

$$I(T) = \frac{n_0^2 s}{N\beta} \exp\left(-\frac{E}{kT}\right) \left[1 + \frac{n_0 s}{N\beta} \int_{T_0}^{T} \exp\left(-\frac{E}{kT'}\right) dT'\right]^{-2}. \tag{1.15}$$

The temperature T_m of a second-order glow peak is obtained from

$$\frac{\beta E}{kT_m^2} = s\left(1 + \frac{2kT_m}{E}\right) \exp\left(-\frac{E}{kT_m}\right). \tag{1.16}$$

1.1.1.4 General-order kinetics

May and Partridge (1964) derived an expression for general-order kinetics by considering the case where none of the assumptions of the first- and second-order

kinetics hold. The expression for general-order kinetics they proposed is given by

$$I(t) = -\frac{dn}{dt} = n^b s^a \exp\left(-\frac{E}{kT}\right). \tag{1.17}$$

The term s^a has dimension of $m^{3(b-1)}s^{-1}$ and b is the order of kinetics. In this case, the TL intensity as a function of temperature can be written as

$$I(T) = s'' n_0 \exp\left(-\frac{E}{kT}\right)\left[1 + \frac{s''(b-1)}{\beta}\int_{T_0}^{T} \exp\left(-\frac{E}{kT'}\right) dT'\right]^{\frac{-b}{b-1}} \tag{1.18}$$

where $s'' = s^a n_0^{(b-1)}$. Equation (1.18) is valid for $b \neq 1$ and reduces to the appropriate equation for first- or second-order kinetics when b approaches 1 or 2. For a general-order glow peak, T_m is given by

$$\frac{\beta E}{kT_m^2} = s\left(1 + \frac{2kT_m(b-1)}{E}\right)\exp\left(-\frac{E}{kT_m}\right). \tag{1.19}$$

1.1.2 Mixed-order kinetics model

The OTOR model has been used to describe experimental features of TL. Despite its utility, this model is not realistic since materials have multiple trapping and recombination centres. In describing TL with the OTOR model, the number of trapped electrons equals the number of trapped holes ($n = m$) and it is assumed that the concentration of conduction electrons is negligible ($n_c \simeq 0$). In practise, in luminescent materials, there exist traps which are stable during TL readout. These "thermally disconnected" traps are known as deep traps. The presence of deep traps implies that the concentration of trapped electrons is different from that of trapped holes. Under the assumption that $n_c \simeq 0$, the charge neutrality condition is now

$$n + h = m \tag{1.20}$$

where h is the concentration of electrons in deep traps. The rate equation for the concentration of electrons trapped in the deep traps is given by

$$\frac{dh}{dt} = (H - h)A_h \tag{1.21}$$

where H is the total concentration of deep traps and A_h is the corresponding trapping probablity. For trapped holes at the recombination centre, the rate equation becomes

$$\frac{dm}{dt} = \frac{dn}{dt} + \frac{dh}{dt}. \tag{1.22}$$

The deep traps can capture electrons released from the shallow trap (thermally unstable trap). They compete with recombination centres for the capture of electrons released from shallow traps Chen and McKeever (1997).

For the special case when $h \simeq H$, $dh/dt \simeq 0$, Kelly and Bräunlich (1970) expressed the TL intensity as

$$I = \frac{(n+h)\,A_m}{(N-n)\,A_n + (n+h)\,A_m}\, n\, s\, \exp\Big(-\frac{E}{kT}\Big) \tag{1.23}$$

Under the assumption of negligible retrapping ($(N-n)\,A_n << (n+h)\,A_m$), Equation (1.23) reduces to

$$I = n\, s\, \exp\Big(-\frac{E}{kT}\Big). \tag{1.24}$$

Equation (1.24) is the first-order TL equation derived earlier (Equation (1.7)). When retrapping is dominant ($(N-n)\,A_n >> (n+h)\,A_m$) and $N >> n$, Equation (1.23) becomes

$$I = \frac{(n+h)\,A_m}{N\,A_n}\, n\, s\, \exp\Big(-\frac{E}{kT}\Big). \tag{1.25}$$

For $A_n = A_m$, Equation (1.23) reduces to

$$I = \frac{n+h}{N+h}\, n\, s\, \exp\Big(-\frac{E}{kT}\Big). \tag{1.26}$$

Equations (1.25) and (1.26) can both be expressed as

$$I = n\, h\, s' \exp\Big(-\frac{E}{kT}\Big) + n^2\, s' \exp\Big(-\frac{E}{kT}\Big) \tag{1.27}$$

where $s' = s\,A_m/N\,A_n$ or $s' = s/(N+h)$. Chen et al. (1981) referred to Equation (1.27) as the mixed-order kinetic equation. It reduces to first-order when $h >> n$ and to second-order if $h << n$.

1.1.3 Optically stimulated luminescence

Optically stimulated luminescence (OSL) is the luminescence produced when a previously irradiated insulator or semiconductor is exposed to light of a specific wavelength (Bøtter-Jensen et al., 2003; Yukihara and McKeever, 2011; Chithambo, 2018). Applications of OSL include retrospective dosimetry (Huntley et al., 1985), personal, space and medical dosimetry (Yukihara and McKeever, 2011). These applications are based on the premise that the luminescence intensity depends on the amount of radiation absorbed by the sample under investigation. The three methods of OSL stimulation are continuous wave stimulation (Huntley et al., 1985), linear modulation (Bulur, 1996) and time-resolved stimulation (Chithambo and Galloway, 2000; Bailiff, 2000).

1.1.3.1 Continuous-wave OSL

Continuous-wave OSL (CW-OSL) is the luminescence stimulated with light of constant intensity. The resulting signal includes a scattered component of the stimulating light which needs to be taken into account during analysis. The experimental setup usually includes a set of band-pass filters used for luminescence detection and a set of long-pass filters to restrict the wavelength range of the stimulating light (Galloway et al., 1997; Chithambo and Galloway, 2001).

As in the case of TL, OSL can be described in terms of first-, second- or general-order kinetics. The OTOR model shown in Figure 1.3 can be used to describe the basic process of OSL emission. All the terms defined previously when describing TL remain valid. The probability of stimulating an electron from the trap is now given by

$$p = \Phi\sigma \tag{1.28}$$

where Φ is the intensity of the stimulating light and σ is the photoionisation cross-section (Bøtter-Jensen et al., 2003). Assuming that retrapping is negligible during optical stimulation, the intensity of the emitted OSL is expressed as

$$I_{OSL}(t) = -\frac{dn}{dt} = np. \tag{1.29}$$

The luminescence intensity is obtained from equation (1.29) as

$$I_{OSL}(t) = n_0 p \exp(-pt) = I_0 \exp(-pt) \tag{1.30}$$

where $I_0 = n_0 p$ is the intensity at time $t = 0$. In this case, the luminescence intensity decreases monotonically and equation (1.30) is known as the first-order kinetics equation for OSL.

If retrapping is dominant during optical stimulation, the OSL signal follows second-order kinetics and is given by

$$I_{OSL}(t) = -\frac{dn}{dt} = \frac{n^2 p}{N}. \tag{1.31}$$

Starting with equation (1.31), time-dependence of the luminescence intensity is obtained as

$$I_{OSL}(t) = \frac{n_0^2 p}{(1 - \frac{n_0 p}{N} t)^2} \tag{1.32}$$

In the general-order case, for intermediate retrapping, the OSL signal is given by

$$I_{OSL}(t) = -\frac{dn}{dt} = \frac{n^b p}{N^{b-1}} \tag{1.33}$$

where b, the order of kinetics, is a dimensionless parameter. In a similar manner, for general-order kinetics, the luminescence intensity is

$$I_{OSL}(t) = \frac{n_0^b p}{N^{b-1}} \left[1 + (b-1)\left(\frac{n_0}{N}\right)^{b-1} pt\right]^{-\frac{b}{b-1}} \tag{1.34}$$

Equation (1.34) gives the OSL intensity for general-order kinetics. It reduces to first- or second-order kinetics when b approaches 1 or 2 respectively.

Figure 1.5 shows a CW-OSL curve of unannealed α-Al_2O_3:C,Mg measured at room temperature during a 1000 s exposure to 470 nm blue-light-emitting diodes after irradiation to 1.0 Gy. For the CW-OSL shown in Figure 1.5, the luminescence was detected with a 7.5 mm thick Hoya U-340 filter (transmission band 270-380 nm). The inset of this figure is CW-OSL of the same sample which increase initially with illumination.

The solid line describing the CW-OSL curve in Figure 1.5 is the sum of three exponentially decreasing functions given by

$$I(t) = I_1 \exp(-\lambda_1 t) + I_2 \exp(-\lambda_2 t) + I_3 \exp(-\lambda_3 t) \tag{1.35}$$

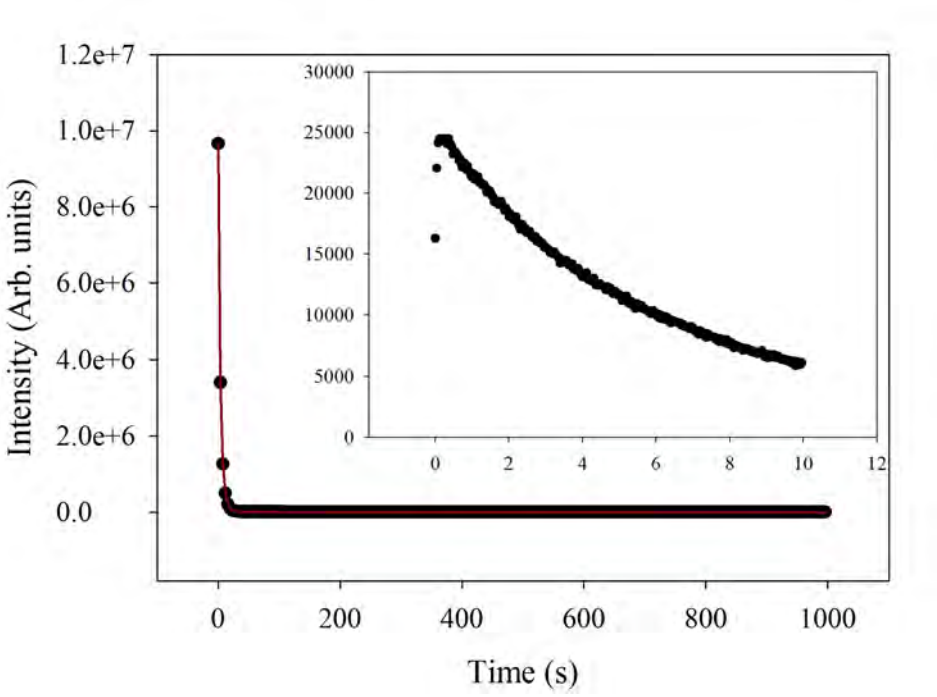

Figure 1.5: A CW-OSL curve of α-Al_2O_3:C,Mg measured at room temperature during a 1000 s exposure to 470 nm blue light after irradiation to 1.0 Gy. The inset shows a CW-OSL curve of the same sample which increases initially with stimulation time.

where I_1, I_2 and I_3 are scaling parameters and λ_1, λ_2 and λ_3 are the decay constants. This is a convenient way of describing a decay curve.

However, not all CW-OSL curves decrease exponentially with stimulation time. Some CW-OSL curves first increase with stimulation time before decreasing thereafter. Examples of such CW-OSL curves have been reported by (Nyirenda and Chithambo, 2017) for α-Al_2O_3:C. Nyirenda and Chithambo (2017) attributed the initial increase of luminescence intensity to charge retrapping and competition effects at electron traps and recombination centres.

1.1.3.2 Linearly modulated OSL

With linearly modulated optical stimulation, the intensity Φ of the stimulating light is increased with measurement time t at a constant rate γ (Bulur, 1996). The luminescence measured is referred to as linear-modulated OSL (LM-OSL) and consists of a set of time-separated peaks (Bulur, 1996; Bøtter-Jensen et al., 1999). Each of these peaks is associated with a specific photoionisation cross-section. The

intensity Φ of the stimulating light is now defined as

$$\Phi(t) = \gamma t. \tag{1.36}$$

For first-order kinetics, the change in the concentration of trapped electrons is expressed as

$$\frac{dn}{dt} = -np = -\gamma\sigma t n \tag{1.37}$$

where $p = \gamma\sigma t$. The luminescence intensity for first-order kinetics becomes

$$I(t) = n_0\gamma\sigma t \exp\left(-\frac{\gamma\sigma t^2}{2}\right). \tag{1.38}$$

The luminescence intensity, as given by equation (1.38), is described by an exponential function that goes through a peak at $t_{max} = \sqrt{1/\gamma\sigma}$. Similar expressions can be derived for second- or general-order kinetics. Figure 1.6 is a LM-OSL curve of α-Al_2O_3:C,Mg measured after irradiation to 1.0 Gy with the power density of the stimulating light increasing linearly from 9 (10%) to 90 mW/cm^2 (100%). As seen in Figure 1.6, the LM-OSL curve goes through a peak at 12 s of stimulation.

1.1.3.3 Time-resolved OSL

Time-resolved OSL, also known as pulsed optically stimulated luminescence (POSL), is the luminescence recorded when the sample is stimulated by a series of short light pulses (Sanderson and Clark, 1994; Markey et al., 1995). TR-OSL aims to separate in time the stimulation and emission of luminescence (Chithambo, 2011). The luminescence signal measured during optical stimulation increases monotonically with time whereas the signal measured after the light pulse decreases with stimulation time (Chithambo, 2011). The luminescence component recorded during stimulation also comprises of scatter from the stimulating light. The advantages of this method over CW-OSL and LM-OSL include the high reduction in background noise and the possibility of repeated measurements since each brief light pulse only stimulates a small proportion of trapped electrons (Chithambo and Galloway, 2000).

Measurements of TR-OSL can be used to evaluate luminescence lifetimes (Galloway, 2002; Chithambo and Ogundare, 2009). The luminescence lifetime is the delay between stimulation and emission (Galloway, 2002; Chithambo and Ogundare,

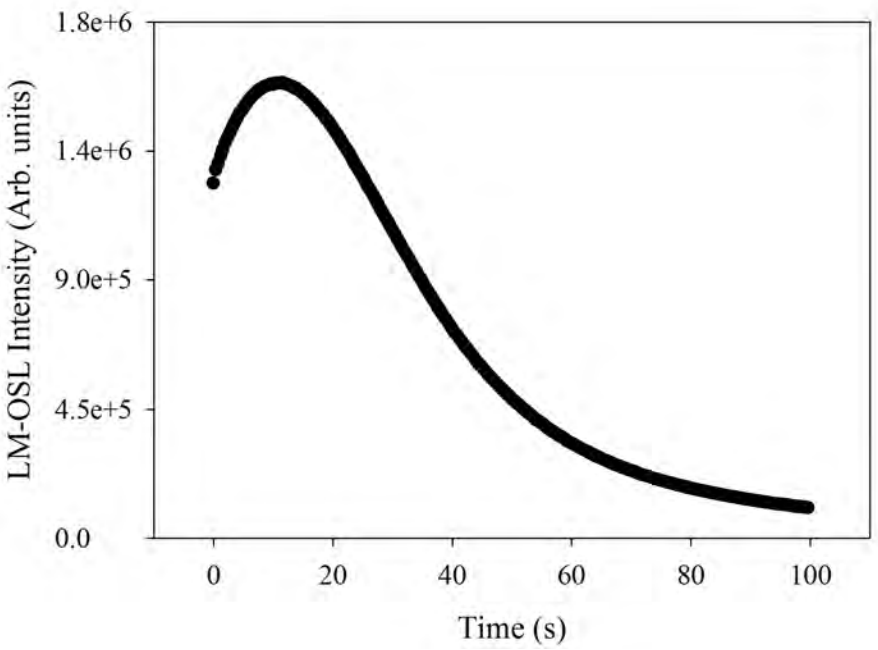

Figure 1.6: A LM-OSL curve of α-Al_2O_3:C,Mg measured at room temperature during a 100 s exposure to 470 nm blue light after irradiation to 1.0 Gy. The power density of the stimulating light was increased linearly from 10 to 100% during measurement.

2009). Various models have been used to explain charge processes involved in TR-OSL. The simplest analytical model of TR-OSL consists of one electron trap and one radiative recombination centre. This model describes the TR-OSL intensity in terms of changes in the concentration of optically stimulated electrons (Chithambo, 2007b,c). A kinetics model based on simulations of experimental data has also been used to explain the luminescence process of TR-OSL (Pagonis et al., 2009) in quartz. A phenomenological model in which the luminescence intensity is expressed as a function of the concentration of excited luminescence centres was also proposed (Yukihara and McKeever, 2011; Chithambo, 2018).

1.2 Aim of the thesis

This thesis aims to contribute towards the understanding of mechanisms of luminescence in α-Al_2O_3:C,Mg using TL and OSL techniques. The dosimetric features of α-Al_2O_3:C,Mg will be investigated for annealed and unannealed samples. The dynamics of the phototransferred peaks from each of these samples will also be investigated. The dependence of illumination time on phototransferred peaks will

also be studied. Lastly, thermally assisted OSL will be used to investigate the presence and role of deep traps in luminescence.

1.3 Synopsis of the thesis

The remaining chapters are organised as follows: Chapter 2 describes the process of phototransferred thermoluminescence and presents some of the models which have been used to explain the dependence of peak intensity on illumination time for phototransferred peaks. Thermal quenching and thermal assistance to optical stimulation are described in Chapter 3. Chapter 4 discusses point defects in α-Al_2O_3:C,Mg. In Chapter 5, the experimental methods are presented. These include the experimental setup and the characteristics of the samples used. Chapter 6 discussed the dosimetric features of α-Al_2O_3:C,Mg for the unannealed and annealed samples. The studies of phototransferred thermoluminescence from the unannealed sample and the samples annealed at 700, 900 and 1200°C for 15 minutes each are presented in Chapters 7-9 respectively. The investigation of thermally assisted optically stimulated luminescence from α-Al_2O_3:C,Mg is discussed in Chapter 10. Chapter 11 concludes the study and makes suggestions for future luminescence research in α-Al_2O_3:C,Mg.

Chapter 2

Phototransferred Thermoluminescence

Phototransferred thermoluminescence (PTTL) is the thermal stimulation for luminescence of electrons which have been optically transferred from deep traps to shallow traps (McKeever, 1985; Chen and McKeever, 1997). The PTTL process consists of four steps namely; irradiation, depletion of electrons in shallow traps, illumination, and thermal stimulation. Electron-holes pairs are created during irradiation. Some of these electrons are trapped at electron traps whereas some holes are captured at recombination centres. After irradiation, the sample is preheated to remove electrons from the shallow traps. The preheated sample is cooled and exposed to light of a specific wavelength in order to transfer some electrons from deep traps into the shallow ones. Finally, the sample is then heated again to monitor luminescence.

PTTL has been observed and studied in common luminescent materials such as; quartz (Milanovich-Reichhalter and Vana, 1990; Wintle and Murray, 1997; Santos et al., 2001; Bertucci et al., 2011; Chithambo et al., 2019; Chithambo and Dawam, 2020), LiF (Bailiff and Poolton, 1991), α-Al_2O_3:C (Walker et al., 1996; Chithambo et al., 2017a), α-Al_2O_3:C,Mg (Kalita and Chithambo, 2017e, 2019; Sob et al., 2021), tanzanite (Chithambo, 2021a) and BeO (Bulur, 2007). PTTL has been suggested as a tool for radiation dosimetry (Bailiff and Poolton, 1991; Bossin et al., 2018); the study of absorption spectra of minerals (Alexander and McKeever, 1998) and as a means to study luminescence mechanisms in α-Al_2O_3:C (Chithambo et al., 2017a).

In PTTL, a trap into which electrons are optically transferred is referred to as an acceptor trap whereas a trap from which these electrons are optically transferred is known as a donor trap.

2.1 Kinetics-based models of PTTL

2.1.1 The two traps one centre model

The simplest energy model used to describe PTTL is one consisting of a shallow trap (an acceptor trap), a deep trap (a donor trap) and a radiative recombination centre as shown in Figure 2.1.

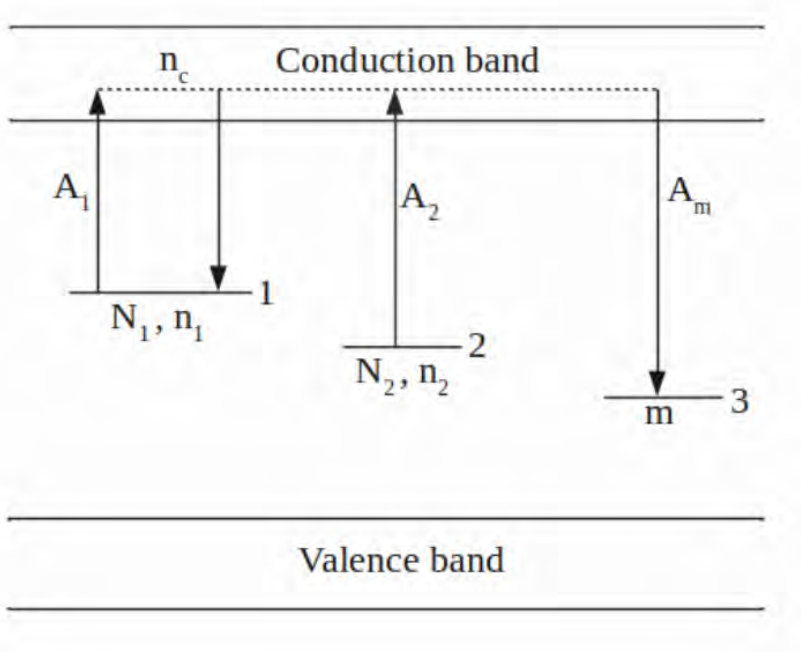

Figure 2.1: Simple model of PTTL showing the flow of charges from the shallow trap (level 1), the deep trap (level 2), and the recombination centre (level 3). Reproduced from Chen and McKeever (1997).

For the model of Figure 2.1, the concentration of electron traps for the trap labelled i is N_i and n_i is the concentration of trapped electrons. A_i denotes the probability of retrapping for trap i. The concentration of hole traps is denoted by M whereas that of trapped holes is denoted by m. In addition, n_c and n_v are the concentration of electrons and holes in the conduction and valence bands respectively.

During the irradiation stage, the trapping of electrons at electron traps and the capture of holes by the recombination centre can be described as:

$$\frac{dn_1}{dt} = A_1(N_1 - n_1)n_c, \tag{2.1}$$

$$\frac{dn_2}{dt} = A_2(N_2 - n_2)n_c, \tag{2.2}$$

$$\frac{dn_v}{dt} = R - A_m^*(M - m)n_v, \tag{2.3}$$

where R is the rate of electron-hole pairs creation and A_m^* is the probability of hole detrapping at the recombination centre. In addition to the flow of charge described by equations (2.1) - (2.3), charge needs to be conserved. This condition is written as

$$n_c + n_1 + n_2 = m + n_v. \tag{2.4}$$

After irradiation, preheating is performed to remove electrons from the shallow trap. It is assumed that after preheating, the new concentration of electrons at level 1 is $n_{10} = 0$, and that of electrons at level 2 is n_{20}. The concentration of electrons and holes in the conduction and valence bands respectively are also assumed to be negligible hence for charge conservation, we have $n_{20} = m_0$ with m_0 being the new concentration of holes.

During illumination, electrons are optically stimulated from the deep trap at a rate f_2. It is assumed that optical stimulation of electrons out of the shallow trap is negligible since at the start of this step $n_{10} = 0$. The flow of charge during this stage can be expressed as

$$\frac{dn_2}{dt} = -n_2 f_2 + A_2(N_2 - n_2)n_c, \tag{2.5}$$

$$\frac{dn_1}{dt} = A_1(N_1 - n_1)n_c, \tag{2.6}$$

$$\frac{dm}{dt} = -A_m m n_c, \tag{2.7}$$

$$\frac{dn_v}{dt} = 0, \tag{2.8}$$

and for charge neutrality;

$$\frac{dn_c}{dt} = -\frac{dn_1}{dt} - \frac{dn_2}{dt} + \frac{dm}{dt}. \tag{2.9}$$

All the terms in equations (2.5) - (2.9) are as previously defined. During illumination, it is assumed that $dn_c/dt \approx 0$. This is the quasi-equilibrium (QE) approximation. Optically stimulated electrons can retrap into the deep trap, transit to the

shallow trap or recombine with holes at the recombination centre. It is assumed that retrapping into the deep trap is negligible, namely that $A_2(N_2 - n_2)n_c \approx 0$. The solutions of equations (2.5) - (2.7) are then given by:

$$n_2(t) = n_{20} \exp(-tf_2), \tag{2.10}$$

$$n_1(t) = N_1[1 - \exp(-Bt)], \tag{2.11}$$

and

$$m(t) = m_0 \exp(-t/\tau) \tag{2.12}$$

where $B = n_c A_1$ and $\tau = 1/n_c A_m$ is the lifetime. There is a non-negligible concentration of electrons in the shallow trap after illumination. Equation (2.10) describes the loss of electrons from the deep trap during illumination while equation (2.11) describes the filling of the shallow trap within that time. The loss of holes at the recombination centre is expressed by equation (2.12). This loss is in part due to the OSL observed during illumination.

At the heating stage, that is after illumination, some of the electrons which are thermally freed from the shallow traps can recombine with holes via the conduction band to emit luminescence. The transport of charge during this stage is described by:

$$\frac{dn_1}{dt} = -n_1 p_1 + A_1(N_1 - n_1)n_c, \tag{2.13}$$

$$\frac{dn_2}{dt} = A_2(N_2 - n_2)n_c, \tag{2.14}$$

and

$$\frac{dm}{dt} = -A_m m n_c = -\frac{m}{\tau}, \tag{2.15}$$

where p_1 is the probability of thermal release of electrons from the shallow trap. At the heating stage, at time t^*, it is assumed that QE approximation is valid and the deep trap is close to saturation such that $n_1(t^*) \ll N_2 - n_2(t^*)$ (Chen and McKeever, 1997). Under these assumptions, the area under the PTTL peak is computed as

$$S(t^*) = \frac{C_s m(t^*) n_1(t^*)}{N_2 - n_2(t^*)} \tag{2.16}$$

where C_s is a constant. By substituting with equations (2.10) - (2.12), the PTTL signal is given by

$$S(t^*) = \frac{C_s \exp(-t^*/\tau) N_1 [1 - \exp(-Bt^*)]}{N_2/n_{20} - \exp(-t^* f_2)} \tag{2.17}$$

As the illumination time increases, the population of electrons in the deep trap progressively becomes negligible and $S(t^*)$ increases towards a maximum. Equation (2.17) therefore describes a monotonically increasing function. This is not always consistent with experimental results.

The dependence of PTTL intensity on stimulation time displays a wide range of behaviour. An example is one where the PTTL dependence on illumination time increases up to a maximum and then decreases thereafter. Figure 2.2 shows an example of the dependence of PTTL intensity, taken as peak height, on duration of illumination for a PTTL peak of unannealed α-Al_2O_3:C,Mg.

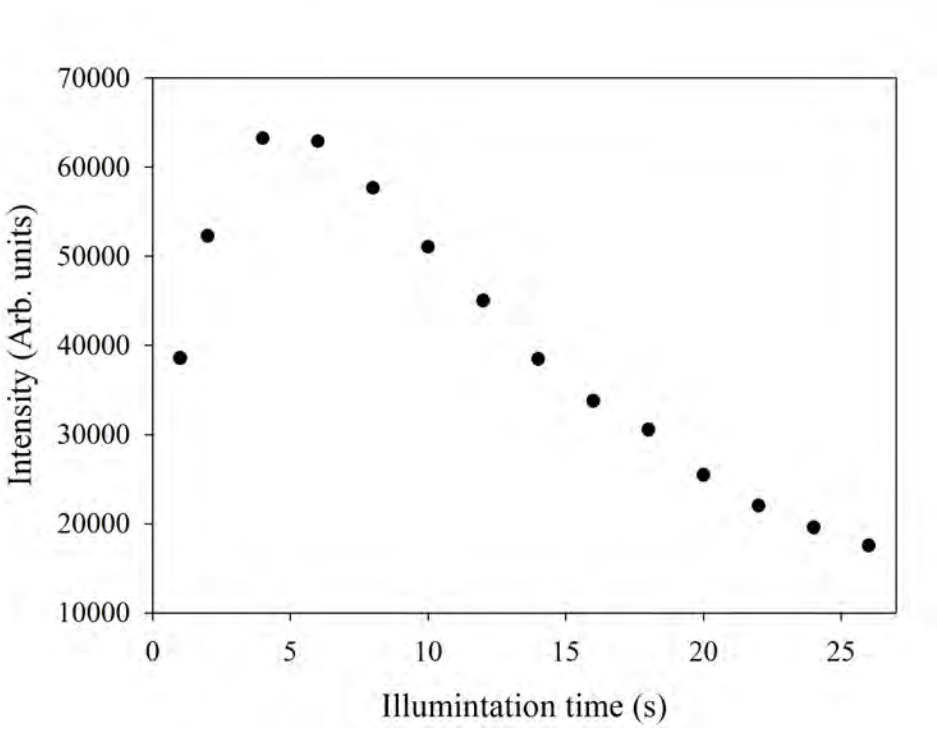

Figure 2.2: Dependence of intensity (peak height) on illumination time for a PTTL peak of unannealed α-Al_2O_3:C,Mg which appears at 43°C. The glow curves from which the PTTL peak is observed were measured at 1°C/s after irradiation to 2.0 Gy, preheating to 60°C and illumination with 470 nm blue.

In describing the charge dynamics during the illumination, no loss of electrons from the shallow trap was assumed. Walker et al. (1996) found that in the case of

α-Al_2O_3:C, electrons are optically bleached from the shallow traps during illumination. For the simple model of Figure 2.1, this loss of electrons due to bleaching can explain the decreasing part of most experimental PTTL curves. However, Alexander et al. (1997); Alexander and McKeever (1998) showed that the PTTL intensity will not necessarily decrease to zero as expected from bleaching but to a non-zero constant value.

2.1.2 The model of Wintle and Murray (1997)

Wintle and Murray (1997) used a model consisting of a shallow trap, a deep trap and a recombination centre to describe the dependence of PTTL intensity on illumination time. The model thus described is similar to the one shown in Figure 2.1. The main point is that Wintle and Murray (1997) neglected retrapping. The concentration of electrons in the shallow trap is denoted by n_1 whereas that of electrons in the deep trap is denoted by n_2. The equations describing charge transfer during illumination are

$$\frac{dn_2}{dt} = -\lambda_2 n_2 \tag{2.18}$$

$$\frac{dn_1}{dt} = -\lambda_1 n_1 + \alpha\lambda_2 n_2 \tag{2.19}$$

where λ_1 and λ_2 are the rates of optical stimulation out of the shallow and deep traps respectively and α is a constant of proportionality. Equation (2.18) refers to the loss of electrons from the deep trap whereas equation (2.19) on the other hand describes the loss of electrons from the shallow trap but also the retrapping of electrons stimulated from the deep trap during illumination. The solutions to coupled equations (2.18) and (2.19) is

$$n_1 = \alpha\frac{\lambda_2 n_{20}}{\lambda_1 - \lambda_2}[e^{-\lambda_2 t} - e^{-\lambda_1 t}] \tag{2.20}$$

where n_{20} is the initial population of electrons in the deep trap. As shown by equation (2.20), the concentration of shallow trap electrons, n_1, initially increases with illumination time before decreasing to a steady value thereafter. Figure 2.3 shows plots of n_1, as defined by equation (2.20), for different values of the constant α. The parameters $\lambda_1 = 0.1s^{-1}$, $\lambda_2 = 0.05s^{-1}$ and $n_{20} = 10^{12}cm^{-3}$ were used. The choice of parameters, for purposes of illustration only, was guided by (Chen and Pagonis, 2011).

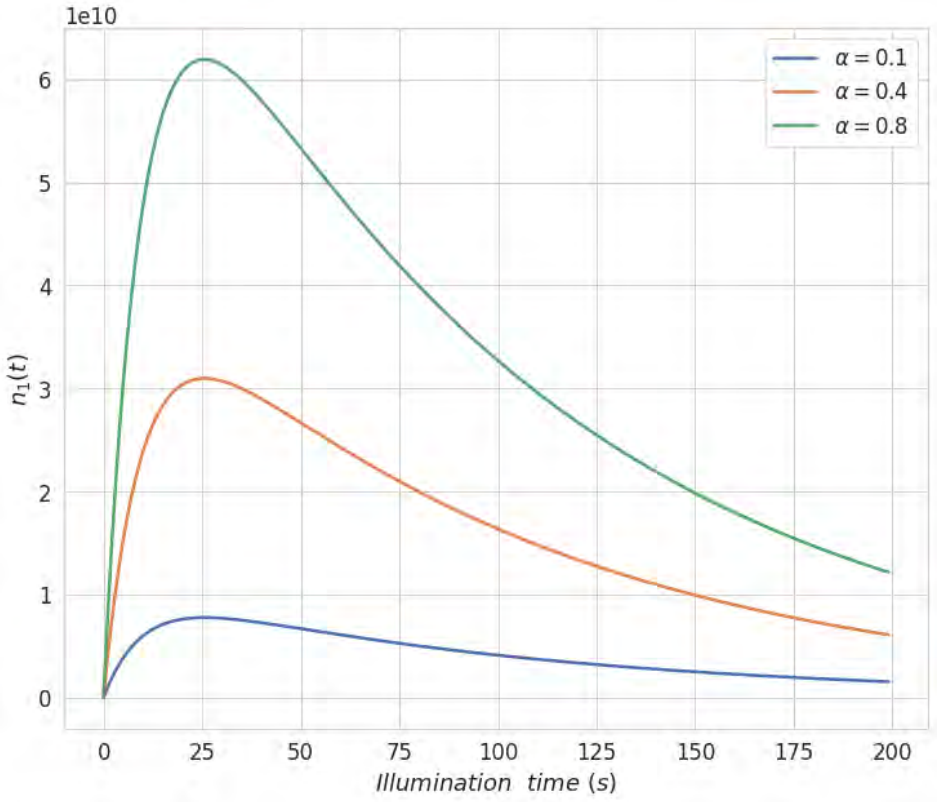

Figure 2.3: Population of shallow trap electrons as a function of illumination time. The simulation parameters are: $\lambda_1 = 0.1$ s^{-1}, $\lambda_2 = 0.05$ s^{-1}, $n_{20} = 10^{12}$ cm^{-3} and $\alpha = 0.1, 0.4, 0.8$.

The work of Wintle and Murray (1997) shows that any ensuing PTTL measured after illumination is proportional to the concentration of electrons in the shallow trap.

2.2 The three traps two centres model

The energy band model of Figure 2.4 can be used to explain the decreasing part of PTTL dependence on illumination time without the requirement of optical bleaching of electrons from the shallow trap (Alexander et al., 1997; Alexander and McKeever, 1998) as observed in the study of Walker et al. (1996). The model (Figure 2.4) consists of a shallow trap (level 1), a deep active trap (level 2), a deep inactive trap (level 3), a radiative recombination centre (level 4), and a non-radiative recombination centre. The deep inactive trap is not necessary for PTTL to occur however, it is useful in explaining non linear dose dependence effects (Chen and McKeever,

1997). Charge conservation is now expressed as

$$n_c + n_1 + n_2 + n_3 = m_4 + m_5 \tag{2.21}$$

where n_3 is the concentration of trapped electrons at the deep inactive trap, and m_4 and m_5 are the concentration of holes captured at the radiative and non-radiative recombination centres respectively. All other terms are as previously defined.

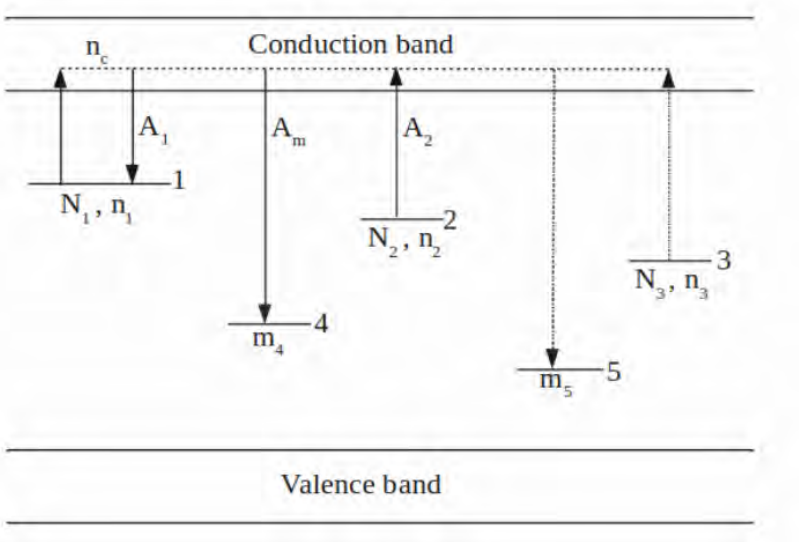

Figure 2.4: Energy band model of PTTL showing the flow of charge from the shallow trap (level 1), the deep trap (level 2), the deep inactive trap (level 3), the radiative recombination centre (level 4), and the non-radiative recombination centre (level 5). Reproduced from Chen and McKeever (1997).

Similar equations describing the transfer of charge during each stage of the PTTL process can be written for this model as in section 2.1. One important feature of this model is that it allows a transfer of holes from the radiative to the non-radiative recombination centre during the heating step of the PTTL process. This implies that in addition to the OSL observed during illumination, holes are also lost by capture at the non-radiative recombination centre. As a consequence of this competition between the two hole centres, the PTTL signal now depends on n_1 and m_4.

In the simple model of Figure 2.1, the concentration of electrons n_1 cannot be greater than that of holes since charge must be conserved. In the model of Figure 2.4 however, it is possible for n_1 to be greater than m_4 at some time t. If we assume that at the start of the heating stage $n_1 < m_4$ then the PTTL signal will grow with illumination time until the active deep trap, n_2, is depleted or there is no longer enough holes at m_4 for electrons to recombine with. the PTTL intensity will

therefore decrease when any of these two situations occurs. The PTTL intensity is then described by

$$S = min(n_1, m_4). \tag{2.22}$$

Alexander et al. (1997) and Alexander and McKeever (1998) showed that the dependence of the PTTL signal on duration of illumination is affected by factors such as the wavelength of the stimulating light, its intensity, and the photoionisation cross-section, σ, from the deep active trap.

2.3 The phenomenological model of Chithambo et. al (2017)

Chithambo et al. (2017a) developed a phenomenological model for the analysis of PTTL dependence on illumination time in which the number of donors is not assumed. In their model, the number of acceptor and donor traps depend on the preheating temperature. For two different preheat temperatures for example, a trap associated with a given peak may act as an acceptor or a donor. This is not the case with the models of Alexander et al. (1997); Alexander and McKeever (1998) or Wintle and Murray (1997) in which the number of acceptors (shallow trap) and donors (deep traps) are fixed. The rate equations describing charge transfer are written for the illumination step only. These equations are written under the assumption that retrapping is negligible and only a portion of electrons stimulated from the donor traps are transferred to an acceptor trap. In principle this applies for first-order kinetics but is a simplifying assumption otherwise. Charge transfer occurs via the conduction band.

Figure 2.5 shows the model of Chithambo et al. (2017a) for α-Al_2O_3:C. The model consists of a shallow trap (ST), a main trap (MT), an intermediate-energy trap (IET), a deep trap (DT), a deep hole trap (DHT) and a recombination centre (R).

In their study Chithambo et al. (2017a) reported that peaks I - III were reproduced under phototransfer for various preheating temperatures. They found that peak I was reproduced under phototransfer after preheating to any temperature between 100 and 500 °C. In that sense, the traps labelled MT, IET, DT act as donors for peak I after preheating to 100 °C whereas the trap labelled ST acts as the acceptor. The transfer of charge during illumination is then expressed as

$$\frac{dn_2}{dt} = -s_2 n_2 \tag{2.23}$$

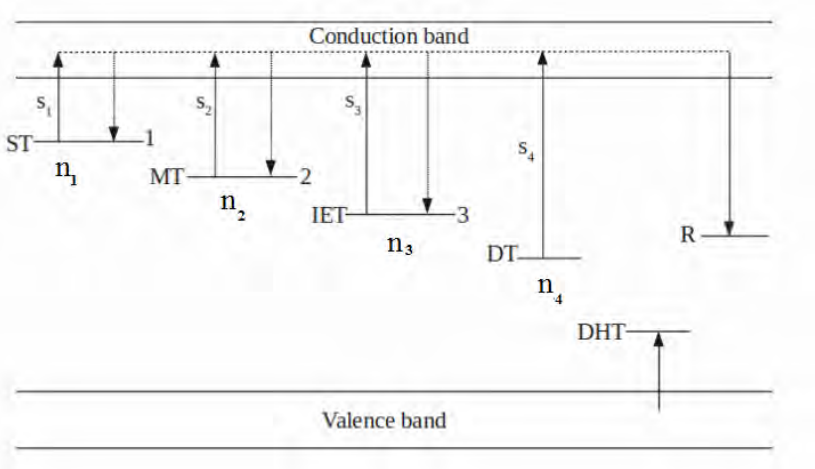

Figure 2.5: Phenomenological model use to describe PTTL in α-Al_2O_3:C by Chithambo et al. (2017a). ST, MT, IET and DT are the shallow-, main-, intermediate-energy and deep electron traps. DHT and R are the deep hole trap and the recombination centre respectively.

$$\frac{dn_3}{dt} = -s_3 n_3 \tag{2.24}$$

$$\frac{dn_4}{dt} = -s_4 n_4 \tag{2.25}$$

$$\frac{dn_1}{dt} = -s_1 n_1 + a_2 s_2 n_2 + a_3 s_3 n_3 + a_4 s_4 n_4 \tag{2.26}$$

where s_i and n_i are the probabilities of electron stimulation and the concentration of electrons for trap i respectively. The stimulation probability $s_i = \Phi\sigma_i$ where Φ is the photon flux and σ_i is the photoionisation cross-section of trap i (Bøtter-Jensen et al., 2003). The constants a_2, a_3 and a_4 are used to quantify the portion of electrons stimulated from the respective donor trap into the acceptor trap. Equations (2.23) - (2.26) describe a general system of a one acceptor and three donors whose solution is

$$n_1(t) = A_1\left(e^{-s_2 t} - e^{-s_1 t}\right) + A_2\left(e^{-s_3 t} - e^{-s_1 t}\right) + A_3\left(e^{-s_4 t} - e^{-s_1 t}\right) \tag{2.27}$$

where $A_1 = a_1 s_2 n_{2i}/(s_1 - s_2)$, $A_2 = a_2 s_3 n_{3i}/(s_1 - s_3)$ and $A_3 = a_3 s_4 n_{4i}/(s_1 - s_4)$. n_{2i}, n_{3i} and n_{4i} are the initial concentration of electrons at the donor traps MT, IET and DT respectively. As shown by Chithambo et al. (2017a), for a given preheat temperature the contribution of a potential donor may be negligible. Hence in addition to solving for a solution such as that given by equation (2.27), the TL

dependence on illumination time of the peak associated with each potential donor is also examined to determine if the contribution from the corresponding trap is significant. As in the model of Wintle and Murray (1997), it is assumed that the PTTL intensity is proportional to the concentration of electrons at the acceptor trap.

We use the model of Chithambo et al. (2017a) for the analysis of PTTL-time profiles of α-Al_2O_3:C,Mg reported in this thesis. PTTL-time profiles of unannealed α-Al_2O_3:C,Mg have also been analysed with this model (Sob et al., 2021). Chithambo et al. (2019) and Chithambo and Dawam (2020) equally applied this model to the analysis of PTTL dependence on illumination time for natural and synthetic quartz respectively.

Chapter 3

Thermally Assisted Luminescence Phenomena

This chapter discusses thermal assistance and thermal quenching; two independent thermodynamic processes which occur simultaneously during luminescence stimulation (Kalita and Chithambo, 2017h).

3.1 Thermal quenching

Thermal quenching refers to the decrease in luminescence efficiency with increasing temperature (Wintle, 1975). Thermal quenching has been observed and studied for many luminescent materials such as quartz (Galloway, 2002; Chithambo and Galloway, 2001; Nanjundaswamy et al., 2002; Bøtter-Jensen et al., 2003; Chithambo and Ogundare, 2009; Pagonis et al., 2010, 2014), Al_2O_3:C (Akselrod et al., 1998; Chithambo et al., 2014, 2015) and Al_2O_3:C,Mg (Kalita et al., 2017a; Kalita and Chithambo, 2017c; Trindade and Jacobsohn, 2018). Thermal quenching manifests itself as the reduction of TL intensity as the measurement temperature increases. For a set of glow curves measured at increasing heating rates, the decrease in peak intensity or peak area with increase in heating rate is ascribed to thermal quenching (Gorbics et al., 1969). In the absence of thermal quenching, the peak intensity and the area under the peak are expected to remain constant. Inverse thermal quenching is observed if the peak intensity or peak area increases with heating rate (Chithambo and Dawam, 2020). Depending on the experimental parameters, it therefore becomes important to account for thermal quenching when evaluating kinetic parameters such as the activation energy (Petrov and Bailiff, 1995). OSL curves measured at elevated temperatures (100 - 200°C) are also affected by thermal quenching (Wintle, 1975; Spooner, 1994; Huntley et al., 1996; Chithambo

and Galloway, 2001; Kalita et al., 2017a). Multiple studies have shown that luminescence lifetimes and luminescence intensity from time-resolved luminescence spectra are affected by thermal quenching (Galloway, 2002; Chithambo, 2003, 2006, 2007b,c).

3.1.1 The Mott-Seitz Mechanism

The Mott-Seitz mechanism, which is based on a configurational coordinate model, is one of the mechanisms suggested to explain thermal quenching in most luminescent materials; including quartz and α-Al_2O_3:C (Chen and Pagonis, 2011). Figure 3.1 is a configurational coordinate diagram describing the Mott-Seitz mechanism for thermal quenching. It shows adiabatic potential energy curves for the ground and excited states of the recombination centre plotted as functions of the configurational coordinate r (Bøtter-Jensen et al., 2003). In this model, electrons captured at the excited state of the recombination centre can undergo either radiative or non-radiative transitions to the ground state of the recombination centre. The radiative transition, depicted as the vertical arrow, results in luminescence emission. The second route on the other hand is an indirect thermally assisted transition to the ground state. The activation energy for thermal quenching is represented by W. In the non-radiative process, the energy is released through phonons.

The probability A_{NR} of the non-radiative process is assumed to be temperature dependent whereas that of radiative process is assumed to be constant (Mott and Gurney, 1948). The luminescence efficiency, defined as the ratio of the radiative and non-radiative probabilities, is given by

$$\eta = \frac{A_R}{A_R + A_{NR}\exp(-W/kT)} = \frac{1}{1 + C\exp(-W/kT)} \tag{3.1}$$

where $C = A_{NR}/A_R$ is a dimensionless constant, W is the activation energy for thermal quenching, k is Boltzmann constant and T is the absolute temperature. The temperature dependence of the luminescence lifetime τ is then expressed as

$$\tau = \eta\tau_{rad} = \frac{\tau_{rad}}{1 + C\exp(-W/kT)} \tag{3.2}$$

where τ_{rad} is the lifetime for radiative transitions (Bøtter-Jensen et al., 2003). In the presence of thermal quenching, the luminescence intensity is expressed as (Petrov and Bailiff, 1995)

$$I = \eta I_0 = \frac{I_0}{1 + C\ \exp(-W/kT)} \tag{3.3}$$

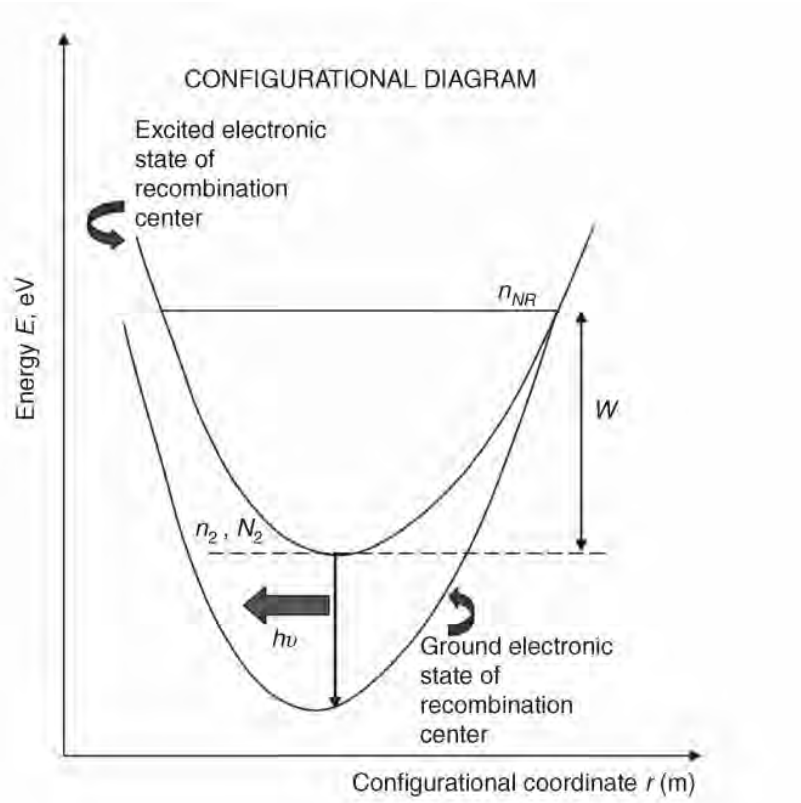

Figure 3.1: A configurational coordinate diagram describing thermal quenching. Reproduced from Chen and Pagonis (2011).

where I_0 is the least quenched intensity. All other parameters are as previously defined.

The model in Figure 3.1 is a fine tool for explaining thermal quenching but does not explain the physics of the process. It is known that the transition from the ^3P excited state to the ^1S ground state at an F-centre is radiative (Brewer et al., 1980; Agulló-López et al., 1988; McKeever et al., 1995). The non-radiative transitions on the other hand are temperature-dependent. It has been reported that the intensity, the width and the position of the main emission band in α-Al_2O_3:C are affected by measurement temperature (Evans, 1995; Zhu et al., 2014; Chithambo et al., 2015). This assumption is probably valid for α-Al_2O_3:C,Mg since the main emission bands in these two samples are associated with oxygen vacancies or their clusters (Summers, 1984; Agulló-López et al., 1988). According to Chithambo et al. (2015), the temperature-dependent increase of width for the 380 and 420 nm emission bands of α-Al_2O_3:C could be due to strong coupling between the F-centre and the lattice. Based on the semiclassical configurational model, the dependence of band width

on temperature can be expressed as

$$\Delta W(T) \approx \Delta W_0 \left(\frac{2k}{\hbar\omega}\right)^{1/2} T^{1/2} \tag{3.4}$$

where ΔW_0 is the width at absolute zero of temperature, k is Boltzmann's constant and $\hbar\omega$ is the energy of the coupling phonon (Chithambo et al., 2015). Equation (3.4) shows that the change in width of the emission bands at 380 and 420 nm becomes prominent with increasing temperature. Using configurational coordinate diagrams (Fig. 11 of their paper), Chithambo et al. (2015) provided a description of the radiative and non-radiative transitions. Descriptions of non-radiative transitions with the aid of such configurational coordinate diagrams have also been provided elsewhere (Fox, 2001; Gaft et al., 2005; Henderson and Imbusch, 2006).

3.1.2 The Model by Nikiforov et al.

Nikiforov et al. (2001) developed a model based on the thermal and optical ionisation of F-centres to explain thermal quenching in Al_2O_3:C. Figure 3.2 shows the band diagram proposed by Nikiforov et al. (2001) to describe thermal quenching in alumina (α-Al_2O_3:C).

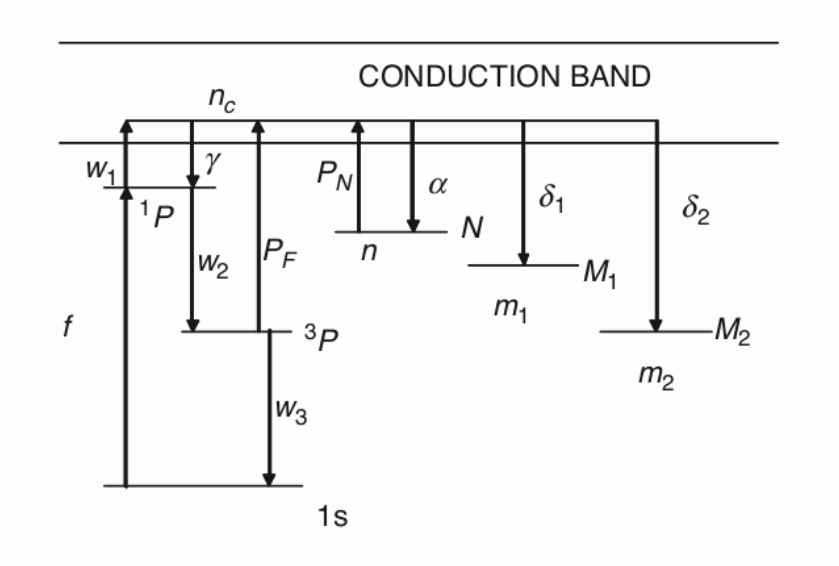

Figure 3.2: Kinetic model of Nikiforov et al. (2001) for thermal quenching in alumina. Reproduced from Chen and Pagonis (2011).

The model shown in Figure 3.2 consists of an F-centre, a dosimetric trap (n, N) and deep traps (m_1, M_1) and (m_2, M_2). The electronic structure of the F-centre

consists of a ground state level, ^1S, and two excited states labelled ^1P (singlet state) and ^3P (triplet state).

In this model, N, M_1 and M_2 (cm^{-3}) denote the concentration of the dosimetric and deep traps. The concentration of trapped carriers at each of these levels is represented by n, m_1 and m_2 (cm^{-3}) respectively; α, δ_1 and δ_2 ($\mathrm{cm}^{-3}\mathrm{s}^{-1}$) are the corresponding capture coefficients. P_N is the probability of thermal stimulation of electrons into the conduction band from the dosimetric trap. The transition probabilities are w_1, w_2 and w_3 (s^{-1}). For instance w_3 denotes the transition probability between the ^3P and the ^1S states of the F-centre. γ is the carrier capture coefficient associated with level ^1P. In the model, thermal quenching results from reduction in concentration of F-centres due to thermal ionisation and optical ionisation. Exposure to UV light (205 nm) leads to an excited F-centre ($\mathrm{F} + h\nu\,(205\,\mathrm{nm}) \longrightarrow \mathrm{F}^*$) which then forms an F^+-centre by releasing an electron ($\mathrm{F}^* \longrightarrow \mathrm{F}^+ + e^-$). This ionisation of F-centres leads to an increase in the concentration of F^+-centres with time. Thermal stimulation of electrons from the ^3P excited state into the conduction band is shown by the transition P_F and its probability is given by

$$P_F = C\exp(-W/kT) \tag{3.5}$$

where all the terms are as previously defined. As P_F increases with temperature, the number of radiative transitions ($^3P \longrightarrow {}^1S$) decreases. Hence, thermal and optical ionisation of the F-centre leads to thermal quenching.

3.2 Thermal assistance

Thermal assistance to optical stimulation refers to the thermal contribution to the photo-eviction of electrons during OSL emission (Spooner, 1994). Thermal assistance manifests itself as an increase in integrated OSL intensity with measurement temperature. As pointed out by Wintle (1975), thermal assistance affects the rate of optical eviction of charge and thereby also affects the initial luminescence and the shape of the OSL curve. For convenience, OSL curves measured above room temperature are sometimes known as thermally assisted OSL (TA-OSL). TA-OSL provides a means of indirectly investigating the signal from deep traps (above 500°C) which are not thermally accessible in conventional TL studies (Huntley et al., 1996; Chithambo and Galloway, 2001; Polymeris and Kitis, 2012; Polymeris et al., 2015a; Meriç et al., 2016; Kalita et al., 2017b; Chithambo, 2021b).

In the presence of thermal assistance, Spooner (1994) observed that the luminescence intensity could be described in term of a Boltzmann term as follows:

$$I(T) = I_0 \exp(-E_a/kT) \tag{3.6}$$

where I, I_0 are the integrated luminescence intensities at temperature T and T_0. In equation (3.6), E_a is the activation energy for thermal assistance and k is Boltzmann constant. Thermal assistance and thermal quenching are observed independently (Chithambo and Galloway, 2001). Combining equations (3.2) and (3.6), the luminescence intensity becomes

$$I(T) = \frac{I_0 \exp(-E_a/kT)}{1 + C \exp(-W/kT)} \tag{3.7}$$

where all the terms are as previously defined. When thermal assistance is due to separate electron traps, the overall luminescence intensity is expressed as

$$I(T) = \frac{I_0 \prod_i^n \exp(-E_{ai}/kT)}{1 + C \exp(-W/kT)} \tag{3.8}$$

where E_{ai} is the activation energy for thermal assistance of the ith electron trap and n is the number of electron traps (Chithambo and Costin, 2017).

Chapter 4

Point defects in α-Al_2O_3:C,Mg

Defects have an impact on the physical, chemical and electrical properties of materials. This chapter describes point defects in α-Al_2O_3:C,Mg and their role in the use of this sample as a luminescence dosimeter.

4.1 Point defects

A defect refers to a disruption in the crystal structure. If such a disruption is localised at a lattice point or over a few atomic sites, it is known as a point defect (Agulló-López et al., 1988; Tilley, 2008). Other types of defects such as dislocations, surface defects and volume defects are also possible (Tilley, 2008). Our discussion will only focus on point defects. Point defects can result from vacancies at atom sites, interstitial elements or impurities (Tilley, 2008). A vacancy occurs when an atom is absent from its site. A vacancy caused by an atom M is denoted by V_M. An interstitial atom occupies a position which should be unoccupied in the lattice. Foreign atoms introduced into the crystal during growth or doping are known as impurities. Figure 4.1 shows point defects in a crystal MX. Defects present in *as grown* crystals are referred to as native or intrinsic defects whereas those arising from external impurities or doping are termed extrinsic defects. Defects can also be induced by exposure of the crystal to nuclear radiation or other forms of radiation.

4.2 Case of α-Al_2O_3:C,Mg

Alpha-alumina (α-Al_2O_3) is a crystallographic form of Al_2O_3 (Doremus, 2008; Riedel and Chen, 2008). Its crystal structure, as shown in Figure 4.2, consists of oxygen anions (O^{2-}) in a slightly distorted hexagonal stacking with aluminium

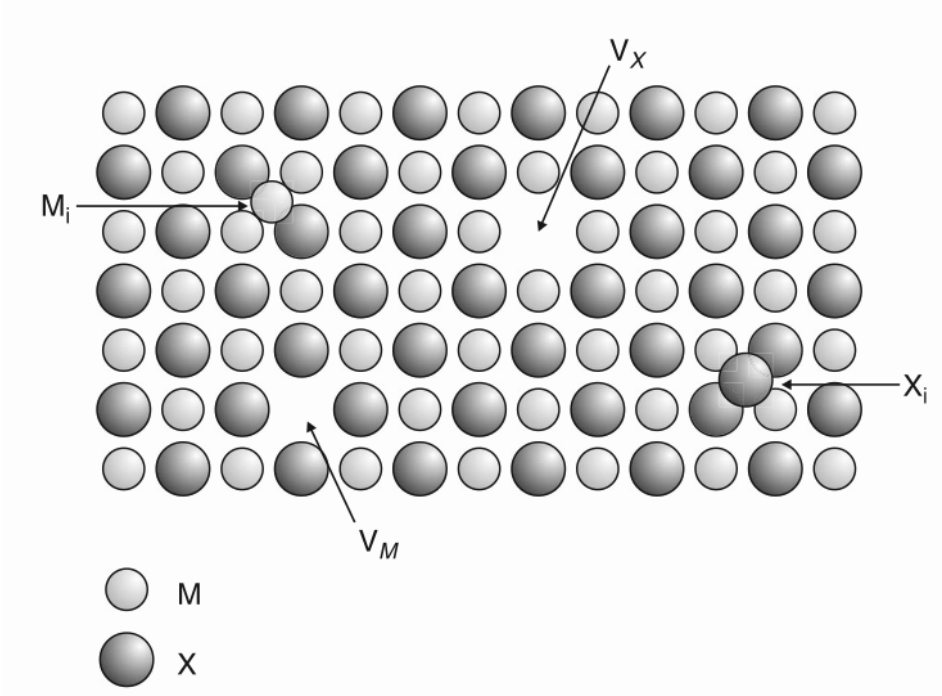

Figure 4.1: Point defects in a crystal of compound MX where V_M is a metal vacancy; V_X a nonmetal vacancy; M_i, a metal self-interstitial; and X_i a nonmetal self-interstitial. The diagram is reproduced from (Tilley, 2008).

cations (Al^{3+}) occupying two third of the octahedral interstices (Doremus, 2008; Riedel and Chen, 2008).

An oxygen vacancy gives rise to an F or F^+ luminescent centre by trapping two or one electron(s) respectively (McKeever et al., 1995). The F-centre is neutral whereas the F^+-centre has a positive charge with respect to its immediate environment in the crystal structure. F and F^+ are not the only electron centres in, say, Al_2O_3:C. α-Al_2O_3:C is a very sensitive thermoluminescence and optically stimulated luminescence dosimeter (Akselrod et al., 1990; Akselrod and McKeever, 1999). F-centres, which have a strong absorption band at 205 nm, are responsible for the main emission at 415 nm in α-Al_2O_3:C and have a luminescence lifetime of $\sim$ 35 ms (Markey et al., 1995; Akselrod et al., 1998; Chithambo et al., 2015). On the other hand, F^+-centres are characterised by absorption bands at 230 and 255 nm; emission at 330 nm and a short lifetime of less than 7 ns (Evans and Stapelbroek, 1978).

α-Al_2O_3:C,Mg, the subject of this study, is also a very sensitive luminescent material developed for optical data storage (Akselrod et al., 2003b), used as a fluorescent nuclear track detector (Akselrod and Sykora, 2011) and investigated for various applications including 2D dosimetry in magnetic resonance guided radio-

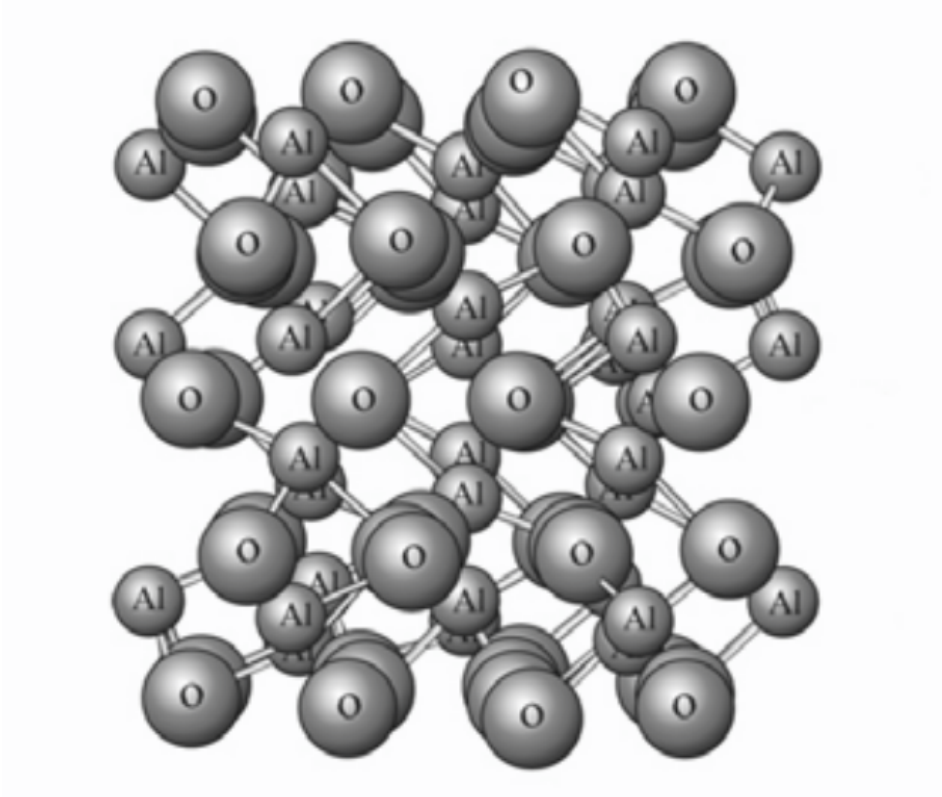

Figure 4.2: Crystal structure of Al_2O_3. It consists of oxygen ions in a hexagonal stacking with aluminium ions occupying two third of the interstitial sites. The diagram is reproduced from (Kouroukla, 2015).

therapy (Shrestha et al., 2020). α-Al_2O_3:C has a high concentration of F and F^+ centres owing to carbon-doping. In addition to these defects, co-doping with Mg is thought to produce additional colour centres such as F^+(Mg), F_2, F_2^{2+}(2Mg) and F_2^+(2Mg) types (Sykora and Akselrod, 2010). An F_2-centre is a cluster of two oxygen vacancies with two trapped electrons each. An F^+-centre can in theory be charge compensated for by an Mg^{2+} ion substituting an Al^{3+} ion. This results into an F^+(Mg) centre. The F_2^{2+}(2Mg) centre is formed when two F^+(Mg) centres are inter-linked. If an F_2^{2+}(2Mg) centre captures an electron, the F_2^+(2Mg) centre is formed. Similarly, if the F_2^+(2Mg) traps an electron, the resulting centre is a neutral F_2(2Mg) centre. Figure 4.3 shows the crystal structure of α-Al_2O_3:C,Mg with some of its point defects.

Owing to the presence of these Mg related electron centres, various luminescence emission bands are generated between 300 and 750 nm in α-Al_2O_3:C,Mg (Akselrod et al., 2003a; Kalita and Chithambo, 2018a; Chithambo et al., 2020). Photoluminescence (PL) measurements have shown that Al_2O_3:C,Mg has four emission bands at 325, 500, 510 and 750 nm. These bands are attributed to F^+(Mg), F_2, F_2^{2+}(2Mg)

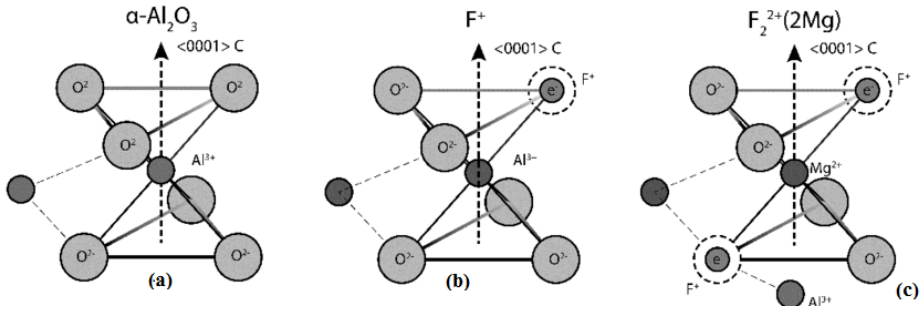

Figure 4.3: Crystal structure of α-Al_2O_3:C,Mg and some of its defects; the ideal lattice cell, one with an F^+-centre, and another containing the F_2^{2+}(2Mg) centre respectively are shown. The diagram is taken from (Kouwenberg, 2018).

and F_2^+(2Mg) centres respectively (Sykora and Akselrod, 2010). Measurements using continuous-wave and time-resolved optically stimulated luminescence as well as radioluminescence also show two prominent emission bands at 330 and 415 nm due to F^+ and F-centres respectively (Chithambo et al., 2020; Sanyal and Akselrod, 2005; Denis et al., 2011b; Yukihara and McKeever, 2011). α-Al_2O_3:C,Mg has several absorption bands and its yellow-green colouration is due to absorption in the blue region at 435 nm (Akselrod et al., 2003b). Annealing at or beyond 700 °C removes the colour as reported by Kalita and Chithambo (2018a). Figure 4.4 shows the absorption spectra of α-Al_2O_3:C,Mg.

A summary of the absorption/excitation and F-type emission bands in Al_2O_3 and Al_2O_3:C,Mg as reported by Trindade and Jacobsohn (2018) are listed in Table 4.1.

Absorption/Excitation (eV)	Emission (eV)	Defect
6.0	3.0	F
5.4, 4.8	3.8	F^+
5.17, 4.86	3.82	F^+(Mg)
4.1, 3.5, 2.75	2.48	F_2
3.54	3.22	F_2^+(Mg)
4.77, 3.7, 2.0	1.65	F_2^+(2Mg)
2.85	2.43	F_2^{2+}(2Mg)

Table 4.1: Absorption/excitation and emission bands of F-related centres in Al_2O_3 and Al_2O_3:C,Mg.

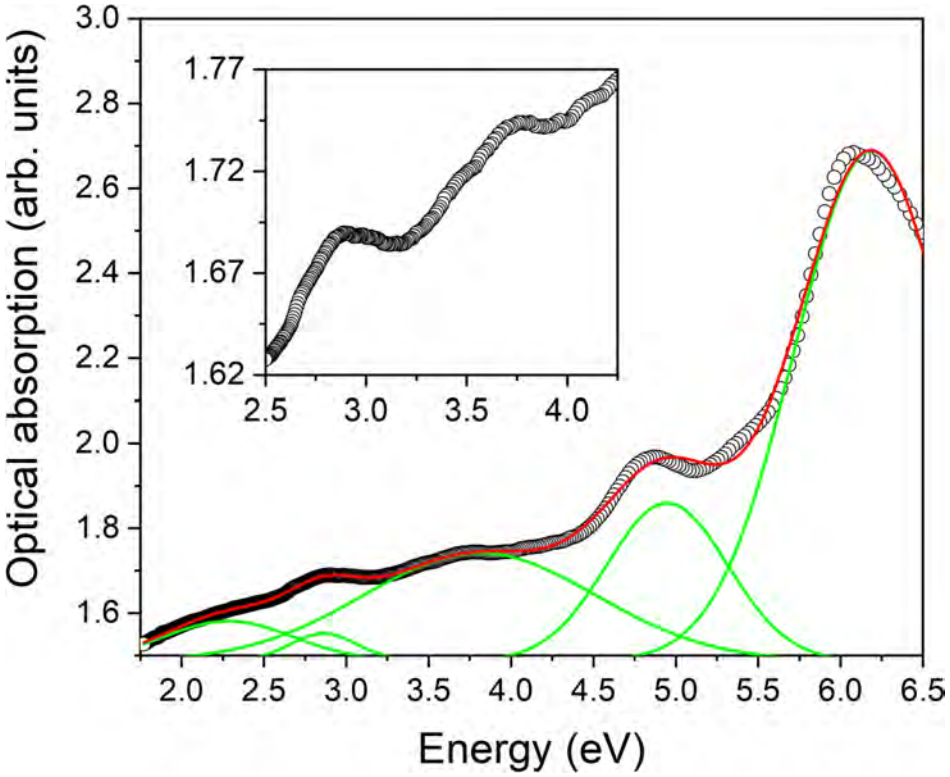

Figure 4.4: Absorption spectra of α-Al_2O_3:C,Mg (open circles) shown with the results of Gaussian (green lines) spectral deconvolution and best fit (red line). The inset highlights the absorption bands between 2.5 and 4.25 eV. The diagram is taken from (Trindade and Jacobsohn, 2018)

Chapter 5

Experimental Details

This chapter describes the luminescence system used for experiments and the samples of α-Al_2O_3:C,Mg used in the study.

5.1 The luminescence measurement system

The Risø TL/OSL DA-20 Luminescence Reader was used for irradiation, stimulation and detection of luminescence from α-Al_2O_3:C,Mg. The Risø TL/OSL Reader consists of two main components namely the Reader and the Controller. The Reader consists of the luminescence detection system, the luminescence stimulation system and the irradiation source. Figure 5.1 is a picture of the Risø TL/OSL DA-20 Luminescence Reader used for our study of α-Al_2O_3:C,Mg. The Controller and the Reader are indicated.

Figure 5.2 is a schematic diagram of the main components of the Luminescence Reader namely the irradiator, the photomultiplier tube, the detection filter, the emission filter, the sample carousel and the heater strip.

Figure 5.1: A picture of the Risø TL/OSL DA-20 Luminescence Reader used for measurements.

The Controller comprises of the electronics used to control the Reader. It also displays the instruction currently being executed. The Controller is connected to a computer via an RS-232 serial cable.

5.1.1 The luminescence detection system

The luminescence detection system consists of a bialkali EMI 9235QB photomultiplier tube (PMT) and a set of transmission filters. The PMT tube has a maximum detection efficiency between 200 and 400 nm. Figure 5.3 shows the quantum efficiency of the PMT tube as a function of the incident photon wavelength. This detection window is suitable for detection of luminescence in α-Al_2O_3:C,Mg the material studied in this thesis. For irradiation doses below 4 Gy, a 7.5 mm thick Hoya U-340 filter with transmission band in the range 270 - 380 nm was used for luminescence detection. For higher doses and whenever necessary, the Hoya U-340 filter together with a 1% absorptive neutral density filter were used to attenuate the luminescence intensity and to prevent damage to the PMT.

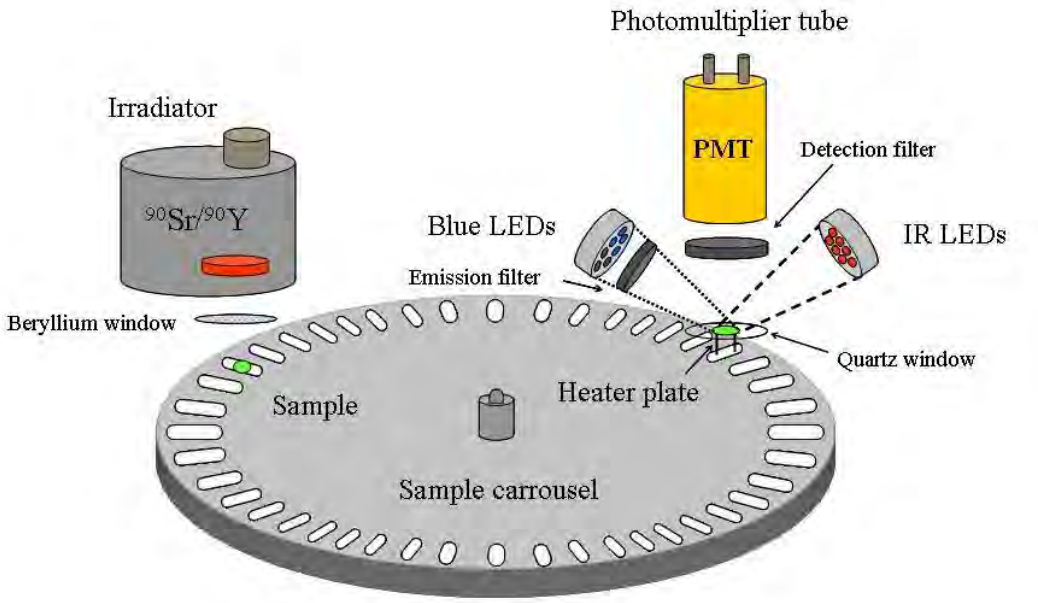

Figure 5.2: Schematic diagram of the Risø TL/OSL Reader (reproduced from the Risø manual (Technical University of Denmark, 2011))

5.1.2 The luminescence stimulation system

Luminescence can be thermally or optically stimulated. The heating system used for thermal stimulation consists of a heater strip and a lift mechanism. For thermal stimulation, the sample is first placed on the carousel which is then rotated to have the sample directly on top of the heater. The heater strip is then raised to ensure contact between the heater and the sample holder. The Risø TL/OSL Reader allows the use of heating rates ranging from 0.1 to 10 °C/s and samples can be heated from room temperature up to 700 °C. Nitrogen is used during heating to properly thermally anchor the sample to its holder (Betts et al., 1993).

Two separate sets of blue and infrared light emitting diodes (LEDS) are provided for optical stimulation. The infrared LEDS emit at 870 nm. For samples of α-Al_2O_3:C,Mg, blue LEDS were used for optical stimulation. The set of blue LEDS consists of 28 LEDS arranged in 4 clusters each with 7 LEDS. The blue LEDS (NICHIA type NSPB-500AS) emit at 470 nm with a full width at half maximum of 20 nm and provide a total power of 80 mW/cm^2 at sample position. The switching

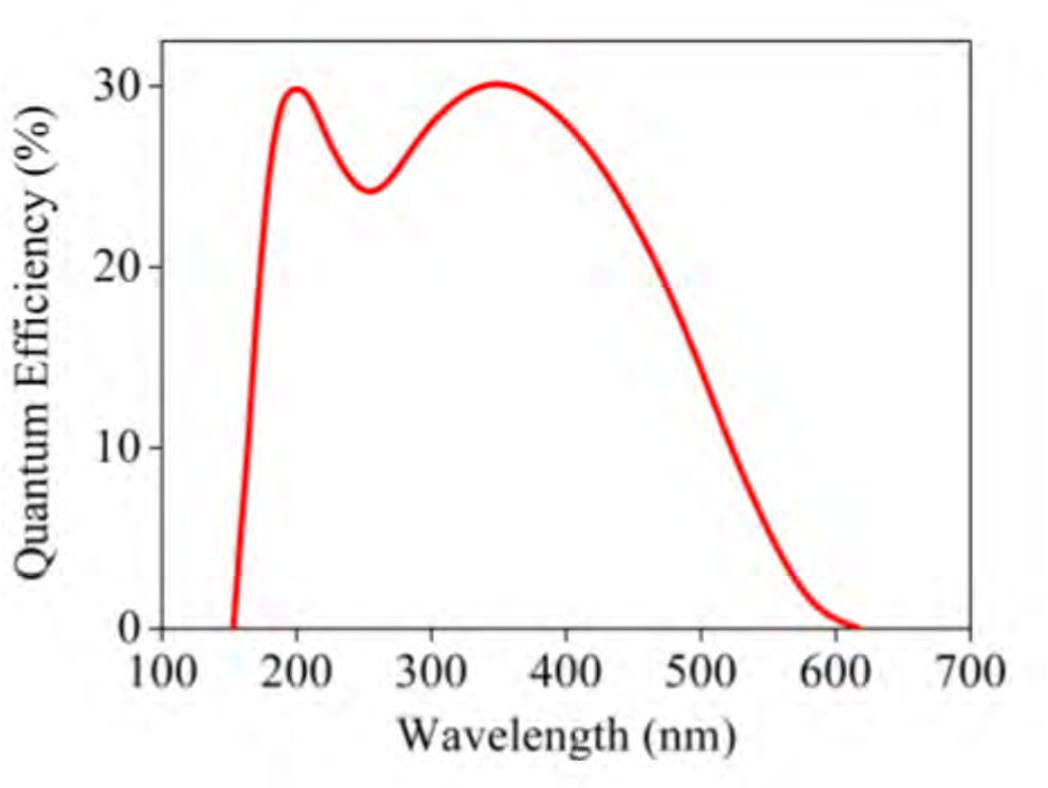

Figure 5.3: Quantum efficient of the EMI 9235QB photomultiplier tube as a function of the photon's wavelength (Technical University of Denmark, 2011)

of the LEDS is controlled by software and their power can be adjusted. Unless it is stated otherwise, the power of the stimulating light was set to 72 mW/cm^2 for measurements.

5.1.3 The irradiation source

Sample irradiation is done *in-situ* with a ^{90}Sr/^{90}Y beta-source. The beta particles emitted from the source have a maximum energy of 2.27 MeV. The activity of the beta source is about 1.48 GBq. The nominal dose rate is 0.1028 Gy/s. Before irradiation, the carousel is rotated to position the sample holder directly below the irradiation source. All irradiations were done at room temperature.

5.2 Samples and preparation

Samples used were trapezoidal shaped Al_2O_3:C.Mg of thickness 0.5 mm and side lengths 8 x 4 mm (Landauer, Inc; Oklahoma, USA) greenish in hue prior to any heat treatment with a mass of 0.060 g (Sob et al., 2021). An unannealed sample

and samples annealed at 700, 900 and 1200 °C for 15 minutes each were used. For each measurement, the sample was affixed to an aluminium disc with the aid of conductive grease and then placed at a given position on the carousel. Figure 5.4 shows the carousel with samples of α-Al_2O_3:C,Mg at positions 21, 28, 33 and 38 respectively. The unannealed sample is at position 28 whereas the samples at positions 33, 38 and 21 are annealed at 700, 900 and 1200°C for 15 minutes respectively. The colour of the sample at position 28 is evident.

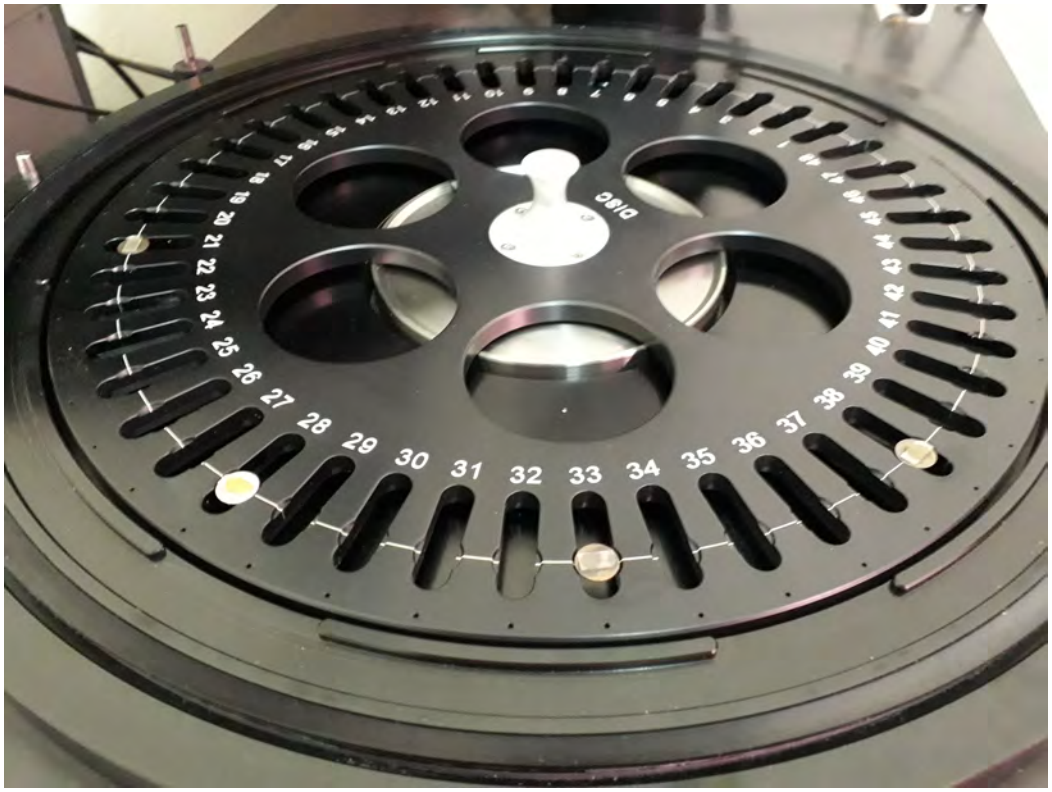

Figure 5.4: A picture of the carousel with samples of α-Al_2O_3:C,Mg at positions 21, 28, 33 and 38 respectively. The unannealed sample is at position 28 whereas the samples at positions 33, 38 and 21 are annealed at 700, 900 and 1200°C for 15 minutes respectively.

Chapter 6

Dosimetric features of α-Al_2O_3:C,Mg

α-Al_2O_3:C,Mg, just as α-Al_2O_3:C, is a material of great interest in radiation dosimetry. Some of the properties of a good dosimeter are a linear response over wide dose range, low fading, good reproducibility and non-toxicity. The dose response and the fading of α-Al_2O_3:C,Mg are reported in this chapter.

The properties of α-Al_2O_3:C have been widely studied (Akselrod et al., 1998; Yukihara and McKeever, 2006; Mishra et al., 2007; Ogundare et al., 2013; Chithambo et al., 2015). The high sensitivity of α-Al_2O_3:C is due to the presence within it of a high concentration of F and F^+-centres resulting from doping of α-Al_2O_3 by carbon (McKeever et al., 1995). The F-centre, the main luminescence centre in α-Al_2O_3:C, emits at 410 nm (Agulló-López et al., 1988) and has a lifetime of $\sim$35 ms at room temperature (Akselrod et al., 1998; Markey et al., 1995). Such a long lifetime limits the use of α-Al_2O_3:C for fast response applications such as 2-dimensional dose mapping and real-time optical fibre dosimetry (Rodriguez et al., 2011). On the other hand, in addition to large concentrations of F and F^+-centres (Akselrod et al., 2003c), co-doping of α-Al_2O_3 by C and Mg also promotes within it the creation of new luminescence centres thought to be F^+(Mg), F_2, F_2^+(2Mg) and F_2^{2+}(2Mg) (Sykora and Akselrod, 2010; Rodriguez et al., 2011; Eller et al., 2013). Using photoluminescence, Sykora and Akselrod (2010) attributed the emission bands at 325, 500, 750 and 510 nm to F^+(Mg), F_2, F_2^+(2Mg) and F_2^{2+}(2Mg)-centres respectively. The F_2^{2+}(2Mg) and F_2^+(2Mg) luminescence centres have a lifetime $<$ 100 ns (Akselrod et al., 2003b) thereby making α-Al_2O_3:C,Mg suitable for applications in fast dose response mapping and real-time optical fibre dosimetry (Ahmed et al., 2016). For α-Al_2O_3:C,Mg, it has been shown that the F^+ and F-centres are the main luminescence centres (Denis et al., 2011a,b; Rodrig-

uez et al., 2011; Chithambo et al., 2020). Denis et al. (2011a,b) found that the OSL emission from α-Al_2O_3:C,Mg is similar to that from α-Al_2O_3:C. Denis et al. (2011a,b) also found that the F^+-centre, characterised by the emission at 330 nm, is more intense in α-Al_2O_3:C,Mg than in α-Al_2O_3:C. It has been shown that the luminescence sensitivity of α-Al_2O_3:C is dependent on annealing temperature (Chithambo, 2004; Yukihara et al., 2004; Yukihara and McKeever, 2006). The depletion of deep electron traps in α-Al_2O_3:C with annealing at 900°C affects the luminescence sensitivity (Chithambo, 2004; Yukihara et al., 2004; Yukihara and McKeever, 2006). In the case of α-Al_2O_3:C,Mg, studies have shown that the F and F^+-centres remain stable up to 1200°C and that some centres such as F_2^{2+}(2Mg) are destroyed for annealing at or above 700°C (Akselrod et al., 2003b; Sykora and Akselrod, 2010). Annealing-induced changes of luminescence centres may affect the luminescence properties of the material. Kalita and Chithambo (2017d) found that TL and OSL sensitivity of α-Al_2O_3:C,Mg was affected by annealing and they attributed the change in sensitivity to the change in the concentration of the F_2^{2+}(2Mg) centre. Kalita and Chithambo (2018a) found that the influence of annealing on F^+ and F-centres emission bands became distinguishable only for dose higher than 10 Gy. Radioluminescence (RL) spectra of Al_2O_3:C,Mg have been studied (Rodriguez et al., 2011; Trindade and Jacobsohn, 2018; Chithambo et al., 2020). Chithambo et al. (2020) investigated the influence of measurement temperature and annealing on the F and F^+ emission in Al_2O_3:C,Mg. In their study, Chithambo et al. (2020) observed RL at 410 nm for the unannealed sample and at 330 and 410 nm for the sample annealed at 1200°C. For the annealed sample, they found that the emission at 330 nm was dominant (Chithambo et al., 2020). Chithambo et al. (2020) equally noted that the F_2^{2+}-centres, responsible for the emission at 520 nm (Rodriguez et al., 2011), were absent or indistinct and suggested that the increase in the concentration of F^+-centres could be due to endothermic dissolution of the F_2^{2+}-centre (Kalita and Chithambo, 2018a).

The dosimetric features of α-Al_2O_3:C,Mg are reported and discussed in this chapter for the conventional TL and PTTL peaks. One of the features studied is the influence of irradiation dose on peak position and peak intensity. The other is the fading of luminescence with delayed stimulation. Section 6.1 deals with the dosimetric features of conventional TL peaks whereas those of PTTL peaks are presented in section 6.2. The use of annealed and unnanealed samples provides a means of investigating the effect of annealing on the reported features. For ease of reference, the unannealed sample is referred to as sample A and the samples annealed at 700, 900 and 1200°C for 15 minutes each as samples B, C and D respectively. Section 6.3 summarises the results.

In order to study the dose dependence of glow peaks, glow curves were repeatedly measured on a sample freshly irradiated at room temperature each time to doses between 0.1 and 8.2 Gy. The sensitivity of the sample coupled with the experimental setup limit the range of doses to which the sample could be exposed without damaging the photomultiplier tube. Each sample was heated at 1°C/s to record a glow curve. The maximum temperature for TL measurements was 500°C. Preheating was used to adequately study higher temperature peaks (at 200°C or above). A 7.5 mm thick Hoya U-340 filter (transmission band 250-390 nm) was used for luminescence detection. In addition to this filter, a 1% absorptive neutral density filter (transmission band 370-800 nm) was also used to attenuate the luminescence intensity and to prevent damage to the photomultiplier tube.

6.1 Dosimetric features of conventional TL peaks

6.1.1 Glow curve structure of conventional TL peaks

Figures 6.1-6.4 show glow curves of samples A, B, C and D measured at 1°C/s after irradiation to 4 Gy each. Sample A (Figure 6.1) has peaks at 51, 86, 184, 220, 312 and 416°C respectively. Earlier measurements on sample A, such as those reported by Sob et al. (2021), revealed peaks at 43, 73, 195, ∼246, 284, ∼336 and 374°C respectively for a heating rate of 1°C/s and a dose of 2.0 Gy. The shift in peak position is an experimental artefact which can be ascribed to the use of a neutral density filter (Kalita and Chithambo, 2017a). For sample B (annealed at 700°C), the glow curves (Figure 6.2) have peaks at 54, 89, 117, 188, 224, 308, 390 and 420°C respectively. Figure 6.3 depicts peaks at 51, 85, 115, 183, 220, 260, 304, 404 for sample C (annealed at 900°C). The 260°C peak is not obvious from Figure 6.3. Its position is inferred from subsequent measurements. For sample D (annealed at 1200°C), as shown in Figure 6.4, the glow peaks are at 60, 90, 118, 191, 256, 310, 380 and 420°C respectively. The peaks of each sample are labelled I through VII. The peak at 117°C in sample B and at 115 and 118°C in samples C and D respectively is labeled IIa. This peak appeared at 100°C in glow curves of annealed samples measured without the neutral density filter. It has been reported to occur in samples annealed at 700°C or above (Kalita and Chithambo, 2017b, 2018a). Akselrod et al. (2003a) reported the disappearance of the absorption and emission bands corresponding to the F_2^{2+}(2Mg)-centre after annealing to 700 °C. Sykora and Akselrod (2010) equally showed that an emission band near 500 nm disappears after annealing to 700°C. This annealing-induced peak is not observed in α-Al_2O_3:C (Yukihara et al., 2004; Chithambo, 2004). This

led Kalita and Chithambo (2017b) to suggest that the peak was due to a new electron trap created after the destruction of the F_2^{2+}(2Mg)-centre. We equally noticed the loss of the yellowish-green colour of the sample following annealing at or above 700°C (see Figure 5.4) as reported by Kalita and Chithambo (2017b). Akselrod et al. (2003a) found that this yellowish-green colour of the sample is due to absorption at 435 nm by the F_2^{2+}(2Mg)-centre. It is noteworthy that peaks I and II of sample D appear after preheating to 250°C as seen in Figure 6.4b. This implies that some of the electrons stimulated from the traps corresponding to peaks IV-VII during preheating get retrapped at the electron traps of peaks I and II. The sample was not illuminated between preheating and heating so, the occurrence of these shallow peaks cannot be ascribed to phototransfer.

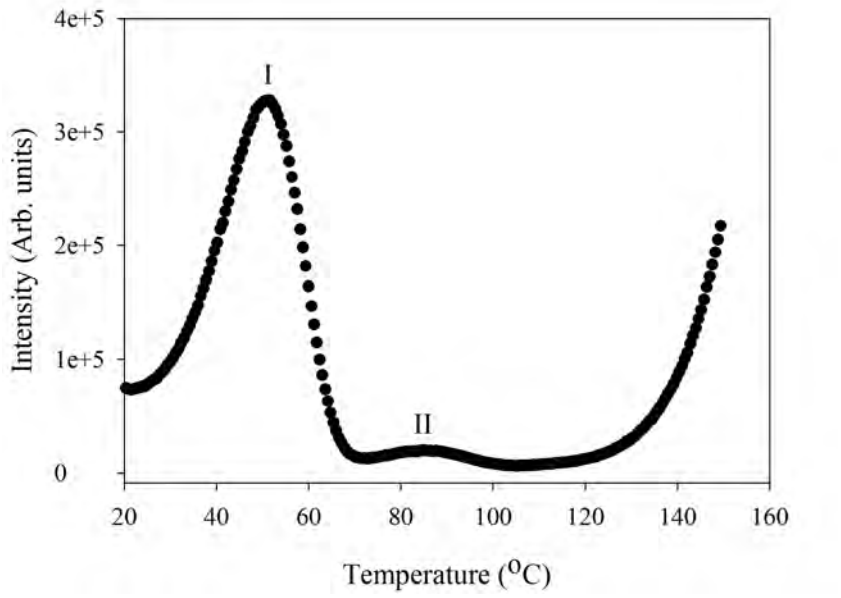

a

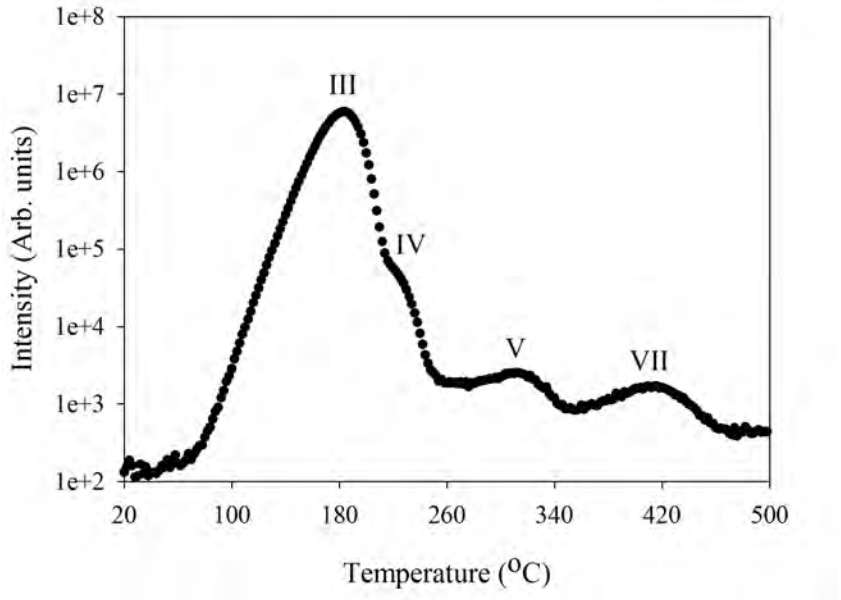

b

Figure 6.1: Glow curves of unannealed α-Al_2O_3:C,Mg (sample A) measured at 1°C/s after irradiation to 4 Gy. The plot in (a) shows peaks I and II whereas the plot in (b), which is obtained after preheating to 150°C, shows peaks III, IV, V and VII. Instead of measuring a single glow curve up to 500°C, the measurement was split for visual clarity of the higher temperature peaks.

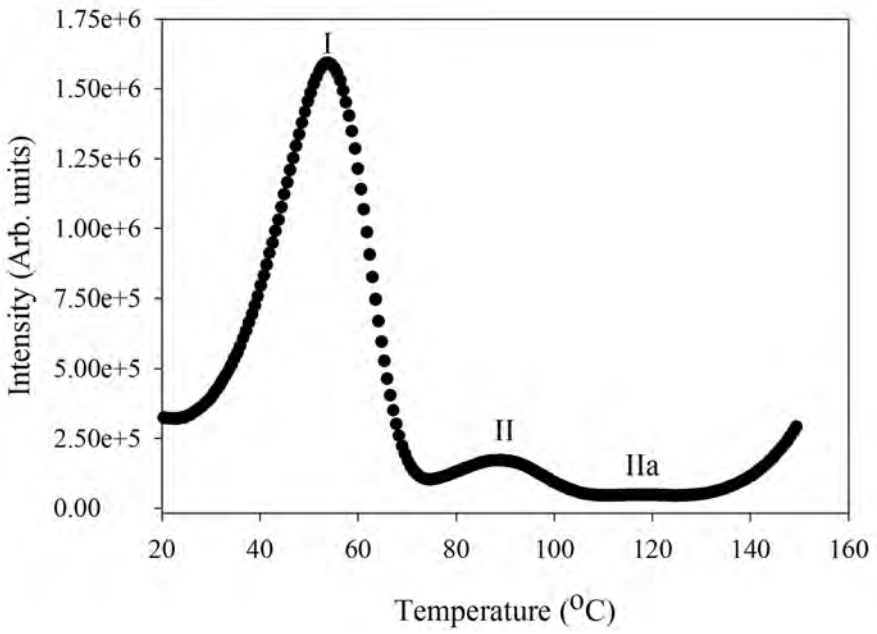

a

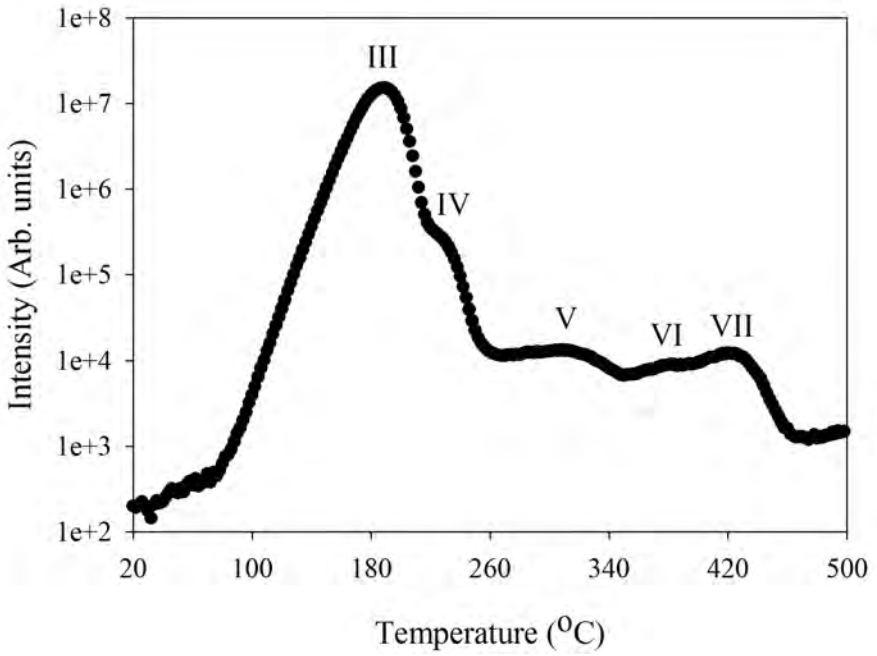

b

Figure 6.2: Glow curves of α-Al_2O_3:C,Mg annealed at 700°C (sample B) measured at 1°C/s after irradiation to 4 Gy. The plot in (a) shows peaks I, II and IIa whereas the plot in (b), which is recorded after preheating to 150°C, shows peaks III-VII.

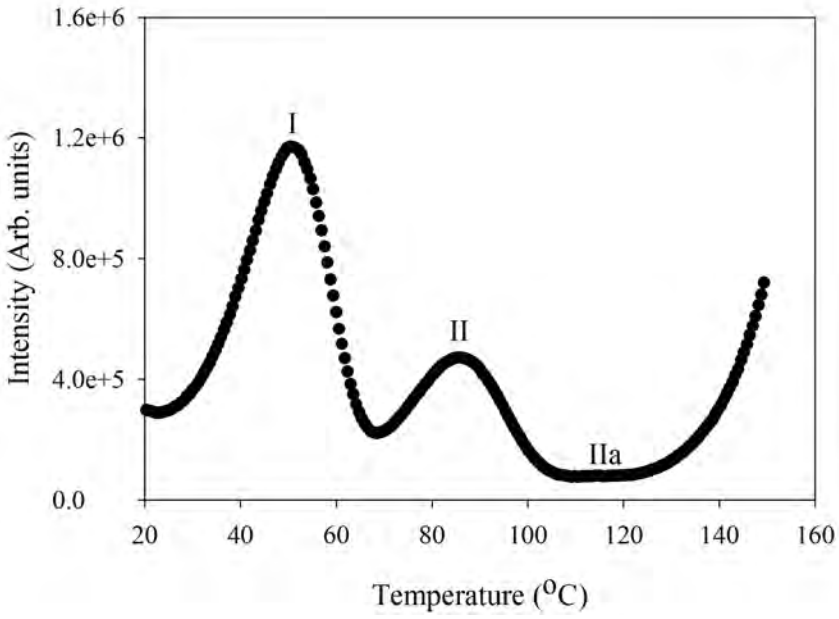

a

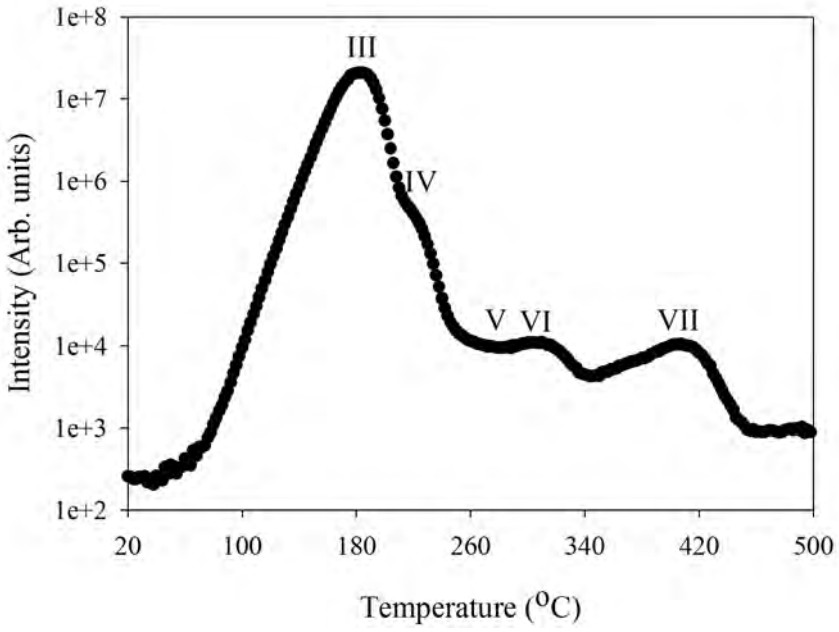

b

Figure 6.3: Glow curves of α-Al_2O_3:C,Mg annealed at 900°C (sample C) measured at 1°C/s after irradiation to 4 Gy. The plot in (a) shows peaks I, II and IIa whereas the plot in (b), recorded after preheating to 150°C, shows peaks III-VII.

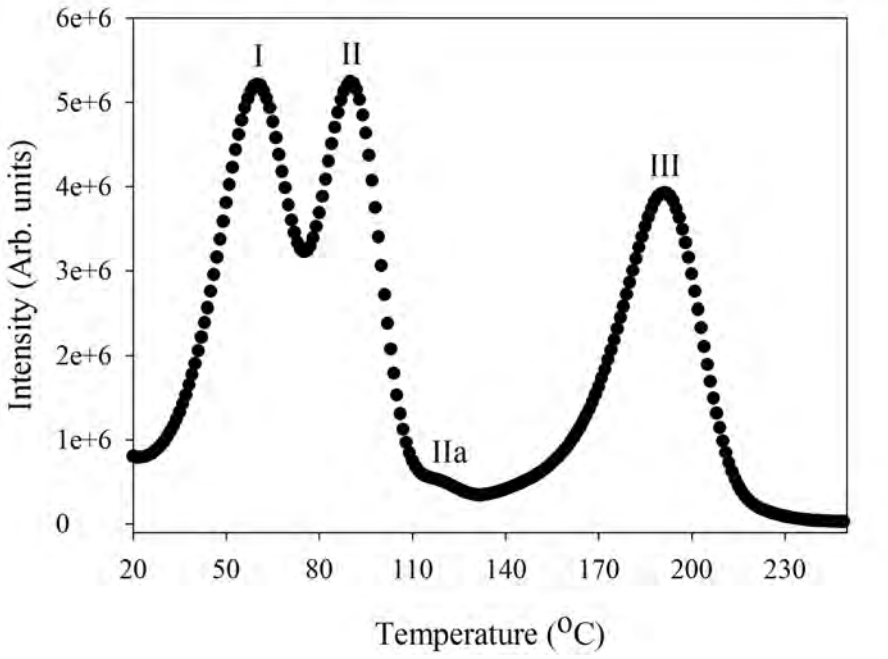

a

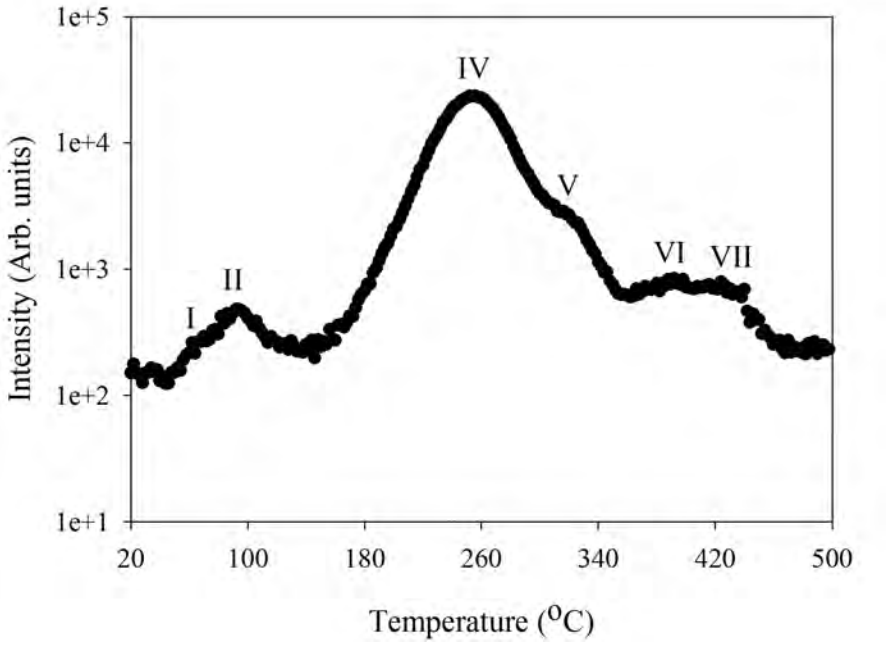

b

Figure 6.4: Glow curves of sample D (annealed at 1200°C) measured at 1°C/s after irradiation to 4 Gy. The glow curve in (a) is measured immediately after irradiation whereas the glow curve in (b) is measured after preheating to 250°C. Peaks I and II appear again after being removed by preheating.

6.1.2 Dose response of conventional TL peaks

The influence of irradiation dose on the position of a glow peak is one way of determining the order of kinetics of that peak (McKeever, 1985; Chen and McKeever, 1997). The position of a first-order peak is independent of dose whereas that of a second-order peak is not. To this effect, plots of peak position against irradiation dose are shown in Figure 6.5 for samples A, B, C and D respectively. Figure 6.5a shows that the position of each peak of sample A is independent of irradiation doses between 0.1 and 7.4 Gy. The results of Figure 6.5a imply that peaks of sample A follow first-order kinetics. Similar results were reported by Kalita and Chithambo (2017f) and by Trindade et al. (2020). Results consistent with first-order kinetics are also shown in Figures 6.5b and 6.5c as reported for samples annealed up to 900°C by Kalita and Chithambo (2017b). The dependence of peak temperature on irradiation dose is shown in Figure 6.5d for peaks I-V of sample D. These peaks also follow first-order kinetics. Peaks VI and VII are not shown because their positions could not be reliably determined. Kalita and Chithambo (2018b) found that all the peaks of sample D with the exception of peak I are first-order peaks.

Figure 6.6 shows the influence of irradiation dose on the intensity of peak I for samples A, B, C and D respectively. The intensity, measured here as peak heights, grows with irradiation dose. For a quantitative analysis of the dose response, we use a suitable arbitrary function. In this case, we write

$$S(x) = a(1 - e^{-bx}) \tag{6.1}$$

where $S(x)$ is the peak intensity corresponding to dose x; a (Arb. units) and b (Gy^{-1}) are positive constants. Given the function of equation (6.1), we compute the supralinearity and superlinearity indices. The supralinearity index is given by:

$$f(x) = \frac{S(x)}{x} \cdot \frac{x_1}{S(x_1)} \tag{6.2}$$

where x_1 is the normalisation dose. The superlinearity index is defined as

$$g(x) = \left[\frac{xS''(x)}{S'(x)}\right] + 1 \tag{6.3}$$

where S' and S'' are the first and second derivatives of the function S. The functions f and g are then used to describe the effect of irradiation dose on the peak intensity (Chen and McKeever, 1997; Pagonis et al., 2006). The dose response is sublinear if $g(x) < 1$ or $f(x) < 1$. For a linear response, $g(x) = 1$ whereas a superlinear response corresponds to $g(x) > 1$. Similarly, a supralinear behaviour is observed when $f(x) > 1$.

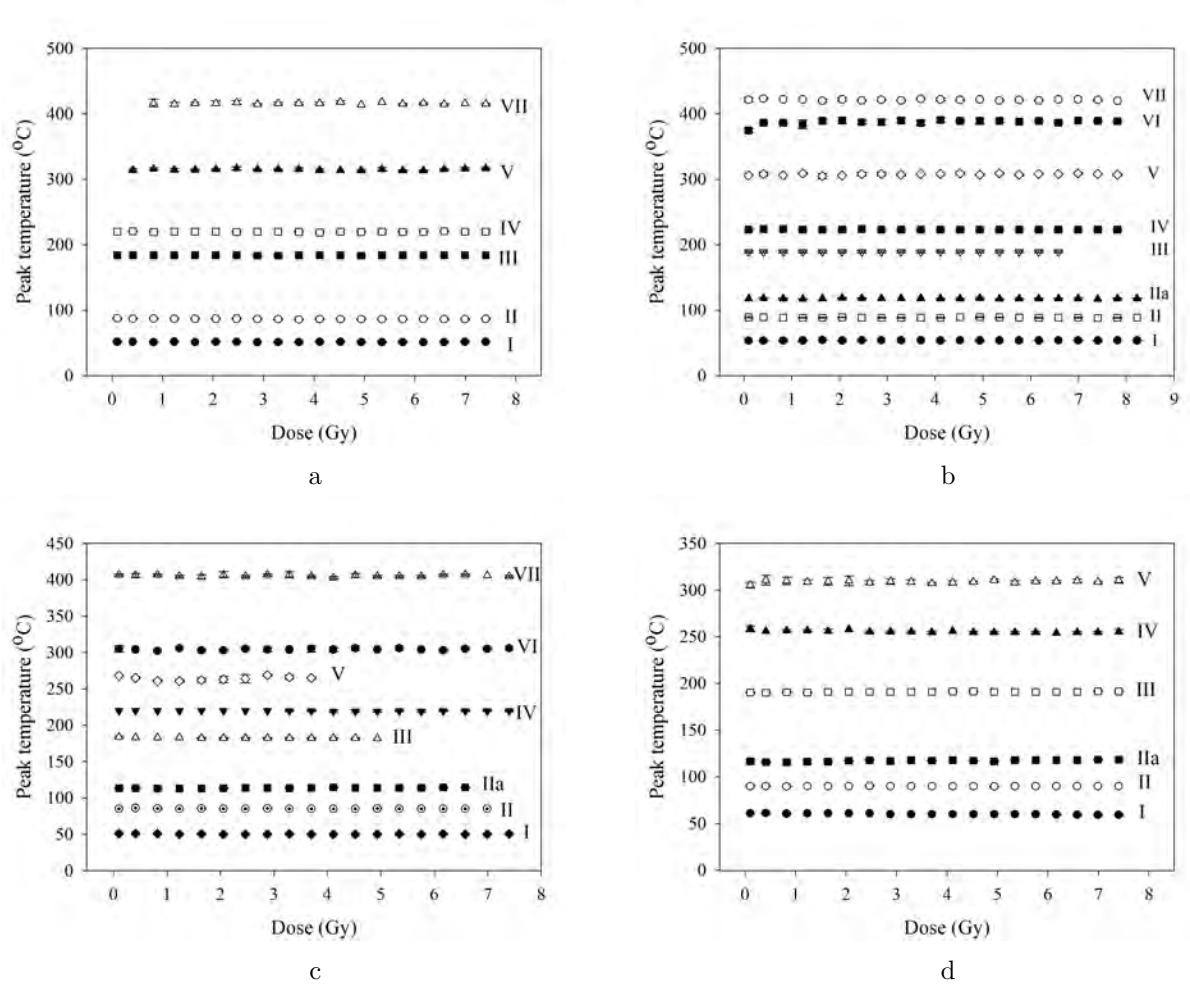

Figure 6.5: Influence of irradiation dose on peak temperature for (a) sample A, (b) sample B, (c) sample C and (d) sample D respectively.

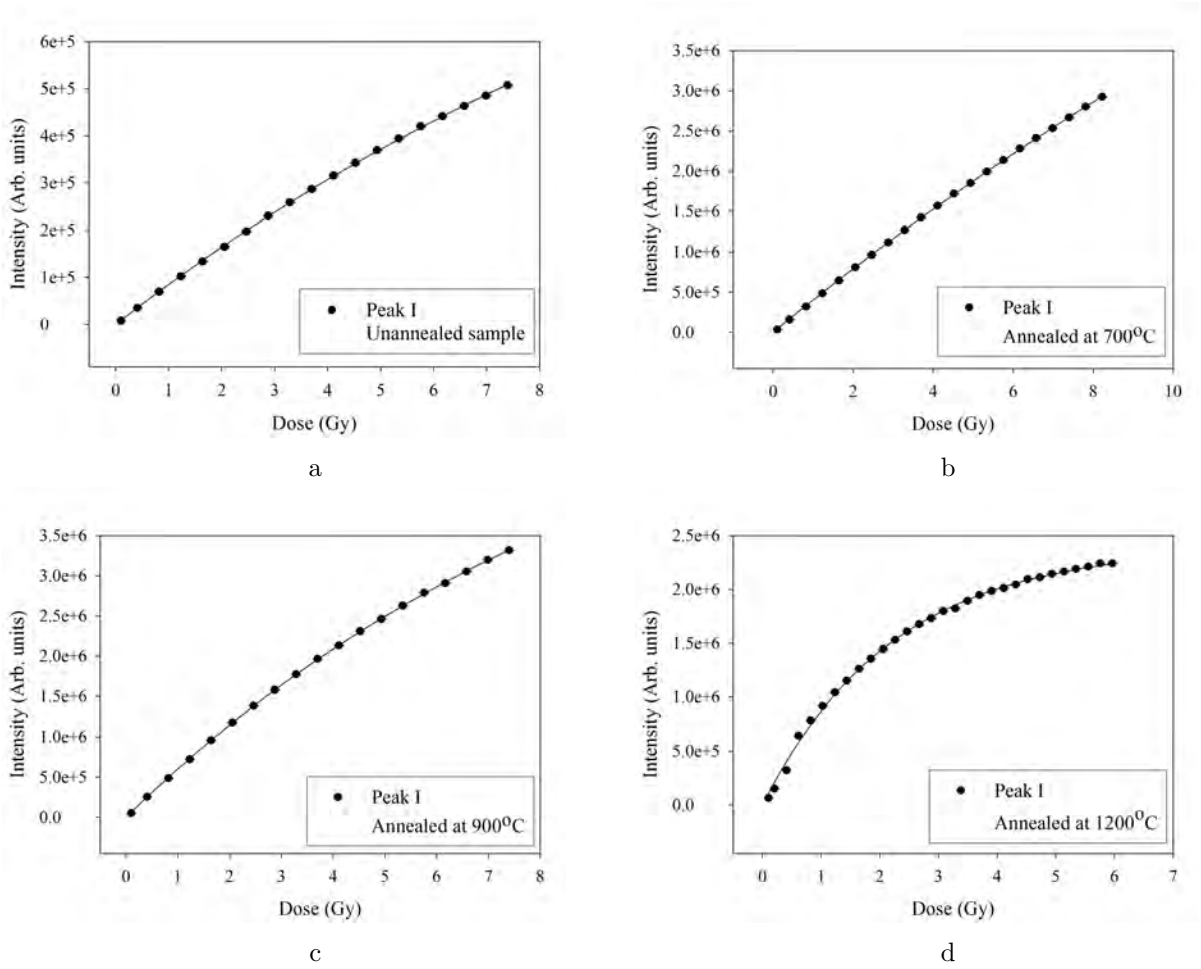

Figure 6.6: Intensity against irradiation dose for peak I of (a) sample A, (b) sample B, (c) sample C and (d) sample D. The solid line in each case is a fit of equation (6.1).

Figure 6.7 shows plots of the supralinearity index f and of the superlinearity index g as functions of irradiation dose for peak I of sample A. The supralinearity index f decreases from 1.00 to 0.78 while the superlinearity index decreases from 0.99 to 0.49 within the same dose range. These results show that the dose response of peak I of sample A is sublinear within 0.1-7.4 Gy. Kalita and Chithambo (2017g) also showed that the dose response of peak I of unannealed α-Al_2O_3:C,Mg is sublinear.

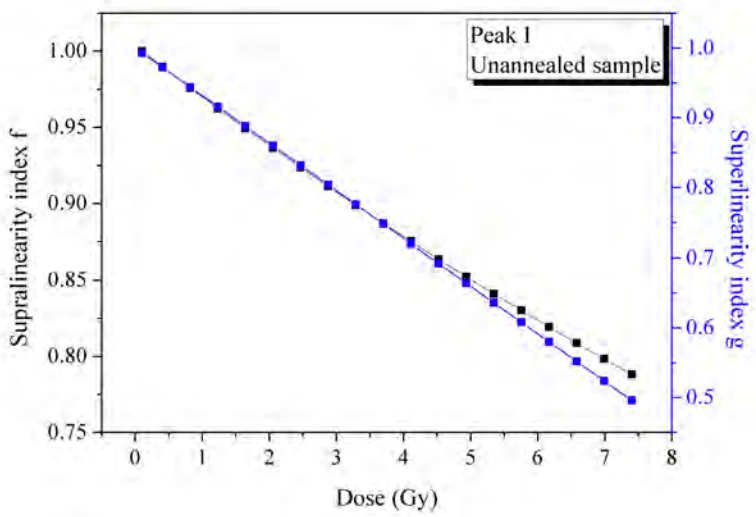

Figure 6.7: Supralinearity index f and superlinearity index g against irradiation dose for peak I.

Using the same analysis, we found that the dose response of peak I of sample B is sublinear for irradiation doses between 0.1 and 8.1 Gy. Similarly for samples C and D, the dose response of peak I is sublinear within 0.1-7.4 Gy. We note that for the dose range used, the response of peak I is sublinear irrespective of annealing temperature.

Figure 6.8 shows the influence of irradiation dose on the intensity of peak II of samples A, B, C and D respectively. For each of these samples, the peak intensity grows monotonically with irradiation dose. The response of peak II of sample A is described by the function

$$S(x) = a(1 - e^{-bx}) + cxe^{-bx} \tag{6.4}$$

where a, b and c are fitting parameters. For peak II of sample B, the dose response

is fitted with the expression

$$y = ax^c \tag{6.5}$$

where a (Arb.units/Gy) and c are positive constants. For samples C and D, the response of peak II is fitted with equation (6.1).

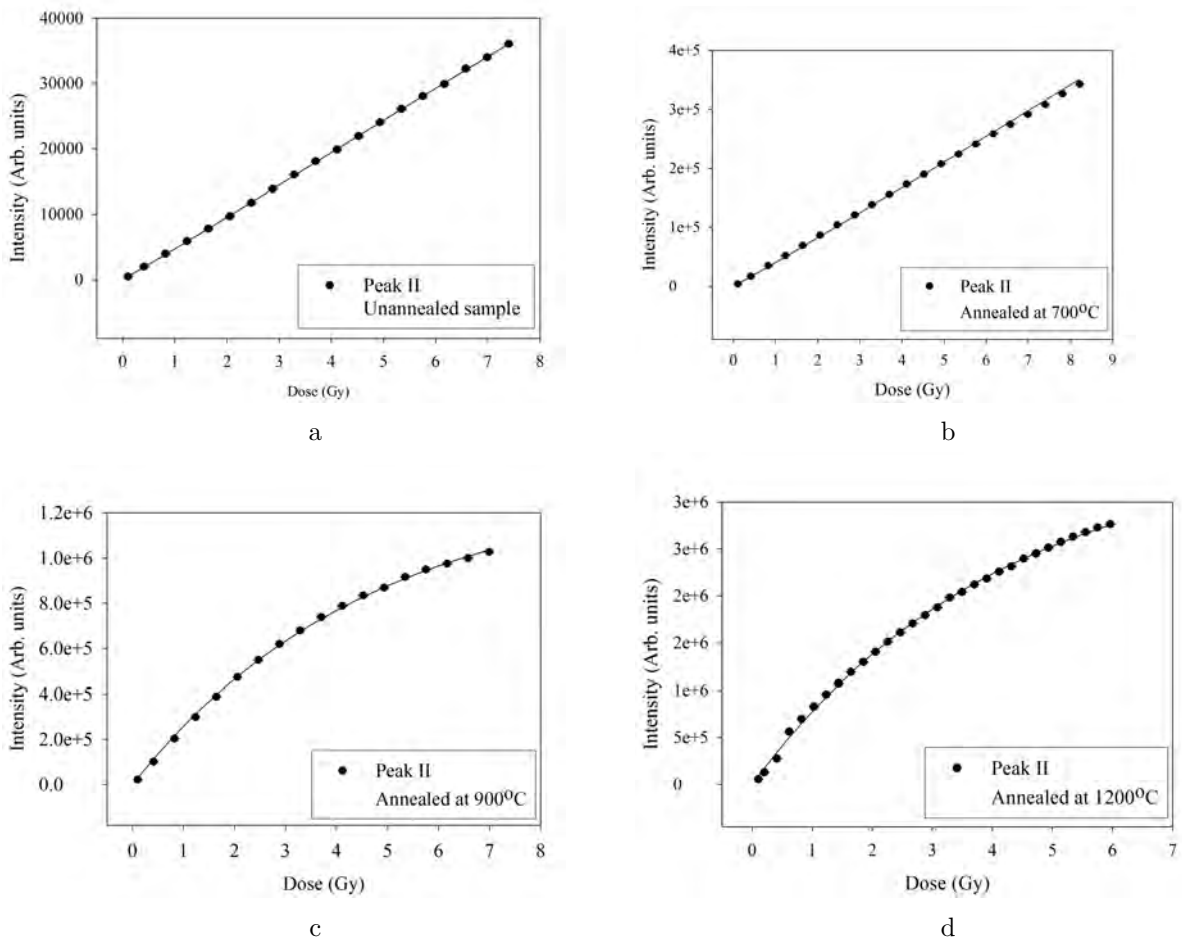

Figure 6.8: Dependence of TL intensity on irradiation dose for peak II of (a) sample A, (b) sample B, (c) sample C and (d) sample D. For sample A, the solid line is a best fit of equation (6.4). In (b) it is a best fit of equation (6.5) and in (c) and (d), the lines are best fits of equation (6.1).

The supralinearity and the superlinearity indices for peak II of sample A as functions of dose are shown in Figure 6.9.

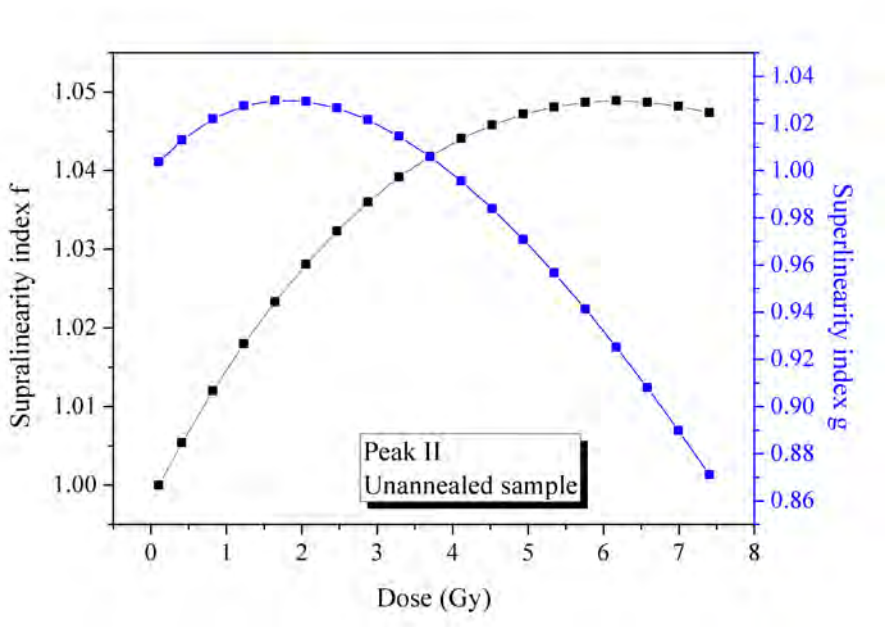

Figure 6.9: Supralinearity index f and superlinearity index g against irradiation dose for peak II.

The supralinearity index, f, of peak II of sample A increases from 1.00 to 1.05 with irradiation doses from 0.1 to 7.0 Gy and then decreases slightly thereafter. On the other hand, the superlinearity index g remains greater than 1.00 for doses up to 4.0 Gy and then decreases monotonically thereafter to 0.87. Hence, according to the superlinearity index g, peak II of sample A is superlinear with irradiation doses up to 4.0 Gy and then sublinear thereafter with irradiation doses up to 7.4 Gy. This result is in agreement with that of Kalita and Chithambo (2017g) on the response of peak II of unannealed α-Al_2O_3:C,Mg for doses up to 10 Gy. Using the same method as before, it was found that the dose response of peak II of sample B is linear for doses between 0.1 and 8.2 Gy. For sample C (Figure 6.8c), the analysis of the superlinearity index g shows that the dose response of peak II is sublinear within 0.1-7.1 Gy. This is equally the case for peak II of sample D (Figure 6.8d) for doses up to 6.1 Gy.

The influence of irradiation dose on the intensity of peak IIa for samples B, C and D is shown in Figure 6.10. For each of these samples, the intensity of peak IIa grows with dose. For sample B, the peak response is fitted with equation (6.5). Its superlinearity index g is constant at $\sim$1.00 within margin of error. This implies that peak IIa of sample B is essentially linear within 0.1 - 8.2 Gy. The response

of peak IIa of sample C is fitted with equation (6.1) and it is sublinear for doses between 0.1 and 6.5 Gy. Similarly, for sample D, the dose response of peak IIa is sublinear within 0.1-6.1 Gy.

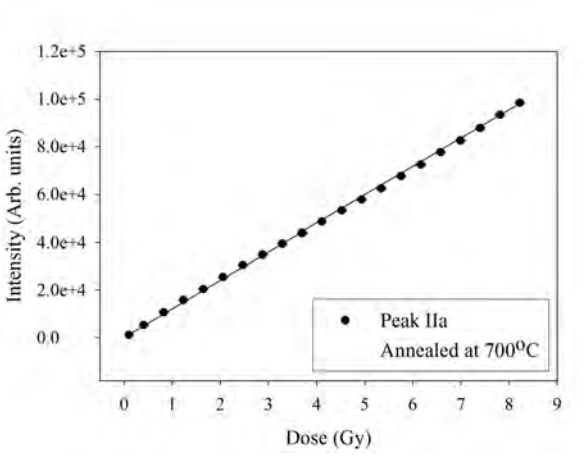

a

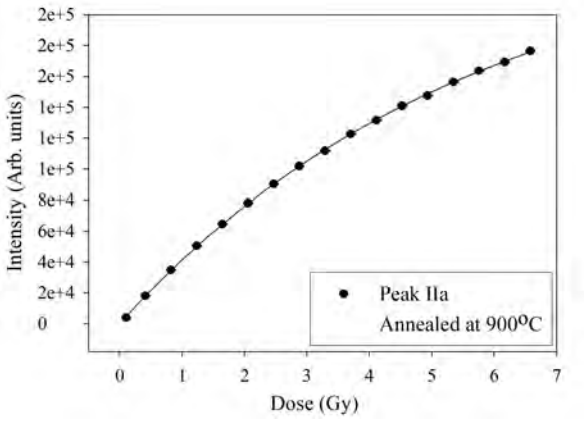

b

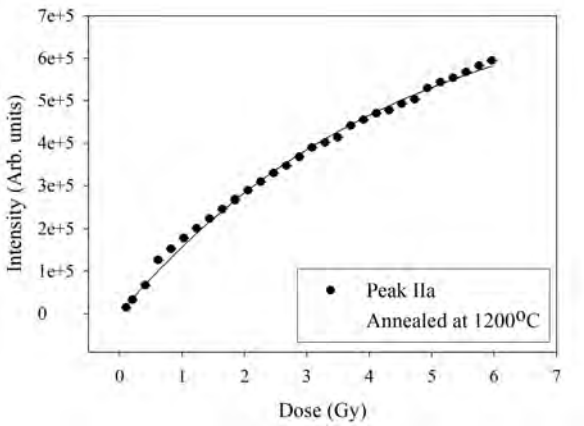

c

Figure 6.10: Effect of irradiation dose on the intensity of peak IIa of (a) sample B, (b) sample C and (c) sample D. In (a) the response is fitted with equation (6.5) whereas in (b) and (c), it is fitted with equation (6.1).

The influence of irradiation dose on the intensity of peak III is shown in Figure 6.11 for samples A, B, C and D respectively. For sample A (Figure 6.11a), the peak intensity increases continuously with irradiation dose and is best approximated with the expression

$$S(x) = y_0 + ax + bx^2, \tag{6.6}$$

where y_0, a and b are constants. The same method of analysis described earlier shows that the dose response of peak III of sample A is superlinear for doses from 0.1 to 7.4 Gy.

The intensity of peak III of sample B (Figure 6.11b) increases with dose up to 5.5 Gy. Its response, fitted with equation (6.5), is linear with dose up to 5.0 Gy. For sample C, the intensity of peak III also grows with dose up to 4.8 Gy. The solid line through the data of this peak is a fit of equation (6.1) and the dose response is sublinear. For peak III of sample D (Figure 6.11d), the data shows a trend towards saturation for doses above 2.0 Gy.

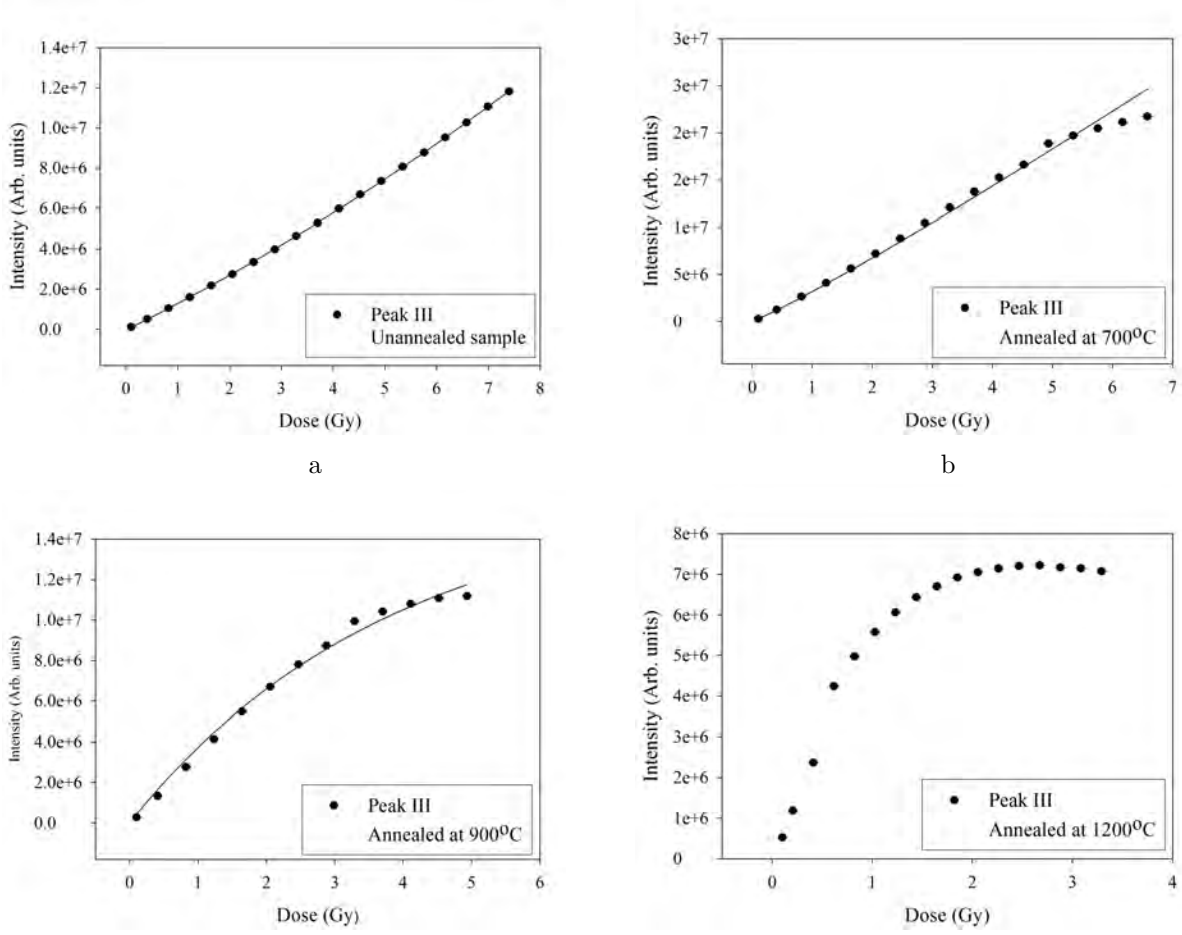

Figure 6.11: Dependence of intensity on irradiation dose for peak III of (a) sample A, (b) sample B, (c) sample C and (d) sample D.

Figure 6.12 shows the growth of intensity against irradiation dose for peak IV of samples A, B and D. The dose response of the peak for each of these samples is best approximated by equation (6.1). The analysis of superlinearity and supralinearity indices show that peak IV of sample A is sublinear up to 7.4 Gy whereas for samples B and D, the corresponding peaks are sublinear up to 7.9 and 6.1 Gy respectively.

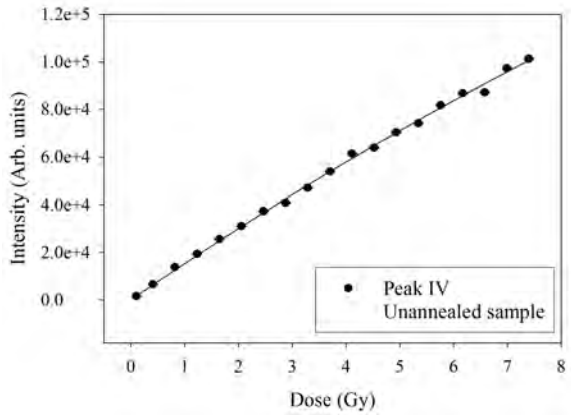

a

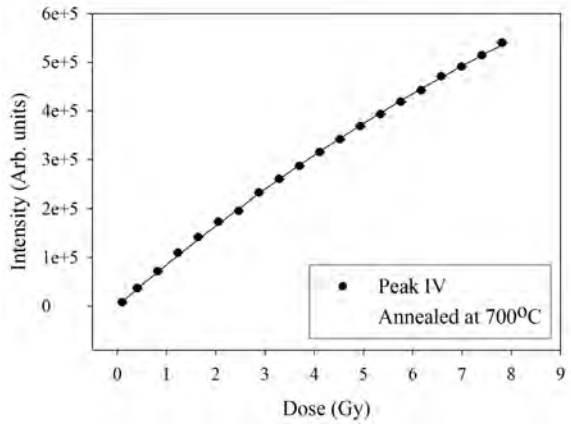

b

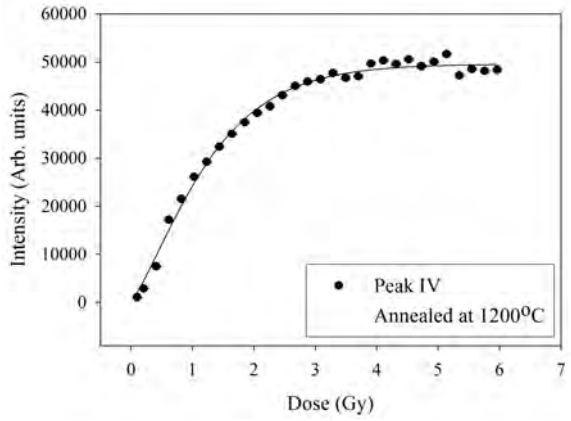

c

Figure 6.12: Intensity of peak IV against irradiation dose for (a) sample A, (b) sample B and (c) sample D. For each of these sample, the dose response is fitted with equation (6.1).

The intensity of peak V against irradiation dose is shown in Figure 6.13 for samples A, B, C and D. Peak V of sample A increases with irradiation doses from 0.1 to 7.4 Gy as shown in Figure 6.13a. Its dose response is best described by equation (6.6) and the same analysis used earlier shows that this peak is superlinear with irradiation doses from 0.1 to 7.4 Gy.

Figure 6.13b shows that the intensity of peak V of sample B increases with irradiation dose between 0.1 and 7.9 Gy. The response is best fitted with equation (6.5) and it is linear. For sample C the same analysis shows that the corresponding peak is sublinear up to 3.7 Gy whereas for sample D, the dose response of the peak is sublinear within 0.1-6.1 Gy.

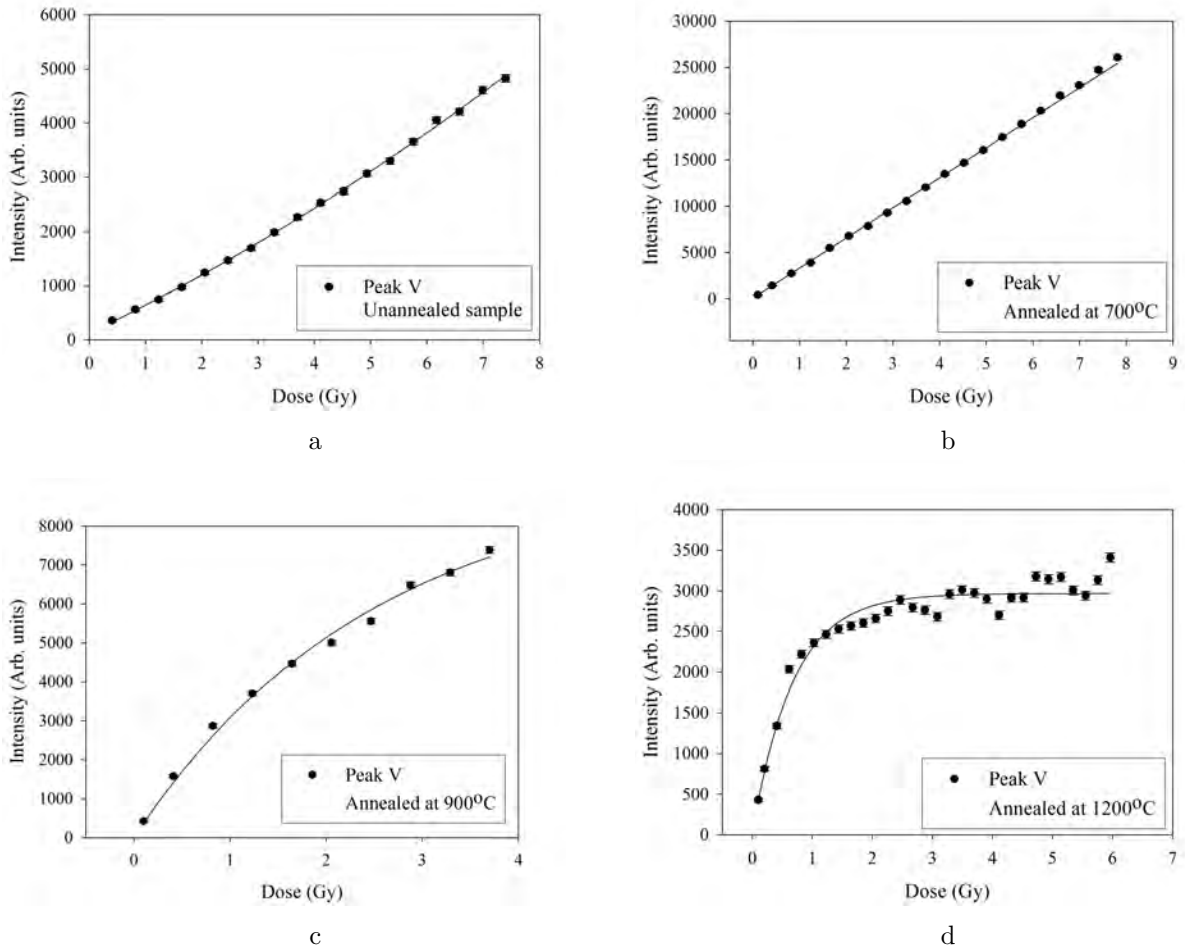

Figure 6.13: Influence of irradiation dose on the intensity of peak V for (a) sample A, (b) sample B, (c) sample C and (d) sample D.

The dependence of intensity on irradiation dose is shown in Figure 6.14 for peak VI of sample B. Its intensity increases monotonically with irradiation dose. A fit of equation (6.5) is also shown. The data shows a linear growth with dose up to 6.0

Gy. The response of this peak could not be studied for the other samples.

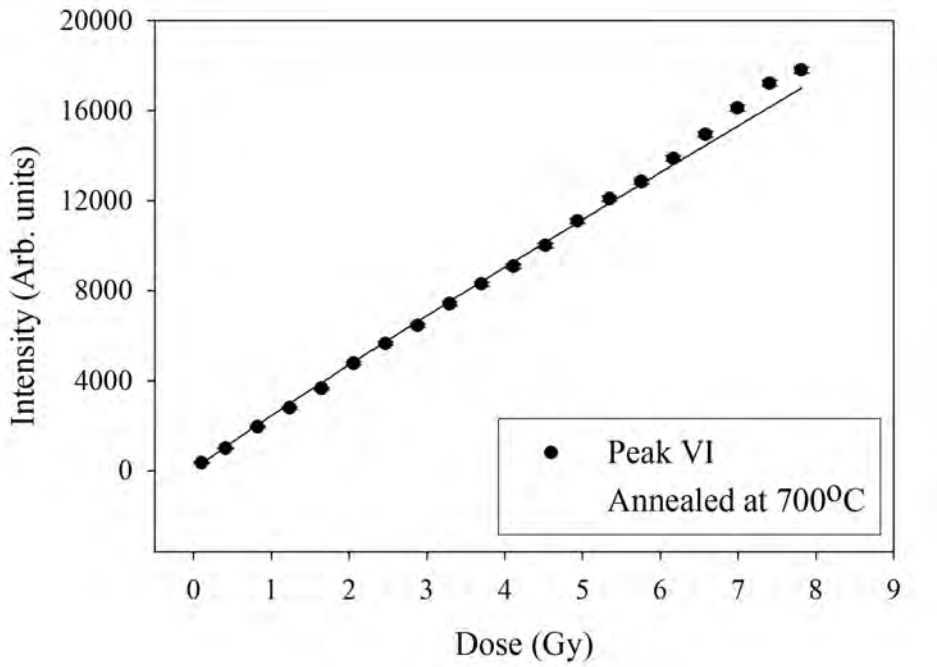

Figure 6.14: Dependence of irradiation dose on the intensity of peak VI of sample B. The solid line is a fit of equation (6.5).

Figure 6.15 shows the intensity of peak VII with irradiation dose for samples A, B and C each fitted with equation (6.5). For each sample, the intensity of peak VII grows with dose. Using the same analysis as before, we find that peak VII of sample A is superlinear within 0.1-7.4 Gy. For samples B and C, the response of peak VII is linear with doses up to 6.0 and 7.4 Gy respectively.

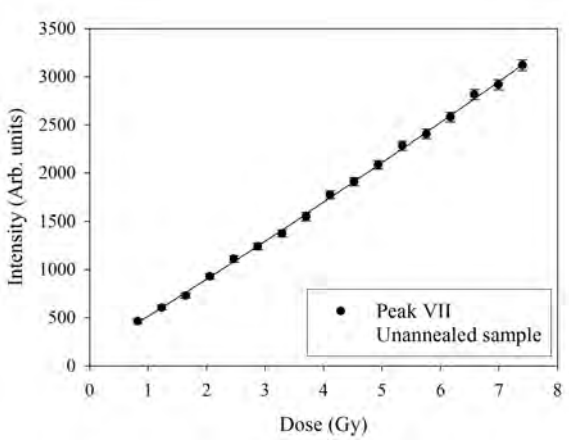

a

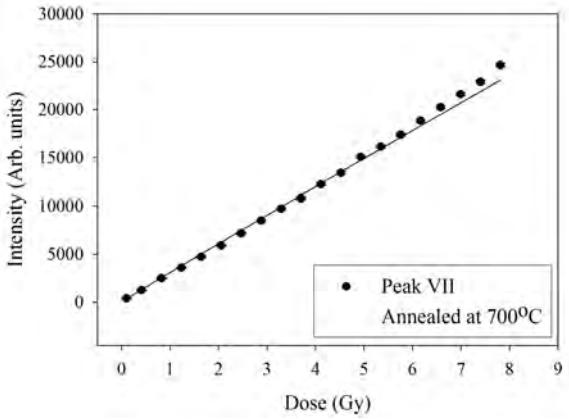

b

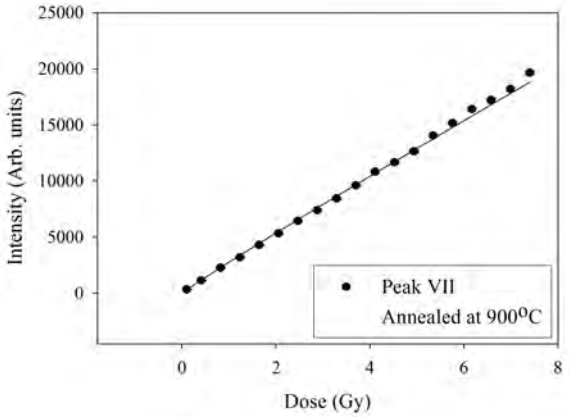

c

Figure 6.15: Dependence of intensity on irradiation dose for peak VII of (a) sample A, (b) sample B and (c) sample C. For each sample, the peak response is fitted with equation (6.5).

6.2 Dosimetric features of phototransferred TL peaks

6.2.1 PTTL glow curve structure

Figure 6.16 shows glow curves of samples A, B, C and D each measured after irradiation to 4 Gy, preheating to 120°C and illumination for 10 s. Preheating to 120°C is intented to remove peaks I, II and IIa of each sample. Peaks A1 and A2 in Figure 6.16a are the PTTL peaks corresponding to peaks I and II respectively. Peak A1 appears at 54°C whereas peak A2 occurs at 90°C. Figure 6.16a also shows peaks III, IV, VI and VII which are not removed after preheating to 120°C.

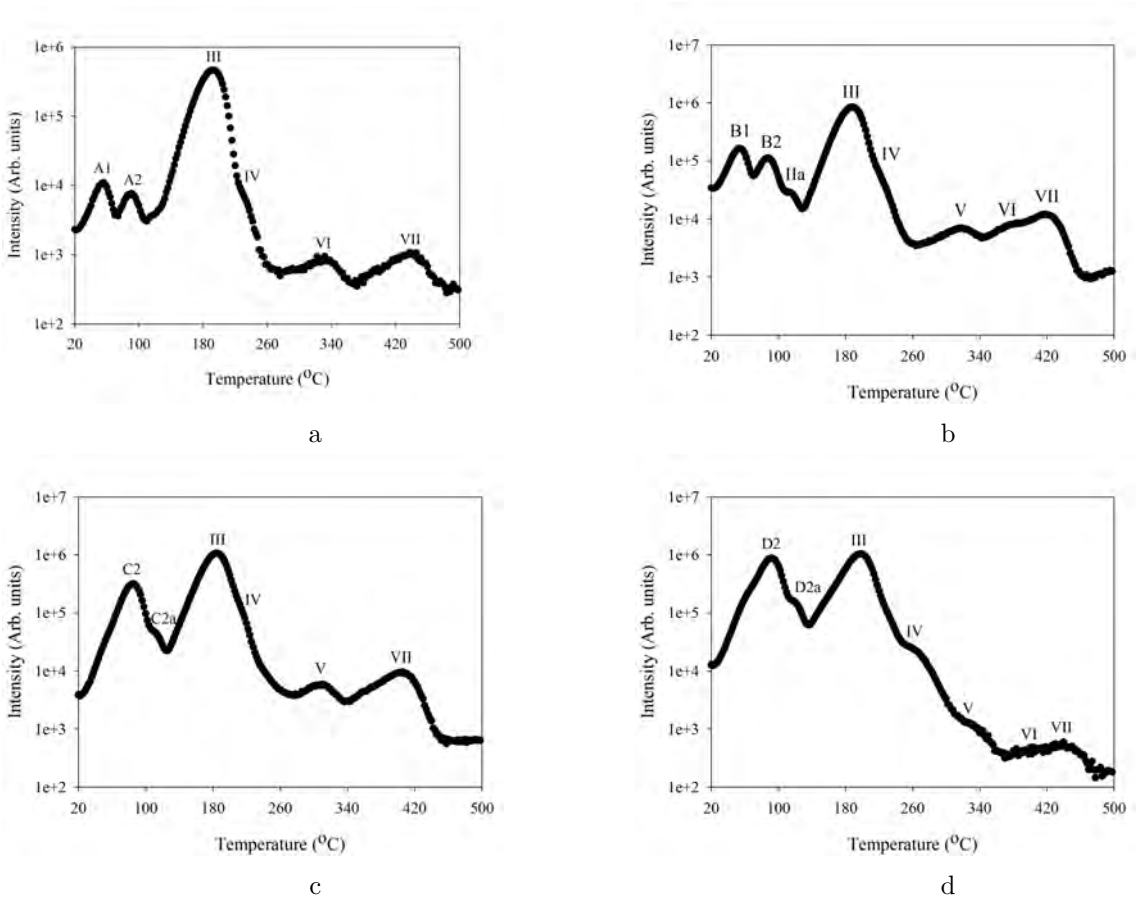

Figure 6.16: Glow curves of α-Al_2O_3:C,Mg measured at 1°C/s after irradiation to 4.1 Gy, preheating to 120°C and illumination for 10 s. Peaks A1, A2, B1, B2, C2, C2a, D2 and D2a are due to phototransfer.

Figure 6.16b is a glow curve measured under the same experimental conditions for sample B. The glow peaks B1 at 54°C, B2 at 88°C and B2a at 113°C are due to phototransfer. Similar glow curves are shown in Figures 6.16c and 6.16d for samples

C and D. Peaks II and IIa of sample C are reproduced under phototransfer as peaks C2 and C2a at 88 and 113°C respectively. For sample D, the PTTL peaks are D2 at 92°C and D2a at 116°C.

Glow curves of samples B, C and D each recorded under the same experimental conditions with the exception of a 200°C preheat are shown in Figure 6.17. Preheating to 200°C removes peaks I-III of each sample. Following this preheat, peaks I-III of each sample are reproduced under phototransfer. Peaks B3 and C3 each occur at 189°C whereas peak D3 appears at 196°C.

In summary, although each sample has multiple peaks, only peaks I-III are reproduced under phototransfer. Peak IV of sample D is also reproduced under phototransfer as shown later in the text.

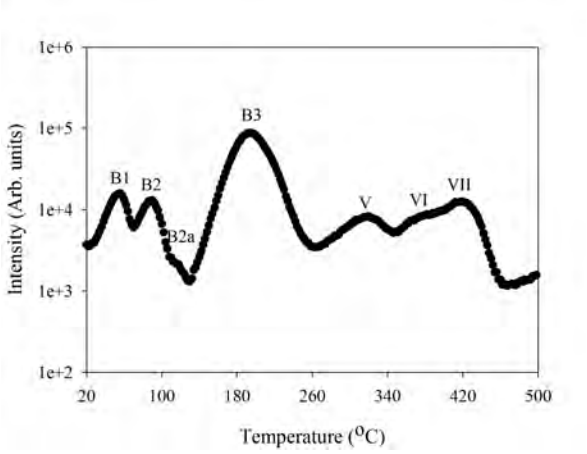

a

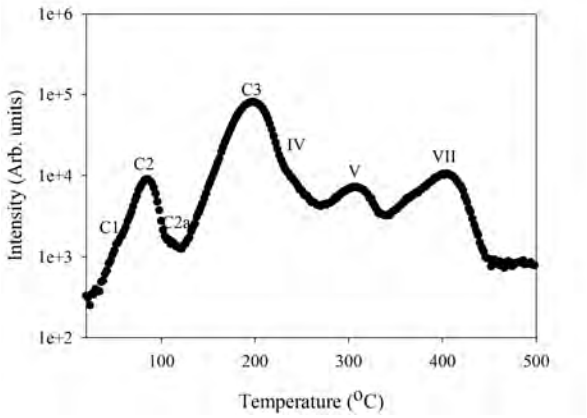

b

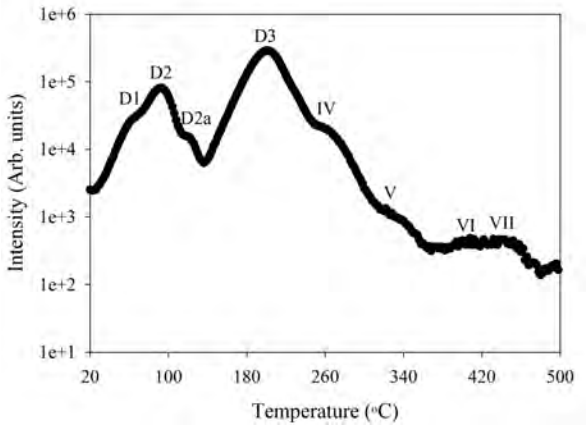

c

Figure 6.17: Glow curves of α-Al_2O_3:C,Mg measured at 1°C/s after irradiation to 4 Gy, preheating to 200°C and illumination for 10 s. Peaks I-III of each sample are reproduced under phototransfer.

6.2.2 Dose response of PTTL peaks

6.2.2.1 Dependence of peak position on dose

This section reports and discusses the dose response of phototransferred peaks of samples A, B, C and D respectively. The dependence of peak position on irradiation dose for the PTTL peaks of these samples is shown in Figure 6.18 for preheating to 120°C and in Figure 6.19 for preheating to 200°C. Figure 6.18a shows the positions of peaks A1, A2, III, VI and VII against irradiation dose. It is observed that peaks A1 and A2 are independent of irradiation dose. Hence, they follow first-order kinetics as do the corresponding conventional peaks.

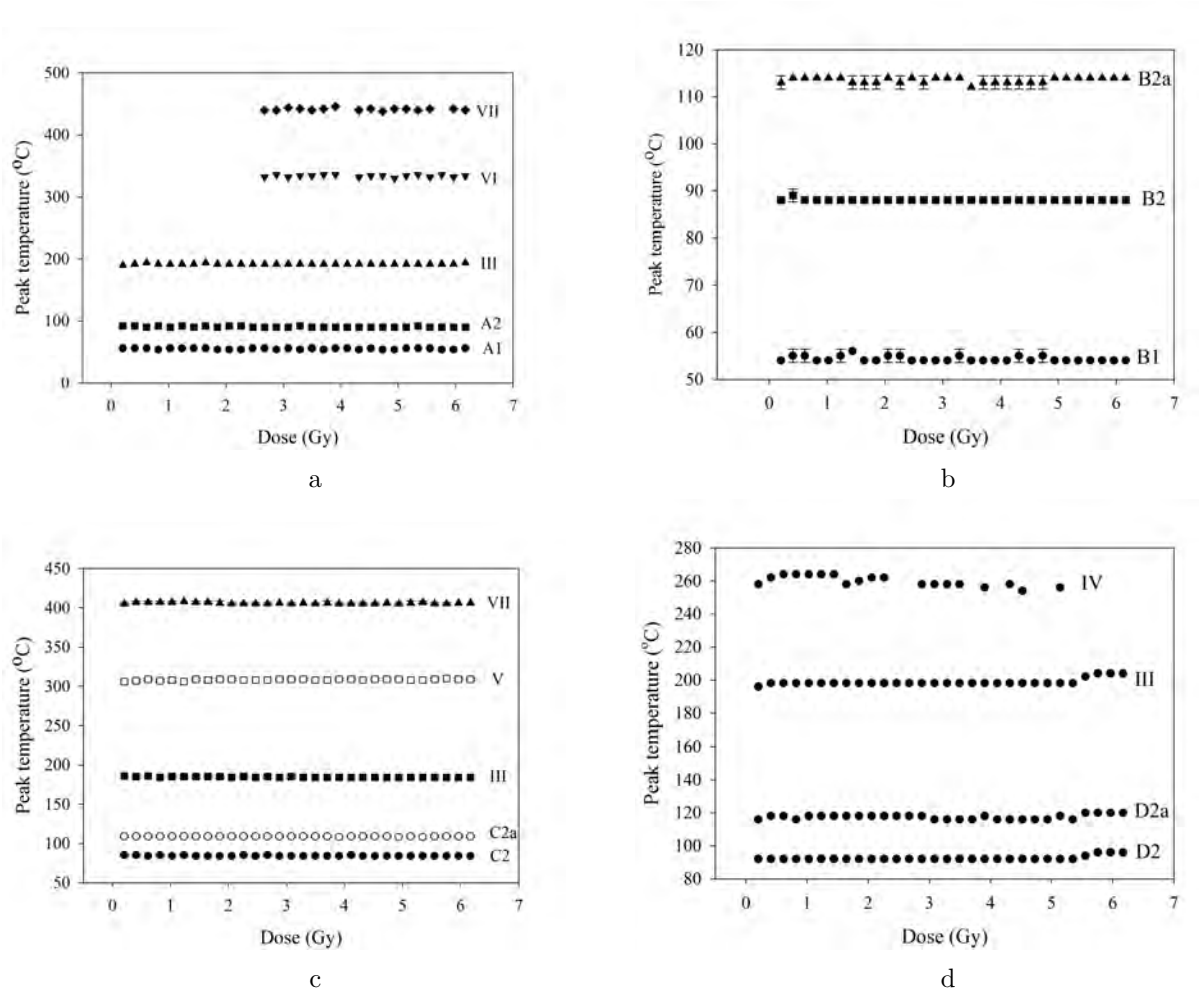

Figure 6.18: Dependence of peak position on irradiation dose for peaks of (a) sample A, (b) sample B, (c) sample C and (d) sample D. Peaks A1, A2, C2, C2a, D2 and D2a are due each due to phototransfer after preheating to 120°C and illumination for 10 s.

Figure 6.18b shows that the positions of peaks B1, B2 and B2a are each independent of irradiation dose. Similar results are shown in Figure 6.19a for peaks B1, B2, B2a and B3 respectively following preheating to 200°C. These results are characteristic of first-order glow peaks. The dependence of peak position on irradiation dose is shown in Figures 6.18c and 6.19b for sample C. The positions of peaks C2, C2a and C3 are independent of irradiation dose showing that these are first-order glow peaks just as their conventional counterparts. The dependence of peak position on irradiation dose for D2, D2a and D3 is shown in Figures 6.18d and 6.19c. Just as their conventional counterparts, peaks D2, D2a and D3 are independent of irradiation dose, and can therefore be categorised as first-order glow peaks. Kalita and Chithambo (2019) studied the dosimetric features of the phototransferred peaks of α-Al_2O_3:C,Mg annealed at 1200°C and found that the phototransferred peaks corresponding to peaks I, II, IIa and III of their sample were reproduced at the same positions. Kalita and Chithambo (2019) also concluded that these peaks follow the same kinetics as their conventional counterparts.

In summary, all phototransferred glow peaks follow first-order kinetics.

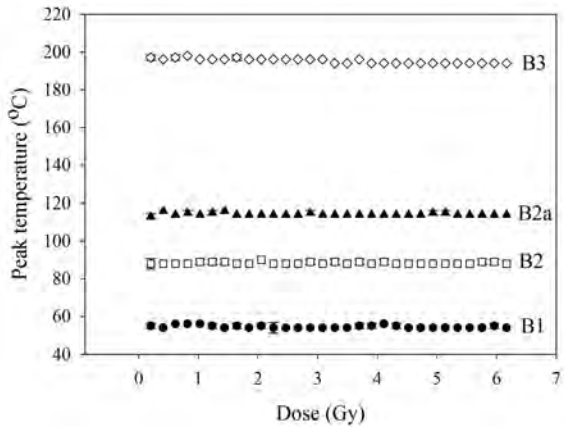

a

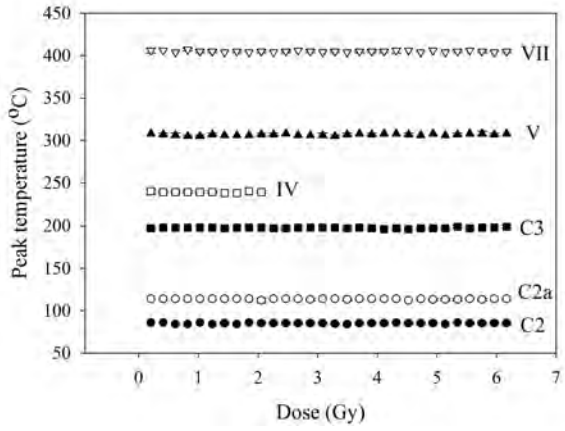

b

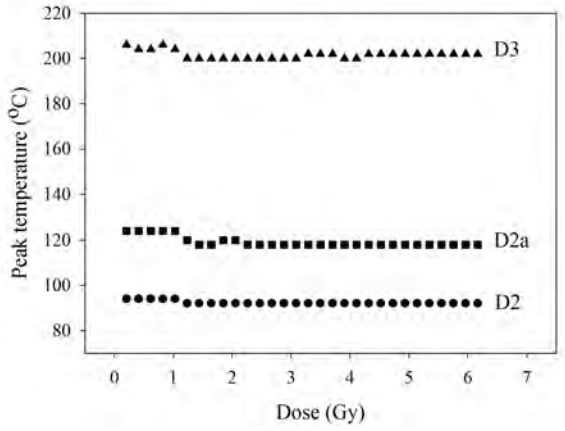

c

Figure 6.19: Dependence of peak position on irradiation dose for (a) sample B, (b) sample C and (c) sample D. The PTTL peaks of each sample are due to phototransfer after preheating to 200°C and illumination for 10 s.

Figure 6.20 shows the dependence of intensity on irradiation doses between 0.2 and 6.1 Gy for peaks A1 and B1. For each of these two peaks, the intensity grows with dose. The response of peak A1 is best approximated with equation (6.4) whereas that of peak B1 is fitted with equation (6.1).

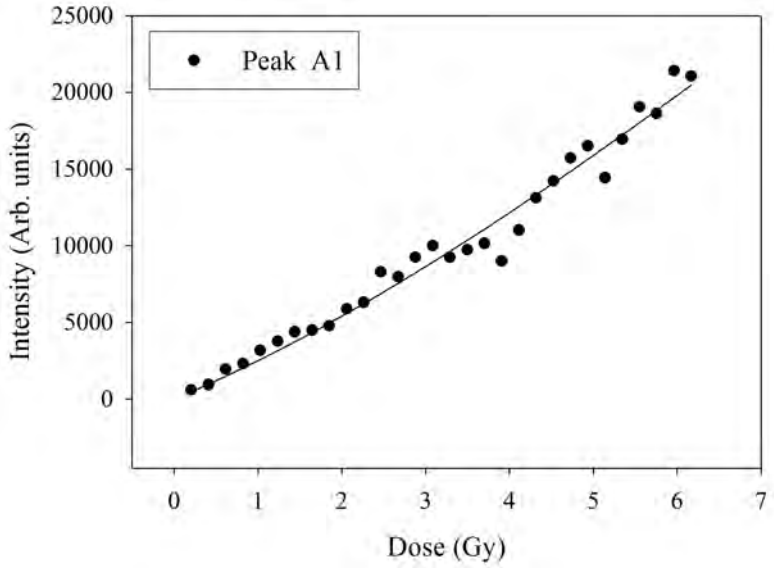

a

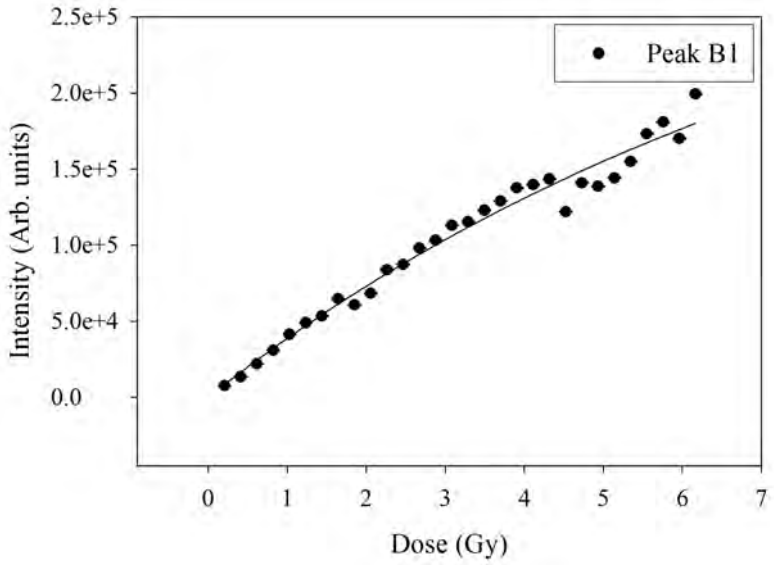

b

Figure 6.20: Influence of irradiation dose on peak intensity for (a) peak A1 and (b) peak B1. The solid line through the data is a fit of equation (6.4) for peak A1 and of equation (6.1) for peak B1.

The supralinearity index f and the superlinearity index g of peak A1 as functions of irradiation dose are shown in Figure 6.21. The index f increases from 1.00 to 1.43 with doses between 0.2 and 6.2 Gy. The index g on the other hand increases from 1.03 to 1.24 with irradiation doses up to 3.5 Gy and then decreases to a final value 1.20 Gy. Irrespective of the irradiation dose, g remains greater than 1.00 hence, the dose response of peak A1 is superlinear. This result differs from that of peak I, of conventional TL, which is sublinear within the same dose range.

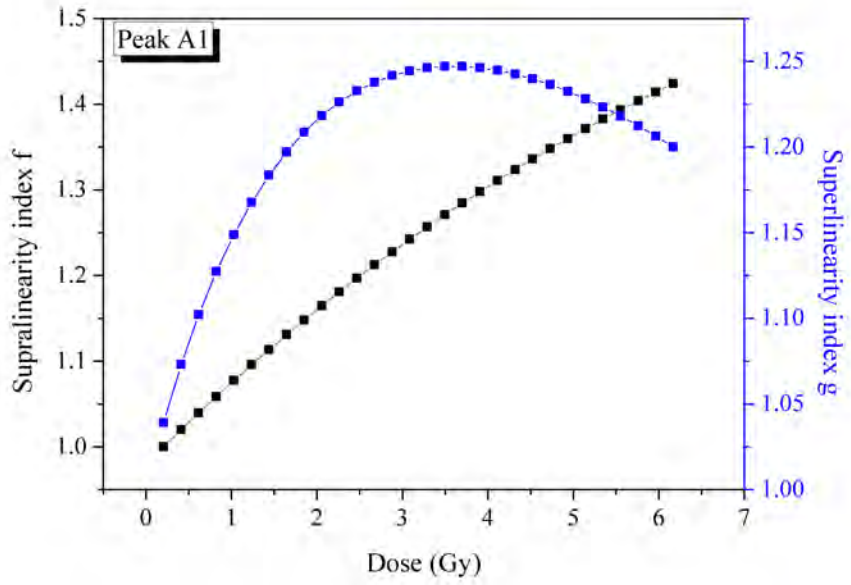

Figure 6.21: Supralinearity index f and superlinearity index g of peak A1 against irradiation dose.

The analysis of superlinearity and supralinearity indices shows that just as peak I of sample B, peak B1 has a sublinear dose response within 0.1-6.1 Gy

The influence of irradiation dose on the intensity of peaks A2, B2, C2 and D2 is shown in Figure 6.22 for doses between 0.2 and 6.1 Gy. Figures 6.22a and 6.22b show that the intensity of peaks A2 and B2 each increases monotonically with dose. For Peaks C2 and D2 (Figures 6.22c and 6.22d) on the other hand, the data show trends towards saturation for doses above 3.5 and 4.5 Gy respectively.

The line through the data points of peak A2 in Figure 6.22a is the best fit from equation (6.5). Analysing the response using the supralinearity index f and the superlinearity index g (plot omitted), it is found that peak A2 is linear with doses up to 6.2 Gy in contrast with peak II of this sample which is sublinear within 4.0-7.4 Gy as reported in section 6.1.

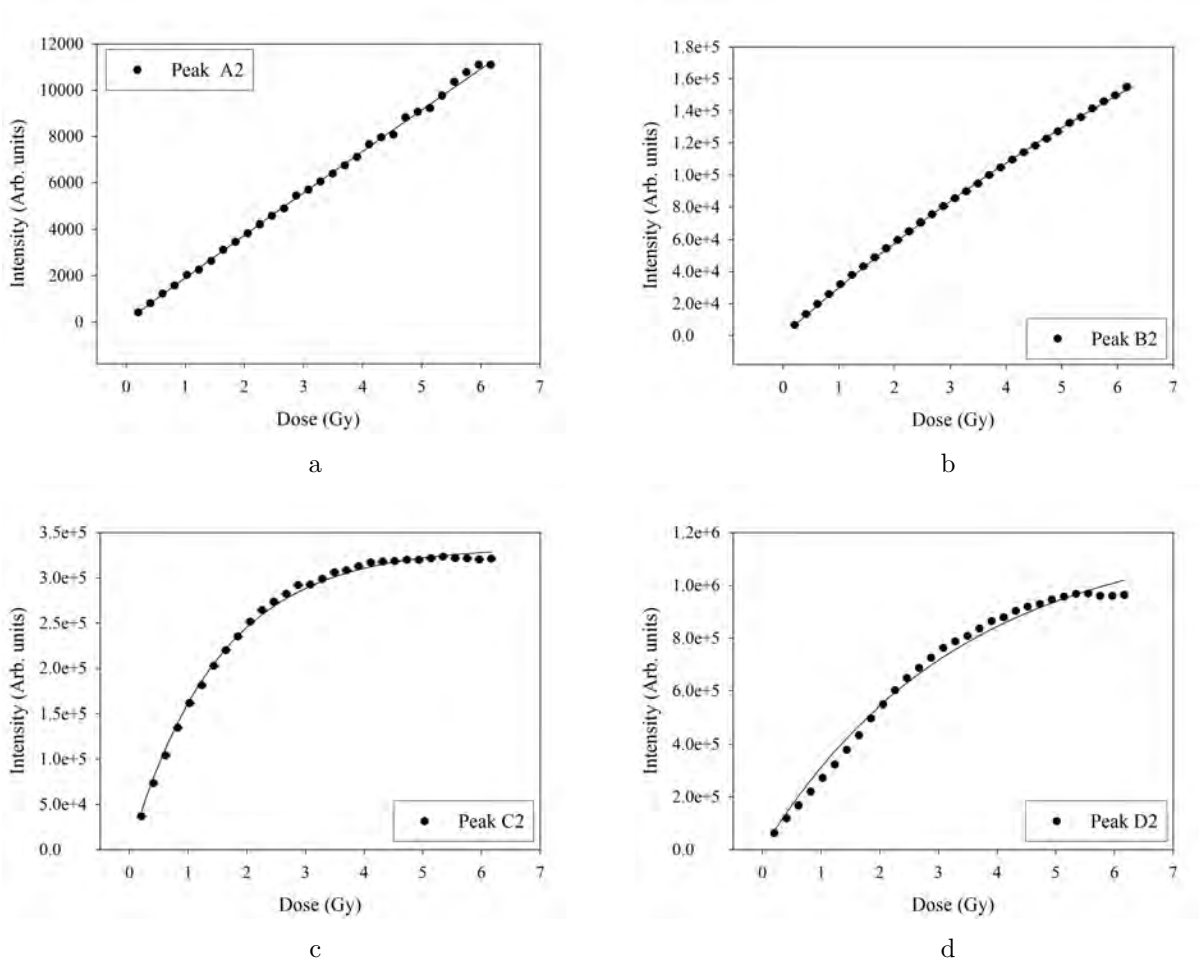

Figure 6.22: Dependence of intensity on irradiation dose within 0.1-6.2 Gy for (a) peak A2, (b) peak B2, (c) peak C2 and (d) peak D2.

The dose response of peak B2 is fitted with equation (6.1) and the analysis of the corresponding indices f and g shows that it is sublinear within 0.1-6.1 Gy. Similarly, the dose response of peaks C2 (Figure 6.22c) and D2 (Figure 6.22d) are each described by equation (6.1) and they are each sublinear as the corresponding conventional peaks.

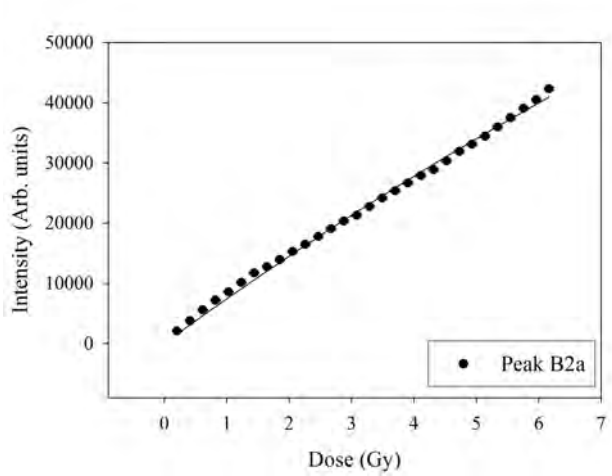

a

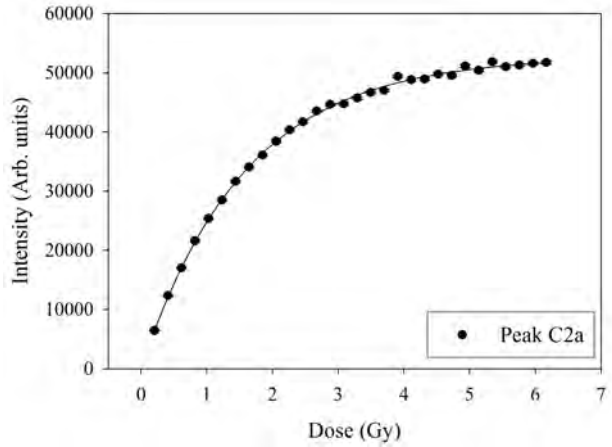

b

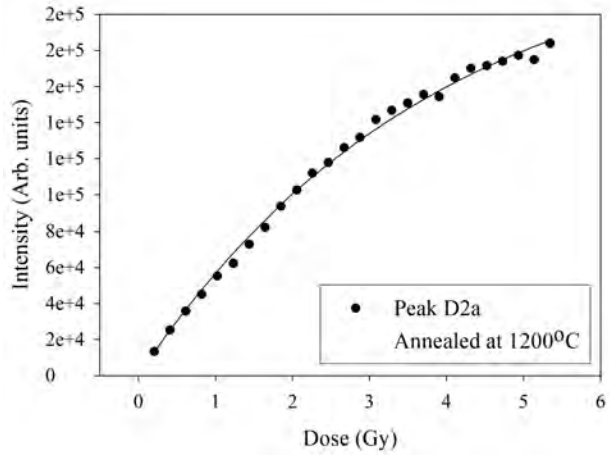

c

Figure 6.23: Effect of irradiation dose on the intensity of peaks (a) B2a, (b) C2a and (d) D2a respectively. The solid line through the data points of each peak is a fit of equation (6.1).

Figure 6.23 shows the influence of irradiation dose on peak intensity for B2a, C2a and D2a respectively. The solid line through the data of each peak is a fit of equation (6.1). The same analysis used earlier shows that for each of peaks B2a, C2a and D2a, the response is sublinear within 0.2-6.2 Gy.

Preheating to 300°C is intented to remove peaks I-IV of each sample. For sample A, peaks I-III are reproduced by phototransfer as peaks A1, A2 and A3 at 54, 90 and 190°C whereas for sample D, peaks II, IIa, III and IV are reproduced as PTTL peaks D2, D2a, D3 and D4 at 92, 116, 196 and 262°C respectively. A glow curve of sample D meant to illustrate peak D4 is shown in Figure 6.24 for a dose of 4.1 Gy, a 300°C preheat and illumination for 10 s. The dose response of peak D4 could not be studied because it could not be isolated from peak V for certain doses.

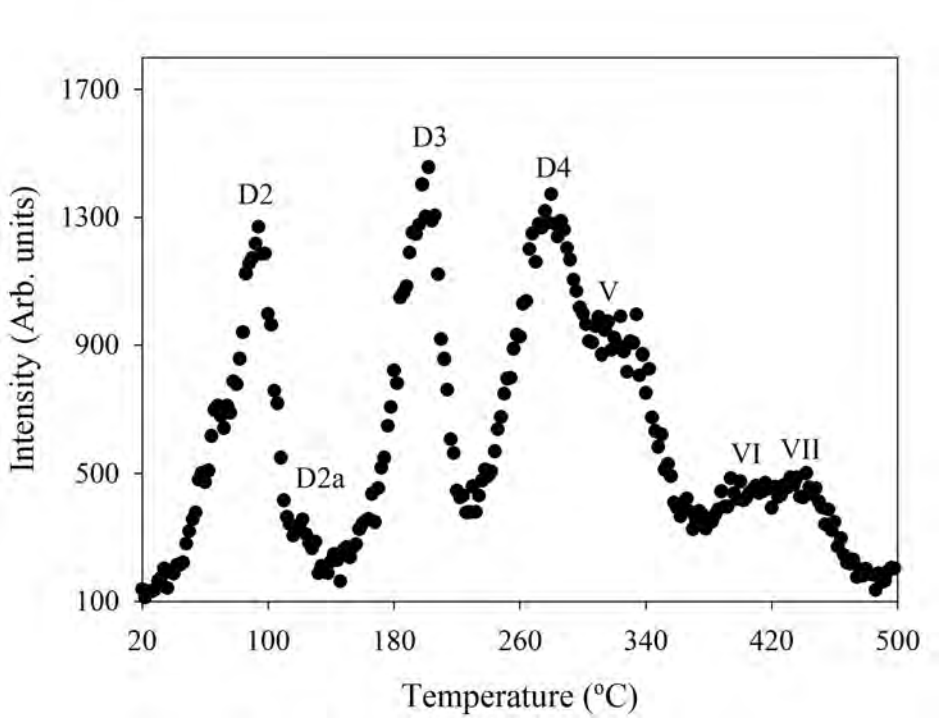

Figure 6.24: Glow curve of sample D measured at 1°C/s after irradiation to 4.1 Gy, preheating to 300°C and illumination for 10 s.

Figure 6.25 shows the effect of irradiation dose on peak position for the PTTL peaks of samples A and D following preheating to 300°C. The position of peak A3 is not affected by irradiation dose. This is also the case for peaks A1 and A2 as shown earlier for a 120°C preheat. This observation implies that peak A3 also follows first-order kinetics as peak III in a conventional glow curve of this sample (Figure 6.1).

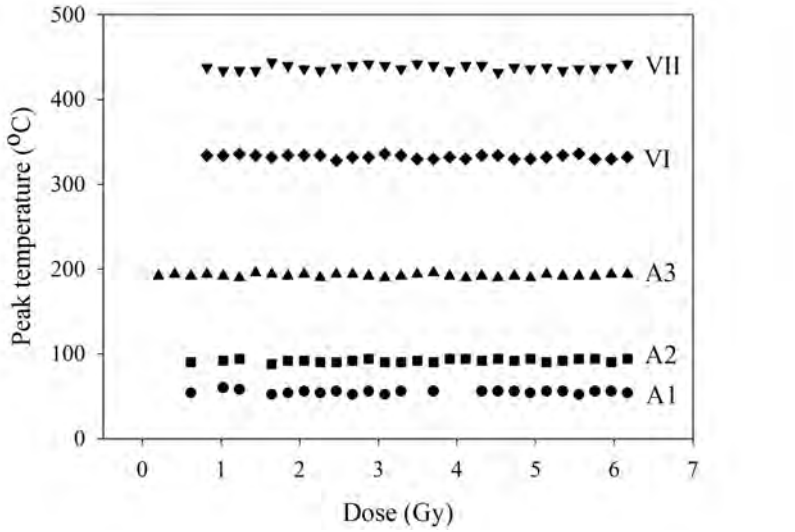

a

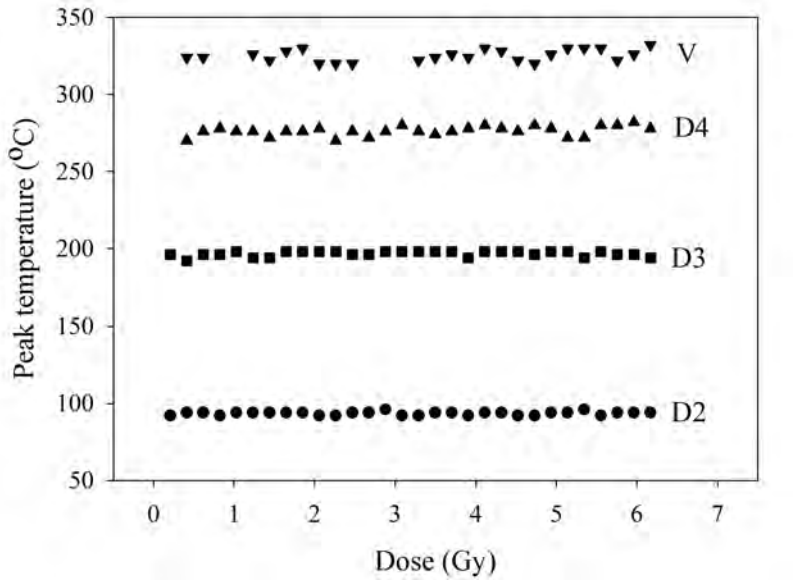

b

Figure 6.25: Influence of peak position on irradiation dose for (a) sample A and (b) sample D. Peaks A1-A3 and D1-D4 are due to phototransfer after preheating to 300°C and illumination for 10 s.

Previous studies (Kalita and Chithambo, 2017e; Sob et al., 2021) have shown that peaks V-VII of unannealed α-Al_2O_3:C,Mg are not reproduced by phototransfer. For this reason, preheating temperatures above 300°C were not used to investigate the dose response of any potential PTTL peaks resulting from peaks V-VII of each sample. The dependence of peak intensity on irradiation doses between 0.1 and 6.2

Gy is shown in Figure 6.26 for peaks A3, B3, C3 and D3 respectively. The data for peaks A3 and D3 are for preheating to 300°C. For peaks A3, B3 and C3, the respective intensity grows with irradiation dose. For peak D3 on the other hand, the intensity seems to saturate for doses above 3.0 Gy. The response of peaks B3, C3 and D3 are each fitted with equation (6.1). However the fit for peak D3 is not reliable. The same analysis performed before shows that peaks B3 and C3 are sublinear within 0.1-6.1 Gy. Kalita and Chithambo (2019) reported that the dose response of phototransferred peaks corresponding to each of peaks II, IIa, III of sample D is linear within 1-15 Gy. Their results differ from those reported here for sample D.

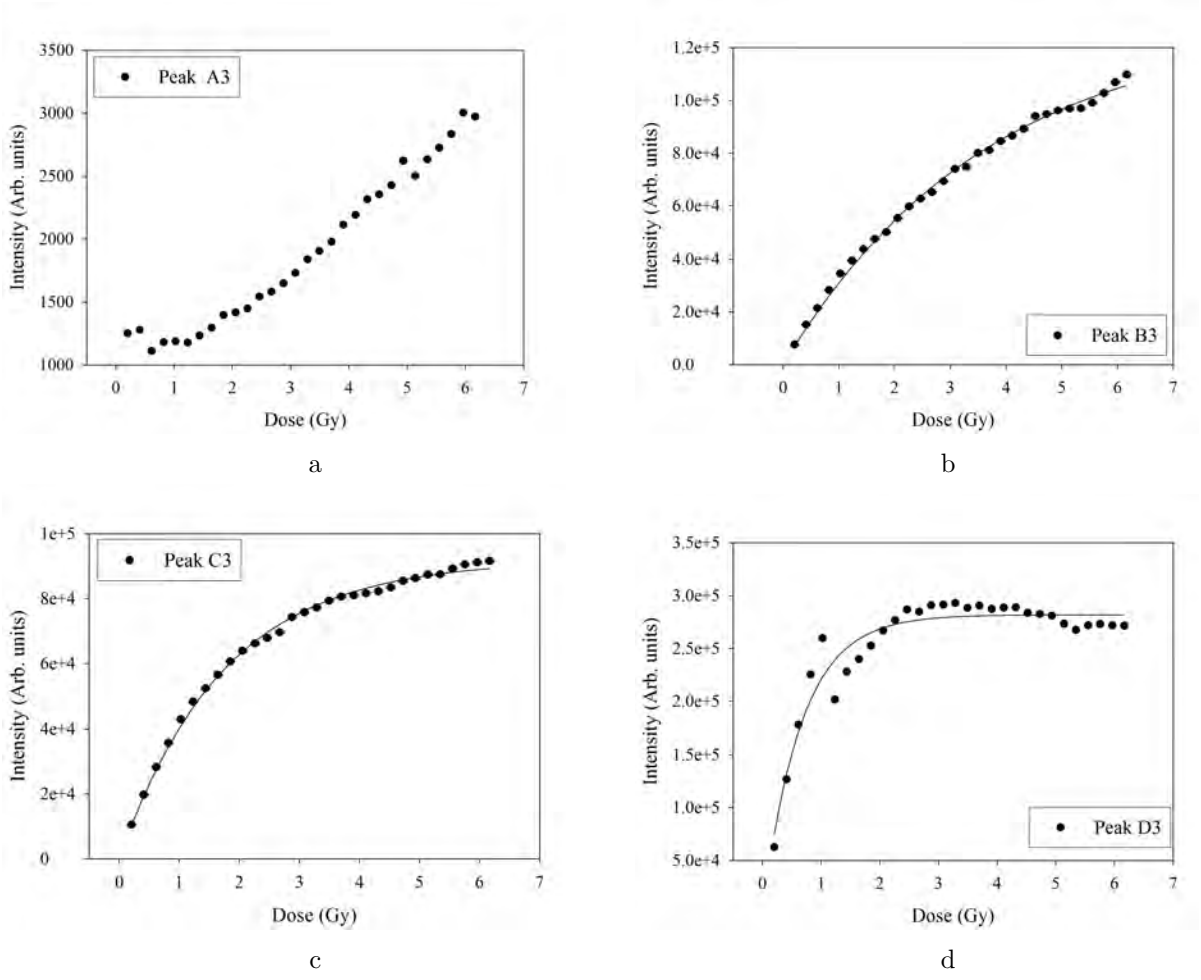

Figure 6.26: Dependence of peak intensity on irradiation dose for peaks (a) A3, (b) B3, (c) C3 and (d) D3 respectively.

Tables 6.1-6.4 summarise some of the dosimetric features of samples A, B, C and D respectively. For each peak, the features listed are the dose response and the order of kinetic *b*.

Table 6.1: Dose response features of unannealed α-Al_2O_3:C,Mg (sample A)

Peak	T_m (°C)	Dose range (Gy)	Dose Response	Order of kinetic b
I	51	0.1 - 7.4	sublinear	1
II	86	0.1 - 4.0	superlinear	1
		4.0 - 7.4	sublinear	
III	184	0.1 - 7.4	superlinear	1
IV	220	0.1 - 7.4	sublinear	1
V	312	0.1 - 7.4	superlinear	1
VII	416	0.1 - 7.4	superlinear	1
A1	54	0.1 - 6.1	superlinear	1
A2	90	0.1 - 6.1	sublinear	1

Table 6.2: Dose response features of α-Al_2O_3:C,Mg annealed at 700°C (sample B)

Peak	T_m (°C)	Dose range (Gy)	Dose response	Order of kinetics
I	54	0.1 - 8.2	sublinear	1
II	89	0.1 - 8.2	linear	1
IIa	117	0.1 - 8.2	linear	1
III	188	0.1 - 5.0	linear	1
IV	224	0.1 - 7.9	sublinear	
V	308	0.1 - 7.9	linear	1
VI	390	0.1 - 6.0	linear	1
VII	420	0.1 - 6.0	linear	1
B1	54	0.2 - 6.1	sublinear	1
B2	88	0.2 - 6.1	sublinear	1
B2a	113	0.1 - 6.1	sublinear	1
B3	189	0.1 - 6.1	sublinear	1

6.3 Fading of the luminescence signal

Fading manifests as a decrease in luminescence intensity with delayed stimulation. It is due to the spontaneous eviction of electrons from traps between irradiation and stimulation (Chen and McKeever, 1997). The fading of glow peaks of α-Al_2O_3:C,Mg was investigated. Such a study gives an insight into the stability of the electron traps corresponding to each glow peak and is therefore relevant to luminescence dosimetry. During each measurement, the irradiated sample was left at room temperature for a specific time before being heated to record luminescence.

Table 6.3: Dose response features of α-Al_2O_3:C,Mg annealed at 900°C (sample C)

Peak	T_m (°C)	Dose range (Gy)	Dose response	Order of kinetics b
I	51	0.1 - 7.4	sublinear	1
II	85	0.1 - 7.1	sublinear	1
IIa	115	0.1 - 6.5	sublinear	1
III	183	0.1 - 4.8	sublinear	1
IV	220			
V	260	0.1 - 3.7	sublinear	1
VI	304			
VII	404	0.1 - 7.4	linear	1
C2	88	0.1 - 6.2	sublinear	1
C2a	113	0.1 - 6.2	sublinear	1
C3	189	0.1 - 6.2	sublinear	1

Table 6.4: Dose response features of α-Al_2O_3:C,Mg annealed at 1200°C (sample D)

Peak	T_m (°C)	Dose range (Gy)	Dose response	Order of kinetics b
I	60	0.1 - 6.2	sublinear	1
II	90	0.1 - 6.1	sublinear	1
IIa	118	0.2 - 5.3	sublinear	1
III	191			1
IV	256	0.2 - 6.0	sublinear	1
V	310	0.1 - 7.4	sublinear	1
VI	∼380			
VII	∼420			
D2	92	0.2 - 6.2	sublinear	1
D2a	116	0.2 - 5.3	sublinear	1
D3	196	0.2 - 6.2	sublinear	1

In this study of fading, the neutral density filter was not used.

6.3.1 Fading of conventional TL peaks

For this study, glow curves of sample A were measured for delay times between 0 and 48 hours. For each measurement, the sample was irradiated to 1.0 Gy at room temperature and then heated at 1°C/s to stimulate luminescence after a

given delay. Figure 6.27 shows two glow curves; one measured immediately after irradiation and the other one measured 6 hours later. Peaks I and II are indistinct in the glow curve measured after a 6 hours delay as shown in Figure 6.27b. The initial rise region of peak III of the delayed glow curve is comprised of a remnant from peak II. Plots of TL intensity against delay time are not shown for peaks I and II because these peaks had faded to a level where they could not be measured as evidenced in the glow curve measured after 6 hours in Figure 6.27b.

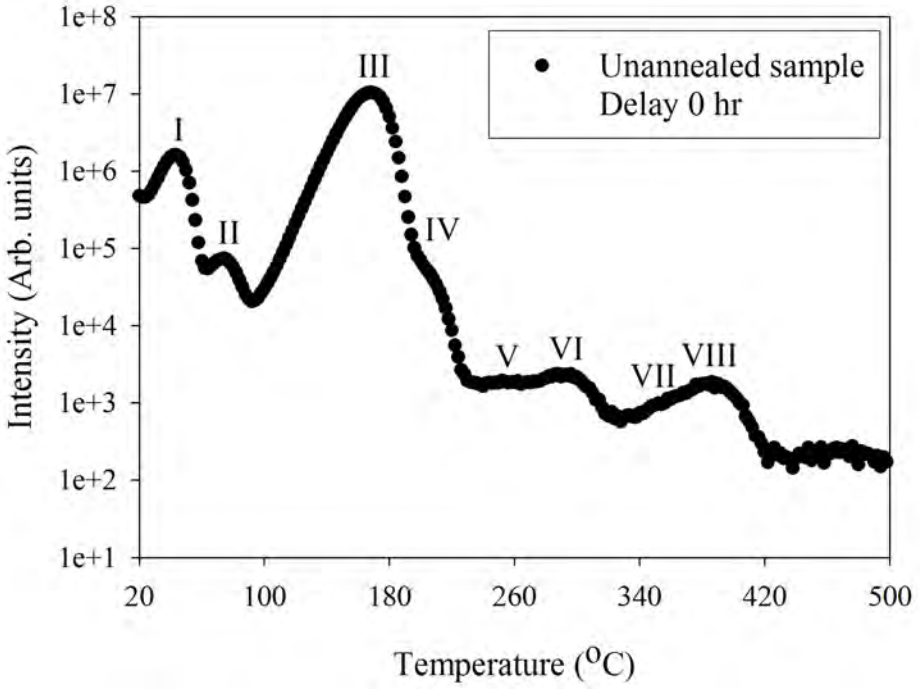

a

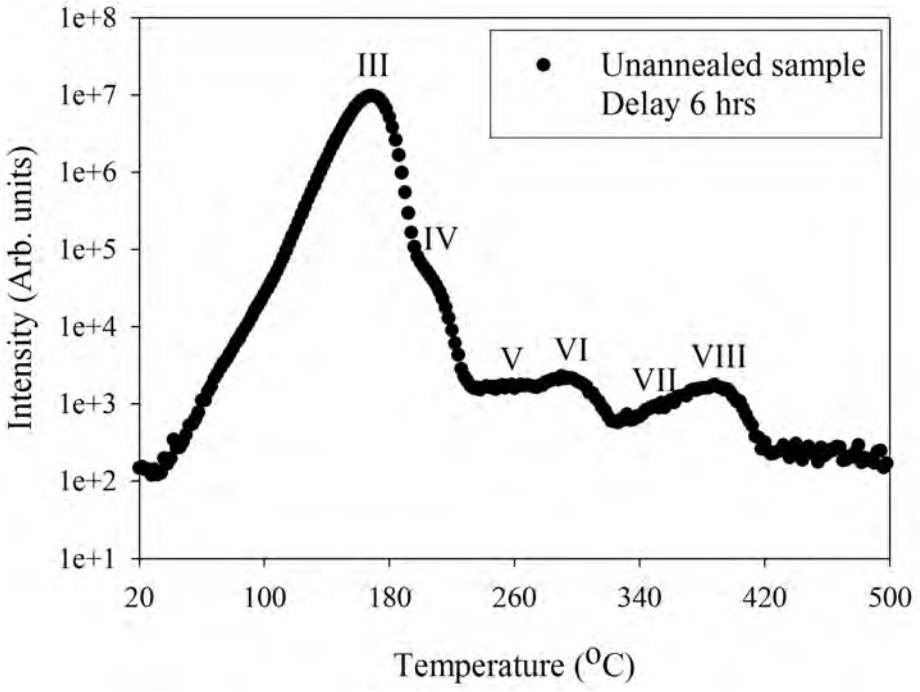

b

Figure 6.27: Glow curves of unannealed α-Al_2O_3:C,Mg (sample A) measured at 1°C/s after irradiation to 1.0 Gy. The glow curve in (a) is measured immediately after irradiation whereas that in (b) is measured 6 hours after irradiation.

The effect of delayed stimulation on the intensity and the position of peak III is shown in Figure 6.28. Peak III fades slowly with delay between irradiation and stimulation;. Its intensity decreasinges to 902.8% of its initial value after a 486 hours delay and to 90% after a delay of 48 hours.

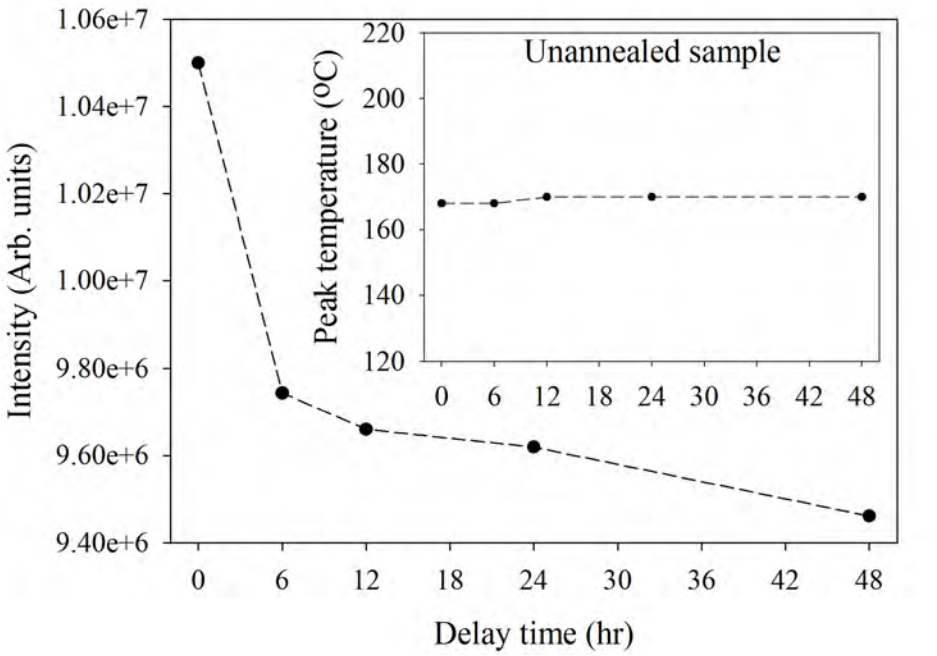

Figure 6.28: Effect of delayed stimulation on peak III of unannealed α-Al_2O_3:C,Mg (sample A). The intensity of peak III against delay is shown on the main graph whereas the dependence of its position on delay time is shown in the inset. The dotted line is visual guide which shows the trend in the data.

Figure 6.29 shows the glow curve measured immediately after irradiation and the one measured 48 hours after. Just as in the case of peak III, the influence of delay stimulation on peaks IV-VIII is minimal. The results of Figures 6.28 and 6.28 show that the electron traps corresponding to peaks III-VIII remain stable with storage times up to 48 hrs. Regarding the fading of peak III of the unannealed sample (sample A), Kalita and Chithambo (2017f) observed that the peak faded to ∼22% of its initial intensity within 2400 s after irradiation and thereafter to ∼14% within 64800 s (18 hrs). Kalita and Chithambo (2017f) suggested that the fading may be due to the escape of electrons from the main trap through the shallow traps (peaks I and II) by quantum tunneling. In this study, we observed that peak III remains stable after 48 hrs. The difference in results might be specific to the samples.

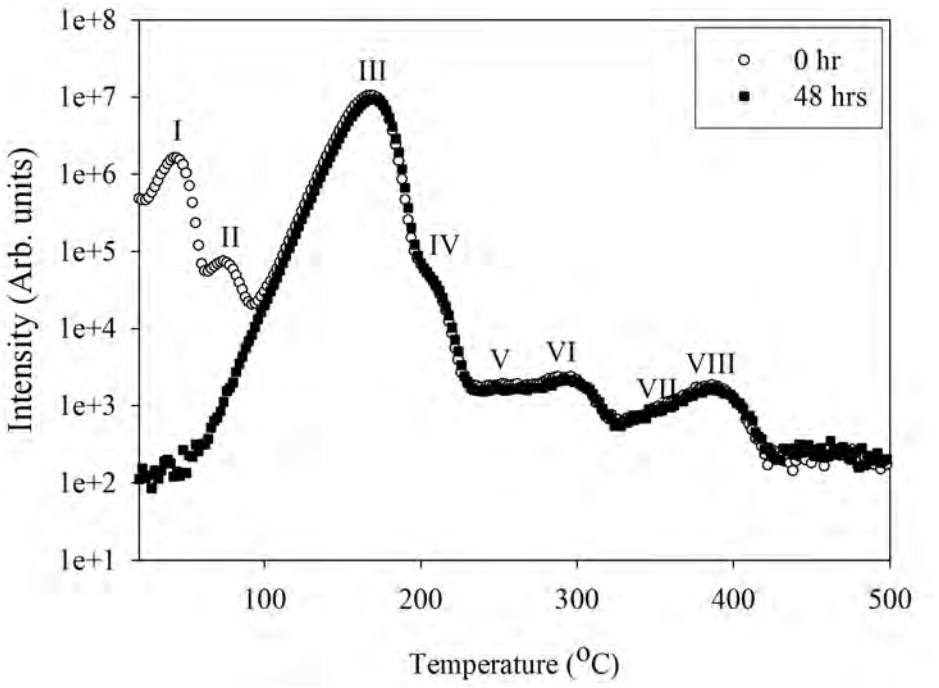

Figure 6.29: Glow curves of unannealed α-Al_2O_3:C,Mg (sample A) measured at 1°C/s after irradiation to 1.0 Gy. The open symbols are for the glow curve measured immediately after irradiation whereas the full symbols represent the glow curve measured after a 48 hours delay.

6.3.2 Fading of phototransferred TL peaks

We now report the influence of delayed stimulation on the phototransferred peaks of samples A, B, C and D for preheating temperatures of 100, 120 and 200°C. Each glow curve was measured following irradiation to 3.0 Gy, preheating and illumination for 12 s. In this case, a delay was allowed between illumination and thermal stimulation. Delay times ranged from 0 to 320 s. The preheating temperature, irradiation dose, duration of illumination and the delay times were chosen in order to reliably examine the phototransferred peaks of each sample. The neutral density filter was not used. Figure 6.30 shows two glow curves of sample A; the first measured immediately after illumination and the second 320 s after illumination.

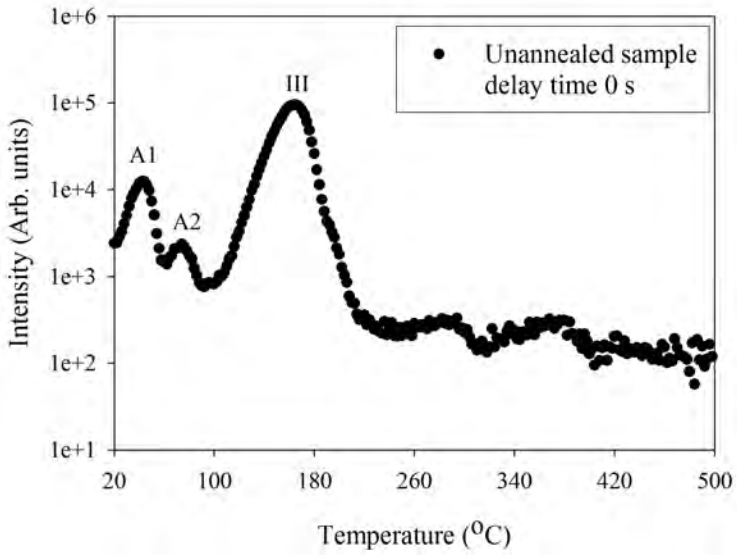

a

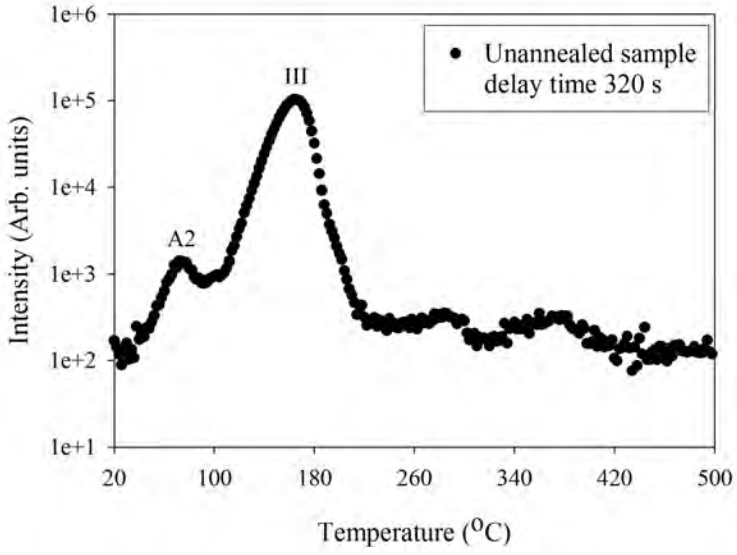

b

Figure 6.30: Glow curves of sample A measured at 1°C/s after irradiation to 3.0 Gy, preheating to 100°C and illumination for 12 s. The glow curve in (a) is measured immediately after illumination whereas the one in (b) is recorded 320 s after illumination.

Peaks A1 and A2 are reproduced at 44 and 72°C respectively. These two peaks appear at the same positions as the corresponding conventional peaks. The glow curve of Figure 6.30b shows that peak A1 has faded completely for a 320 s delay.

Figure 6.31 shows the influence of delay between illumination and measurement

on peaks A1, B1, C1 and D1. The fading of peaks A1, B1 and C1 can each be described exponentially as

$$I(t) = I_0 \exp(-\gamma t), \tag{6.7}$$

where I_0 is the initial intensity, γ is the decay constant and t is the delay time. The intensity of peak A1 decreases to about 50% of its initial value within 70 s and only 17% of the initial intensity is left after a 300 s delay. The decay constant γ found from the fit in Figure 6.31a is 0.0082 s^{-1}. The lifetime of peak A1, computed as $1/\gamma$, is approximately 122 s. Peak A1 is unstable as its conventional counterpart namely; peak I. Kalita and Chithambo (2017g) observed that peak I fades within 300 s for a dose of 1.0 Gy and a heating rate of 1°C/s and within 600 s for a dose of 4.0 Gy. Peak B1 appears at 46°C, the same temperature as that of peak I of sample B. For this preheat, the lifetime of B1 is 118 s. Peak B1 is unstable and fades within the same timeframe as peak A1. Similarly, peak C1 occurs at 46°C and its lifetime is 136 s. For peak D1, the intensity decreases monotonically with delay time up to 160 s. Beyond 160 s, peak D1 was indistinct from peak D2 and could no longer be measured.

Figure 6.32 shows the intensity of peaks A2, B2, C2 and D2 against delay time for a 100°C preheat. As seen in Figure 6.32a, the intensity of peak A2 increases initially with delay time before decreasing monotonically thereafter. Peak A2 is an effective competitor for electrons lost from other traps. As other peaks fade, any such additional contributions decrease. For peaks B2, C2 and D2 (Figures 6.32b-6.32d), the intensity decreases monotonically with delay. In contrast to peaks A1, B1, C1 and D1, peaks A2, B2, C2 and D2 could still be measured after a 5000 s delay.

The effect of delay on peaks B1, C1 and D1 for a 120°C preheat is shown in Figure 6.33. The behaviour of these peaks is similar to that of the corresponding peaks after preheating to 100°C. The decay of peaks B1 and C1 is exponential and the lifetimes of these two peaks for this preheat are 108 and 111 s respectively.

The influence of delayed stimulation on the intensity of peaks B2, C2 and D2 following preheating to 120°C is shown in Figure 6.34. The peaks fade in a manner similar to that observed for a 100°C preheat.

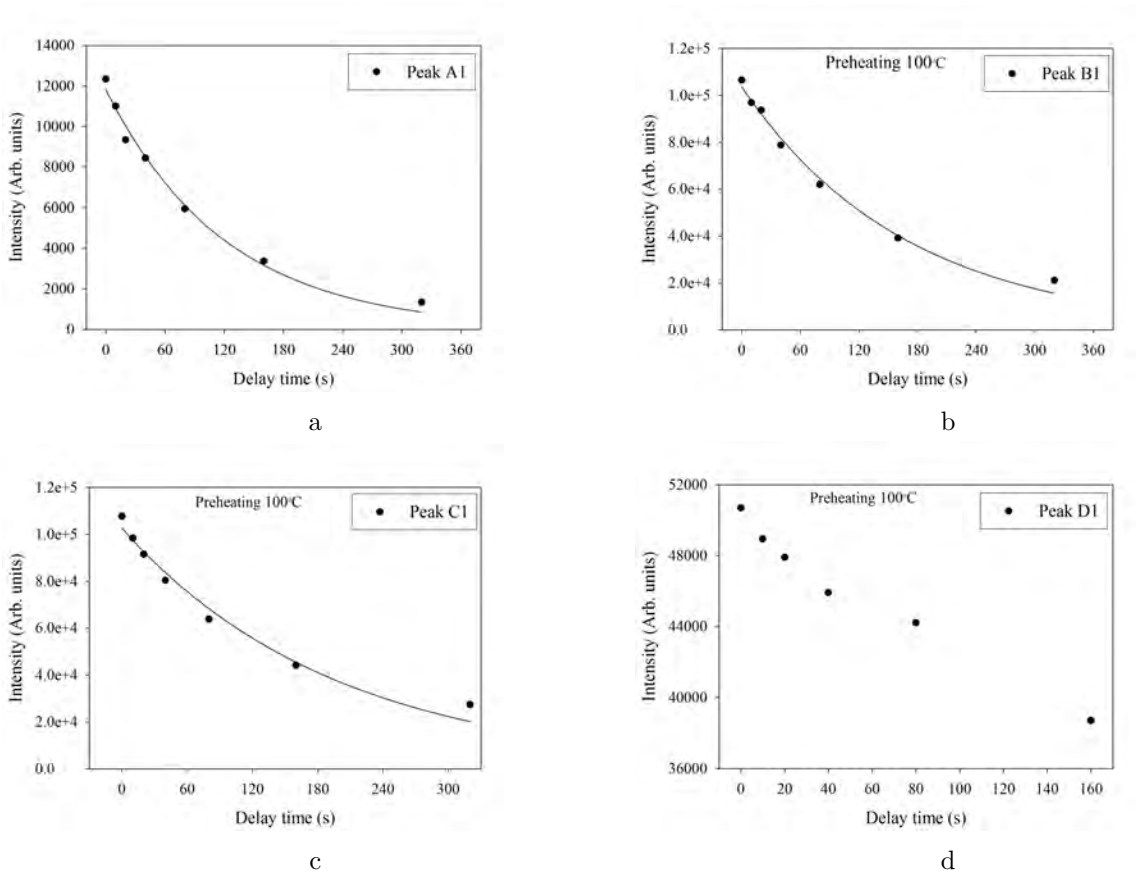

Figure 6.31: Influence of delay on the intensity of (a) peak A1, (b) peak B1, (c) peak C1 and (d) peak D1. Each data point corresponds to a measurement at 1°C/s after irradiation to 3.0 Gy, preheating to 100°C and illumination for 12 s. Peaks A1, B1, C1 and D1 appear at 44, 46, 46 and 52°C respectively. The solid line is the best fit of equation (6.7).

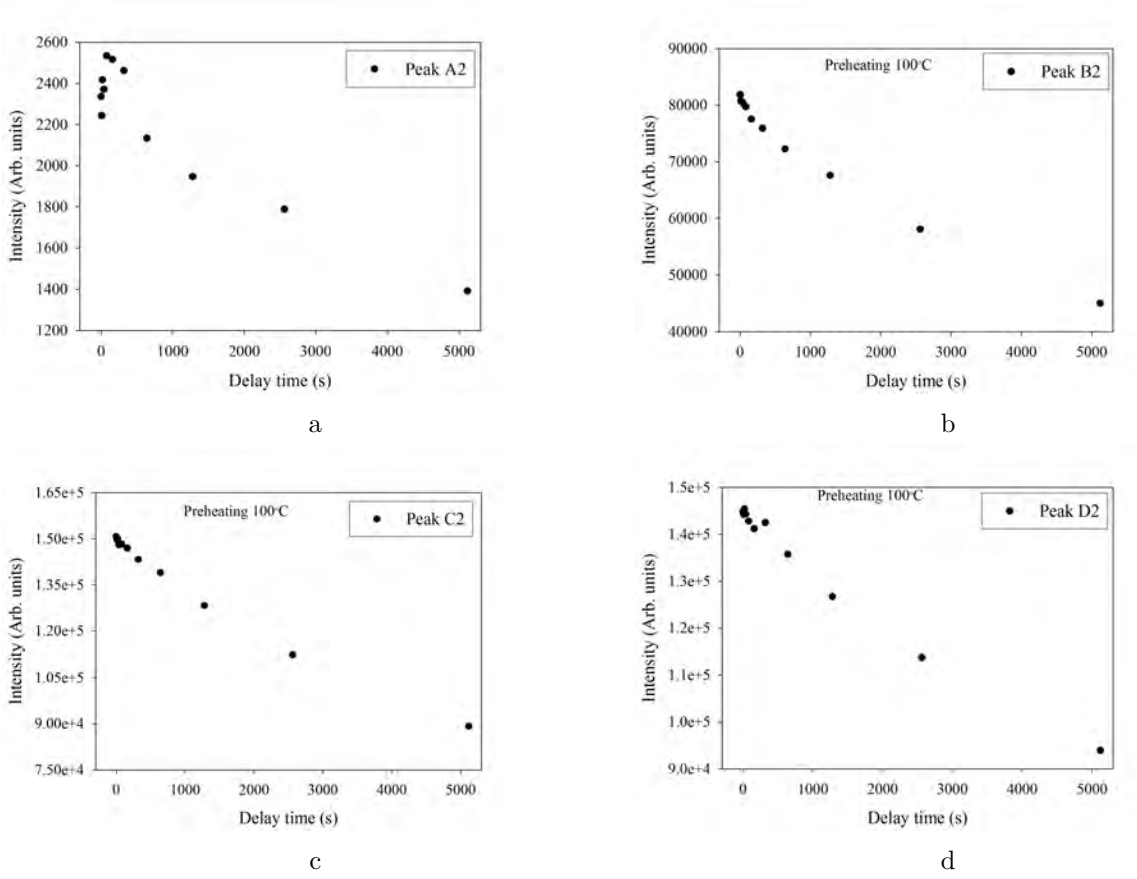

Figure 6.32: Influence of delay on the intensity of (a) peak A2, (b) peak B2, (c) peak C2 and (d) peak D2. Each data point corresponds to a measurement at 1°C/s after irradiation to 3.0 Gy, preheating to 100°C and illumination for 12 s. Peaks A2, B2, C2 and D2 appear at 72, 76, 76 and 80°C respectively.

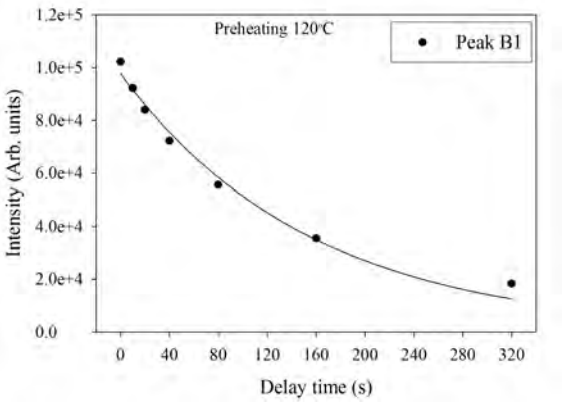

a

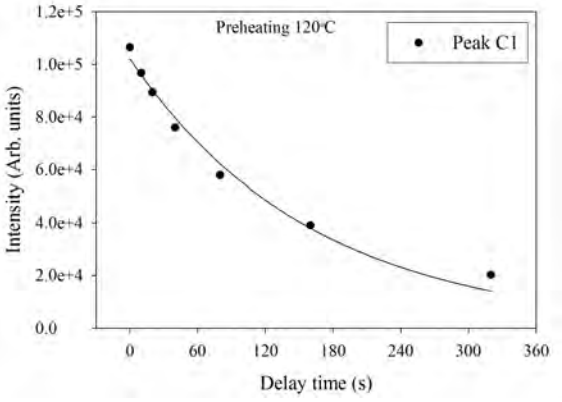

b

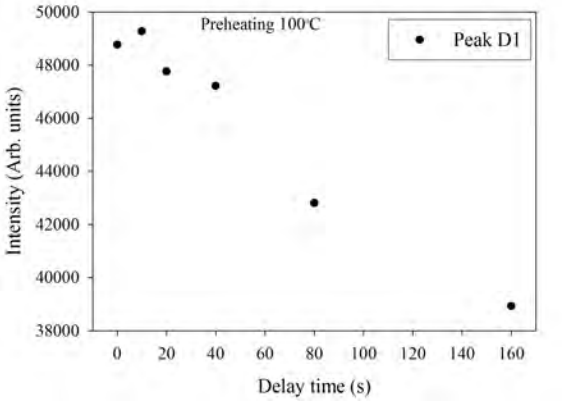

c

Figure 6.33: Influence of delay on the intensity of (a) peak B1, (b) peak C1 and (c) peak D1. Each data point corresponds to a measurement at 1°C/s after irradiation to 3.0 Gy, preheating to 120°C and illumination for 12 s. Peaks B1, C1 and D1 appear at 46, 46 and 52°C respectively. The solid line is the best fit of equation (6.7).

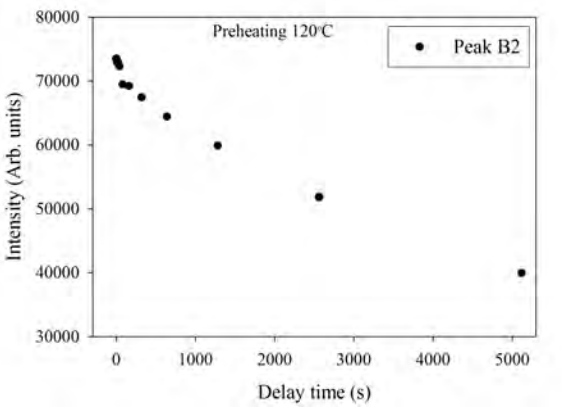

a

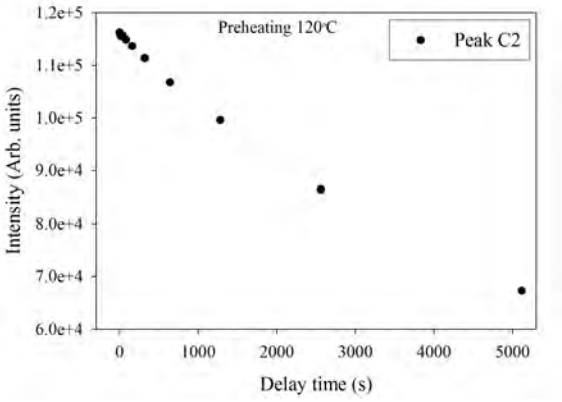

b

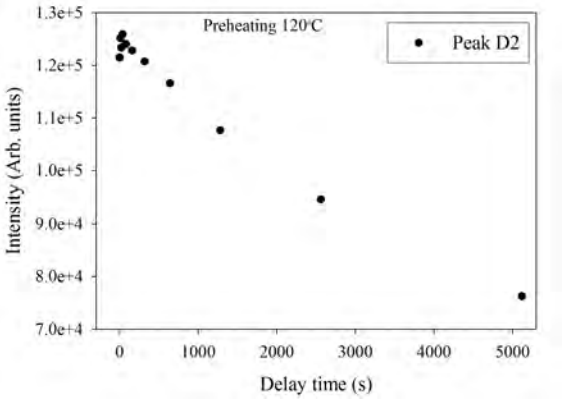

c

Figure 6.34: Influence of delay on the intensity of (a) peak B2, (b) peak C2 and (c) peak D2. Each data point corresponds to a measurement at 1°C/s after irradiation to 3.0 Gy, preheating to 120°C and illumination for 12 s. Peaks B2, C2 and D2 appear at 76, 76 and 80°C respectively.

Figure 6.35 shows the fading of peaks B1, C1, B2 and C2 respectively following

preheating to 200°C. As for preheating to 100 and 120°C, the fading of peak B1 can be described with an exponential decay. Peaks B1 and C1 fades to 28 and 49% of their initial intensity respectively within 320 s. The intensity values of PTTL corresponding to peak I or II in each sample decrease by 1 or 2 order of magnitude after preheating to 200°C. Following this preheat, the electron trap of peak III, the main donor for these PTTL peaks in each sample, is depleted. For samples B, C and D, peak IIa at 100°C is reproduced under phototransfer after preheating to 200°C. We also note the presence of a PTTL peak near 140°C (peak C2b) for sample C. The influence of delayed stimulation on peak B2a, C2a, D2a or C2b could not be studied reliably.

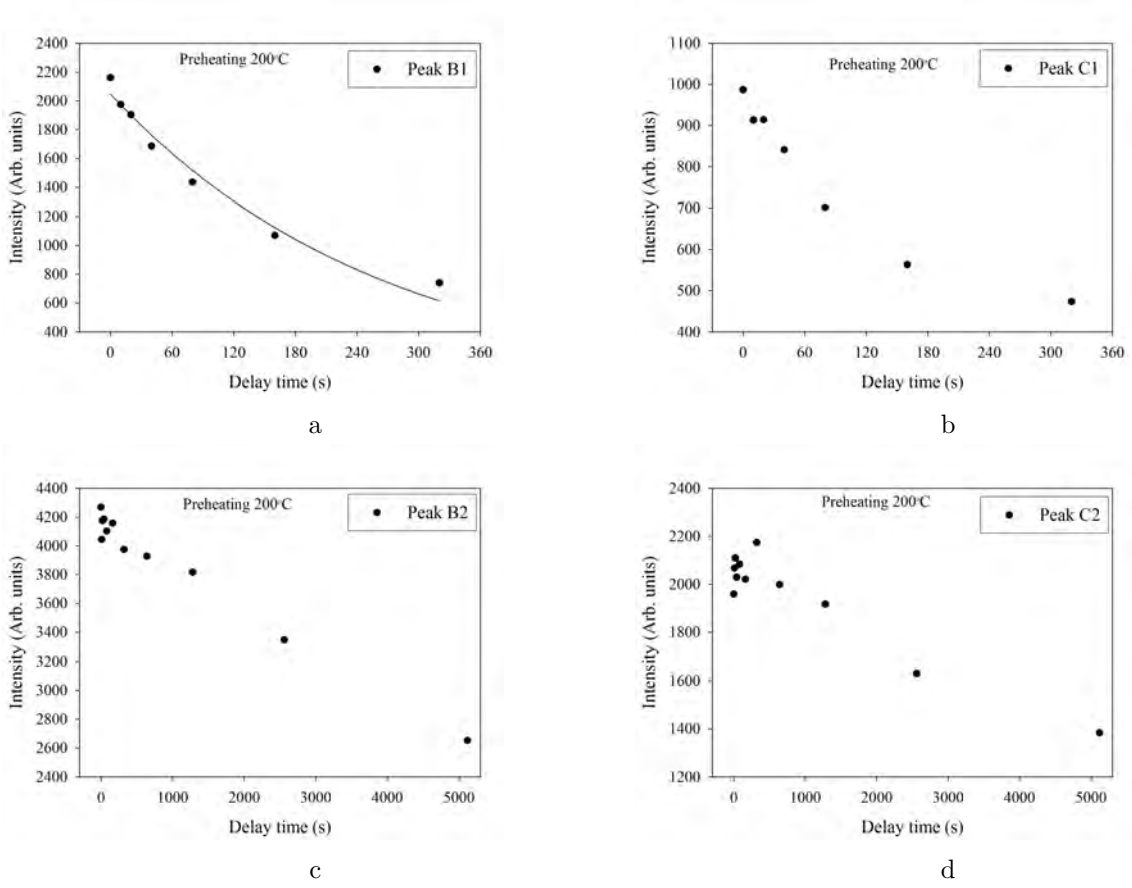

Figure 6.35: Influence of delay on the intensity of (a) peak B1, (b) peak C1, (d) peak B2 and (d) peak C2. Each data point corresponds to a measurement at 1°C/s after irradiation to 3.0 Gy, preheating to 200°C and illumination for 12 s. The solid line is the best fit of equation (6.7).

6.4 Summary

Glow peaks of α-Al_2O_3:C,Mg reported in this study follow first-order kinetics irrespective of annealing up to 1200°C. Similar results on the order of kinetics of glow peaks in α-Al_2O_3:C,Mg have been reported elsewhere (Kalita and Chithambo, 2017f,b,e, 2018b; Trindade et al., 2020). For annealing to 700°C or above, there is a new peak induced at 100°C; labelled here as IIa. The use of the neutral density filter affects the structure and the shape of the glow curves as reported by Kalita and Chithambo (2017a). For instance, peak IIa of sample B appears at 117°C instead of 100°C as found in glow curves measured without this filter. We observed that the dose response of a PTTL peak is not necessarily similar to that of the corresponding peak in conventional TL. The PTTL peaks occur at the same positions as the associated TL peaks and they also follow first-order kinetics. The dose response of peak I is sublinear within 0.1-8.1 Gy; it is therefore not affected by annealing up to 1200°C. For peak I of unannealed α-Al_2O_3:C,Mg Kalita and Chithambo (2017g) found a sublinear dose response within 1-10 Gy. Similar results have also been reported by Kalita and Chithambo (2018b) for peaks I, II and IIa of the sample annealed at 1200°C within 1-10 Gy.

Peaks III, V and VII of sample A each have a superlinear dose response within 0.1-7.4 Gy whereas peak IV is sublinear within the same range. For peak II of this sample, the response is superlinear up to 4.0 Gy and then sublinear thereafter with doses up to 7.4 Gy. This result is in agreement with that of Kalita and Chithambo (2017g) for peak II of their unannealed sample. Peak A1, the PTTL peak corresponding to peak I of sample A, has a superlinear response within 0.1-6.1 Gy whereas peak A2 is sublinear within the same dose range. In contrast, Kalita and Chithambo (2017e) observed a linear dose response between 1 and 15 Gy for each of the phototransferred peaks corresponding to peaks I and II. For peak III, Kalita and Chithambo (2017a) reported a superlinear response within 0.1-30 Gy followed by a sublinear response thereafter up to 100 Gy. However in a subsequent study, the response of this peak was found to be sublinear within 0.1-10 Gy (Kalita and Chithambo, 2017g). The main differences in the two studies were the dose range and the use of a neutral density filter. We note that the result reported here for peak III of sample A is consistent with that of Kalita and Chithambo (2017a). For the main peak of unannealed α-Al_2O_3:C, Kalita and Chithambo (2017g) found a sublinear response within 1-4 Gy followed by a superlinear response up to 10 Gy. However, previous studies (Yukihara et al., 2003; Chithambo, 2004) reported a linear response within 1-10 Gy followed by a superlinear response up to 30 Gy and a sublinear response above 30 Gy. As stated by Kalita and Chithambo (2017g),

in addition to the choice of dose range and of detection filters, the change in the sensitivity of these samples with re-use also affect the dose response.

For sample B, which is annealed to 700°C, peaks II, IIa, III and V-VII are linear within 0.1-8.2 Gy. The dose range specific to each of these peaks is listed in Table 6.2. PTTL peaks B1-B3 which correspond to peaks I-III of sample B each show sublinearity with doses up to 6.1 Gy. On the other hand, peak IV just as peak I of this sample is sublinear for doses up to 7.9 Gy.

With the exception of peak VII which has a linear dose response within 0.1-7.4 Gy, the conventional glow peaks and the PTTL peaks of sample C studied here each have a sublinear response with 0.1-7.4 Gy. The dose range specific to each of these peaks is shown in Table 6.3.

Regarding sample D, peaks I, II, IIa, IV and V each have a sublinear dose response within 0.1-7.4 Gy. The specific range of interest for each peak is shown in Table 6.4. The PTTL peaks D2, D2a and D3 which correspond to peaks II, IIa and III each have a sublinear dose response within 0.2-6.2 Gy.

Peak I of each sample is unstable and fades within 300 s. This is equally the case for the associated PTTL peak. Peak A1 has a lifetime of 122 s. For peak B1 and C1 the respective lifetimes are 118 and 136 s. Peak I of α-Al_2O_3:C,Mg has a shallow trap with an activation energy of ∼0.85 eV and the peak suffers from phosphorescence at room temperature (Kalita and Chithambo, 2017f). The fading of peak I of each sample is due to phosphorescence. In a study on the nature and identity of the traps in α-Al_2O_3:C, Zhu et al. (2014) showed that under oxygen rich conditions, some Al are replaced by C and this results in an electron trap at ∼0.72 eV near the conduction band. It is known that peak I of α-Al_2O_3:C has an activation energy of ∼0.72 eV (Chithambo et al., 2014). In α-Al_2O_3:C,Mg, the corresponding peak has an activation energy of ∼0.85 eV. This led Kalita and Chithambo (2017f) to suggest the trap corresponding to peak I in α-Al_2O_3:C,Mg was of a similar origin however, the difference in activation energies was due to crystallographic structural changes resulting from lattice stressing since the radius of C is smaller than that of Mg. Peak II of each sample on the other hand could be measured with delay time up to 5000 s. For the unannealed sample (sample A), the intensity of peak II increased initially with delay; suggesting that this peak is an effective competitor for electrons lost from other traps. The fading of peak II of each sample can also be ascribed to phosphorescence since the corresponding trap is shallow with an activation energy of ∼ 0.96 eV. Peak III of sample A remains stable with delay up to 48 hrs. The influence of dose on fading was not investigated. However, Kalita and Chithambo (2017g) found that the rate of fading of peaks I-III of unannealed α-Al_2O_3:C,Mg was affected by dose. Kalita and Chithambo (2019) studied the

fading properties of α-Al_2O_3:C,Mg annealed at 1200°C for delay times between 1 and 18000 s for peaks I-III and found that these peaks faded at different rates with peak I being the most unstable and the rate of fading was influencing by annealing temperature.

Chapter 7

Illumination-time-dependent profiles of phototransferred thermoluminescence of unannealed α-Al_2O_3:C,Mg

This chapter deals with the analysis of time-dependent profiles of phototransferred thermoluminescence (PTTL) of unannealed α-Al_2O_3:C,Mg. The qualitative analysis of these time-dependent PTTL profiles is based on theoretical predictions whereas the mathematical analysis of these profiles is based on experimental results. This work has been published by Sob et al. (2021).

7.1 Introduction

In conventional thermoluminescence (TL), the signal is stimulated by controlled heating of a sample immediately after irradiation (McKeever, 1985; Chen and McKeever, 1997). The luminescence ensues directly from the recombination with holes of electrons thermally stimulated from electron traps which are populated during the irradiation. On the other hand, in PTTL the irradiated sample is first preheated to a specific temperature and, after cooling, exposed to light of a specific wavelength before being heated again to monitor any luminescence (Chithambo et al., 2019; Chithambo and Dawam, 2020). The temperature the sample is preheated to is chosen so that one or several peaks in a glow curve are removed during the preheating. Any peak which appears at a temperature below the preheating temperature following illumination and subsequent heating is a PTTL peak since it is induced by optical transfer of electrons from electron traps (donors) not emptied during

preheating. For convenience we refer to the deep electron source traps as donors and the lower temperature electron traps where electrons are phototransferred to as acceptors. Although this generic description assumes that higher-temperature lying electron traps will act as donors and the lower-temperature ones as acceptors during PTTL, it has been shown that this is not always the case (Chithambo et al., 2019; Chithambo and Dawam, 2020). As a case in point, studies of PTTL in annealed synthetic quartz (Chithambo and Dawam, 2020) as well as in natural quartz annealed at 1000°C (Chithambo et al., 2019) have shown that some supposed donors can act as acceptors for certain combinations of preheating temperature and duration of optical exposure. Kalita and Chithambo (2017e) studied the PTTL of unannealed Al_2O_3:C,Mg and reported the presence of three PTTL peaks at 45, 74 and 163°C respectively for a heating rate of 1°C/s and illumination by 470 nm blue light. From that study, Kalita and Chithambo (2017e) concluded that the induced PTTL peaks follow the same order of kinetics as the corresponding peaks in the conventional TL glow curve. This work follows in the same vein as that of Chithambo et al. (2017a) which reported on a systematic analysis of PTTL in α-Al_2O_3:C by relating each PTTL peak to sets of donors the number of which was determined by experiment. The mathematical formulation here is completely based on experimental results. PTTL of Al_2O_3:C,Mg was described in qualitative terms (Kalita and Chithambo, 2017e, 2019). The aim of this chapter is to describe the PTTL of Al_2O_3:C,Mg both qualitatively and mathematically by relating the PTTL to a system of donor electron traps. The PTTL time-response profiles are described using systems of an acceptor and, donors the number of which depends on the preheating temperature.

7.2 Analysis of PTTL-time profiles

7.2.1 Glow curve characteristics

Figure 7.1 shows a glow curve measured after irradiation to 2.0 Gy (solid symbols). As determined by thermal cleaning, the glow curve has eight peaks at 43.3±0.1, 73.0±1.4, 164.7±1.3, 195.3±1.7, ∼246, 284±1.9, ∼336 and 374.4±3.0°C. The peaks are referred to hereafter as I through VIII respectively. These are identified in Fig. 7.1 except peaks V and VII which are indistinct here. A glow curve measured after preheating to 60°C, intended to remove peak I, and illumination for 10 s is shown for comparison. Peak I is reproduced under phototransfer as indicated.

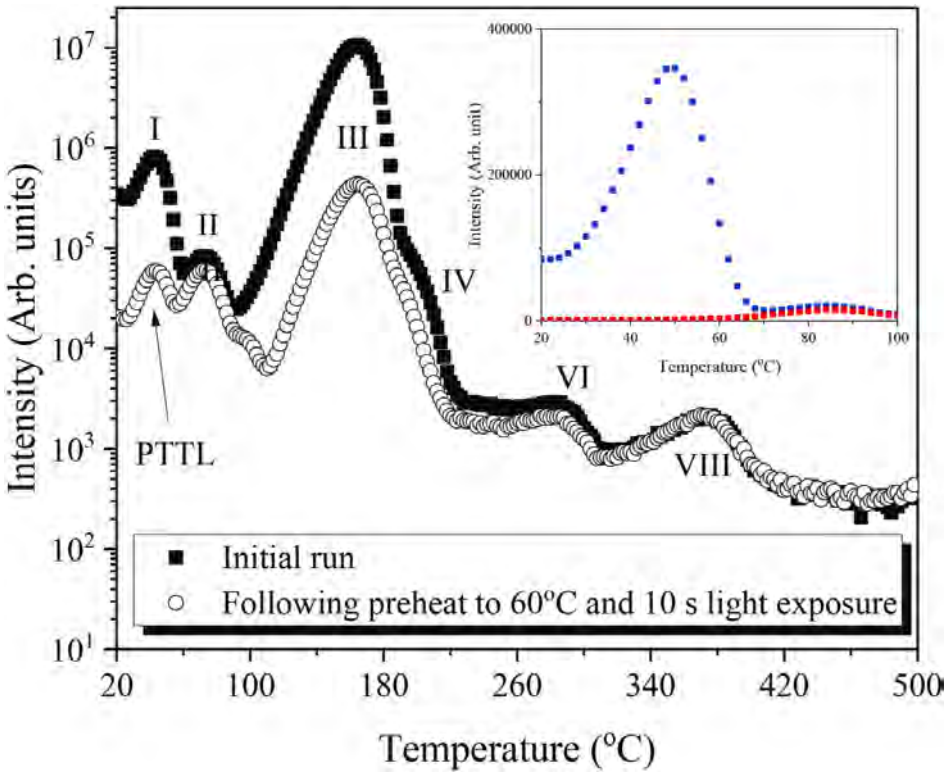

Figure 7.1: Glow curves of unannealed Al_2O_3:C,Mg measured at 1°C/s following irradiation to 2.0 Gy (solid symbols) and another obtained after preheating to 60 °C and subsequent illumination for 10 s (open symbols). The positions of clear peaks except peaks V and VII which are not obvious here, are shown for reference. The inset shows, for comparison, separate glow curves measured with and without preheating where the one with preheating omitted the light exposure step. This is intended to emphasize the nature of the reproduced peak (open circles) as being due to PTTL only.

7.2.2 Determining the role of electron traps as acceptors or donors using partial heating

The role of each electron trap either as an acceptor or a donor in the observed PTTL was investigated by partially heating and illuminating the irradiated sample. The procedure is known as pulse annealing. The technique was to progressively increment the preheating temperature used prior to illumination and to monitor the intensity (as peak heights) of any peaks present after the preheat. In the measurements, the unannealed sample was preheated from 60 to 600°C at 20°C intervals after irradiation and illuminated for 10 s each time. Each such pulse annealing measurement was repeated three times and the intensities plotted are averages from these measurements. For ease of reference, any PTTL peaks corresponding to peaks I-VIII will be referred to as A1, A2, A3....

7.2.2.1 Effect of partial heating on peaks I and II

Figure 7.2(a) shows the dependence of the PTTL intensity on the preheating temperature for peaks A1 and A2 at 43 and 73°C respectively.

The intensity of peak A1 increases with preheating temperature between 80 and 140°C. Peak A1 then decreases rapidly in intensity thereafter from 140 to 200°C. Notably, peak A2 decreases in intensity over the same preheating temperatures. Beyond 200°C, the intensity of both peaks continues to decrease but do so very slowly. For preheating temperatures beyond 400°C, it is no longer possible to measure peaks A1 and A2. The behaviour of peak A1 between 80 and 140°C requires comment. The intensity of an acceptor peak should remain stable as long as donors are not significantly depleted or decrease if they are. In that sense, the possible donors for peak A1 correspond to electron traps for peaks II - VIII. Preheating to 140°C only affects the electron trap for peak II at 73°C. Since the intensity of peak A1 increases as peak II is removed, the change must be due to a decreased role of the electron trap for peak II as a competitor for electrons that should otherwise produce peak A1. Examples of similar competition effects have been observed and discussed for PTTL in natural and synthetic quartz (Chithambo et al., 2019; Chithambo and Dawam, 2020). Peak II (at 73°C) decreases in intensity between 80 and 120°C. This implies that peak II acts as a donor for peak A1 over these temperatures. The decrease in intensity of PTTL peaks A1 and A2 up to 180°C must be due to the progressive depletion of charge from the electron trap of peak III. Increasing the preheating temperature from 200°C onwards has little effect on the PTTL intensity of peaks A1 and A2. Thus although the putative donors for PTTL peaks A1 and A2 are the electron traps for peak III-VIII, the main donor is evidently the electron trap for peak II.

7.2.2.2 Effect of partial heating on peak III

Figure 7.2(b) shows the influence of preheating on peak III. This peak appears at 165°C but is only removed and reproduced under PTTL following preheating beyond 180°C. The possible donors for its PTTL are the electron traps for peaks IV-VIII. Although this peak is not a PTTL peak until after preheating beyond 180°C, its intensity slightly increases with preheating initially. Such an increase is counter-intuitive for a supposed donor for PTTL recorded at peaks A1 and A2. This means one of two things. Either the electron trap for peak III is itself a competitor or the change also reflects the decreased role of another competitor trap which in this case is the electron trap for peak A2. Beyond 180°C, where peak III is reproduced as PTTL, that is, as A3, there is a sharp decrease in intensity. This decrease

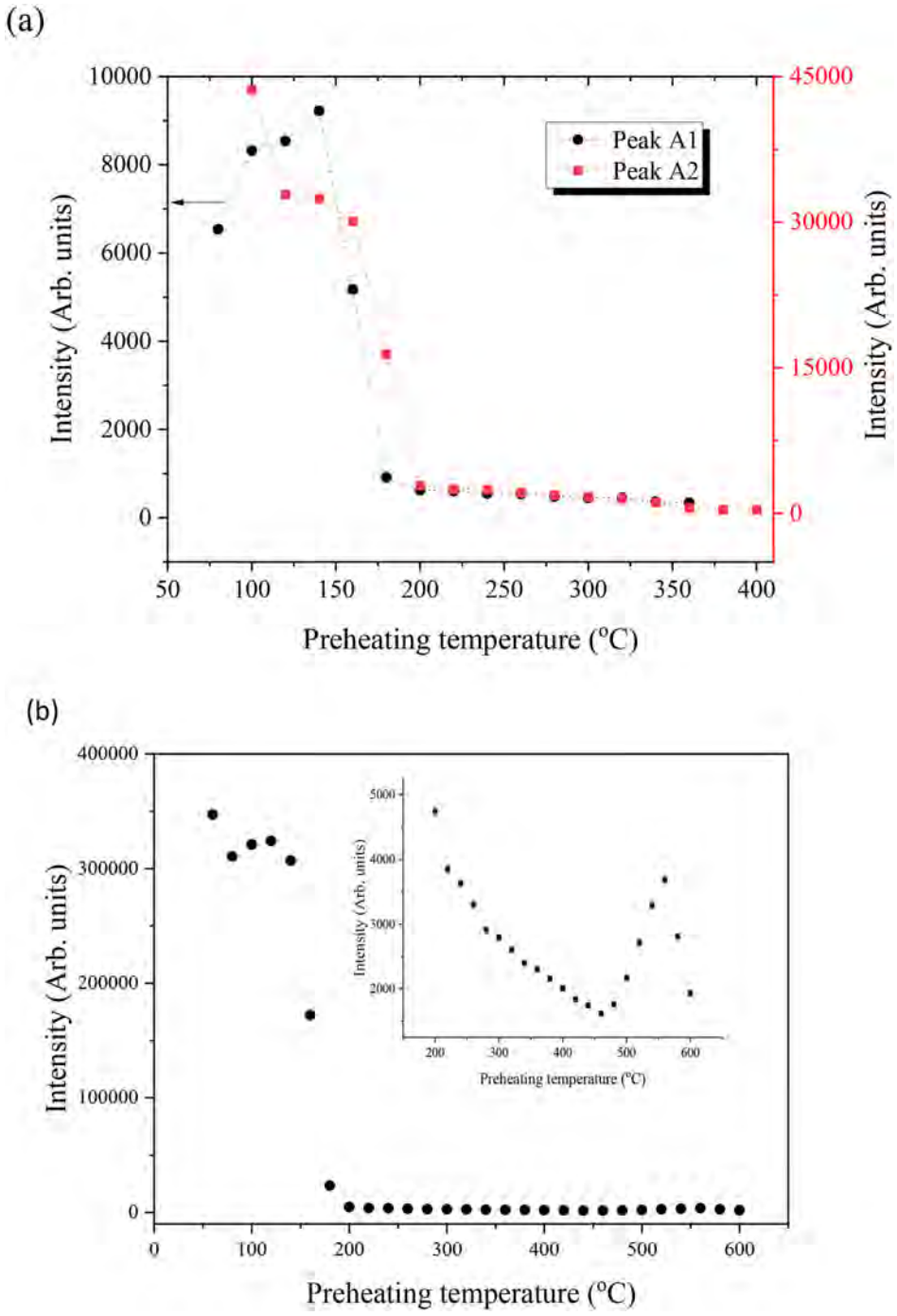

Figure 7.2: Dependence of PTTL intensity on preheating temperature for peaks A1 and A2 (a) and peak III (b). The dotted lines in (a) are only visual guides. The sudden increase in signal beyond 500°C in (b) is ascribed to the effect of deep hole traps.

is likely caused by depletion of charge at supposed donors IV-VIII. The inset to Figure 7.2(b) shows the region from 200 to 600°C whose fine detail is obscured

by the high intensity signals in the main graph. The PTTL intensity decreases monotonically from 200 to 460°C. Peak A3 then becomes more intense reaching maximum emission at 560°C before decreasing with further preheating up to 600°C. Although PTTL observed beyond 500°C can be associated with deep electron traps, it is unlikely that this would cause a sudden and significant increase in signal as shown in Figure 7.2(b) inset. We will explain later how the result is associated with a deep hole trap.

7.2.2.3 Effect of partial heating on peak IV

Peak IV, which is on the falling edge of peak III, is reproduced under phototransfer for certain combinations of preheating temperature and duration of illumination. However, the peak was found unsuitable for analysis because it could not be clearly isolated.

7.2.2.4 Effect of partial heating on peaks V-VIII

Peaks V-VIII are not reproduced under phototransfer.

7.2.3 Qualitative description of the dependence of PTTL intensity on illumination time

The dependence of PTTL intensity on illumination time is discussed for peaks A1, A2 and A3. Although peak IV is also reproduced under phototransfer, the resultant peak (A4) could not be properly isolated for such a study. For completeness and to help explain the PTTL, the influence of illumination on the intensity of the supposed donor peaks that is, any peaks not removed by preheating is also reported. The purpose of this is to confirm whether any assumed donors act as such and how important their involvement in the process is. In the measurements, an irradiated and subsequently preheated sample was illuminated by 470 nm blue light to different durations.

7.2.3.1 PTTL of peak I after preheating to 60°C

In the first test to measure the illumination-time dependence of peak A1, the sample was preheated to 60°C. Figure 7.3 shows the dependence of PTTL intensity on illumination time for peak A1.

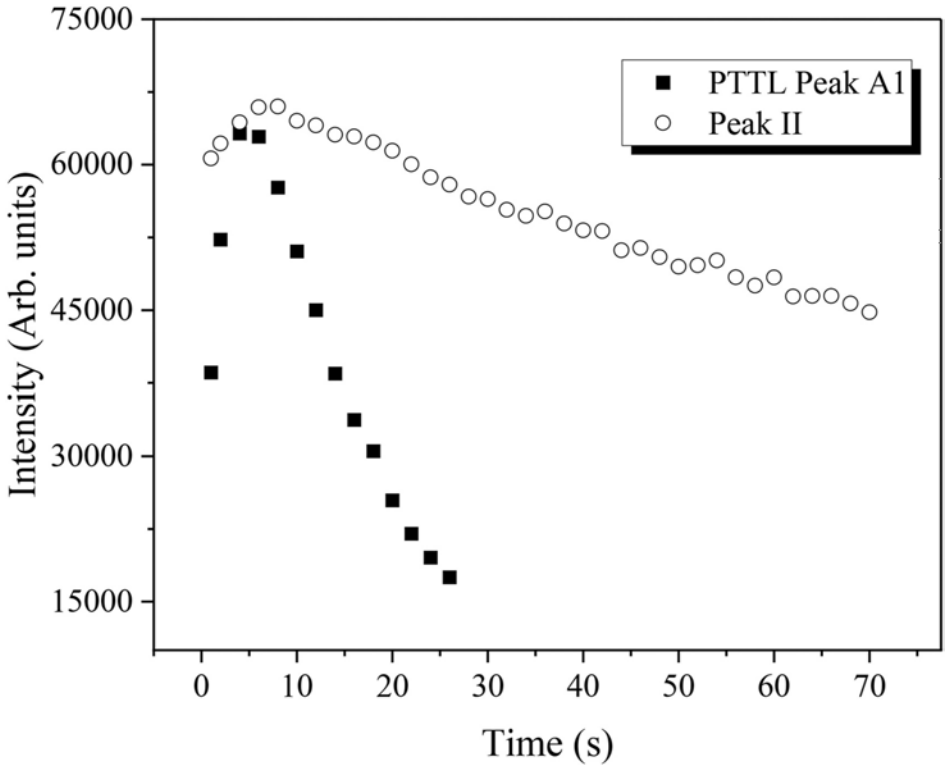

Figure 7.3: Dependence of intensity on duration of illumination for peaks A1 and II.

The intensity of peak A1 goes through a maximum with illumination time up to 26 s. For longer illumination periods than this, peak A1 can no longer be distinguished from peak II at 73°C. The possible donors for the PTTL of peak A1 are electron traps for peaks II-VIII since these are not removed by preheating to 60°C. For comparison, the behaviour for peak II is also shown in Figure 7.3. The intensity of this peak increases with illumination time up to 6 s before decreasing thereafter. This profile suggests that at the start of illumination the electron trap responsible for peak II acts as an acceptor but with further illumination this trap serves as a donor for peak A1. Figure 7.4 shows the dependence of TL intensity on illumination time for the other donor peaks, namely, III and IV (Figure 7.4(a)), and in Figure 7.4(b) for donors V, VI and VIII.

The intensity of all these peaks decreases with illumination time. Of all these peaks, the most intense one is peak III. To illustrate this point, for 2 s illumination, the intensity of peaks II and IV is only 2% that of peak III. The intensities of peaks V, VI and VIII are even lower at only about 0.05% that of peak III. Thus the main donor for peaks A1 and A2 is the electron trap for peak III. The contribution of the donor peaks as identified (and possibly of VII as well) to the PTTL of peak A1 is negligible.

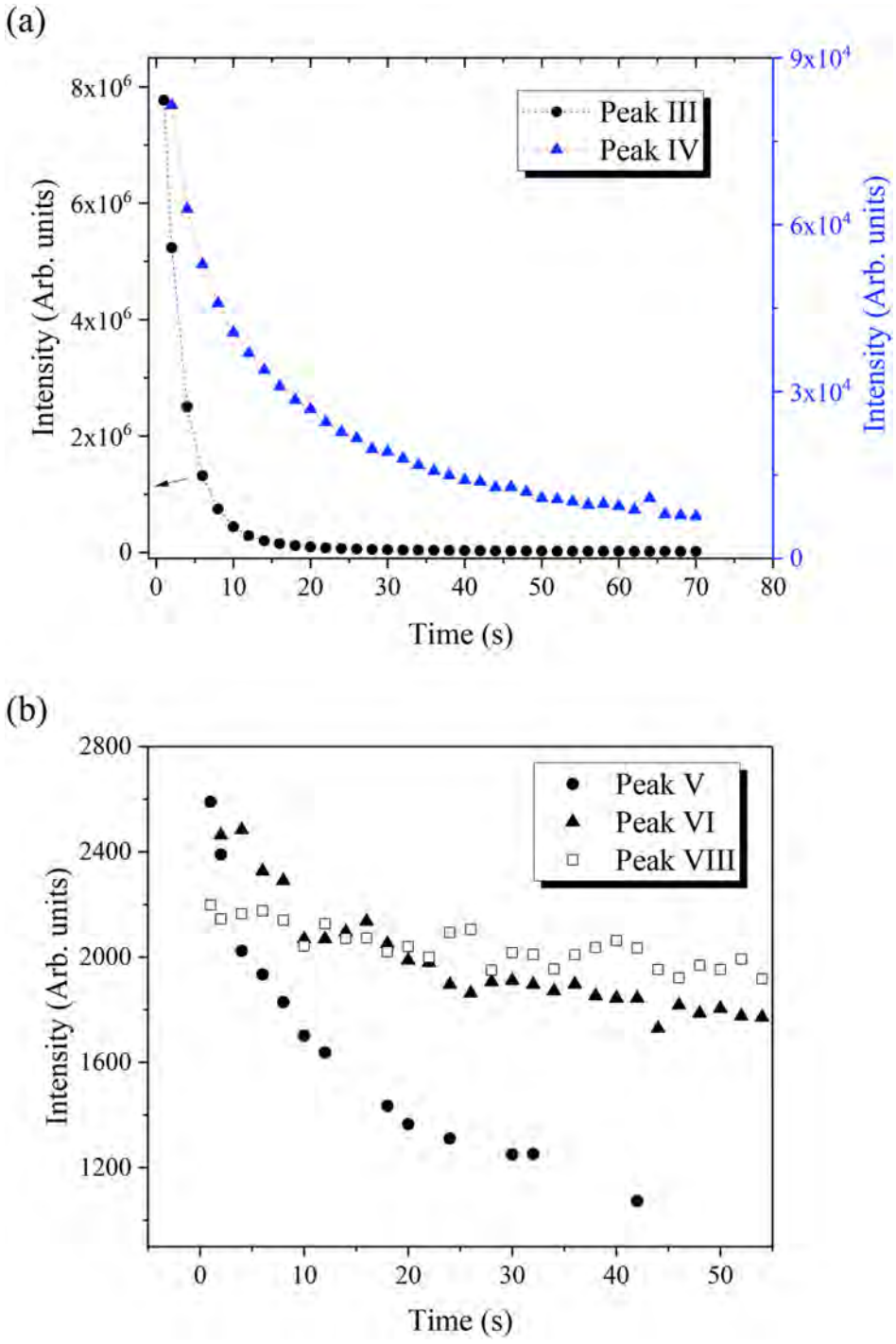

Figure 7.4: The change of TL intensity with illumination time for peaks III and IV (a) and for peaks V, VI and VIII (b). The dashed lines are only visual guides.

7.2.3.2 PTTL from peaks I and II after preheating to 100°C

Preheating to 100°C removes peaks I and II at 43 and 73°C respectively. These two peaks are reproduced by phototransfer (as A1 and A2) at the same positions.

Figure 7.5(a) shows that the intensity of peaks A1 and A2 both initially increase with illumination and then decrease thereafter. Figure 7.5(b) shows the dependence of TL intensity on illumination time for peaks III and IV and in the inset, for peaks VI and VIII.

Peak VII is indistinct, could not be monitored, and so is not discussed. The intensity of all peaks shown in Fig. 7.5(b) decrease with illumination time confirming their role as possible donors for the PTTL at peaks A1 and A2. Comparing intensities, one finds that the main contributor electron traps for PTLL peaks A1 and A2 correspond to peaks III and IV with peak III being dominant.

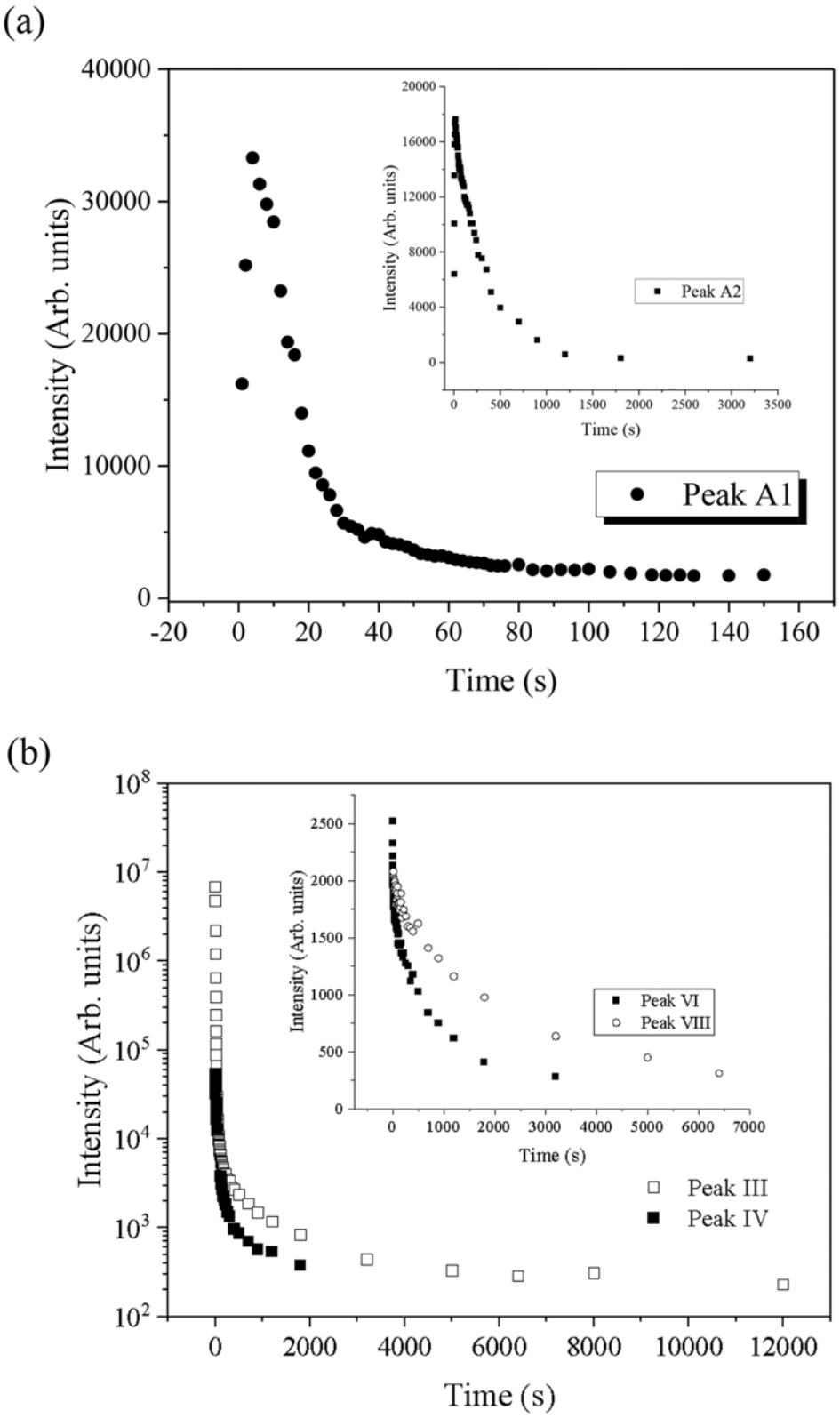

Figure 7.5: The change of TL intensity with illumination time for peak A1 following preheating to 100°C and in the inset, for peak A2 (a). The same feature for peaks III and IV, and in the inset for peaks VI and VIII (b). Peak V was indistinct and could not be monitored.

7.2.3.3 PTTL after preheating to 300°C

When the sample is preheated to 300°C, peaks I-VI are removed by preheating. However, only peaks I, II, III and IV are reproduced by phototransfer. This occurs for various combinations of preheating temperature and duration of illumination as shown in Figure 7.6.

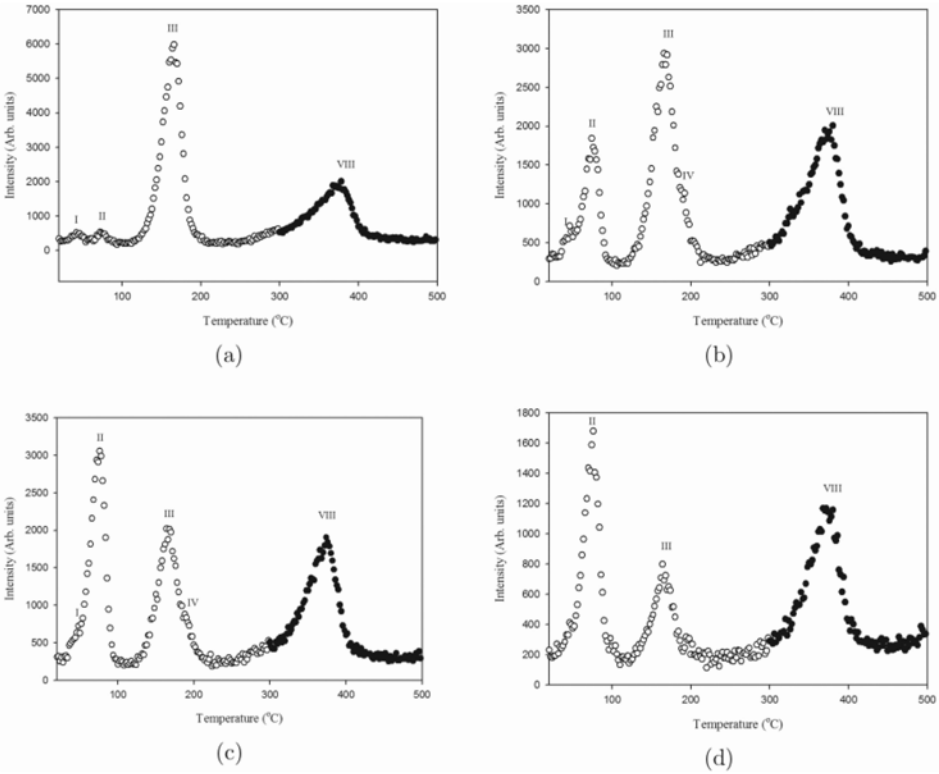

Figure 7.6: Glow curves of unannealed Al_2O_3:C,Mg measured at 1°C/s following irradiation to 2 Gy, preheating to 300°C and illumination for 4 s (a) 40 s (b) 120 s (c) and 1200 s (d). The position of the otherwise indistinct peak IV is only included in (b) and (c) for reference.

Peak IV, which appears on the falling edge of peak III, is also reproduced for certain illumination times above 40 s but is otherwise indistinct and could not be analysed. Likewise, although peak I is reproduced by phototransfer, its intensity was too low to allow for a proper analysis of the dependence of its intensity on illumination time. Peaks V and VI are not reproduced by phototransfer.

Figure 7.7 shows the dependence of PTTL intensity on duration of illumination for peaks A2 and A3. Whereas the intensity of peak A2 displays the archetypal shape, that of peak III decreases monotonically.

The possible donors for this PTTL are electron traps corresponding to peaks VII and VIII. Of these only peak VIII could be monitored (see Figure 7.6) and its

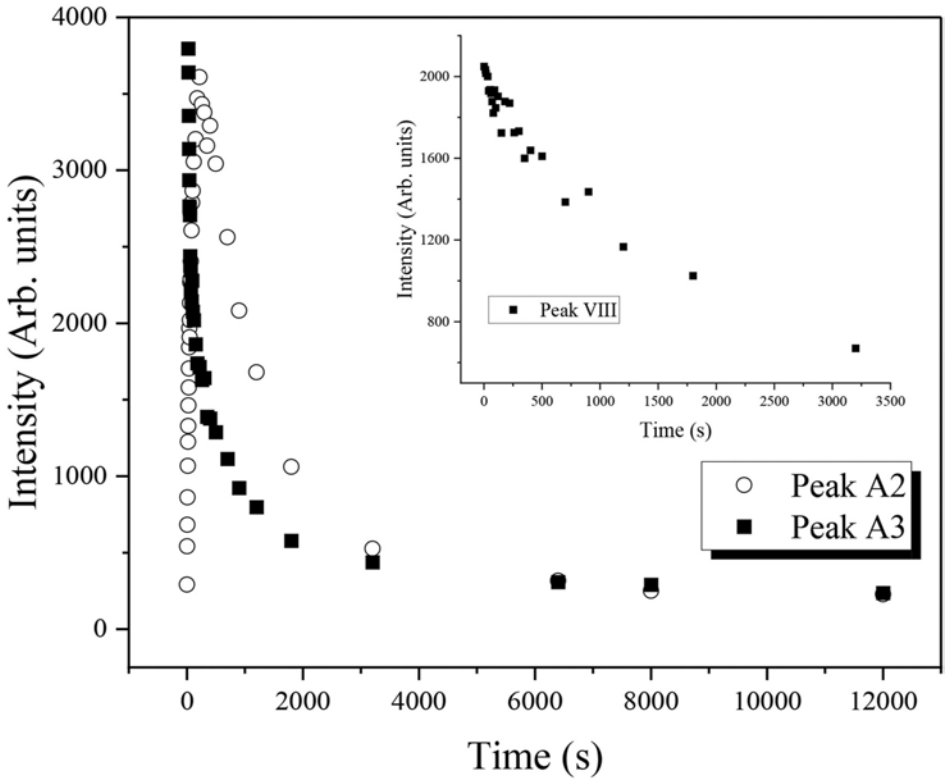

Figure 7.7: PTTL intensity against duration of illumination for peaks A1 and A2 following preheating to 300°C and, in the inset, the change in TL intensity with illumination time for peak VIII.

intensity decreases consistently with illumination time (Figure 7.7, inset).

7.2.3.4 PTTL after preheating to 400°C

Preheating to 400°C removes all peaks in the TL glow curve. Peaks I, II and III are regenerated by phototransfer (as A1, A2 and A3). However, except for peak A3, the intensities of the two other acceptor peaks were too low for analysis. The intensity of peak A3 goes through a maximum before decreasing at longer illumination times. The supposed donor in this case is the deep trap(s). The plot for the time-dependence of peak A3 is shown in Figure 7.8

7.2.4 Mathematical analysis of PTTL time-response profiles

The dependence of PTTL intensity on duration of illumination used for photo-transfer was discussed qualitatively in the preceding section. We will proceed to analyse the same mathematically. The analysis will be informed by experimental results presented in sections 7.2.2 and 7.2.3. To aid the discussion, Table 7.1 lists

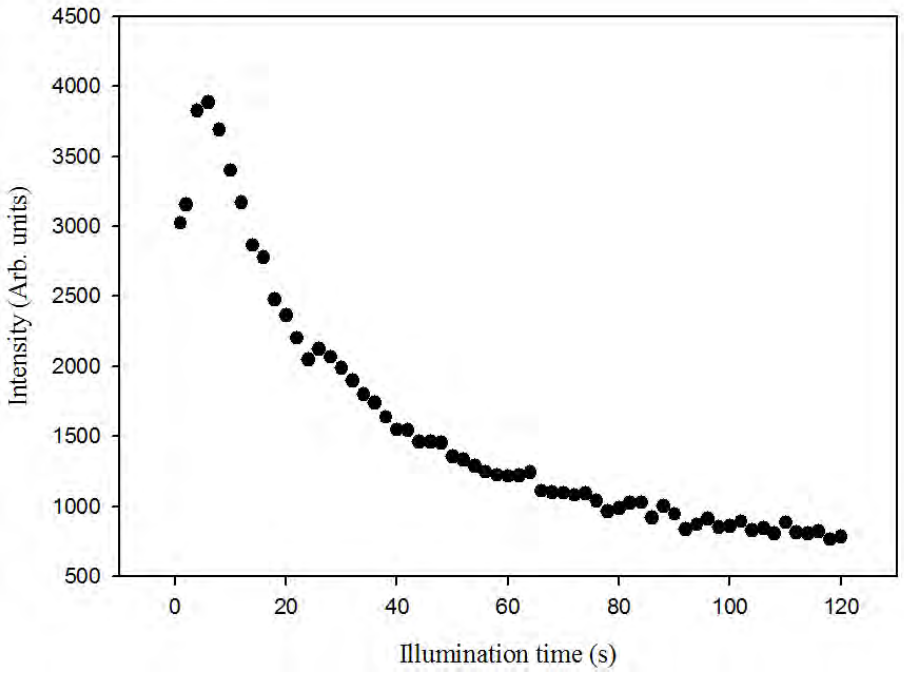

Figure 7.8: PTTL intensity against illumination time for peak A3 following preheating to 400°C.

the observed TL and PTTL peaks. Conventional TL peaks are labelled I-VIII. The PTTL peaks corresponding to these peaks are referred to as A1, A2, ... These are the same labels used thus far. The electron traps listed as 'possible donors' are the theoretically expected ones. This is because, in theory, the electron trap of any peak at temperatures beyond that of one that has been removed by preheating, can serve as a donor in the PTTL process. The main donors suggested by the partial heating experiment (section 7.2.2) and as reflected by PTTL time-response profiles (section 7.2.3) are listed separately in Table 7.1. The analysis will be based on the latter two lists rather than the ideal theoretical list. The concentration of trapped electrons at the i^{th} electron trap will be denoted by N_i and the optical stimulation probabilities as s_i. The equations describing the change in the concentration of trapped electrons are written for the illumination step only. Retrapping is neglected because, as has been shown several times previously, the peaks follow first-order kinetics (Kalita and Chithambo, 2017f,a,b,c). Each family of equations is unique to each system and has a particular solution. This solution is applied to the experimental data for that particular system. The main assumption as before (Chithambo et al., 2019; Chithambo and Dawam, 2020) is that only a portion of electrons released from a donor trap end up at the acceptor electron trap to produce PTTL. The method used here is the same one developed by Chithambo

et al. (2017a) and applied previously on quartz (Chithambo et al., 2018, 2019; Chithambo and Dawam, 2020). The method used here and elsewhere (Chithambo et al., 2017a, 2018, 2019; Chithambo and Dawam, 2020) should be distinguished from the kinetics-based method of say, Alexander and McKeever (1998) where non-linear rate equations are used to relate the concentration of holes at a recombination centre to the concentration of electrons at electron traps and in the conduction band. Here, the transport of electrons involved in the PTTL process is described at the irradiation, preheating, illumination and heating stages. The coupled non-linear differential equations developed this way do not have analytical solutions and thus require numerical approximations to solutions. These numerical solutions are then used to generate plots of PTTL intensity as a function of illumination time by considering various assumptions such as, say, negligible retrapping or the number of electron traps involved in the process. Our approach differs from this method in several respects. We formulate differential equations only at the illumination stage. These equations describe the transfer, to an acceptor, of a proportion of electrons optically stimulated from a donor. The number of donors for any acceptor peak is determined by experiment. The sets of these equations have analytical solutions which are then applied directly to experimental data.

Table 7.1: A summary of TL peaks, their corresponding PTTL peaks, donors and photoionization cross-section (P. cross-section (cm^2)). In the study corresponding to 300 °C, only peak III could be monitored as a donor.

	TL	PTTL			P. cross-section (cm^2)				
Peak label	T_m (°C)	Peak label	Preheating temp (°C)	Possible donors	Main donor[a]	Main donor[b]	Acceptor	Donor	Donor
I	43	A1	60	II III IV V VI VII VIII	III	III	3.26e-18	3.92e-19	
			100	II III IV V VI VII VIII	III	III IV	1.95e-18	6.93e-19	4.82e-20
			300						
II	73	A2	100	III IV V VI VII VIII	III	III IV	2.17e-18	2.17e-18	1.53e-20
			300			VII VIII	4.70e-21	8.52e-20	
III	165	A3	300	IV V VI VII VIII	IV V VI	VII VIII	5.25e-18	2.42e-19	4.70e-21
			400	DT	DT	DT	5.44e-18	3.10e-19	4.70e-21
IV	195	A4	300	N/A	N/A	N/A			
V	246	N/A			N/A	N/A			
VI	284	N/A			N/A	N/A			
VII	336	N/A			N/A	N/A			
VIII	374	N/A			N/A	N/A			

[a] ✓ From pulse annealing study.
[b] ✓✓ From time-response study.

7.2.4.1 Time-dependence of PTTL after preheating to 60°C

Preheating to 60°C followed by illumination produces only peak A1. As shown in Table 7.1, there is only one dominant donor for the PTTL, the electron trap for peak III. Therefore, the PTTL time-response profile for peak A1 can be described in terms of a system of one acceptor and one donor with rate equations as follows:

$$\frac{dN_3}{dt} = -s_3 N_3 \tag{7.1}$$

$$\frac{dN_1}{dt} = -s_1 N_1 + \alpha_3 s_3 N_3 \tag{7.2}$$

where α_3 is a constant of proportionality and all other parameters are as defined before. Equation (7.1) describes the loss of electrons from the donor. Equation (7.2) takes into account not only the transfer of electrons from the donor but the possibility of loss due to illumination at the acceptor. The solution of the coupled set Eqs. (7.1) and (7.2) is

$$N_1(t) = A(e^{-s_3 t} - e^{-s_1 t}) \tag{7.3}$$

where $A = \alpha_3 s_3 N_{3i}/(s_1 - s_3)$ and N_{3i} is the initial concentration of trapped electrons at the donor trap at the start of illumination. Increasing the number of donors to two by considering both peaks III and IV as contributors did not produce any improvement in the fit. This supports the qualitative conclusion that although in theory there are 7 donors, the main contributor to the PTTL is the electron trap for peak III.

7.2.4.2 PTTL following preheating to 100°C

When the sample is preheated to 100°C, only peaks A1 and A2 are reproduced under phototransfer. The main contributors to the PTTL correspond to electron traps for peaks III and IV. Thus in this case we have two separate systems of one acceptor and two donors. Therefore the rate equations describing charge transfer responsible for peak A1 or A2 are

$$\frac{dN_3}{dt} = -s_3 N_3 \tag{7.4}$$

$$\frac{dN_4}{dt} = -s_4 N_4 \tag{7.5}$$

$$\frac{dN_j}{dt} = -s_j N_j + \gamma_3 s_3 N_3 + \gamma_4 s_4 N_4 \tag{7.6}$$

where γ_3 and γ_4 are proportionality constants, (s_j, N_j) is either (s_1, N_1) or (s_2, N_2) depending on which one of the two PTTL peaks is considered. The solution to the coupled first order linear differential Eqs. set (7.4-7.6) is

$$N_j(t) = A_1(e^{-s_3 t} - e^{-s_j t}) + A_2(e^{-s_4 t} - e^{-s_j t}) \tag{7.7}$$

where $A_1 = \gamma_3 s_3 N_{3i}/(s_1 - s_3)$ and $A_2 = \gamma_4 s_4 N_{4i}/(s_1 - s_4)$.

7.2.4.3 PTTL following preheating to 300°C

Preheating to 300°C removes peaks I to VI. Peaks A1, A2, A3 and A4 are reproduced by phototransfer. However, only peaks A2 and A3 were sufficiently intense and distinct for analysis. The only possible donors in this case are the electron traps for peaks VII and VIII (see Table 7.1) although in practise peak VII could not be monitored. Experimental tests (see section 7.2.3.3) suggest that the electron trap for peak VIII is the only dominant donor. On this basis, the time-response profile of the PTTL of peaks A2 and A3 were analysed using the two options of one acceptor and one donor (Eq. 7.3) or one acceptor and two donors (Eq. 7.7). It was found that only the second option could properly describe the result. In this particular case, the PTTL of either peak A2 or A3 cannot result from a single donor.

7.2.4.4 PTTL following preheating to 400°C

Preheating to 400°C removes all peaks in the conventional TL glow curve. Although peaks I, II and III are reproduced by phototransfer, only peak A3 was found suitable for further analysis. In theory, its PTTL corresponds to a simple system of one acceptor and one donor, a deep electron trap, and should be described by an expression similar to Eq. (7.3). However, we could not obtain a satisfactory fit by considering a system consisting of one acceptor and one donor. The lowest possible number of donors which yielded a satisfactory fit was two using an expression of the same form as Eq. (7.7). We therefore assume that the PTTL following preheating to 400°C can be ascribed to the contribution of at least two deep electron donor traps.

7.2.5 Applications of the mathematical model

Figures 7.9 and 7.10 show applications of the models to experimental data. Figure 7.9(a) shows the PTTL time-response profile of peak A1 after preheating to 60°C. The solid line through data is the best fit of Eq. (7.3). Figure 7.9(b) shows the result for peak A1 after preheating to 100°C fitted with Eq. (7.7). The best fit of the same expression on peak A2 after preheating to 100°C and to 300°C are shown in Figures. 7.9(c) and 7.9(d).

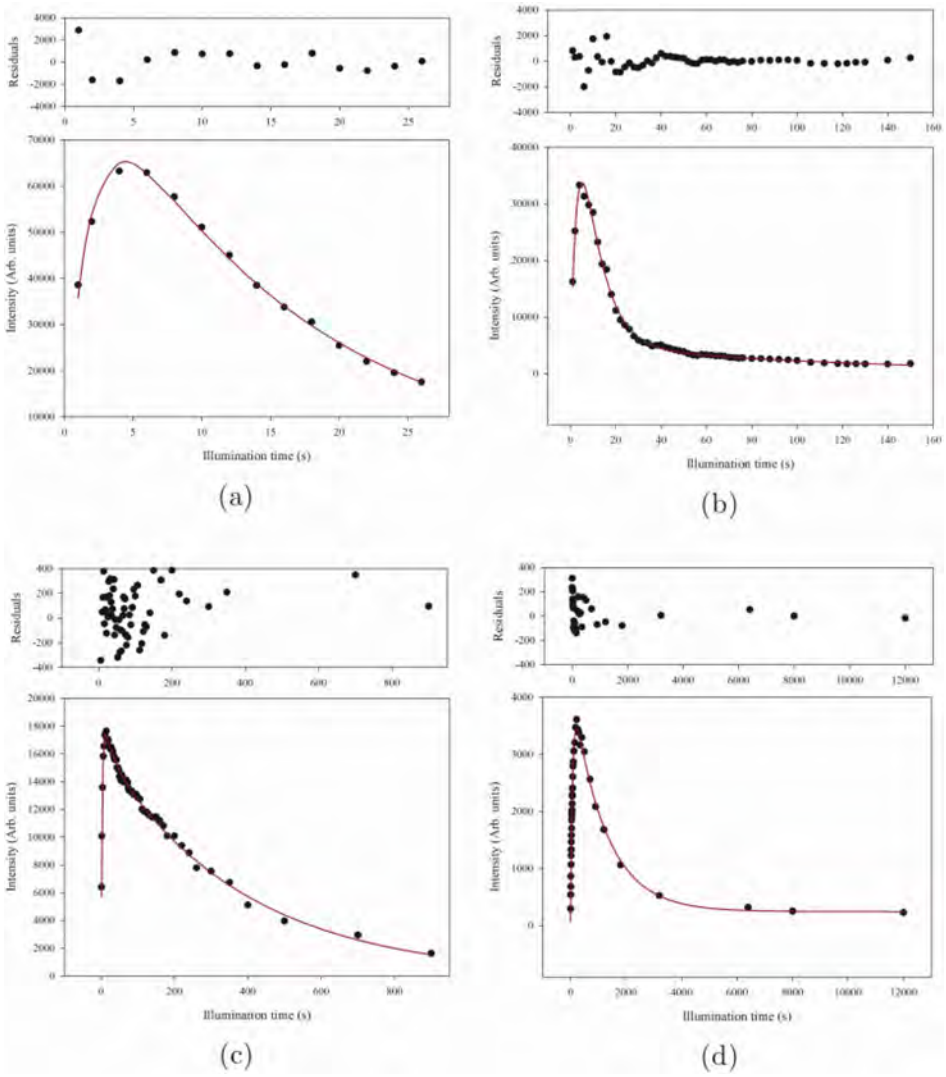

Figure 7.9: PTTL intensity against duration of illumination of peak A1 following preheating to 60 °C (a) and to 100 °C (b) the change for peak A2 following preheating to 100 °C and to 300 °C (d). All data is shown fitted with Eq. (7.7) except for (a) with is fitted with Eq. (7.3)

The PTTL time-response profile of peak A3 after preheating to 300°C and 400°C are shown in Figures. 7.10(a) and 7.10b respectively. Both are shown fitted with

Eq. (7.7). In all cases, except perhaps for Figure. 7.10(a), the experimental data is satisfactory described by the models as evident in the residuals fluctuating about zero.

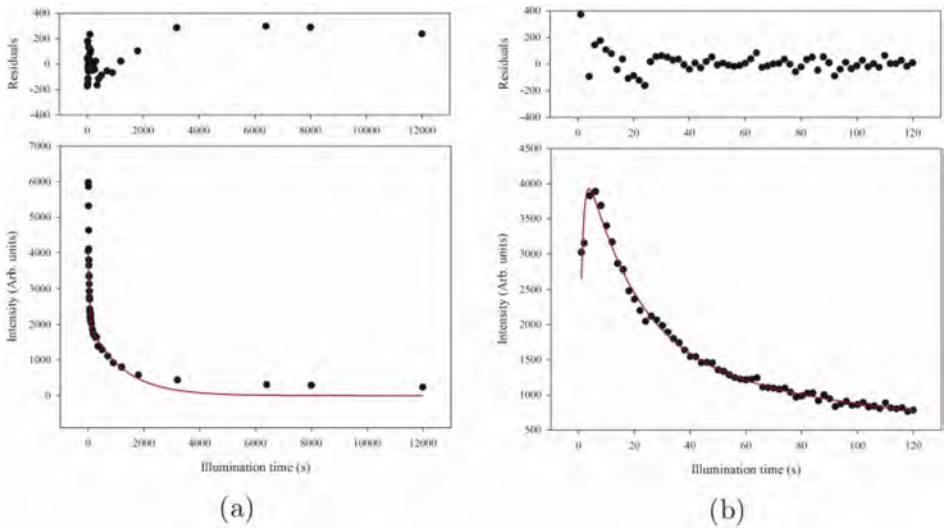

Figure 7.10: PTTL intensity against duration of illumination of peak A3 following preheating to 300 °C (a) and to 400 °C (b).

The stimulation rate $s = \Phi\sigma$ where Φ is the incident photon flux and σ the photoionization cross-section, this provided a means to determine the latter. In this study, we had $\Phi = 1.70 \times 10^{17}$ cm^{-2} s^{-1}. Examples of values of s are $s_1 = 0.5547 \pm 0.0253 s^{-1}$ and $s_3 = 0.0667 \pm 0.0021 s^{-1}$ in the fit for peak A1 after preheating to 60°C. The photoionization cross-section calculated for the various peaks are included in Table 7.1 and range between 10^{-21}-10^{-18} cm^2. The inset of Figure 7.2(b) showed a notable response of PTTL to preheating. Peak A3 increases with preheating up to 560°C before decreasing with further preheating up to 600°C. As stated, this sudden and significant increase in signal is unlikely to be associated with deep electron traps. Yukihara et al. (2003) suggested that deep hole traps become unstable between ~530 and 600°C in Al_2O_3:C. We conclude that the same process is responsible for the result observed in Fig. 7.2(b) inset. A similar type of generation of holes was used by Chithambo (2004) to explain the dose response in Al_2O_3:C. Heating in this temperature region produces a large number of holes. Some of these holes are captured at F centres converting them to F^+ centres. As known, the recombination of an electron with an F^+ centre produces an excited F centre. Luminescence, including TL, at 420 nm results following relaxation of the electron from an excited 3P to the 1S ground state at the F-centre McKeever et al. (1995). Therefore the TL or PTTL intensity in this case reflects changes in the concentration of holes owing to preheating between 500 and 600°C as observed. To our knowledge, this is the first demonstration of involvement of deep

hole traps in the PTTL of Al_2O_3:C,Mg. As a final point, we note the behaviour of peak II in Figure. 7.3. The intensity of this peak does not decrease consistently with illumination as expected of a donor but instead increases for the first 6 s before the expected decrease appears. This behaviour is classified as a competition effect. This is defined as processes that enhance or depress the capture of charge at electron traps during illumination and how this affects the output from acceptors or contribution of donors (Chithambo et al., 2019; Chithambo and Dawam, 2020). The conventional interpretation of PTTL assumes that when electrons are released from donor traps during illumination, they can move to a recombination centre, get re-trapped or transit to acceptors. Although this idealized description aids the formulation of mathematical expressions to describe phototransfer, the real effects are far more complex and affected by competition effects. These have been investigated in detail in quartz (Chithambo et al., 2019; Chithambo and Dawam, 2020) and were briefly discussed for PTTL in α-$A1_2O_3$:C (Chithambo et al., 2018). Competition effects in Al_2O_3:C,Mg may involve not only electron traps but also hole traps.

7.3 Summary

This chapter dealt with a comprehensive study of PTTL in unannealed Al_2O_3:C,Mg and developed a mathematical description of the observed PTTL dependence on illumination time. The experimental PTTL was described as separate systems of an acceptor and, donors the number of which is affected by various combinations of preheating and illumination. The systems were analysed as coupled sets of linear first order differential equations describing the charge transfer at the illumination step. Particular solutions were applied to experimental data. The study also revealed the presence and role of deep hole traps beyond 500°C which contribute to the PTTL observed for the unannealed sample. The study suggests that competition effects in Al_2O_3:C,Mg may involve not only electron traps.

Chapter 8

Illumination-time-dependent profiles of phototransferred thermoluminescence of α-Al_2O_3:C,Mg annealed at 700 and 900°C

This chapter reports the phototransferred thermoluminescence of α-Al_2O_3:C,Mg annealed at 700 and 900°C for 15 minutes each. Qualitative and quantitative description of the PTTL is presented. For a given PTTL peak, the number of donors depends on the preheating temperature. The PTTL time-response profiles are then mathematically described by systems consisting of an acceptor and donors. For ease of reference, samples annealed at 700 and 900°C are referred to as B and C. For each measurement of PTTL, the sample was irradiated to 3.0 Gy, preheated to a specific temperature and cooled down immediately thereafter. The sample was then exposed to 470 nm blue light of optical power density 72 mW/cm^2 for a time during which some electrons were transferred from deeper traps to emptied shallower ones. Following light exposure, the sample was heated again to monitor PTTL. All illuminations were performed at 20°C and all measurements carried out at 1°C/s.

8.1 Glow curve characteristics

Figure 8.1 shows glow curves of samples B and C measured at 1°C/s following irradiation to 3.0 Gy.

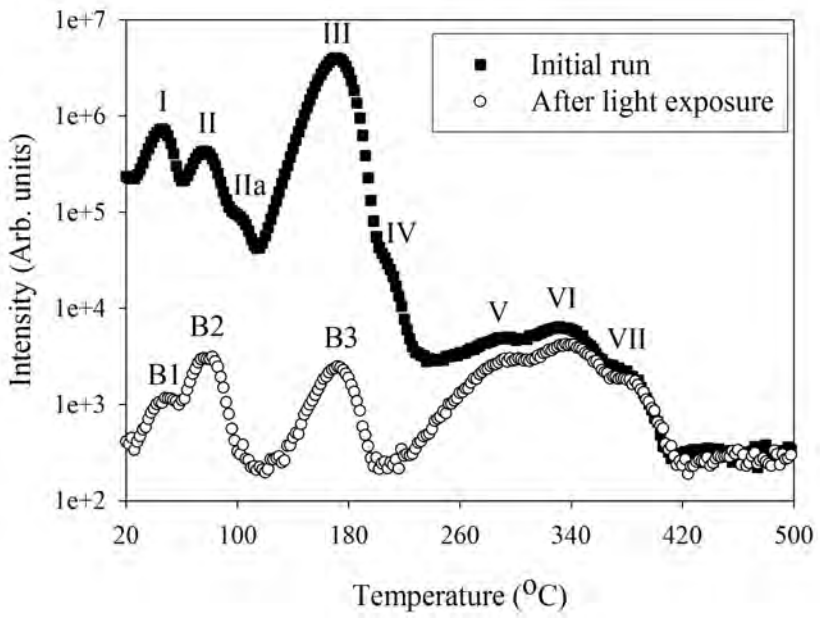

a

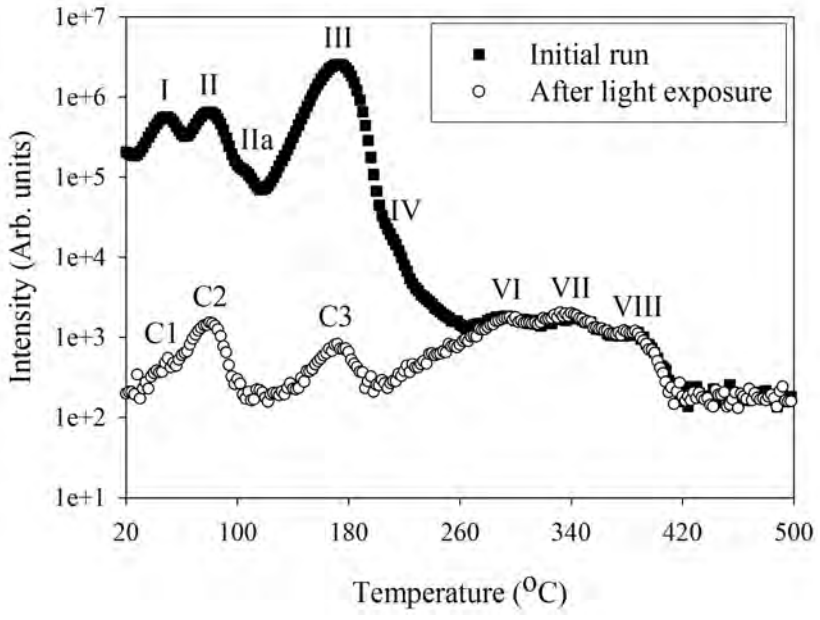

b

Figure 8.1: Glow curves of annealed α-Al_2O_3:C,Mg measured at 1°C/s following irradiation to 3.0 Gy for (a) sample B and (b) sample C. The glow curves recorded after preheating to 260°C and subsequent illumination for 12 s are represented with the open symbols. PTTL peaks B1, B2 and B3 are observed for sample B whereas PTTL peaks C1, C2 and C3 are found for sample C.

The glow curve of sample B has eight peaks at 46, 76, 100, 170, 199, 290, 330 and 375°C respectively. For sample C, the peaks are at 49, 80, 100, 174, 206, 235, 290, 335 and 375°C respectively. These peaks are referred to as I, II, IIa and III through VIII respectively. Examining the glow curves of each sample, we note the presence of peak IIa at 100°C. This peak has been reported in samples annealed at or above 700°C (Kalita and Chithambo, 2017b, 2018b,a). Glow curves measured after preheating to 260°C and illumination for 12 s are also shown for each sample. Preheating to 260°C is intended to remove peaks I-IV of sample B and peaks I-V of sample C. Peaks I, II and III of each sample are reproduced under phototransfer for this preheat as shown in Figures 8.1a and 8.1b.

8.2 Determining the role of electron traps as acceptors or donors using partial heating

Partial heating and subsequent light exposure were used to investigate the role of each electron trap either as an acceptor or a donor in the observed PTTL. Sample B (annealed at 700°C) and sample C (annealed at 900°C) were preheated from 60 to 600°C at 10°C intervals after irradiation to 3.0 Gy and illumination for 12 s each time. For ease of reference, PTTL peaks corresponding to peaks I-VII of sample B are referred to as B1-B7 whereas PTTL peaks corresponding to peaks I-VIII of sample C are referred to as C1-C8.

8.2.1 Effect of partial heating on peaks I, II and IIa

A PTTL peak say B1 is observed only after peak I of sample B has been removed by preheating. In Figures 8.2 and 8.3, the labels of the observed PTTL peaks are used. However it is understood that each of these peaks only becomes a genuine PTTL peak above a certain preheat temperature.

Figure 8.2a shows the dependence of the PTTL intensity on the preheating temperature for peaks B1, B2 and B2a. The intensity of peak B1 is constant with preheating temperature from 80 to 150°C and then decreases rapidly from 150 to 180°C. Beyond 180°C, the intensity of peak B1 decreases at slower rate. Peak B2 behaves in a manner similar to peak B1 with preheating temperatures from 100 to 310°C and then decreases at a faster rate. Peak II of sample B only becomes a PTTL peak after preheating above 90°C hence the initial decrease in intensity up to 100°C is expected because the corresponding trap is being depleted. For peak B2a, which appears near 100°C, the intensity decreases from 60 to 320°C. However, the rate of decrease varies within this interval. The most significant drop

in intensity occurs between 150 and 210°C. The behaviour of peaks B1, B2 and B2a within the interval 100-150°C is expected of an acceptor peak when donors are not significantly depleted. Beyond 180°C, the intensity of each peak continues to decrease but does so very slowly. Above 400°C, we could no longer measure peaks B1, B2 and B2a. Peak III of sample B, which is its main peak, is within 150-200°C where the intensity of each of the observed PTTL peak decreases rapidly. The electron trap of this peak is therefore a main donor to the electron traps associated with peaks I, II and IIa of sample B respectively.

Figure 8.2b shows the dependence of the intensity on preheating temperature for peaks C1, C2 and C2a. The intensity of each of these peaks decreases with preheating temperatures from 60 up to 200°C. Beyond 200°C, only peak C2 could still be measured and, its intensity decreases slowly up to 350°C. The influence of preheating temperature on the intensity of peaks C1, C2 and C2a shows that peak III (at 174°C) of this sample is the main donor of electrons for the associated acceptor traps. The PTTL-temperature profile of peak C2 suggests that electron traps above 200°C are also donors.

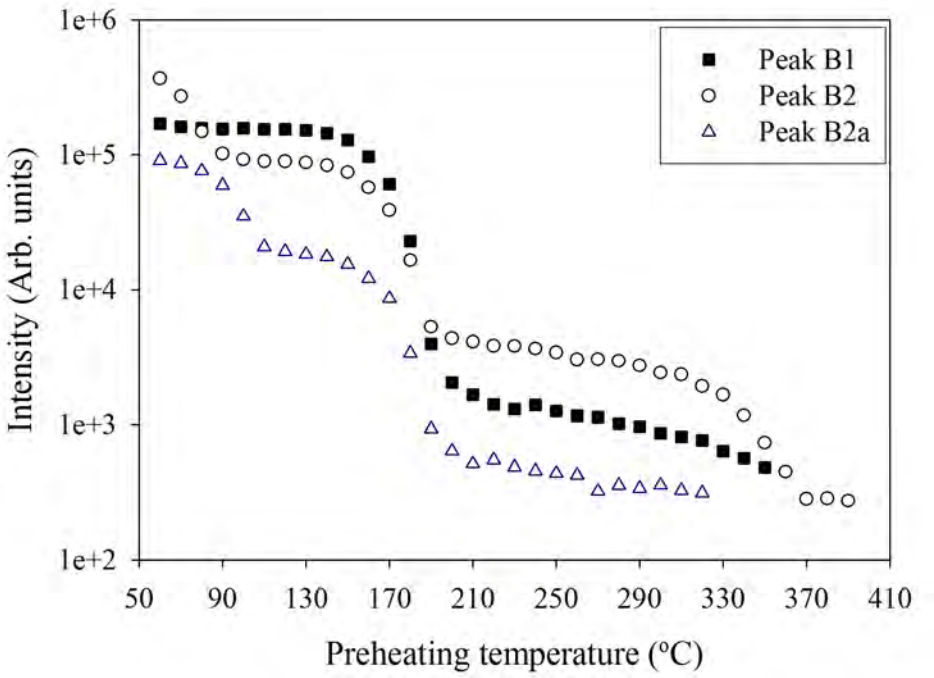

a

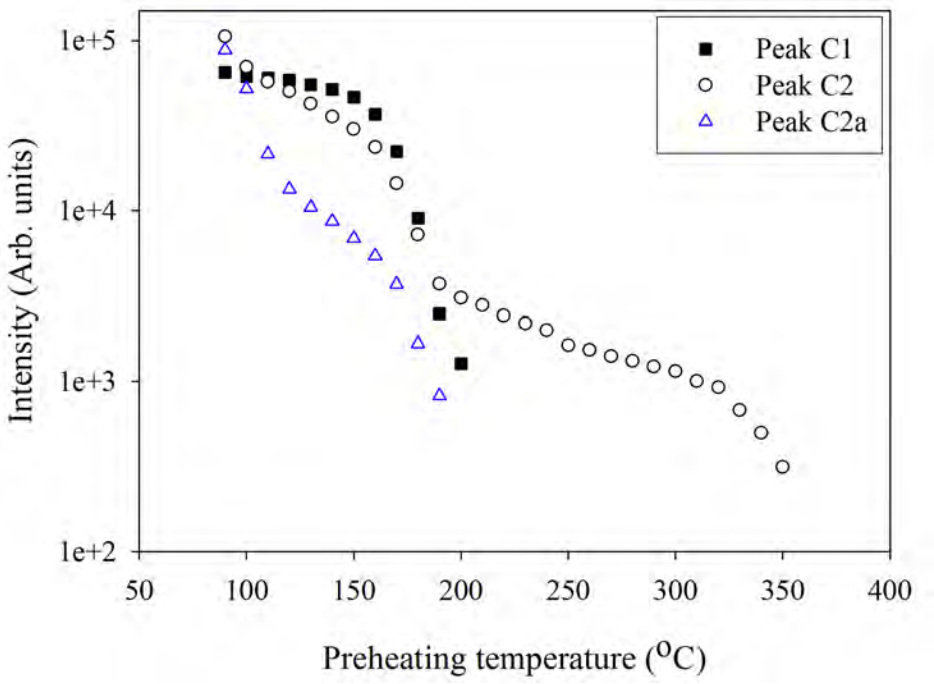

b

Figure 8.2: Dependence of PTTL intensity on preheating temperatures for peaks B1, B2 and B2a (a) and for peaks C1, C2 and C2a respectively.

8.2.2 Effect of partial heating on peak III

Figure 8.3 shows the dependence of PTTL intensity of peaks B3 and C3 on preheating temperature. The intensity of peak B3 is nearly constant with preheating temperatures from 100 up to 150°C as expected of an acceptor peak. From 150 to 200°C, the intensity of this peak decreases sharply since it is being depleted, that is acting as a donor. From 200°C, its intensity decreases at a slower rate. Peak C3 shows a similar profile. These results imply that the traps corresponding to peaks IV-VII of sample B or peaks IV-VIII of sample C are the donors. The significance of their contribution will be investigated by monitoring the intensity of these peaks with light exposure.

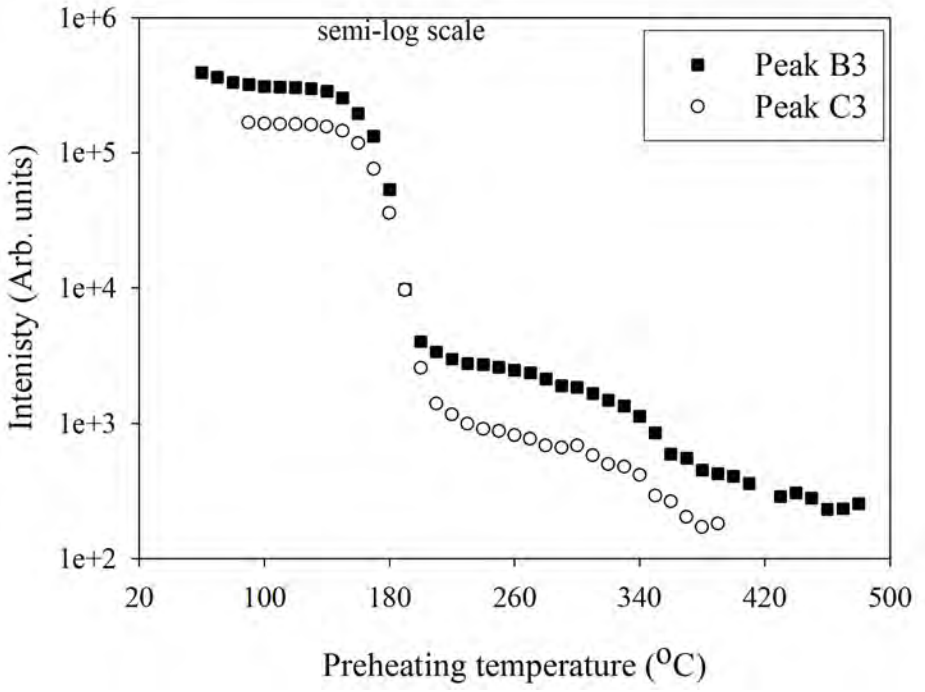

Figure 8.3: Dependence of PTTL intensity on preheating temperatures for peaks B3 and C3 respectively.

8.2.3 Effect of partial heating on peaks IV-VIII

Peak IV of sample B, which is on the falling edge of peak III is reproduced for preheating to 260°C and illumination for 7000 s or 10000 s respectively. However its intensity is low and it is not reproduced for higher preheats. Figure 8.4 shows a glow curve in which PTTL peak B4 is observed following preheating to 260°C and

illumination for 7000 s. None of peaks V-VII of sample B or of peaks IV-VIII of sample C are reproduced under phototransfer.

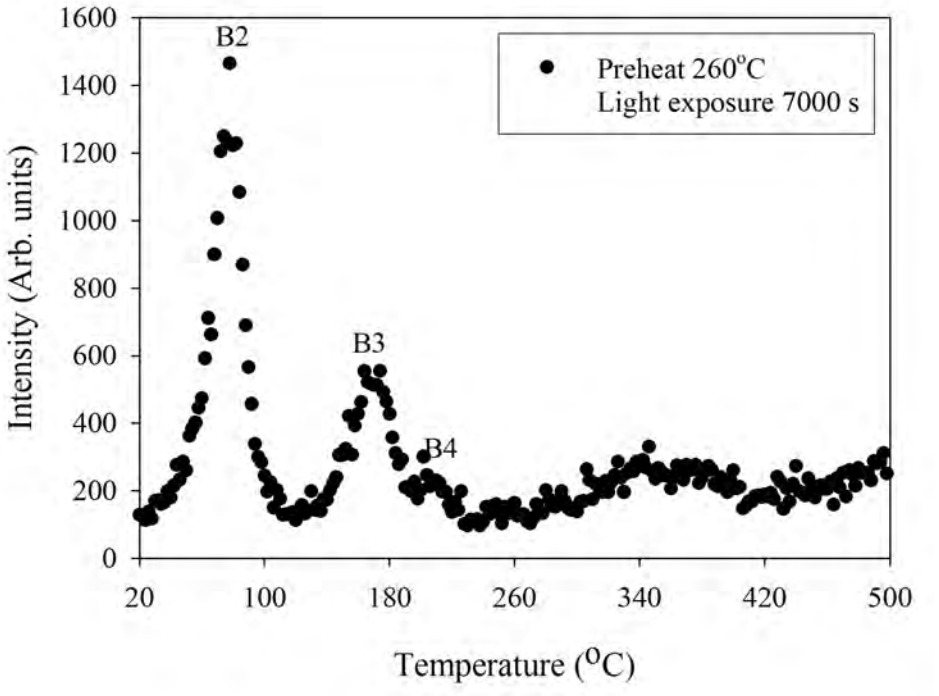

Figure 8.4: A glow curve of sample B recorded at 1°C/s after preheating to 260°C and illumination for 7000 s. Peak B4, at 202°C, is the PTTL peak corresponding to peak IV.

Tables 8.1 and 8.2 list the 'possible' or theoretical donors for each of the observed PTTL peaks of samples B and C for the preheating temperatures used.

8.3 Qualitative description of the dependence of PTTL intensity on illumination time

8.3.1 PTTL from peaks I and II after preheating to 100°C

Figure 8.5a shows the dependence of PTTL intensity on illumination time for peaks B1 and C1 following preheating to 100°C. The intensity of peak B1 increases with illumination time up to 16 s and then decreases monotonically thereafter. Peak C1 behaves in a similar manner. Peaks B1 and C1 are reproduced at 46 and 49°C respectively; the same position as their corresponding peak under conventional TL.

Table 8.1: TL peaks, their corresponding PTTL peaks and possible donors for sample B.

	TL	PTTL		
Peak label	T_m (°C)	Peak label	Preheating temp (°C)	Possible donors
I	46	B1	100	IIa-VII
			120	III-VII
			200	IV-VII
			260	V-VII
			360	VII
II	76	B2	100	IIa-VII
			120	III-VII
			200	IV-VII
			260	V-VII
			360	VII
IIa	100	B2a	200	IV-VII
			260	V-VII
III	170	B3	200	IV-VII
			260	V-VII
			360	VII
IV	199			
V	290			
VI	330			
VII	375			

Figure 8.5b shows the dependence of PTTL intensity on illumination time for peaks B2 and C2. The intensity of peak B2 reaches a maximum at 32 s of illumination time before decreasing monotonically thereafter. For peak C2, the maximum intensity occurs at 64 s and its dependence on illumination time is similar to that of peak B2. The intensity values of peak C2, the sample annealed at 900°C, are higher than those of peak B2. This is not the case for peaks B1 and C1. The possible donors for the PTTL for sample B are the electron traps for peaks IIa-VII since these are not removed by preheating to 100°C. For peaks C1 and C2, the possible donors are the electron traps for peaks IIa-VIII.

Figure 8.6a shows the influence of illumination time on the TL intensity of peaks IIa

Table 8.2: TL peaks, their corresponding PTTL peaks and possible donors for sample C.

	TL	PTTL		
Peak label	T_m (°C)	Peak label	Preheating temp (°C)	Possible donors
I	49	C1	100	IIa-VIII
			120	III-VIII
			200	IV-VIII
			260	VI-VIII
II	80	C2	100	IIa-VIII
			120	III-VIII
			200	IV-VIII
			260	VI-VIII
			360	VIII
IIa	100	C2a	200	IV-VIII
			260	VI-VIII
IIb	∼140	C2b	200	IV-VIII
			360	VIII
III	174	C3	200	IV-VIII
			260	V-VIII
			360	VIII
IV	206			
V	235			
VI	290			
VII	335			
VIII	375			

and III for sample B. The intensity of peak IIa goes through a maximum and then decreases with illumination time up to 1024 s. We note that peak IIa which appears at 100°C is not fully removed by preheating to 100°C. The TL time-response profile of this peak suggests that at the start of illumination it acts as a competitor for optically stimulated electrons from higher temperature traps; however, with further illumination its role as a donor becomes prominent. For peak III, the most intense of these peaks, the TL intensity drops rapidly within the first 150 s of illumination and then decreases slowly thereafter.

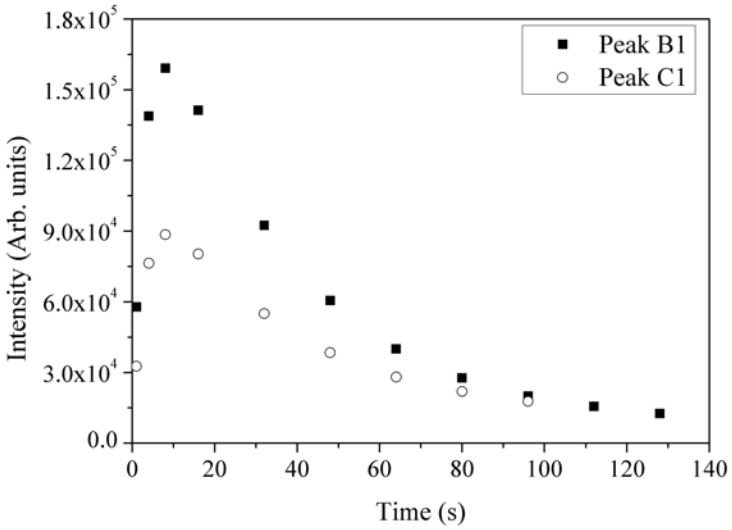

a

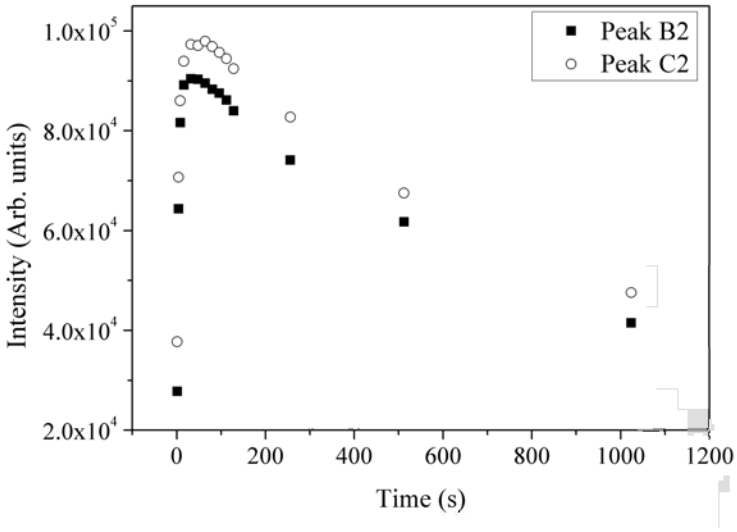

b

Figure 8.5: Dependence of PTTL intensity on duration of illumination for peaks B1 and C1 (a) and, for peaks B2 and C2 (b).

Figure 8.6b shows the dependence of TL intensity on illumination time for peaks IV-VII of sample B. In each case, the TL intensity decreases with illumination time. For peak VII however, the intensity decreases very slowly. In order to estimate the significance of each of these peaks as a donor, a ratio of intensities between each of peaks IV-VII and peak III was plotted. These ratios are referred to as relative intensities. Figure 8.7 depicts the relative intensity of peaks IV-VII as functions of

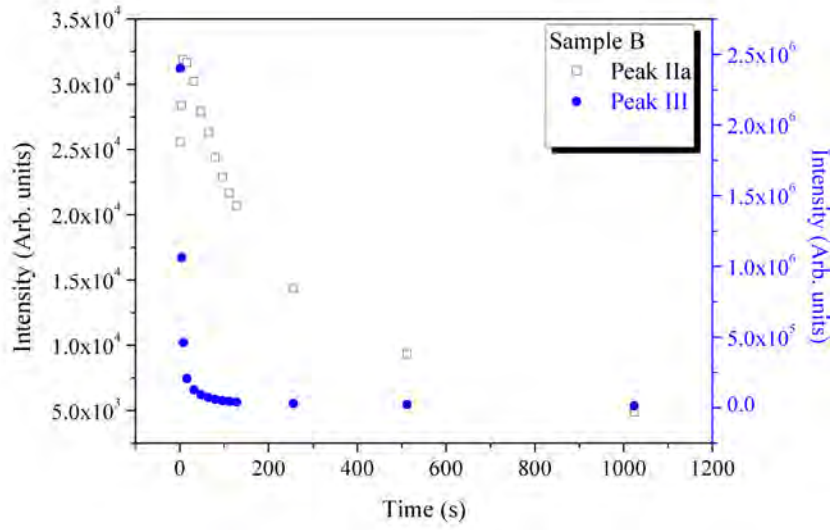

a

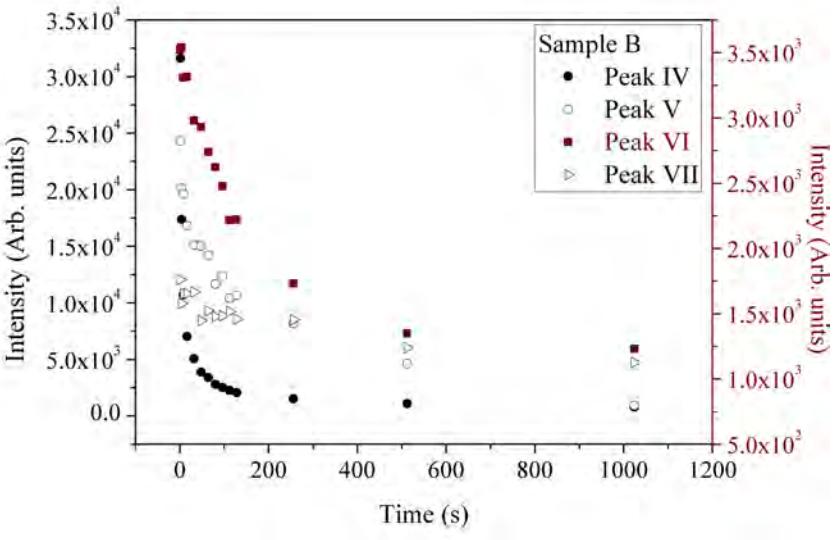

b

Figure 8.6: Dependence of TL intensity on illumination time following preheating to 100 °C for peaks IIa and III (a) and, for peaks IV-VII (b).

illumination time. This analysis of relative intensities shows that the electron traps corresponding to peaks IIa and III are the main donors. As shown in Figure 8.7b, the contribution from electron traps associated with peaks IV-VII can be neglected.

A similar analysis showed that for sample C, electron traps corresponding to peaks IIa and III are the main donors for PTTL peaks C1 and C2.

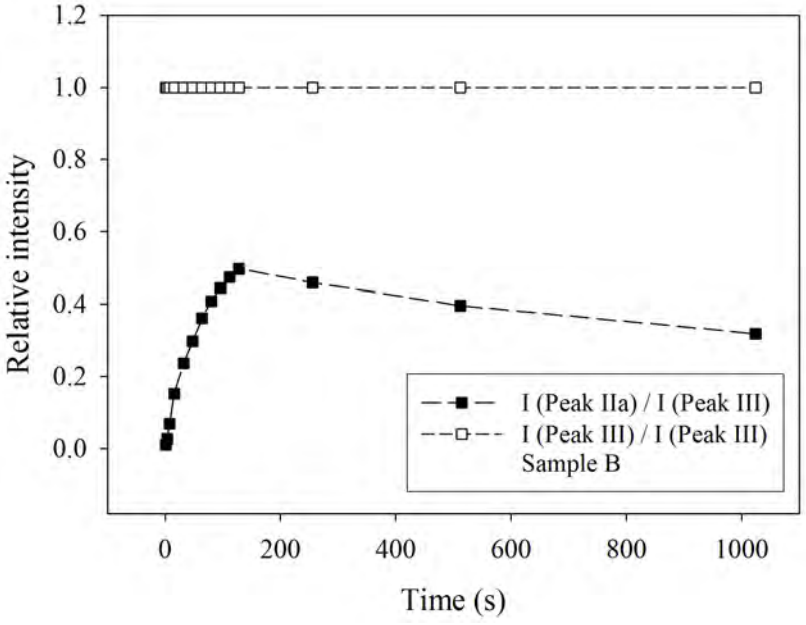

a

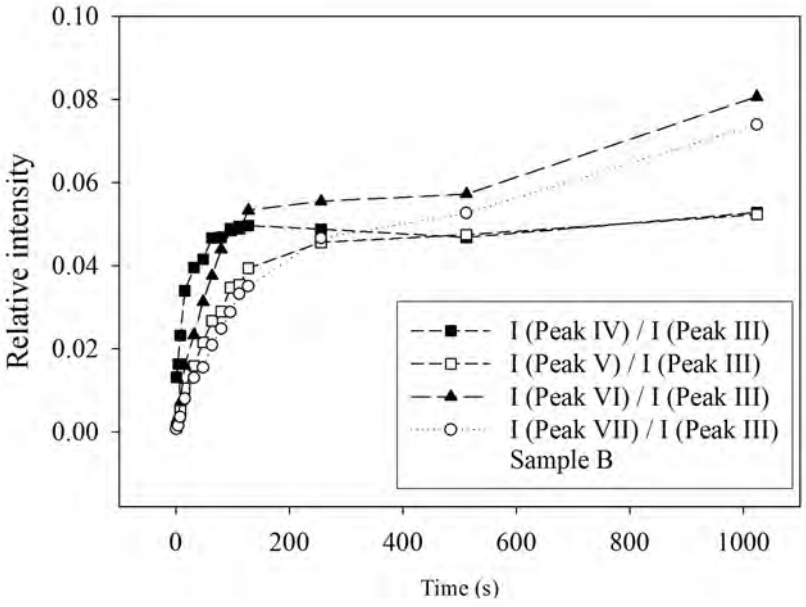

b

Figure 8.7: Relative intensity of (a) peaks IIa and III and of (b) peaks IV-VII of sample B following preheating to 100°C. The dotted lines are visual guides.

8.3.2 PTTL following preheating to 120°C

Peaks I, II and IIa of samples B and C are removed after preheating to 120°C. Following illumination and heating again, peaks I and II are reproduced under phototransfer as B1 and B2 for sample B and as C1 and C2 for sample C.

Figure 8.8a shows the dependence of PTTL intensity on illumination time for peaks B1 and C1 whereas Figure 8.8b shows that of peaks B2 and C2. The PTTL intensities of all these peaks each increases with illumination time up to a maximum and then decreases thereafter.

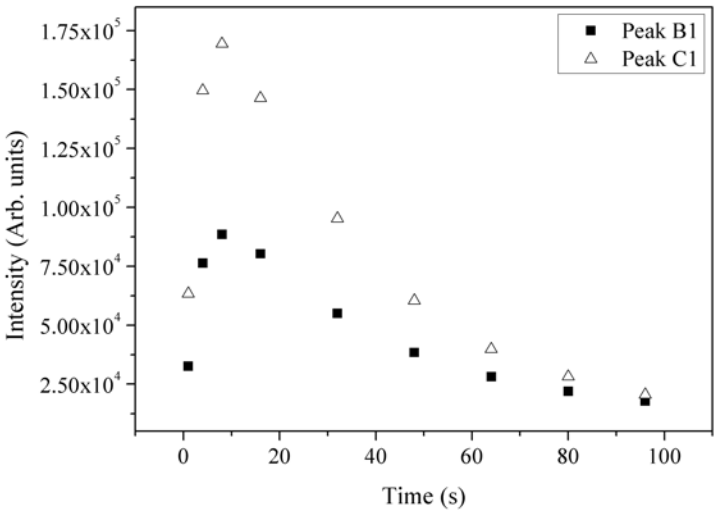

a

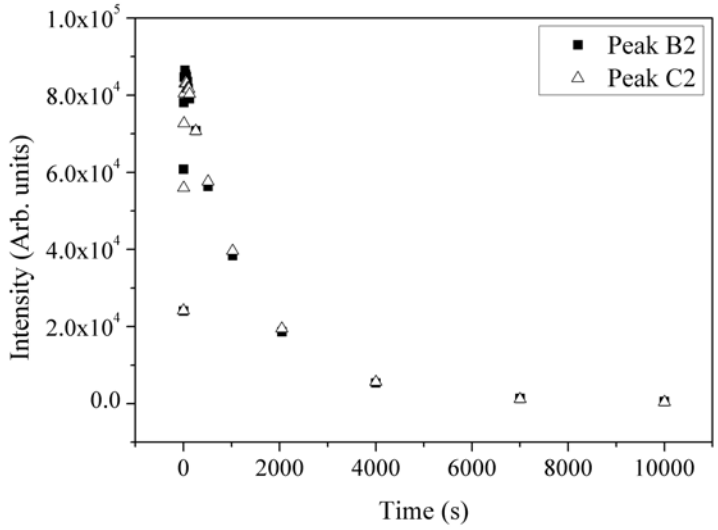

b

Figure 8.8: Dependence of PTTL intensity on illumination time after preheating to 120°C for peaks B1 and C1 (a) and, (b) for peaks B2 and C2 respectively.

Following preheating to 120°C, the possible donors for sample B are the electron traps of peaks III-VII as reported in Table 8.3. Figure 8.10 shows the dependence of TL intensity on illumination time for peaks III-VII of sample B after preheating to 120°C. The TL time-response profiles of peaks III and VI are shown on the main graph while those of peaks IV, V and VII are in the inset. As for preheating to 100°C, the intensity of peak III decreases to less than 40% of its initial value within the first 150 s of illumination time. For peaks IV-VII, the respective TL intensity each decreases monotonically with illumination time. The relative intensity of peaks III-VII is shown in Figure 8.11 and its analysis leads to peaks III and VI of sample B as the main donors for peaks B1 and B2 following preheating to 120°C. The contributions of the donors associated with peaks IV, V and VII are negligible since the relative intensity of each of these peaks is below 0.20.

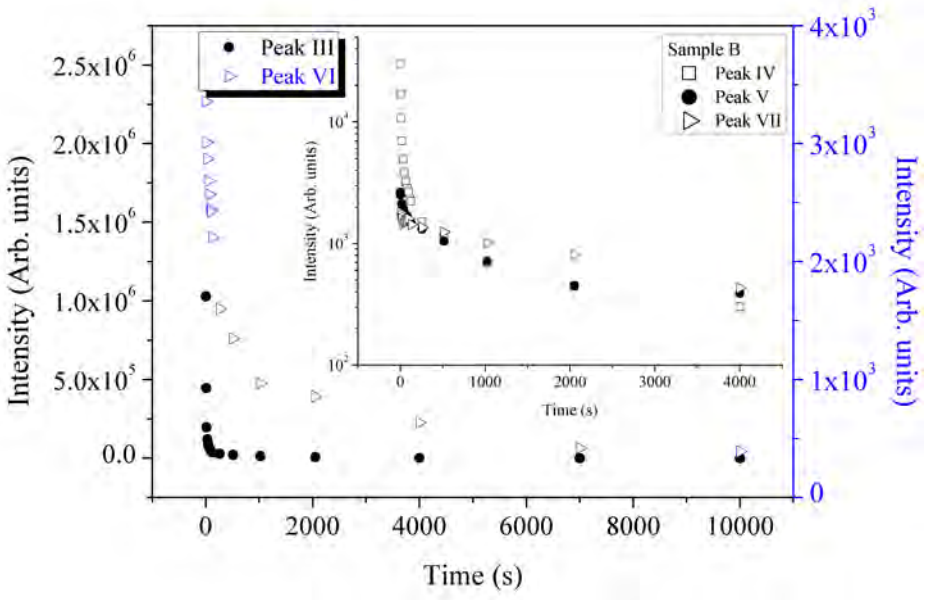

Figure 8.9

Figure 8.10: Dependence of TL intensity on illumination time after preheating to 120 °C for peaks III-VII of sample B.

A similar analysis of the TL time-response profiles of peaks III-VIII of sample C shows that the electron trap of peak III is the main source for the PTTL resulting in peaks C1 and C2 respectively.

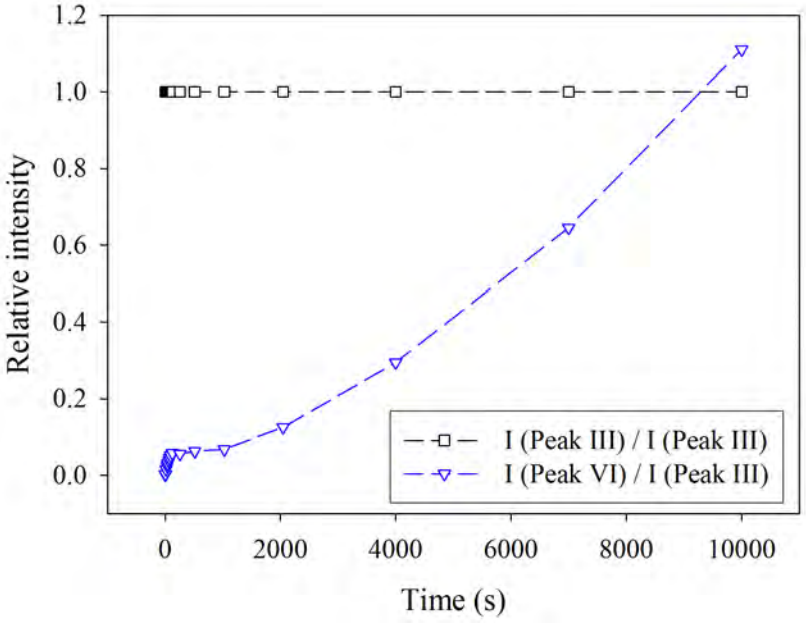

a

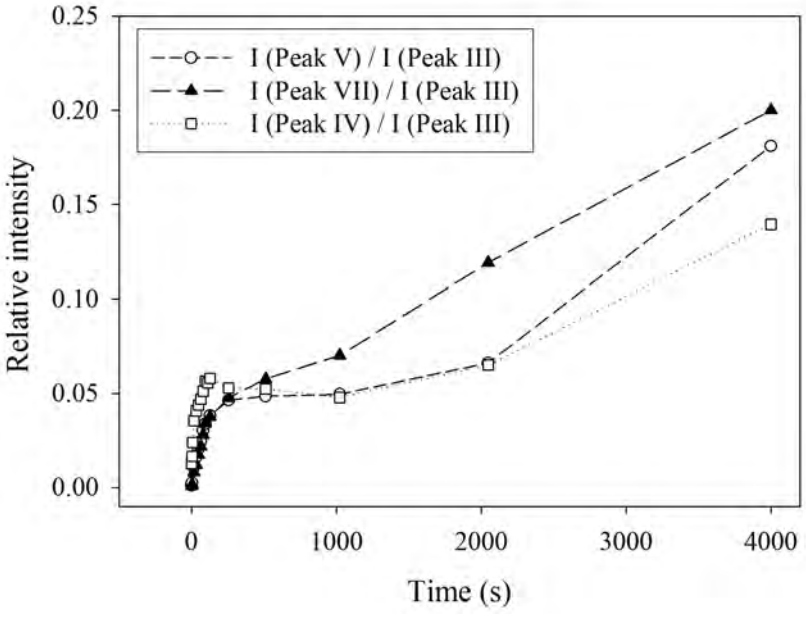

b

Figure 8.11: Relative intensity of (a) peaks III and IV and of (b) peaks V-VII of sample B following preheating to 120°C. The dotted lines are visual guides.

8.3.3 PTTL following preheating to 200°C

Preheating to 200°C removes peaks I-III of samples B and C. Peak IV of these two samples is also partially removed. Following this preheating, peaks I, II, IIa and III are reproduced under phototransfer as peaks B1, B2, B2a and B3 for sample B and as C1, C2, C2a and C3 for sample C. In addition to these PTTL peaks, we also observed a PTTL peak near 140°C for sample C. This peak is denoted here as C2b. Figure 8.12 shows glow curves measured after irradiation to 3.0 Gy for sample C. The glow curve measured immediately after irradiation is represented with the solid symbols whereas as the one measured after preheating and subsequent illumination is shown with the open symbols.

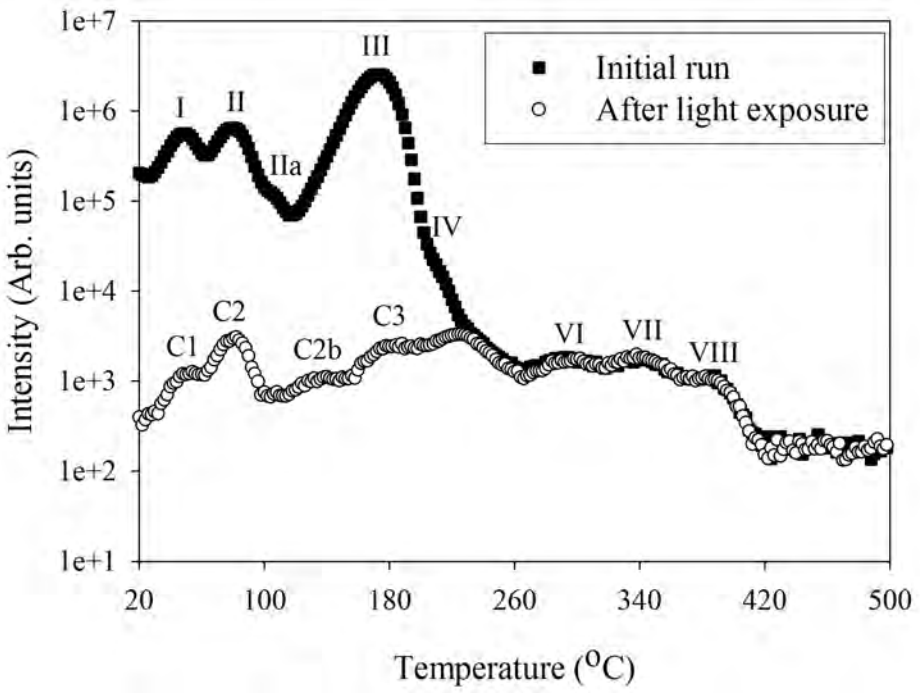

Figure 8.12: Glow curve measured at 1 °C/s for sample C after irradiation to 3.0 Gy (solid symbols). The glow curve obtained after preheating to 200 °C and subsequent illumination for 12 s (open symbols) are also shown for comparison.

Figure 8.13a shows the dependence of PTTL intensity on illumination time for peaks B1 and C1 following preheating to 200°C. The intensity of peaks B1 and C1 increases with illumination. Beyond 80 s and 90 s of illumination time respectively, the peaks could no longer be measured.

Figure 8.13b shows the dependence of PTTL intensity on illumination time for peaks B2 and C2 following preheating to 200°C. The intensity of each of these

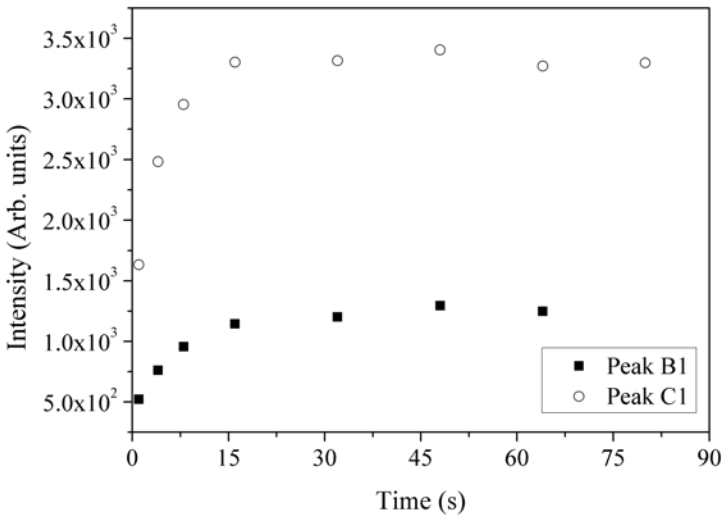

a

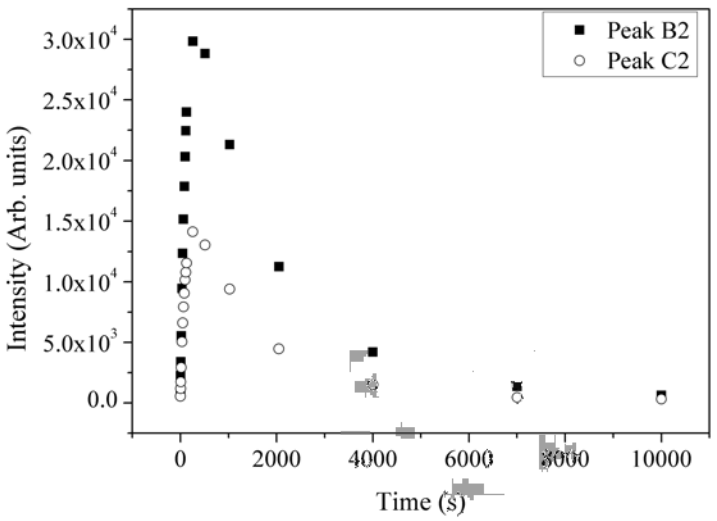

b

Figure 8.13: Dependence of PTTL intensity on illumination time after preheating to 200 °C for peaks B1 and C1 (a) and, (b) for peaks B2 and C2 respectively.

peaks initially goes through a maximum and decreases thereafter.

The results of Figures 8.5, 8.8 and 8.13 show that the illumination time at which the maximum PTTL intensity is reached changes with preheating temperature. For peak B2 for example, the maximum PTTL intensity is reached at 16, 32, or 256 s after preheating to 100, 120 or 200°C respectively.

Figure 8.14 shows the dependence of PTTL intensity on duration of illumination

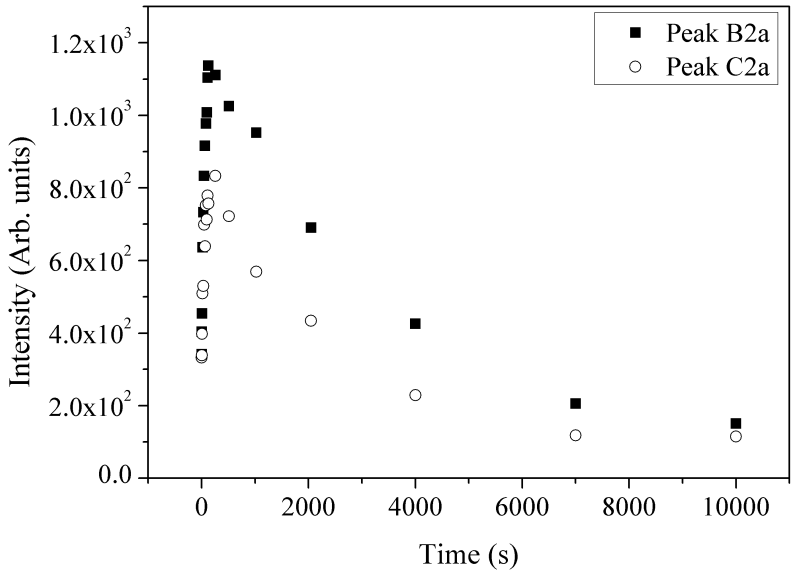

Figure 8.14: Dependence of PTTL intensity on illumination time after preheating to 200 °C for peaks B2a and C2a

for peaks B2a and C2a following preheating to 200°C. The intensity of each of these peaks goes through a maximum before decreasing monotonically with illumination up to 10000 s.

The dependence of PTTL intensity on exposure time for peak C2b following preheating to 200°C is shown in Figure 8.15. The intensity is independent of duration of illumination up to 80 s and it is very low in comparison to that of the other PTTL peaks of this sample. The PTTL intensity against illumination time is shown in Figure 8.16 for peaks B3 and C3. For each of these peaks, the intensity increases initially with illumination time up to 256 s and then decreases monotonically thereafter.

For sample B, the possible donors are electron traps of peaks IV-VII which are not emptied after this preheat. For sample C, they are those of peaks IV-VIII. The analysis of their relative intensities shows that the electron traps corresponding to these peaks are indeed donors for observed PTTL following preheating to 200°C. The relative intensity of each of peaks IV-VII is shown in Figure 8.17. A similar analysis shows that the donors for sample C are the electron traps of peaks IV-VII.

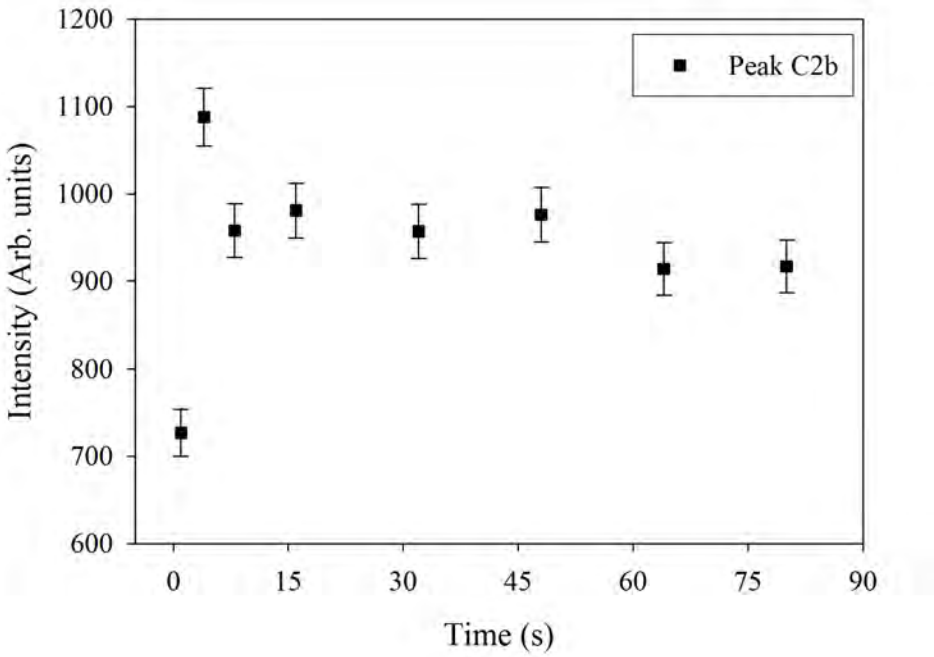

Figure 8.15: Dependence of PTTL intensity on illumination time after preheating to 200 °C for peak C2b.

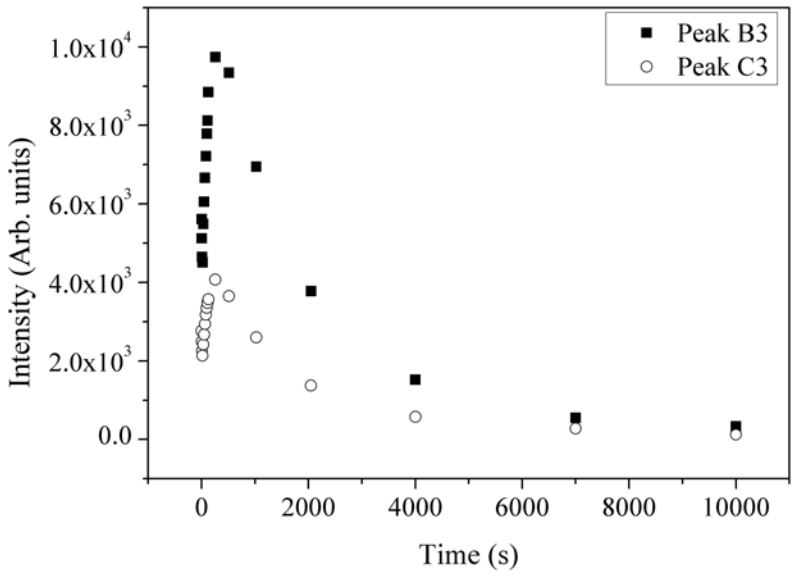

Figure 8.16: Dependence of PTTL intensity on illumination time after preheating to 200 °C for peaks B3 and C3.

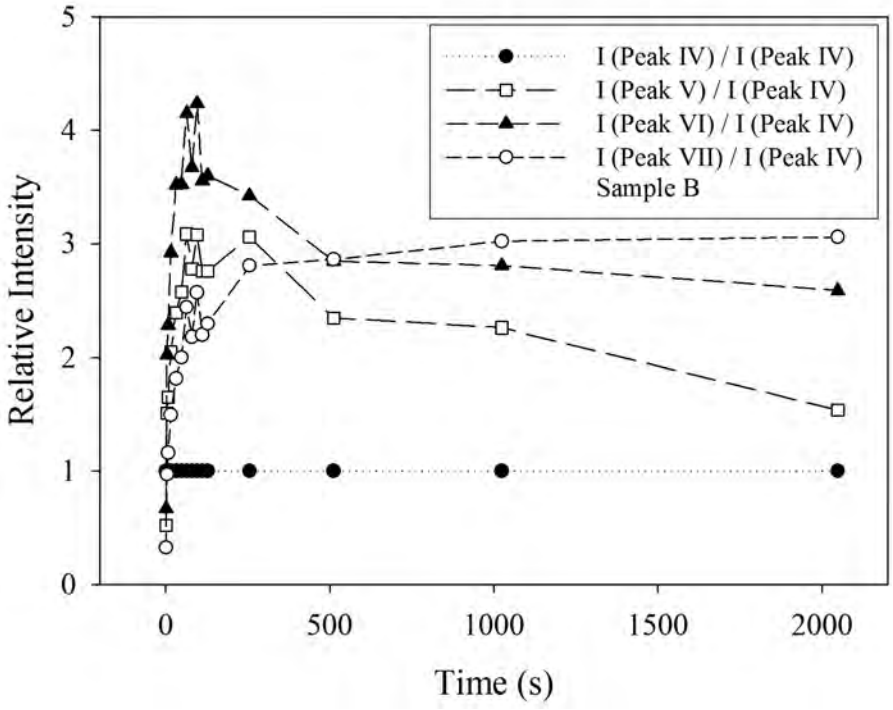

Figure 8.17: Relative intensity for peaks IV-VII following preheating to 200°C. The dotted lines are visual guides which show the trend in the data.

8.3.4 PTTL following preheating to 260°C

Preheating to 260°C removes peaks I-IV of sample B and peaks I-V of sample C. For sample B, the observed PTTL peaks are B1, B2, B2a and B3 whereas for sample C, they are C1, C2, C2a and C3 respectively. Figure 8.18a shows the dependence of PTTL intensity of peaks B1 and C1 on illumination time after preheating to 260°C. The intensity of peak B1 increases with illumination time up to 96 s and could no longer be measured. For this preheat, Peak C1 is observed for illumination time up to 16 s. For higher exposure time, the peak could no longer be measured. Peak B1 becomes indistinct and is obscure by peak B2 as the exposure time increases. The same observation is made for peak C1.

Figure 8.18b shows that for peaks B2 and C2, the respective PTTL intensity increases with illumination time up to 256 s and then decreases monotonically thereafter with further illumination up to 10000 s.

The dependence of intensity on illumination time for peaks B2a and C2a, as shown in Figure 8.19, behaves as those of peaks B2 and C2 respectively. Peak B2a reaches its maximum at 256 s whereas for peak C2a, the maximum occurs at 512 s.

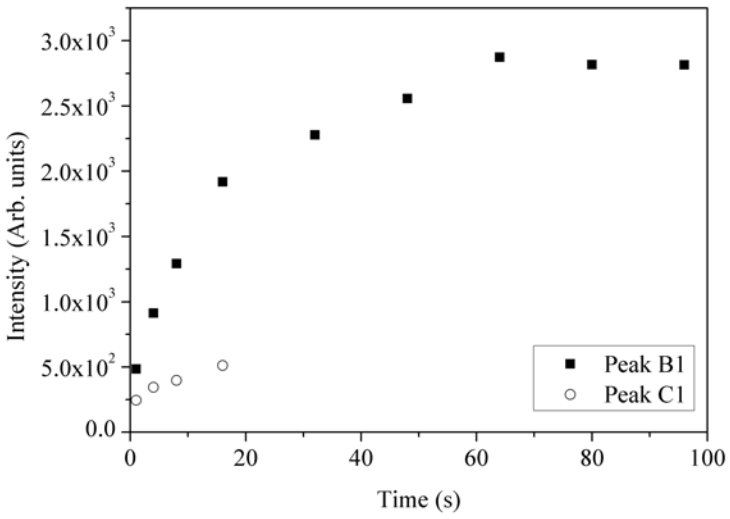

a

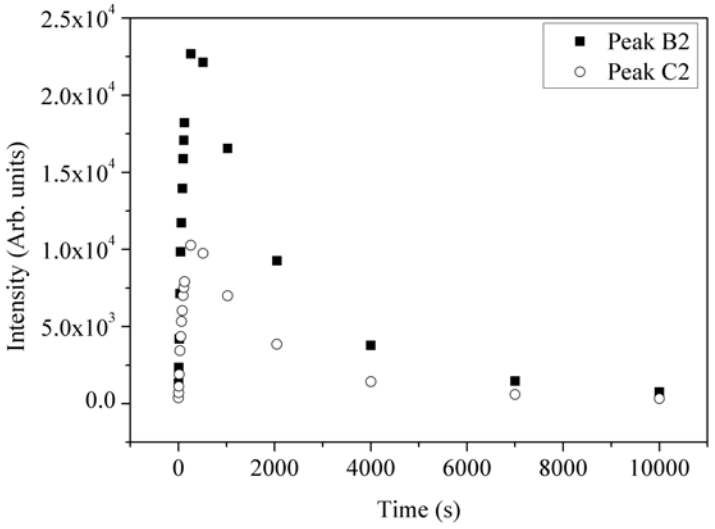

b

Figure 8.18: Dependence of PTTL intensity on illumination time after preheating to 260 °C for peaks B1 and C1 (a) and, for peaks B2 and C2 (b).

The dependence of PTTL intensity on illumination time for peaks B3 and C3 after preheating to 260°C is shown in Figure 8.20. The intensity of these peaks each increases with illumination time up to 256 s and then decreases monotonically thereafter up to 10000 s.

For sample B the analysis of relative intensities for peaks V-VII shows that their electron traps are the respective donors for the PTTL peaks B1, B2, B2a and B3.

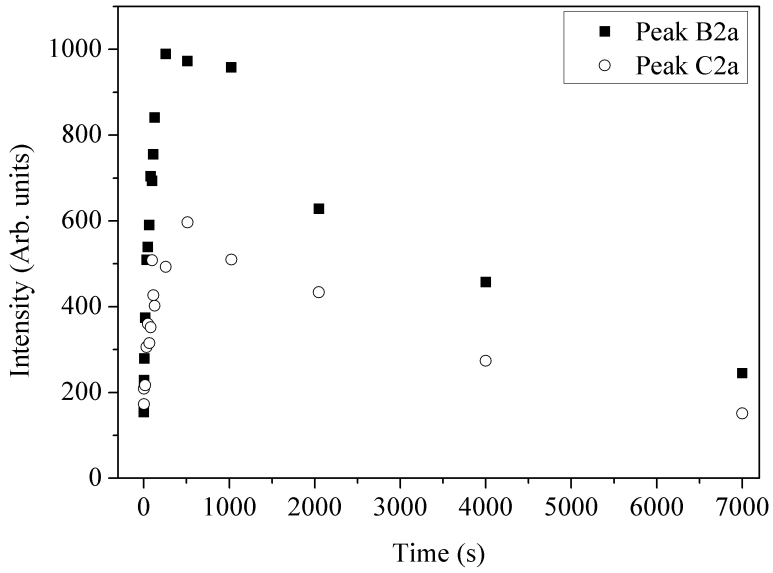

Figure 8.19: Dependence of PTTL intensity on illumination time after preheating to 260 °C for peaks B2a and C2a respectively.

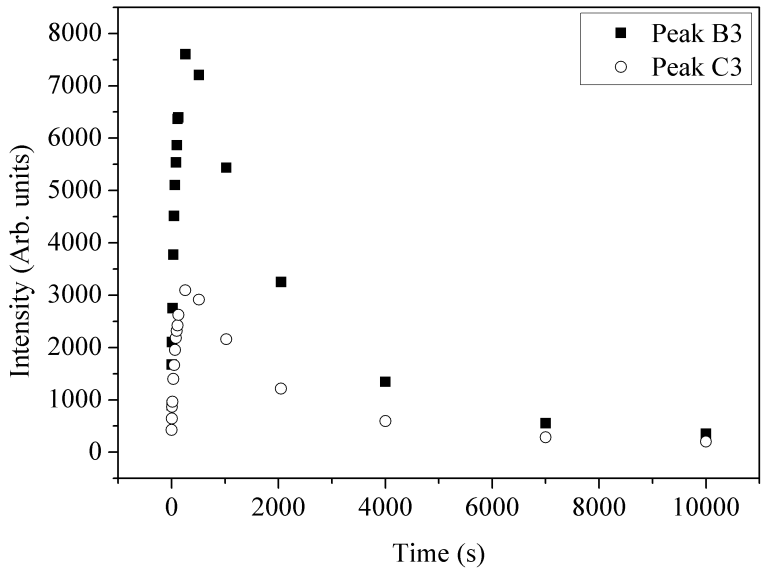

Figure 8.20: Dependence of PTTL intensity on illumination time after preheating to 260 °C for peaks B3 and C3.

The same analysis reveals that for sample C, the donors are the traps associated with peaks VI-VIII.

8.3.5 PTTL following preheating to 360°C

Following preheating to 360°C, all but the last peak of each sample are completely removed. Hence with the exception of deep traps, the electron trap of this remaining peak is the only donor in each case. For sample B, the resulting PTTL peaks are B1, B2 and B3 whereas for sample C, they are C2 and C3. Figure 8.21a shows the dependence of PTTL intensity on illumination time for peak B1. The intensity of peak B1 first increases with illumination time up to 48 s and decreases thereafter with illumination time up to 500 s. For peak B2, the intensity grows with illumination up to 512 s and then decreases slowly thereafter as shown in Figure 8.21b.

Figure 8.22 shows that the intensity of peak C2 reaches a maximum at 512 s and then decreases thereafter. As seen in Figure 8.23, the PTTL-time response profiles of peaks B3 and C3 are similar. The intensity of these peaks each grows with illumination time up to 64 s before decreasing with further illumination time up to 7000 s.

8.3.6 Following preheating to 400°C

For samples B and C, PTTL peaks were not observed after preheating to 400°C and subsequent illumination. For the unannealed sample on the other hand, PTTL peaks were observed as reported by Sob et al. (2021).

8.4 Mathematical analysis of PTTL time-response profiles

This section deals with a quantitative analysis of PTTL time-response profiles of the annealed samples. To aid discussion, the observed TL and PTTL peaks of samples B and C are listed in Tables 8.3 and 8.4. The electron traps listed as 'possible donors' are the theoretically expected ones. The main donors suggested by the partial heating experiment (section 8.2) and as reflected by PTTL time-profiles (section 8.3) are listed separately. The analysis will be based on the latter two lists rather than the ideal theoretical list. N_{ik} will denote the concentration of trapped electrons at the ith electron trap and, s_{ik} the stimulation probabilities for sample k. This method of analysis was developed by Chithambo et al. (2017a) and it was applied on quartz (Chithambo et al., 2018, 2019; Chithambo and Dawam, 2020), α-Al_2O_3:C (Chithambo et al., 2017a) and unannealed α-Al_2O_3:C,Mg (Sob et al., 2021). The main assumptions are that only a portion of electrons released from a

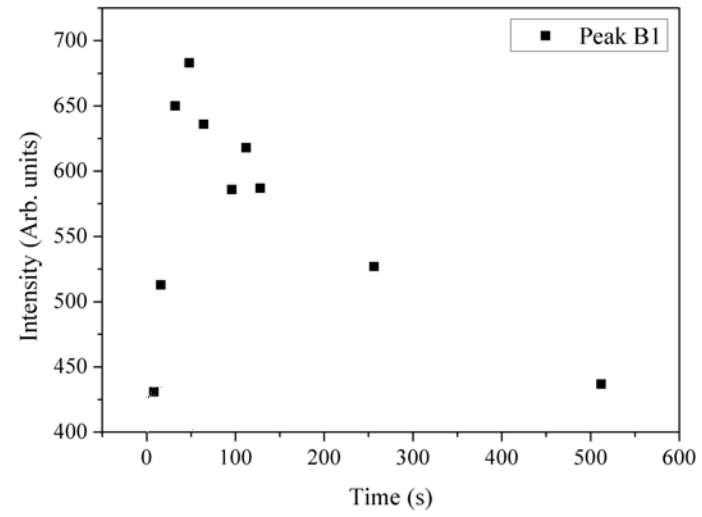

a

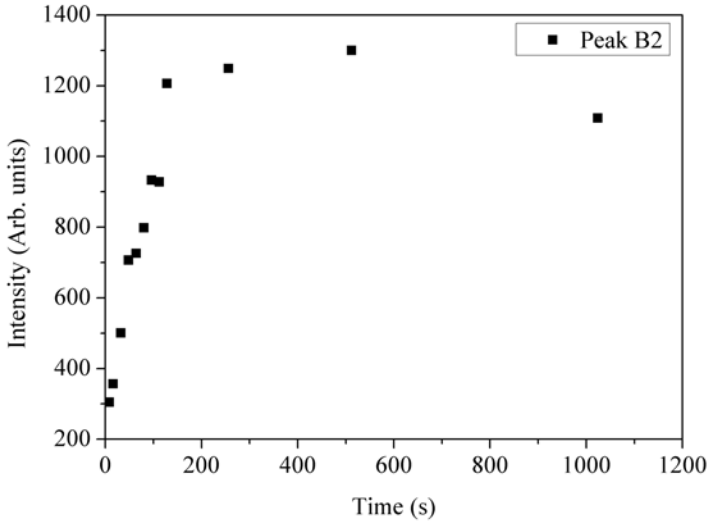

b

Figure 8.21: Dependence of PTTL intensity on illumination time for peak B1 (a) and for peak B2 after preheating to 360 °C (b).

donor trap end up at the acceptor electron trap to produce PTTL; and retrapping is negligible because these peaks follow first-order kinetics. As in the case of the unannealed sample, the equations describing the change in the concentration of trapped electrons are written for the illumination step only. These equations describe the transfer, to an acceptor, of a proportion of electrons optically stimulated from a donor. The number of donors for any acceptor peak depends on the preheat

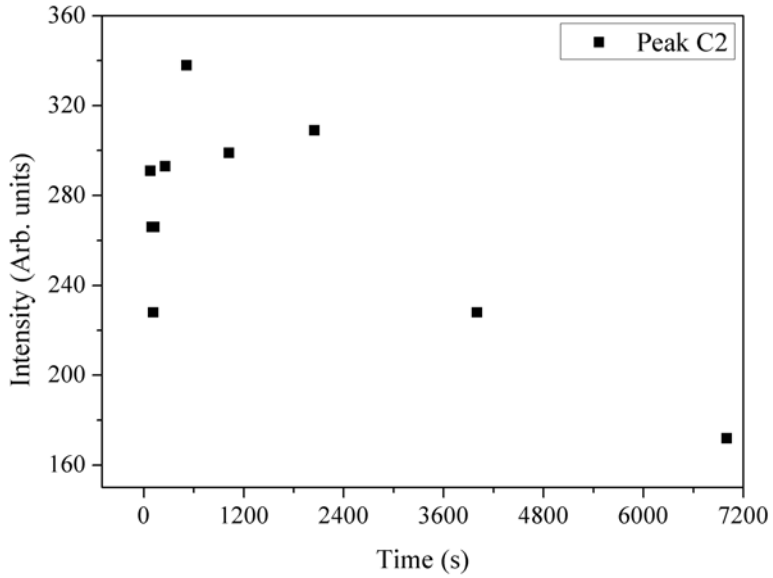

Figure 8.22: Dependence of PTTL intensity on illumination time after preheating to 360 °C for peak C2.

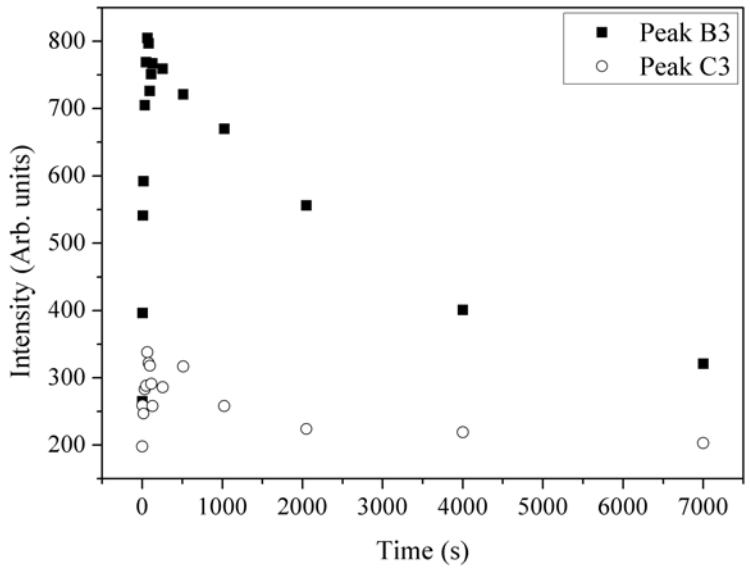

Figure 8.23: Dependence of PTTL intensity on illumination time after preheating to 360 °C for peaks B3 and C3.

temperature. Each coupled set of first-order differential equations has a particular solution. This solution is applied to the experimental data for that particular system. The resulting fits are shown in Figures 8.24-8.27 in section 8.5.

Table 8.3: A summary of TL peaks, their corresponding PTTL peaks, donors and photoionization cross-section (P. cross-section) for sample B

	TL	PTTL				P. cross-section (cm^2)		
Peak label	T_m (°C)	Peak label	Preheating temp (°C)	Possible donors	Main donor[a]	Main donor[b]	Acceptor	Donor	Donor
I	46	B1	100	IIa-VII	III	IIa III	1.48e-19	2.09e-18	
			120	III-VII	III	III VI	1.53e-19	2.20e-18	
			200	IV-VII		IV-VII			
			260	V-VII		V-VII			
			360	VII			5.29e-21	6.80e-19	
II	76	B2	100	IIa-VII	III	IIa III	4.70e-21	1.77e-18	
			120	III-VII	III	III VI	4.70e-21	1.75e-18	
			200	IV-VII		IV-VII	3.53e-21	5.29e-20	
			260	V-VII		V-VII	2.94e-21	5.52e-20	
			360	VII		VII			
IIa	100	B2a	120	III-VII	III	III VI	2.01e-20	3.50e-18	
			200	IV-VII		IV-VII	1.17e-21	3.05e-19	
			260	V-VII		V-VII	1.17e-21	9.29e-20	
			360	VII		VII			
III	170	B3	200	IV-VII		IV-VII	2.94e-21	1.29e-19	
			260	V-VII		V VI	2.35e-21	1.05e-19	
			360	VII		VII	5.88e-22	9.88e-19	
IV	199								
V	290								
VI	330								
VII	375								

[a] ✓ From pulse annealing study.
[b] ✓✓ From time-response study.

Table 8.4: A summary of TL peaks, their corresponding PTTL peaks, donors and photoionization cross-section (P. cross-section) for sample C.

	TL	PTTL				P. cross-section (cm^2)			
Peak label	T_m (°C)	Peak label	Preheating temp (°C)	Possible donors	Main donor[a]	Main donor[b]	Acceptor	Donor	Donor
I	49	C1	100	III-VIII	III	IIa III	1.23e-19	2.20e-18	
			120	III-VIII	III	III	1.33e-19	2.12e-18	
			200	IV-VIII		IV-VII			
			260	VI-VIII	VI-VIII				
			360	VIII		VIII			
II	80	C2	100	III-VIII	III	IIa III	4.11e-21	1.97e-18	
			120	III-VIII	III	III	4.11e-21	1.56e-18	
			200	IV-VIII		IV-VII	4.11e-21	6.00e-20	
			260	VI-VIII		VI-VIII	3.53e-21	5.41e-20	
			360	VIII		VIII			
IIa	100	C2a	120	III-VIII	III	III	1.41e-20	3.17e-18	
			200	IV-VIII		IV-VII	1.17e-21	5.78e-19	
			260	VI-VIII		VI-VIII	1.17e-21	1.10e-19	
			360	VIII		VIII			
IIb	∼140	C2b	200	IV-VIII		IV-VII			
			260	VI-VIII		VI-VIII			
			360	VIII		VIII			
III	174	C3	200	IV-VIII		IV-VII			
			260	VI-VIII		VI-VIII	2.35e-21	8.94e-20	
			360	VIII		VIII			
IV	206								
V	235								
VI	290								
VII	335								
VIII	375								

[a] ✓ From pulse annealing study.
[b] ✓✓ From time-response study.

8.4.1 PTTL following preheating to 100°C

Preheating to 100°C and illumination produces peaks B1 and B2 for sample B and, peaks C1 and C2 for sample C. For each set of peaks, the main donor obtained from pulse annealing study is the electron trap of peak III of the corresponding sample. From PTTL time-response study, the main donors for peaks B1 and B2 are the electron traps of peaks IIa and III as shown in Table 8.3. By considering the dominant donor only (peak III), the PTTL time-response profile for peak B1 or B2 (Figure 8.5) can each be described by a system of one acceptor and one donor. A similar system applies for peak C1 or C2. The rate equations for such a system are:

$$\frac{dN_{3k}}{dt} = -s_{3k}N_{3k} \tag{8.1}$$

$$\frac{dN_{jk}}{dt} = -s_{jk}N_{jk} + \alpha_{3k}s_{3k}N_{3k} \tag{8.2}$$

where k stands for B or C and (s_{jk}, N_{jk}) is either (s_{1B}, N_{1B}), (s_{2B}, N_{2B}), (s_{1C}, N_{1C}) or (s_{2C}, N_{2C}) and α_{3k} are proportionality constants. Equation (8.1) describes the loss of electrons from the donor whereas Equation (8.2) describes not only the transfer of electrons from the donor but also the loss due to illumination at the acceptor. The solution of the coupled sets of equations (8.1) and (8.2) is

$$N_{jk} = A_k(e^{-s_{3k}t} - e^{-s_{jk}t}) \tag{8.3}$$

where $A_k = \alpha_{3k}s_{3k}N_{3ki}/(s_{jk}-s_{3k})$ and, N_{3ki} are the initial concentration of trapped electrons at the donor trap at the start of illumination.

For peak B1, B2, C1 or C2, we first analysed the time profiles on the basis of systems consisting one acceptor and two donors but the resulting fits were not satisfactory. Systems of one acceptor and one donor yielded much better fits for each of their time profiles as shown later in Figures 8.24a and 8.24b.

8.4.2 PTTL following preheating to 120°C

Peaks B1 and B2 are reproduced under phototransfer after preheating to 120°C whereas peaks C1 and C2 are reproduced for sample C. For each of these samples, the electron trap of peak III is the dominant donor found from pulse annealing. The PTTL time-response study of sample B showed that the electron trap of peak VI is also a donor. Hence, the PTTL time-response profiles of sample B can each be

described as systems of one acceptor and two donors whereas those of sample C can be described as systems of one acceptor and one donor. In practise though, the PTTL time-response profile of peaks B1, B2, C1 and C2 were best fitted with expressions of the same form as equation (8.3).

8.4.3 PTTL following preheating to 200°C

Preheating to 200°C removes peaks I-III of samples B and C. For sample B, peaks B1, B2, B2a and B3 are reproduced under phototransfer whereas as for sample C, the PTTL peaks are C1, C2, C2a, C2b and C3. As reported in Tables 8.3 and 8.4, the PTTL time-response study showed that the electron traps corresponding to peaks IV-VII of these sample are the respective donors. In principle, the PTTL time-response profile of any of these PTTL peaks should be described by a system of one acceptor and four donors. The rate equations of charge transfer for such a system are:

$$\frac{dN_{lk}}{dt} = -s_{lk}N_{lk} \tag{8.4}$$

$$\frac{dN_{jk}}{dt} = -s_{jk}N_{jk} + \sum_{l=4}^{7} \alpha_{lk}s_{lk}N_{lk} \tag{8.5}$$

where k stands for B or C; j takes values 1, 2, 2a, 2b or 3 depending on which acceptor the system is being solved for. The donor traps are indexed by l = 4, 5, 6 and 7. The proportionality constant corresponding to a donor trap l of sample k is denoted α_{lk}. For each acceptor trap (k, j), the solution to equations (8.4) and (8.5) is

$$N_{jk} = \sum_{l=4}^{7} A_{lk}(e^{-s_{lk}t} - e^{-s_{jk}t}) \tag{8.6}$$

where $A_{lk} = \alpha_{lk}s_{lk}N_{lki}/(s_{jk} - s_{lk})$ and, N_{lki} is the initial concentration of trapped electrons at donor trap l at the start of illumination. Systems consisting of one acceptor and four donors did not yield satisfactory fit. The time-response profiles of PTTL peaks observed after preheating to 200 °C were best fitted by reducing the number of donors from four to one.

8.4.4 PTTL following preheating to 260°C

Preheating to 260°C removes peaks I-IV of sample B and peaks I-V of sample C. The PTTL peaks of sample B are B1, B2, B2a and B3. The possible donors of

electron traps for sample B are those of peaks V-VII. The PTTL time-response study showed that for this preheat, the electron traps of peaks V-VII are indeed the donors for the observed PTTL. The PTTL peaks of sample C are C2, C2a, C2b and C3 and a similar analysis showed that the electron traps of peaks VI and VII are the donors. Systems of one acceptor and three donors are needed to describe the PTTL time-response profiles of peaks B1, B2, B2a and B3 whereas for the PTTL peaks of sample C, systems of one acceptor and two donors are. However, the time-response profiles were best fitted with expressions derived for systems consisting of a single donor such as equation (8.3).

8.4.5 PTTL following preheating to 360°C

For samples B and C the last preheating temperature for which PTTL time-response profiles were analysed was 360°C. For sample B, preheating to 360°C removes all but peak VII which is only partially removed. The resulting PTTL peaks for sample B are peaks B1, B2 and B3. For sample C, this preheat removes all but peak VIII which is only removed partially. The PTTL peaks for sample C are peaks C2 and C3. For each of these peaks a system consisting of one acceptor and a donor trap yields a satisfactory fit.

8.5 Applications of the mathematical model

Figures 8.24-8.27 show the application of models from Equation (8.3) to experimental data for each of the preheating temperatures used. The PTTL time-response profiles of peaks B1 and C1 after preheating to 100°C are shown in Figure 8.24a. For peaks B2 and C2, the corresponding profiles are shown in Figure 8.24b. The fits obtained from Equation (8.3) following preheating to 120°C are shown in Figure 8.24c for peaks B1 and C1. The PTTL time-response profiles from the same analysis are shown in Figure 8.24d for peaks B2 and C2 after preheating to 120°C.

The PTTL time-response profiles of peaks B2 and C2 after preheating to 200°C were fitted using expressions of the same form as Equation (8.3) as shown in Figure 8.25a. The same analysis is shown in Figure 8.25b for peaks B2a and C2a. Similarly, the PTTL time-response profile of peak B3 fitted with an expression of the same form as Equation (8.3) is shown in Figure 8.25c.

The PTTL time-response profile of peak B1 fitted with Equation (8.3) is shown in Figure 8.26a. The PTTL time-response profiles of peaks B2 and C2 after preheating

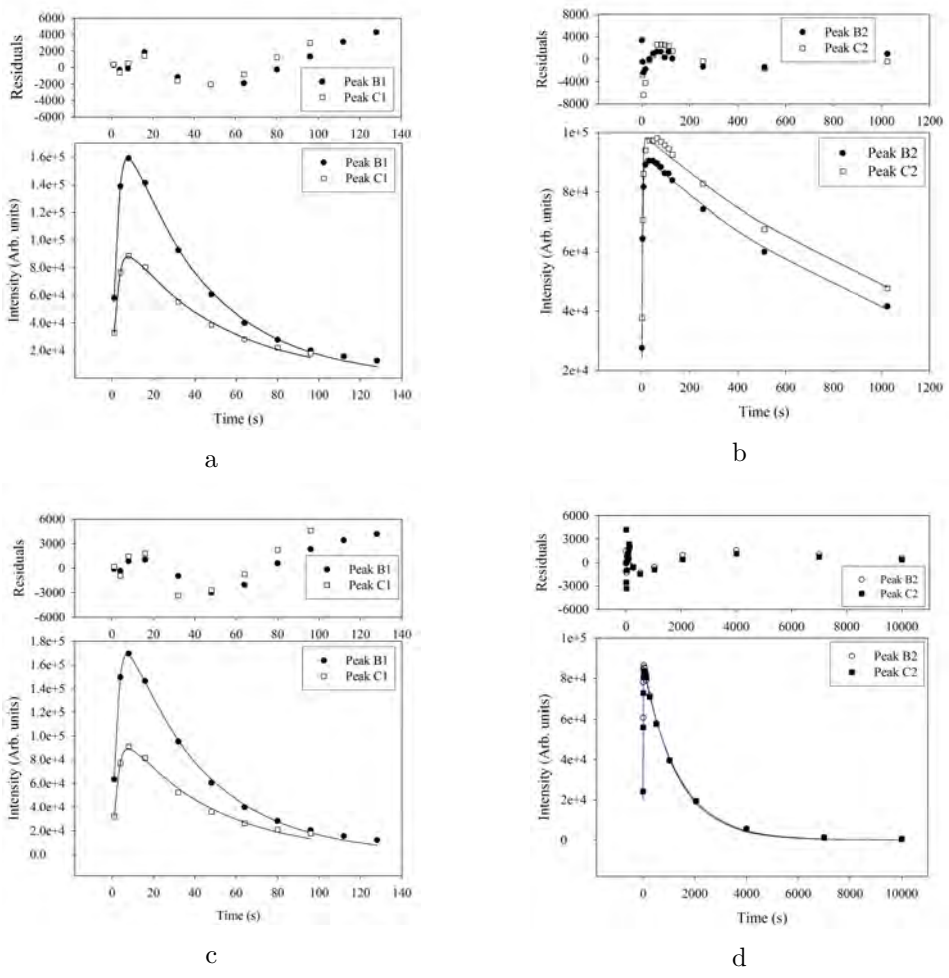

Figure 8.24: PTTL time-response profiles of peaks B1 and C1 (a) and, of peaks B2 and C2 after preheating to 100 °C (b); PTTL time-response profiles of peaks B1 and C1 (c) and, of peaks B2 and C2 after preheating to 120 °C (d).

to 260°C are shown in Figure 8.26b. Figures 8.26c and 8.26d show the PTTL time-response profiles of peaks B2a and C2a and, of peaks B3 and C3 after preheating to 260°C fitted with Equation (8.3).

For preheating to 360°C, the fits with expressions of the same form as Equation (8.3) are shown in Figures 8.27a-8.27d for the PTTL time-response profiles of peaks B1, B2, C2 and B3 respectively.

The optical stimulation probability $s = \Phi\sigma$ is obtained from fitting. It is then used to evaluate the photoionization cross-section σ for each of the observed PTTL peaks. In this study, the incident photon flux $\Phi = 1.70 \times 10^{17}$ cm^{-2} s^{-1} and σ is calculated as s/Φ. The values found are included in Tables 8.3 and 8.4 and range between 10^{-21}-10^{-18} cm^2.

8.6 Summary

A glow curve of α-Al_2O_3:C,Mg annealed at 700°C for 15 minutes (sample B) has peaks at 46, 76, 100, 170, 199, 290, 330 and 375°C when measured at 1°C/s after irradiation to 3.0 Gy. In comparison, for the sample annealed at 900°C (sample C), a glow curve measured under the same conditions consists of peaks at 49, 80, 100, 174, 206, 235, 290, 335 and 375°C. These peaks are labelled I through VII for sample B and I through VIII for sample C. The peak at 100°C, which is observed in both samples, is labelled peak IIa. This peak is due to a new electron trap created after the destruction of the F_2^{2+}(2Mg) centre after annealing at or above 700°C (Kalita and Chithambo, 2017b). Peaks I-III of each of these samples are reproduced under phototransfer for preheating temperatures between 100 and 360°C. For sample C, a PTTL peak is found near 140°C after preheating to 200°C. This peak is obscured by peak III, the dominant peak. In each sample, the electron trap of peak III acts as a donor for the observed PTTL peaks below 150°C. However, the trap of peak III also acts as an acceptor for electrons from higher temperature traps. Due to its position in the glow curve, the transfer of charges to lower temperature traps and from higher temperature trap is favourable. Even though, the role of the electron traps of peaks IV-VII becomes prominent after the removal of peak III by preheating, PTTL time-response profiles of the observed PTTL peaks were best described as systems of one acceptor and one donor.

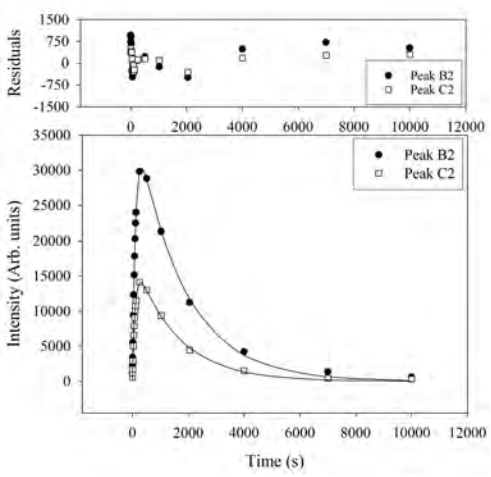

a

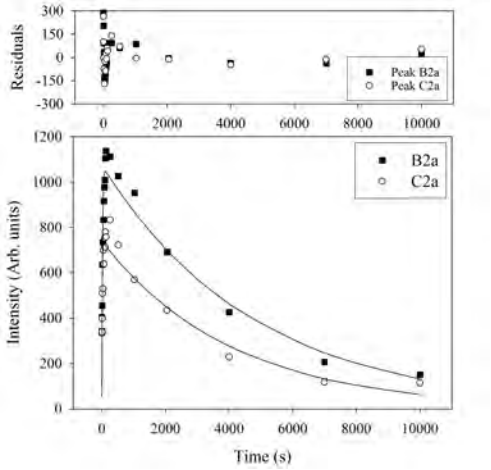

b

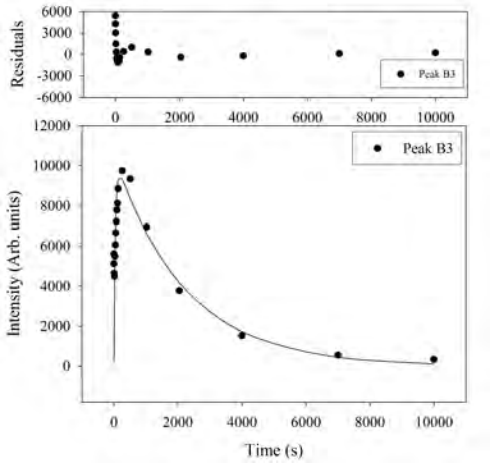

c

Figure 8.25: PTTL intensity against duration of illumination for peaks B2 and C2 (b) and, for peaks B2a and C2a (c) and for peak B3 after preheating to 200 °C (d).

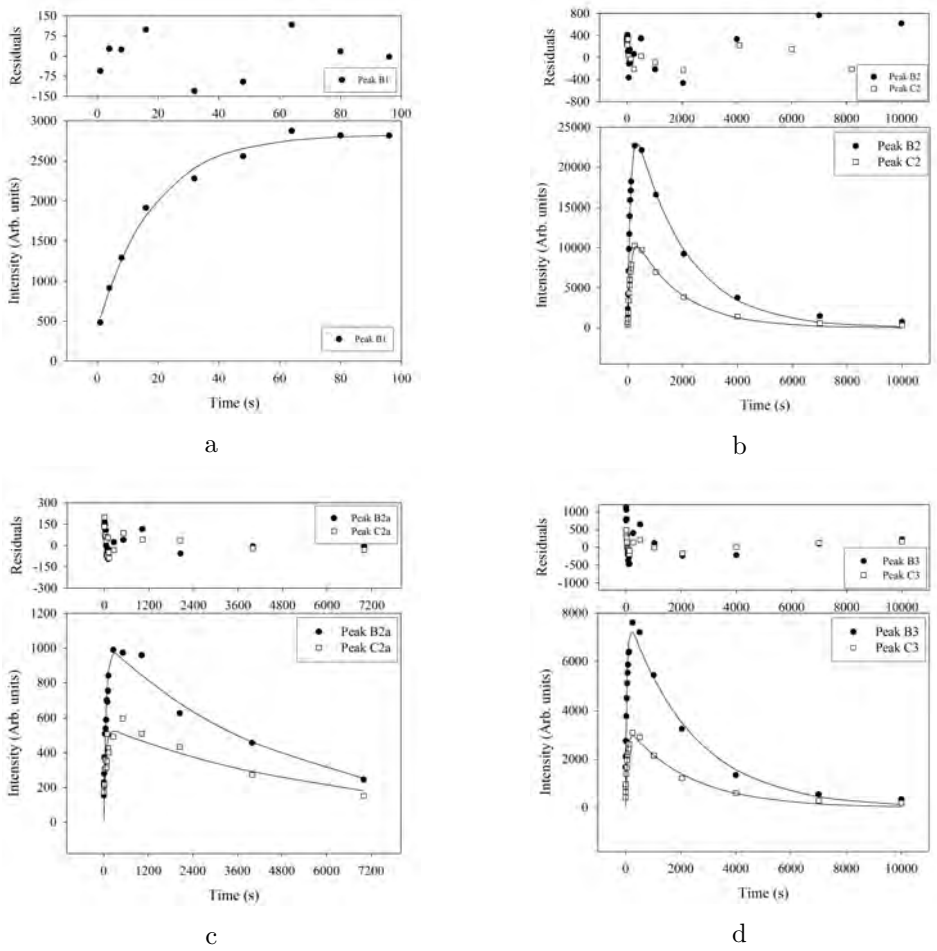

Figure 8.26: PTTL time-response profiles of peak B1 (a) and, of peaks B2 and C2 (b) and, of peaks B2a and C2a (c) and, of peaks B3 and C3 after preheating to 260°C (d).

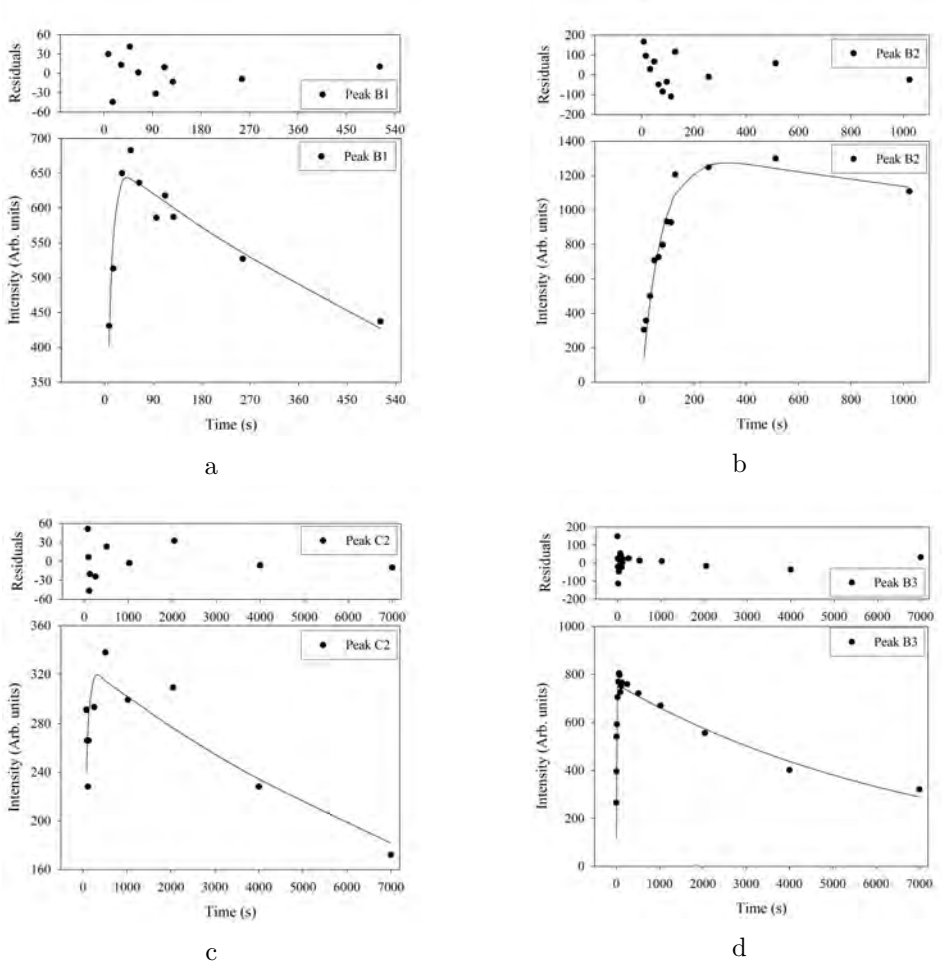

Figure 8.27: PTTL against duration of illumination of peak B1 (a), and of peak B2 (b), and of peak C2 (c), and of peak B3 (d) after preheating to 360 °C.

Chapter 9

Illumination-time-dependent profiles of phototransferred thermoluminescence of α-Al_2O_3:C,Mg annealed at 1200°C

This chapter deals with the phototransferred thermoluminescence (PTTL) of α-Al_2O_3:C,Mg annealed at 1200°C. For the mathematical description of a PTTL peak, a system consisting of an acceptor and, donors the number of which depends on the preheating temperature is used. The sample annealed at 1200°C for 15 minutes is hereafter referred to as sample D. The luminescence sensitivity of α-Al_2O_3:C and α-Al_2O_3:C,Mg is due to their large concentration of F and F^+-centres (Akselrod et al., 1990, 2003a; Chithambo et al., 2015). In addition to these centres, α-Al_2O_3:C,Mg also contains Mg-related centres such as F^+(Mg), F_2^{2+}(2Mg) and F_2^+(2Mg) (Akselrod et al., 2003a). It has been found that the F_2^{2+}(2Mg)-centre disappears after annealing at 700°C while the F and F^+-centres remain stable up to 1200°C (Akselrod et al., 2003a). For α-Al_2O_3:C, studies (Yukihara et al., 2004; Chithambo, 2004; Yukihara and McKeever, 2006) found that annealing at 900°C depletes deep electron traps and that the luminescence sensitivity is affected. In the case of α-Al_2O_3:C,Mg, a new electron centre is formed after annealing at 700°C (Kalita and Chithambo, 2017b). The influence of annealing and beta irradiation on TL spectra of α-Al_2O_3:C,Mg has been investigated (Kalita and Chithambo, 2018a). For the unannealed sample, Kalita and Chithambo (2018a) reported a main emission band from F-centres at ∼410 nm and secondary emission bands at ∼325 and 485 nm attributed to F^+ and F_2^{2+}(2Mg) centres respectively. Except for a decrease in the intensity of the emission at 485 nm, Kalita

and Chithambo (2018a) observed similar bands for samples annealed at 700 and 900°C. In addition, they found that for samples annealed at or above 700°C and for doses greater than 10 Gy, the influence of irradiation dose on the F^+ and F-centres could be easily distinguished. Using radioluminescence, (Chithambo et al., 2020) showed that the 330 nm emission corresponding to the F^+-centre becomes prominent with annealing at 1200°C. The authors also observed that the F and F^+ centres were affected by thermal quenching (Chithambo et al., 2020).

9.1 Glow curve characteristics

α-Al_2O_3:C,Mg is a supersensitive luminescent material whose sensitivity is enhanced by annealing (Kalita and Chithambo, 2017d). Samples annealed at 700 and 900°C were each irradiated to 3.0 Gy at room temperature for measurement (Chapter 8). On the other hand, for the sample annealed at 1200°C (sample D) a dose of 0.2 Gy was sufficient to measure a signal high enough for reliable analysis. In order to measure PTTL, the irradiated sample was preheated, cooled and then exposed to 470 nm blue light of optical power density 72 mW/cm^2. Following illumination, the sample was then heated again at 1°C/s to monitor PTTL.

Figure 9.1 shows glow curves of sample D measured at 1°C/s following irradiation to 0.2 Gy. Solid symbols depict the glow curve measured immediately after irradiation whereas the glow curve recorded after preheating to 120°C and subsequent illumination for 12 s is represented with open symbols.

The glow curve of sample D consists of peaks at 52, 82, 102, 174, 234, 288 and 384°C respectively. These peaks are referred to hereafter as I, II, IIa, III, IV, V and VII respectively. The peak at 335°C (peak VI) is indistinct in the glow curves measured and could not be isolated. For a similar sample of α-Al_2O_3:C,Mg annealed at 1200°C, Kalita and Chithambo (2018b) observed glow peaks at 54, 80, 102, 173, 238, 290, 330 and 387°C after irradiation to 0.2 Gy and heating at 1°C/s. The 100°C peak reported in samples annealed above 600°C (Kalita and Chithambo, 2018a) is also found here. It is labelled peak IIa. The glow curve of sample D measured at 1°C/s after preheating to 120°C and illumination for 12 s has 3 PTTL peaks labelled D1 at 52°C, D2 at 82°C and D2a at 100°C. In addition to these PTTL peaks, the glow curve also consists of peaks III-VII which are not removed after preheating to 120°C. We also observed a peak at ∼140°C; referred here as peak IIb which is reproduced by phototransfer for certain preheat temperatures.

Figure 9.2 shows two glow curves. The glow curve depicted with solid circles is

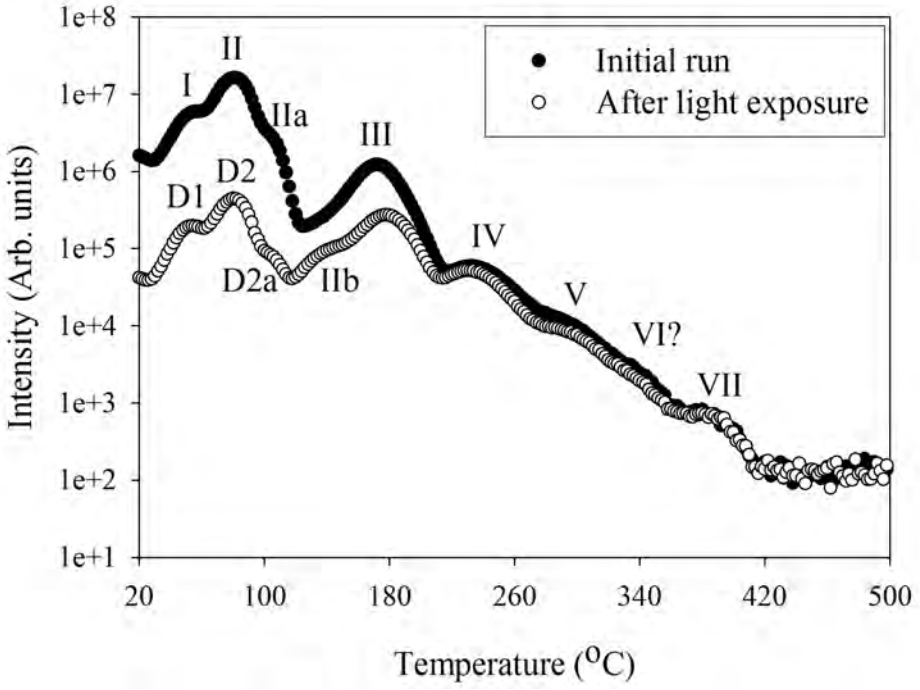

Figure 9.1: Glow curves of sample D measured at 1°C/s following irradiation to 0.2 Gy. Solid symbols depict the glow curve recorded immediately after irradiation and open circles that measured after preheating to 120°C and subsequent illumination for 12 s.

measured immediately after irradiation whereas the one in open circles is recorded after preheating to 260°C and subsequent illumination for 12 s. In both cases, the sample is irradiated to 0.2 Gy and heated at 1°C/s.

The glow curve recorded after preheating to 260°C and illumination for 12 s has 6 PTTL peaks at 56, 82, 104, 142, 170 and 236°C labelled D1, D2, D2a, D2b, D3 and D4 respectively. These PTTL peaks correspond to peaks I-IV which are removed following preheating to 260°C.

9.2 Determining the role of electron traps as acceptors or donors using partial heating

Partial heating and subsequent light exposure were used to investigate the role of each electron trap either as an acceptor or a donor in the observed PTTL. Sample D was preheated from 60 to 600°C at 20°C intervals after irradiation to 0.2 Gy and illuminated for 10 s each time. For ease of reference, any PTTL peaks

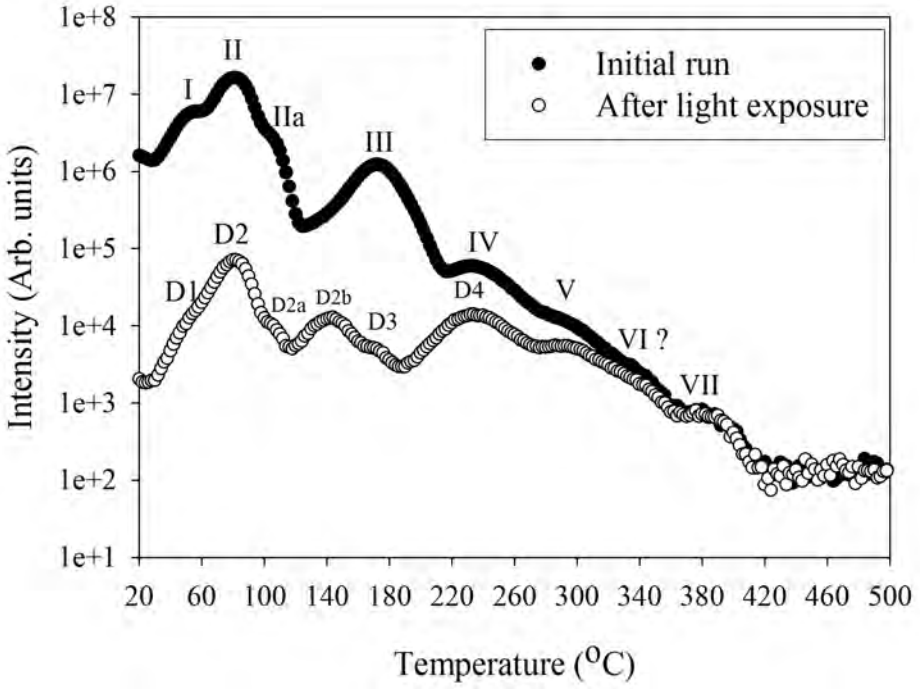

Figure 9.2: Glow curves of sample D measured at 1°C/s after irradiation to 0.2 Gy. Solid symbols represents the glow curve recorded immediately after irradiation whereas the open symbols is for the glow curve obtained after preheating to 260°C and subsequent illumination for 12.

corresponding to peaks I-VII of sample D are referred to as D1-D7.

9.2.1 Effect of partial heating on peaks I, II and IIa

In discussing the dependence of preheating temperature on PTTL intensity, labels for PTTL peaks are used for the whole range of preheating temperatures as seen in Figure 9.3 for example. It is understood that each of these peaks only becomes a genuine PTTL peak from a specific temperature since the corresponding peak in the conventional glow curve needs to be removed before exposure to light to monitor PTTL.

Figure 9.3 shows the dependence of PTTL intensity (peak height) on preheating temperature for peaks D2, D2a and D2b respectively. These are PTTL peaks corresponding to I, II and IIa. We observe a decrease in PTTL intensity for each of these peaks with preheating temperature. For this sample, a drastic drop in intensity with preheating within 150-200°C is not observed for peaks D2, D2a or D2b as found for the corresponding PTTL peaks for the samples annealed at 700

and 900°C (Chapter 8) as well as for the unannealed sample (Chapter 7).

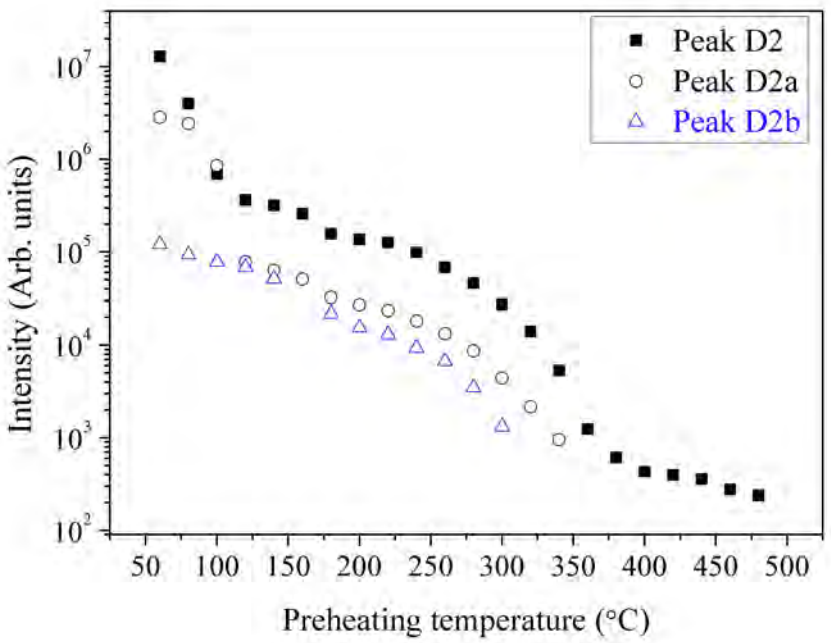

Figure 9.3: Dependence of PTTL intensity on preheating temperatures for peaks D2, D2a and D2b respectively.

Peak I of the conventional TL glow curve of sample D is reproduced under photo-transfer. However, the dependence on preheating temperature of the corresponding peak D1 could not be studied because the peak was not clearly distinct from peak D2. Beyond 350°C of preheating temperature, peaks D2a and D2b could no longer be measured. This is not the case for peak D2 which can be measured up to 460°C. The decrease in PTTL intensity of each of these peaks with preheating temperatures from 60 to 350°C shows that peak III which occurs at 174°C and to a lesser extend peaks IV and V at 234 and 288°C are the main donors of electrons for the observed PTTL peaks.

9.2.2 Effect of partial heating on peaks III and IV

Figure 9.4 shows the dependence of PTTL intensity for peaks D3 and D4 on preheating temperature. For peak D3 the intensity decreases from 60 to 80°C but is nearly constant from 100 to 140°C and then decreases up to 180°C. There is a gap in data points from 180 to 280°C followed by a slow decrease up to 400°C. Within 180 - 280°C, we observed peak D2b to such an extent that D3 is obscured. PTTL is only observed from peak III, namely peak D3, when peak D2b which is

on the rising edge of peak III is no longer observed. This suggests that the competition for electrons from possible donors between 180 to 280°C is dominated by the electron trap of peak D2b. The intensity of peak D4 is constant with preheating temperature up to 200°C and then decreases monotonically thereafter.

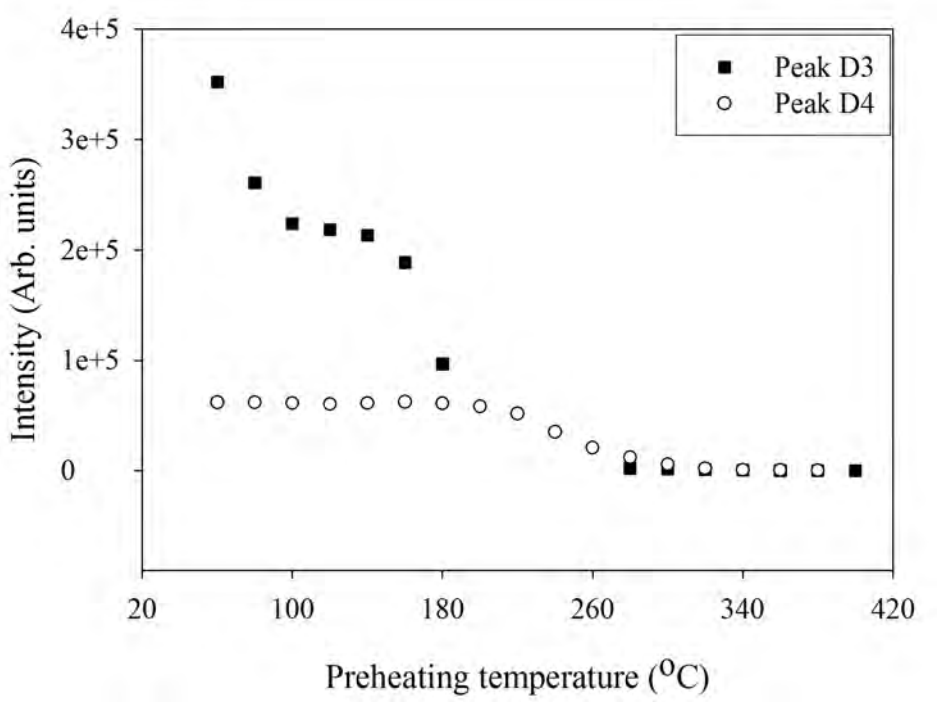

Figure 9.4: Dependence of PTTL intensity on preheating temperatures for peaks D3 and D4 respectively.

Peaks D3 and D4 are observed as PTTL peaks only after preheating beyond 180 and 240°C respectively. Hence, the initial behaviour of peaks D3 and D4 with preheating up to 140 and 200°C respectively is expected since the corresponding traps are not yet depleted significantly. The result for peak D4 shows that peak IV of sample D is a donor of electrons for PTTL peak D3.

9.2.3 Effect of partial heating on peaks V and VII

Peak IV of sample D is reproduced under phototransfer and the dependence of its intensity on preheating temperature is shown in Figure 9.4. Peaks V and VII of sample D are not reproduced under phototransfer.

Table 9.1 lists the 'possible' or theoretical donors for each observed PTTL peaks for the preheating temperatures used.

Table 9.1: TL peaks, their corresponding PTTL peaks and possible donors

	TL	PTTL		
Peak label	T_m (°C)	Peak label	Preheating temp (°C)	Possible donors
I	52	D1	120	III IV V VII
			200	IV V VII
			260	V VII
			350	VII
II	82	D2	120	III IV V VII
			200	IV V VII
			260	V VII
			350	VII
IIa	102	D2a	120	III IV V VII
			200	IV V VII
			260	V VII
			350	VII
IIb	∼140	D2b	200	IV V VII
			260	V VII
			350	VII
III	174	D3	200	IV V VII
			260	V VII
			350	VII
IV	234	D4	260	V VII
			350	VII
V	288			
VII	384			

9.3 Qualitative description of the dependence of PTTL intensity on illumination time

For sample D, which is annealed at 1200°C for 15 minutes, PTTL is observed only when peak II is completely removed from the glow curve hence the first PTTL peaks here were found after preheating to 120°C. This is not the case for the unannealed sample and the samples annealed at 700 and 900°C. The intensity of peak II was

monitored with illumination time for glow curves measured at 1°C/s following irradiation to 0.2 Gy, preheating to 70°C and light exposure. The intensity of peak II was found to decrease monotonically with illumination suggesting that the population of electrons lost during illumination was higher than that gained.

9.3.1 PTTL following preheating to 120°C

Peaks I, II and IIa of sample D are removed after preheating to 120°C. These peaks are reproduced as PTTL peaks at 52, 82 and 104°C respectively and are labelled D1, D2 and D2a. Figure 9.5 shows the dependence of PTTL intensity on illumination time for peak D1 after preheating to 120°C. The peak reaches its maximum intensity at 16 s of illumination time before decreasing thereafter. Beyond 50 s of illumination time peak D1 could no longer be measured.

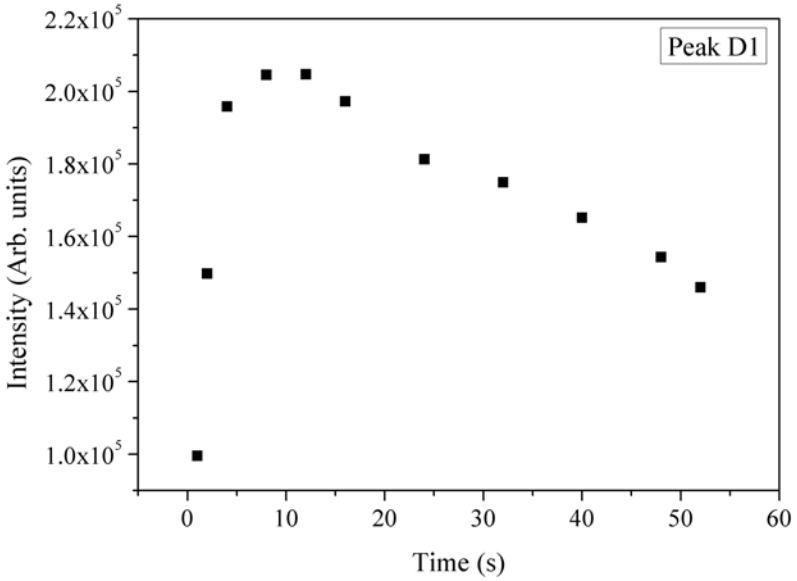

Figure 9.5: Dependence of PTTL intensity on illumination time after preheating to 120°C for peak D1.

Figure 9.6 shows the dependence of PTTL intensity on illumination time for peak D2 after preheating to 120°C. The intensity of peak D2 increases with illumination time up to 128 s and then decreases monotonically to a steady level thereafter. For this peak, the PTTL could still be measured with illumination time up to 20000 s.

The dependence of TL intensity on duration of illumination for peaks III, IV, V and VII are shown in Figure 9.7. Figure 9.7a shows the dependence of TL intensity on illumination time after preheating to 120°C for peaks III and IV of sample D. The

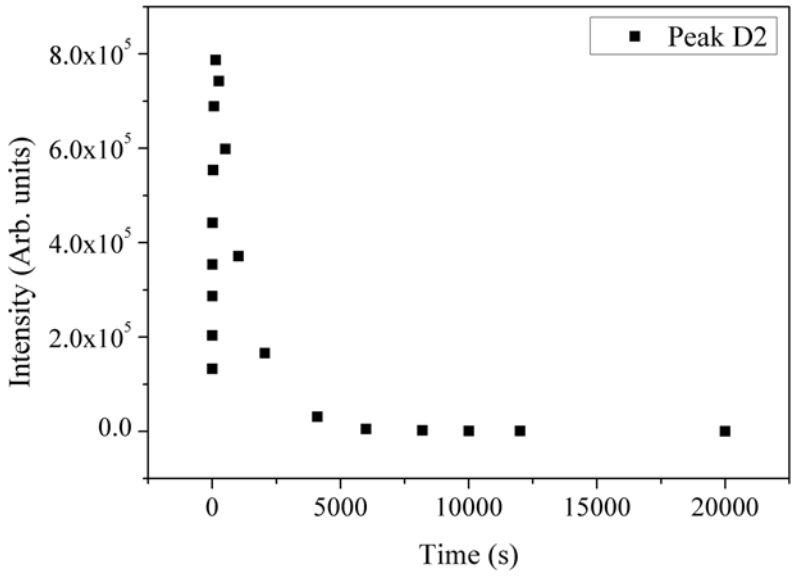

Figure 9.6: Dependence of PTTL intensity on illumination time after preheating to 120°C for peak D2.

intensities of peaks III and IV which are close in magnitude decrease monotonically with illumination time falling to less than 50% of their initial values within the first 2000 s of illumination time. Figure 9.7b shows the TL intensity against illumination time after preheating to 120°C for peaks V and VII of sample D respectively. The TL intensities of peak V and VII decrease continuously with illumination time up to 1024 s. The inset of Figure 9.7b shows the intensity of peak D2a ($\sim$ 100°C) against illumination time. The intensity of this peak first increases with illumination time up to 10 s and then decreases monotonically thereafter.

The possible donors for sample D after preheating to 120°C are the electron traps of peaks III, IV, V and VII respectively. Peak IIb, which is on the rising edge of peak III, is also a potential donor but its contribution can be neglected since it cannot be clearly isolated from peak III for this preheating temperature.

In order to evaluate the contribution of each potential donor, the relative intensity of each of peaks III, IV, V and VII is computed as the ratio between the peak intensity and that of the most intense peak for the shortest duration of illumination used. Following preheating to 120°C, peak IV is initially the most intense. Figure 9.8 shows the relative intensity for peaks III, IV, V and VII. As shown in Figure 9.8a, the relative intensity of peak III increases initially to 1.14 with illumination up to 4096 s and decreases thereafter to 0.91. That of peak IV is constant at 1.00 since it is taken as reference. For peak V, the relative intensity

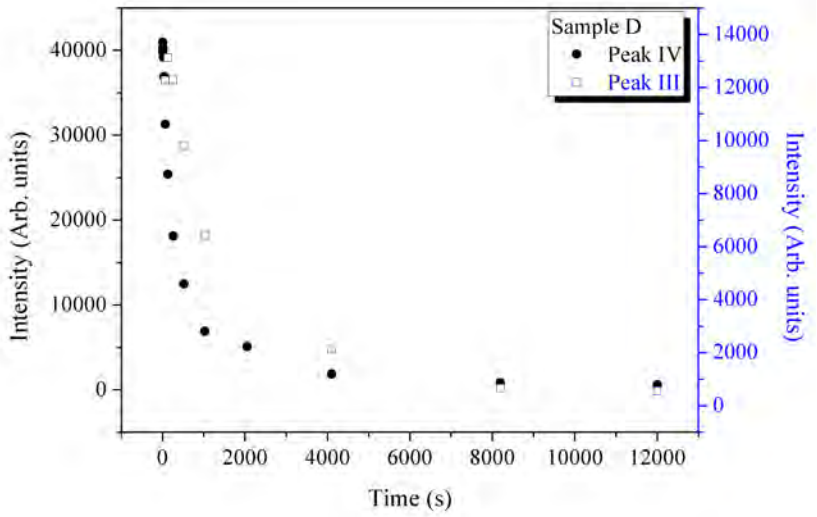

a

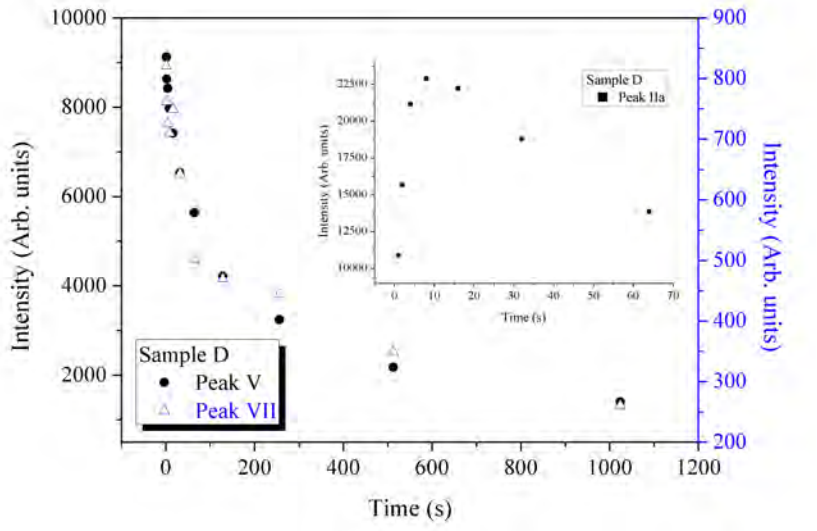

b

Figure 9.7: Dependence of TL intensity on illumination time after preheating to 120°C for peaks III and IV (a) and for peaks V and VII for sample D (b).

varies between 0.23 and 0.20 with illumination time up to 1024 s whereas as for peak VII, it is below 0.05 for any length of illumination. Based on this analysis, the electron traps corresponding to peaks III and IV are the main donors. There is a small but negligible contribution from peak V.

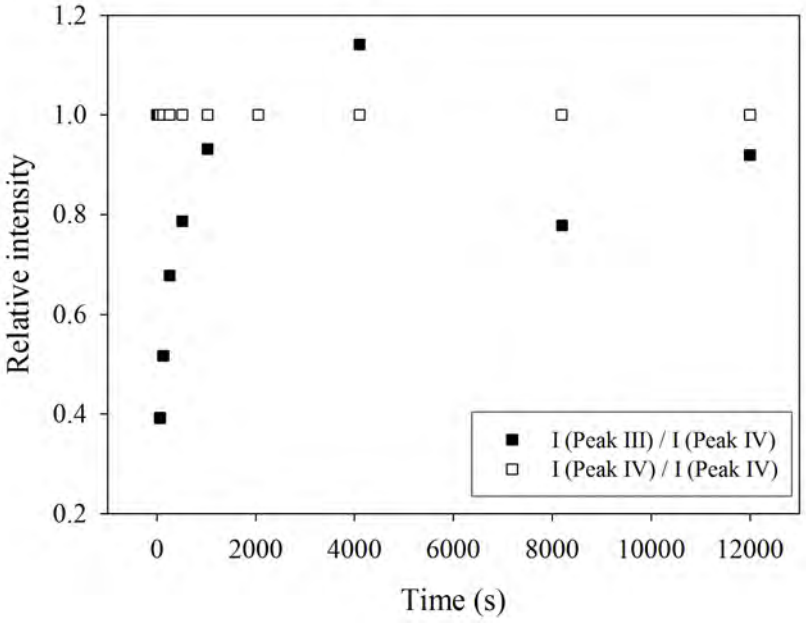

a

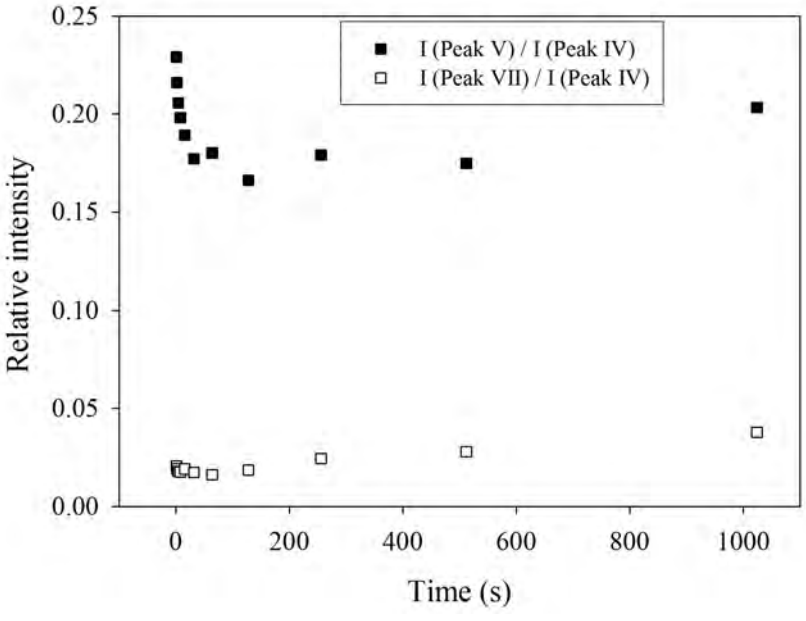

b

Figure 9.8: Relative intensity of (a) peaks III and IV and of (b) peaks V and VII on illumination time after preheating to 120°C.

9.3.2 PTTL following preheating to 200°C

Preheating to 200°C is intended to remove peaks I-III. The PTTL peaks observed subsequently are peaks D1, D2, D2a and D3. In addition to these, a PTTL peak near 140°C denoted D2b is also observed. Peaks D2, D2a, D2b and D3 occur at 80, 104, 142 and 170°C respectively. The PTTL time-response of peak D1 could not be studied because it is indistinct from peak D2 in this case. Figure 9.9 shows a glow curve measured immediately after irradiation to 0.2 Gy (solid symbols) and one measured after irradiation to 0.2 Gy, preheating to 200°C and illumination for 12s where PTTL peaks D1, D2, D2a and D2b are apparent.

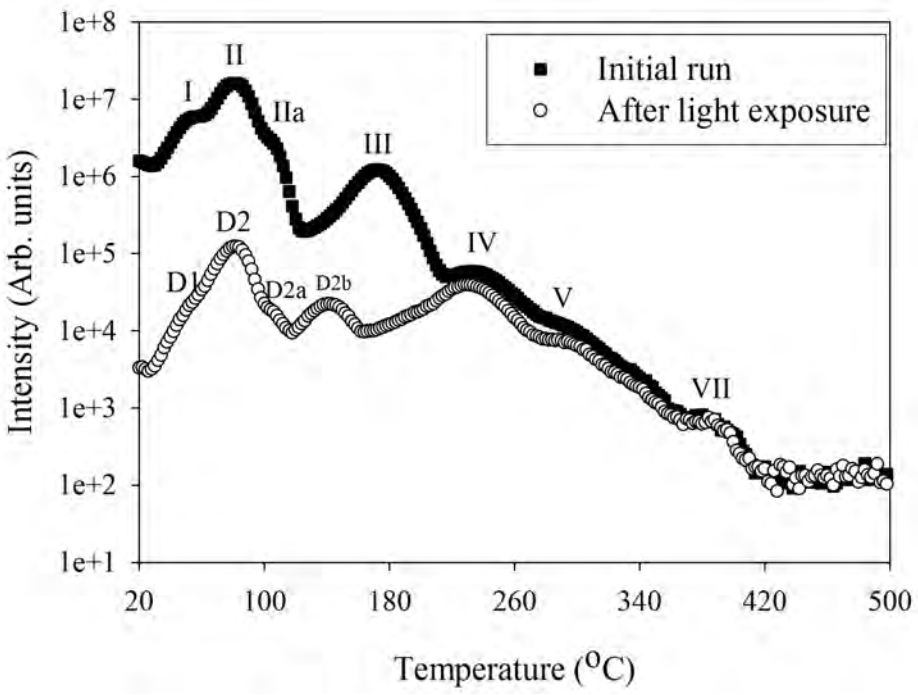

Figure 9.9: Glow curve of sample D measured at 1°C/s after irradiation to 0.2 Gy (solid symbols). The glow curve obtained after preheating to 200°C and subsequent illumination for 12 s (open symbols) is also shown for comparison.

Figure 9.10 shows the dependence of PTTL intensity on illumination time for peak D2 after preheating to 200°C.

The intensity of peak D2 first increases with illumination time before decreasing monotonically thereafter with further illumination up to 12000 s. Figure 9.11a shows the dependence of PTTL intensity of peak D2a on illumination time after preheating to 200°C. The intensity of this peak reaches a maximum at 128 s of illumination time before decreasing monotonically thereafter with illumination time

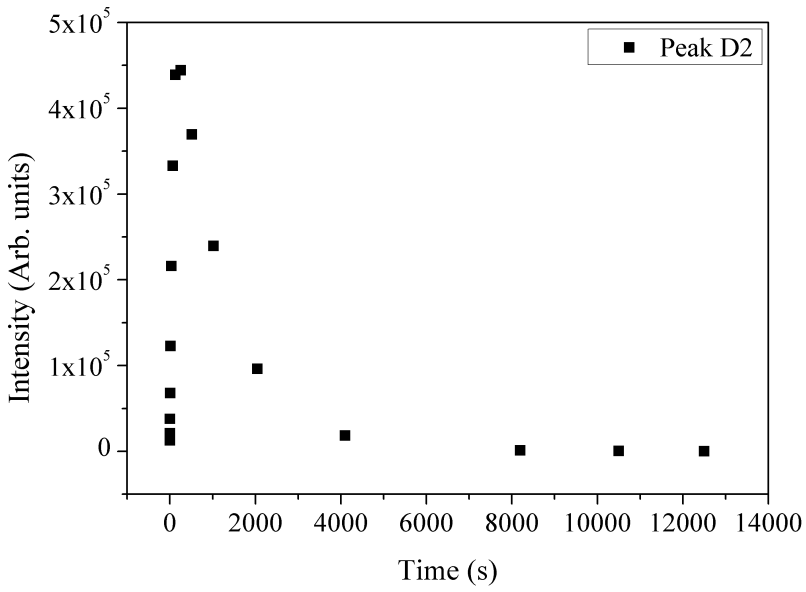

Figure 9.10: Dependence of PTTL intensity on illumination time after preheating to 200 °C for peak D2.

up to 4096 s.

Figure 9.11b shows the dependence of PTTL intensity on illumination time for peak D2b following preheating to 200°C. For peak D2b, the PTTL intensity initially increases with illumination time up to 8 s before decreasing monotonically thereafter with further illumination time up to 65 s. In contrast to peak D2 which can be measured following illumination time up to 12000 s, peak D2b can only be measured for much shorter illumination times. For peak D3, the intensity decreases monotonically with illumination time up to 8192 s as shown in Figure 9.12.

The supposed donors are therefore electron traps of peaks IV, V and VII.

Figure 9.13 shows the dependence of TL intensity on illumination time for peaks IV, V and VII. The intensity of each of these peaks decreases monotonically with illumination time. Peaks V and VII are only observed up to 2000 s of illumination time whereas peak IV can be measured up to 4000 s of illumination time. The relative intensity of each of these peaks is plotted in Figure 9.14. Its analysis shows that peak IV is the main donor. There is a small contribution from peak V and a negligible one from peak VII.

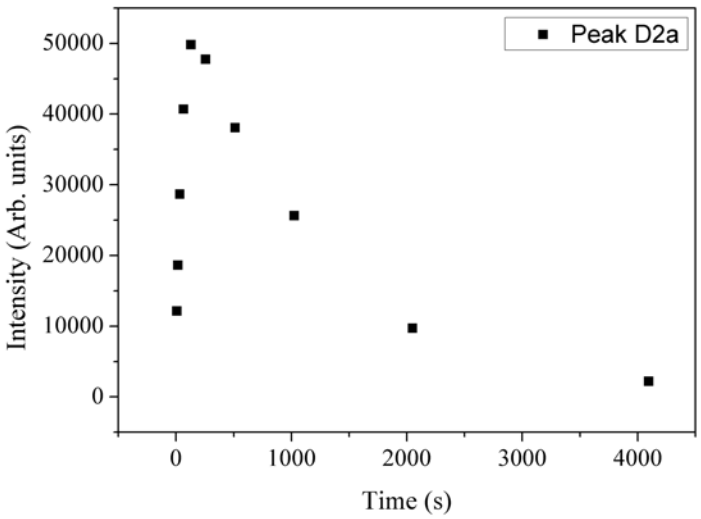

a

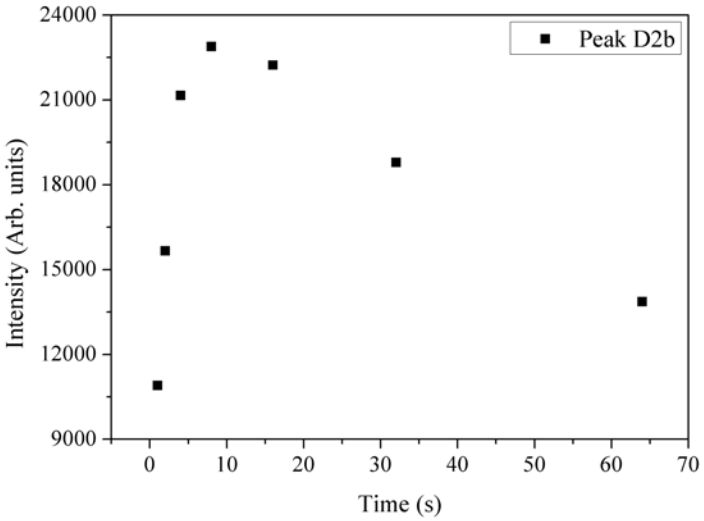

b

Figure 9.11: Dependence of PTTL intensity on illumination time after preheating to 200 °C for peak D2a (a) and, for peak D2b.

9.3.3 PTTL following preheating to 260°C

Preheating to 260°C removes I-IV of sample D. PTTL peaks D2, D2a, D2b, D3 and D4 which correspond to peaks I-IV respectively are observed after subsequent illumination and heating. These peaks occur at 82, 104, 142, 170 and 236°C respectively. Figure 9.15 shows that the intensity of peak D2, following preheating to 260°C, first increases with illumination time up to 256 s before decreasing mono-

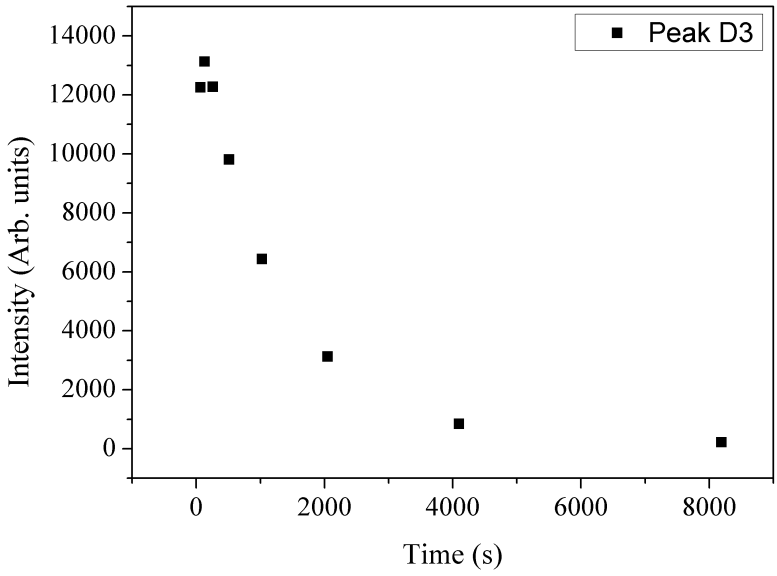

Figure 9.12: Dependence of PTTL intensity on illumination time after preheating to 200 °C for peak D3 (b).

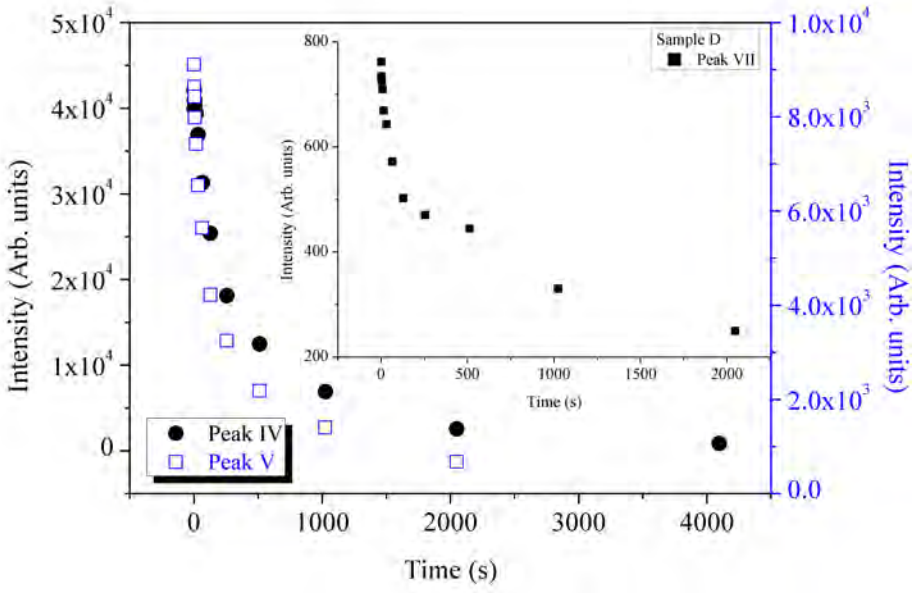

Figure 9.13: Dependence of TL intensity on illumination time following preheating to 200 °C for peaks IV, V and VII of sample D.

tonically thereafter with further illumination time up to 8192 s. Peak D2a, whose profile is shown in Figure 9.16a, behaves in a similar manner.

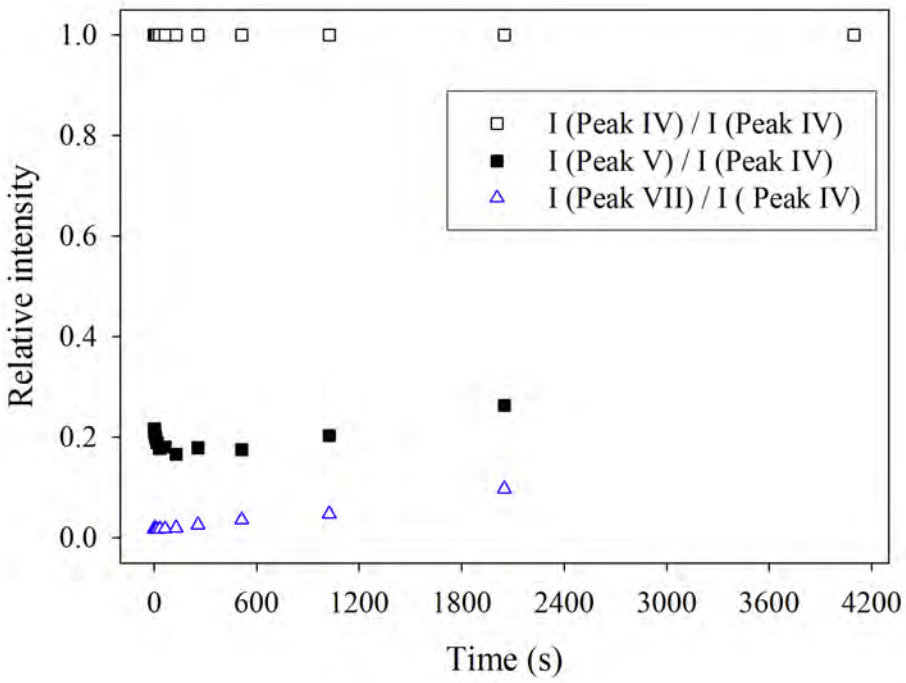

Figure 9.14: Relative intensity of peaks IV, V and VII of sample D on illumination time after preheating to 200°C.

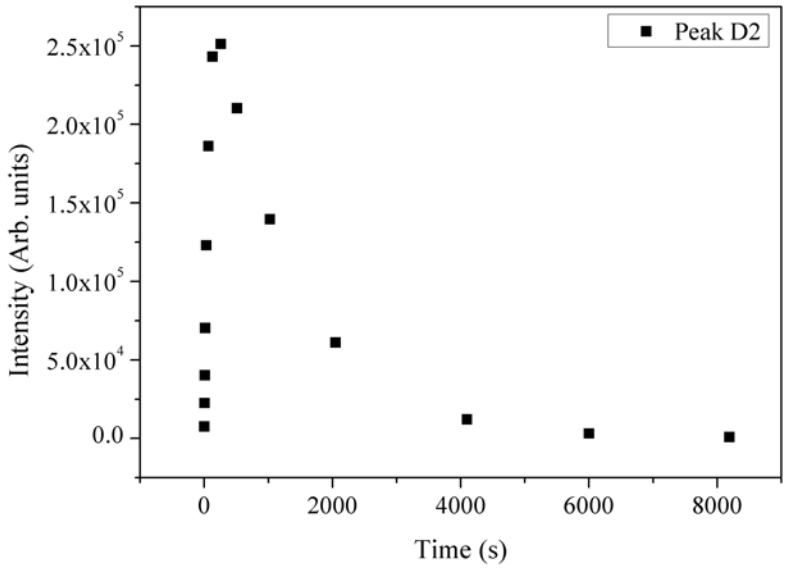

Figure 9.15: Dependence of PTTL intensity on illumination time after preheating to 260 °C for peak D2.

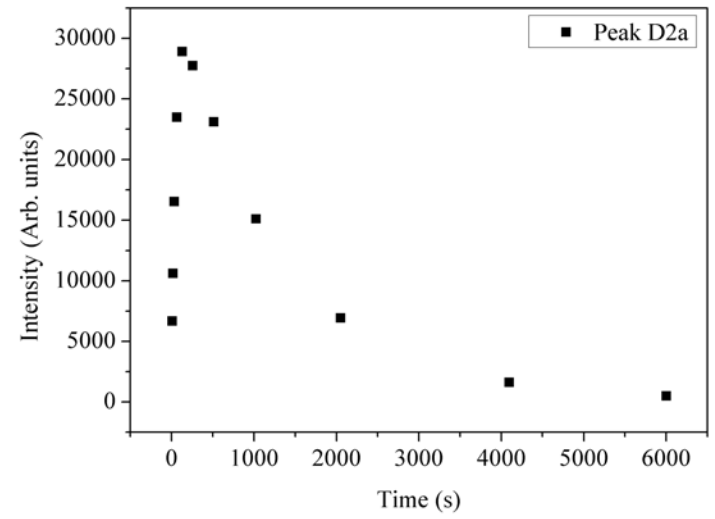

a

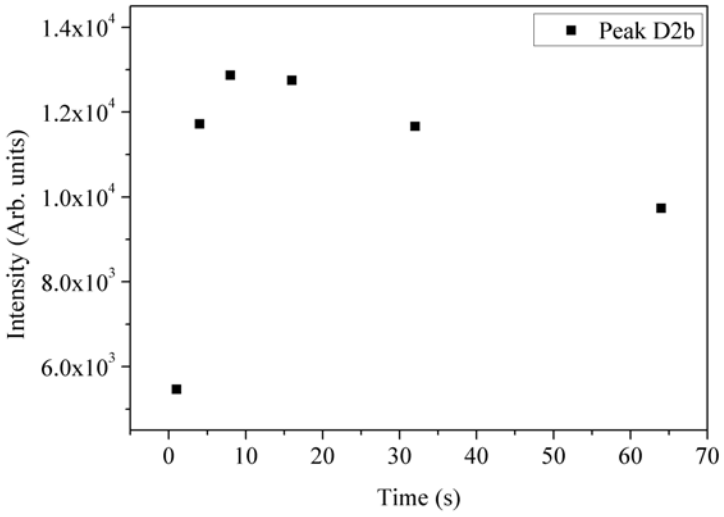

b

Figure 9.16: Dependence of PTTL intensity on illumination time after preheating to 260 °C for peaks D2a (a) and D2b (b) respectively.

For peak D2b, the intensity increases with illumination time up to 8 s before decreasing thereafter with further illumination up to 64 s as shown in Figure 9.16b. For exposure time greater than 64 s, peak D2b could no longer be measured because peak D3 became prominent. Figure 9.17 shows the dependence of PTTL intensity on illumination time for peak D3 after preheating to 260°C.

For peak D3, the intensity reaches a maximum at 128 s of light exposure time before

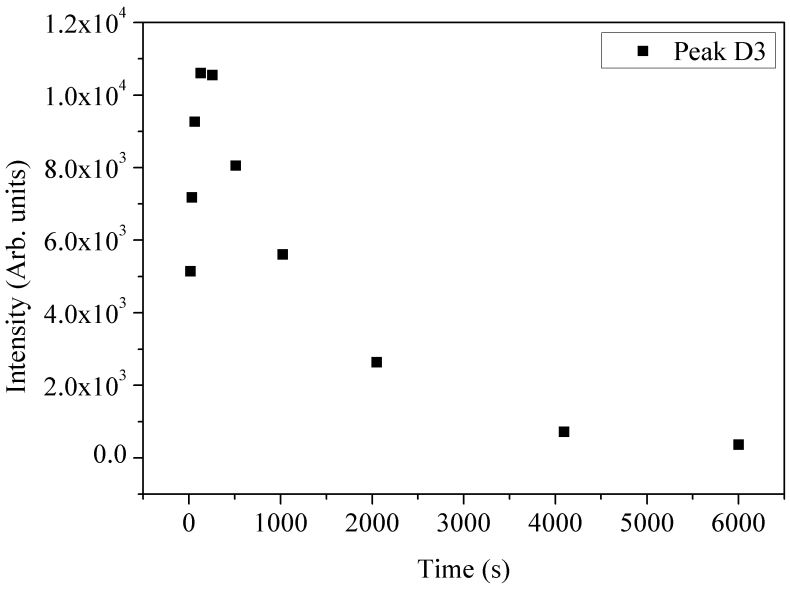

Figure 9.17: Dependence of PTTL intensity on illumination time after preheating to 260 °C for peak D3.

decreasing monotonically thereafter with illumination time up to 6000 s. For this sample, peak IV is reproduced by phototransfer as peak D4. The corresponding peak of samples B (annealed at 700°C) or C (annealed at 900°C) is not reproduced. Figure 9.18a shows the dependence of intensity on illumination time for peak D4 after preheating to 260°C and in the inset following preheating to 350°C.

For preheating to 260°C, the PTTL intensity increases with illumination time up to 64 s before decreasing monotonically thereafter. The electron traps associated with peaks V and VII are the supposed donors of the observed PTTL peaks since they are not removed by preheating to 260°C. The dependence of TL intensity on illumination time for each of these two peaks is shown is Figure 9.18b. In each case, the TL intensity decreases continuously with illumination. The ratio between the intensity of peak V and that of peak VII as a function of illumination shows that peak V is the main donor for this preheat.

9.3.4 PTTL following preheating to 350°C

Following preheating to 350°C, all the peaks with the exception of peak VII of sample D are removed. Hence with the exception of deep traps, the electron trap of this remaining peak is the only donor. The observed PTTL peaks are D1, D2, D2a, D3 and D4. They occur at 56, 82, 102, 171 and 240°C respectively. Figure 9.19

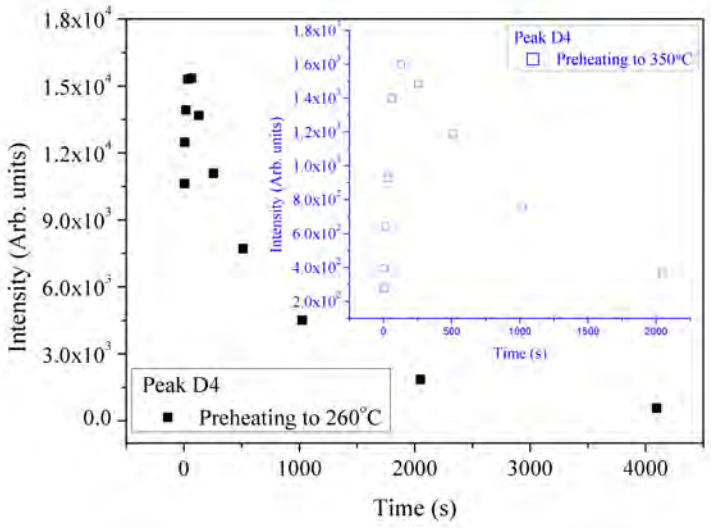

a

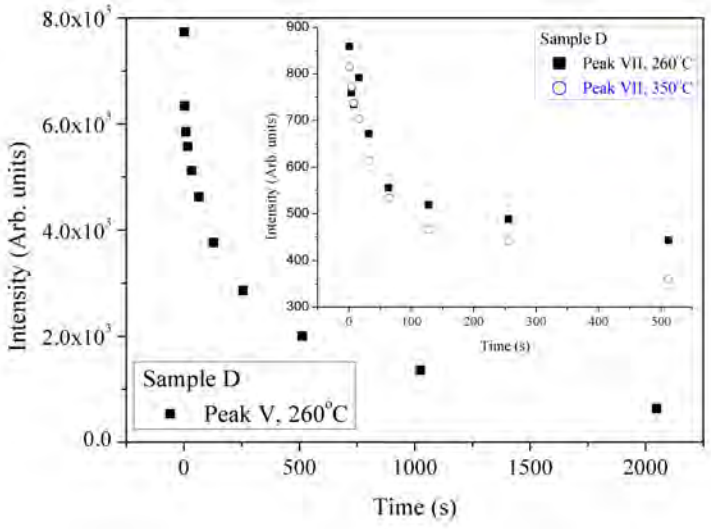

b

Figure 9.18: Dependence of PTTL intensity on illumination time after preheating to 260°C and, to 350°C for peak D4 (a) and dependence of TL intensity on illumination time after preheating to 260°C and to 350°C respectively (b).

shows the dependence of PTTL intensity on illumination time for peak D1. The intensity of peak D1 increases initially with illumination time up to 125 s and then decreases slightly. Beyond 256 s, the peak could no longer be measured.

Figure 9.20a shows the dependence of intensity on illumination time for peak D2. The peak intensity increases to a maximum with illumination time up to 512 s and

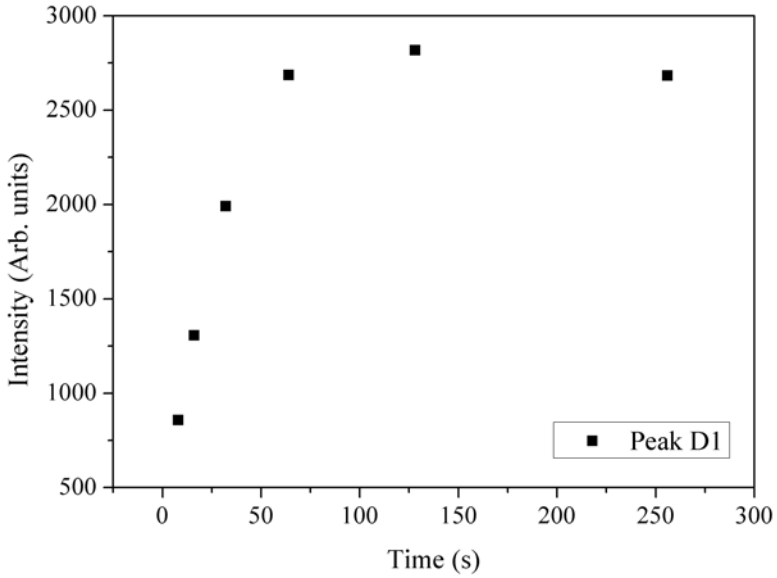

Figure 9.19: Dependence of PTTL intensity on illumination time for peak D1 after preheating to 350 °C.

then decreases thereafter.

Figure 9.20b shows the dependence of PTTL intensity on illumination time for peak D2a. The intensity of this peak reaches a maximum at 256 s and then decreases monotonically with exposure time up to 2048 s.

Figure 9.21 shows the dependence of PTTL intensity on illumination time for peak D3 after preheating to 350°C. Peak D3 reaches its maximum intensity at 256 s and then decreases monotonically with further illumination time up to 2048 s. Peak D4, as shown in the inset of Figure 9.18a, behaves in a similar manner as peak D3 except that its maximum intensity is reached at 128 s. The TL intensity of peak VII, which is not completely removed following preheating to 350°C, is shown in the inset of Figure 9.18b.

9.3.5 PTTL Following preheating to 400°C

Peak D2 is found after preheating to 400°C and exposure to light for 10 s. However its intensity is low and for higher illumination times, it is not observed. The main donor of this peak is bleached for this preheat. Hence, the PTTL-time profile of peak D2 could not be studied for this preheat. Figure 9.22 shows a TL glow curve of sample D measured at 1°C/s after irradiation to 0.2 Gy, preheating to 400°C

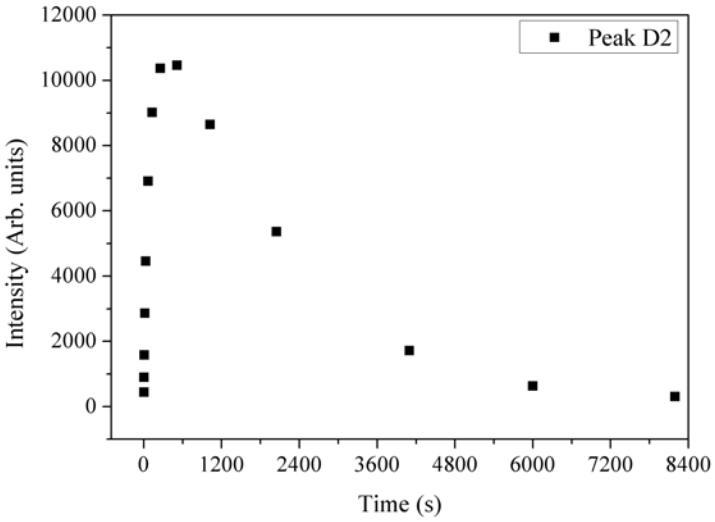

a

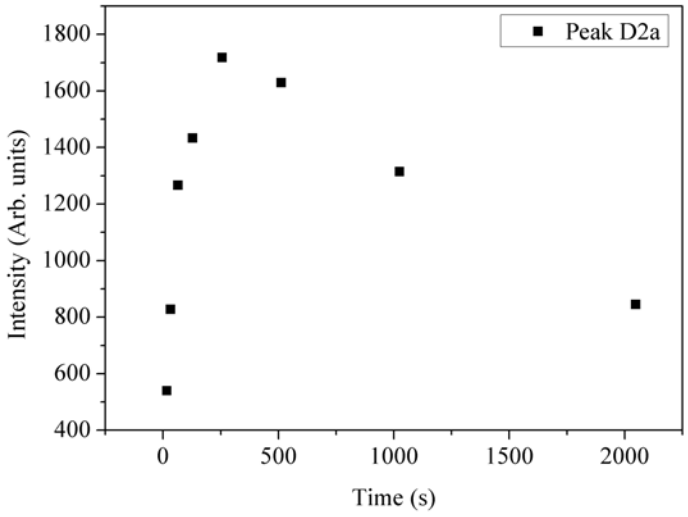

b

Figure 9.20: Dependence of PTTL intensity on illumination time after preheating to 350 °C for peak D2 (a) and for peak D2a (b).

and illumination for 10 s. For the unannealed sample on the other hand, PTTL peaks were found as reported by Sob et al. (2021).

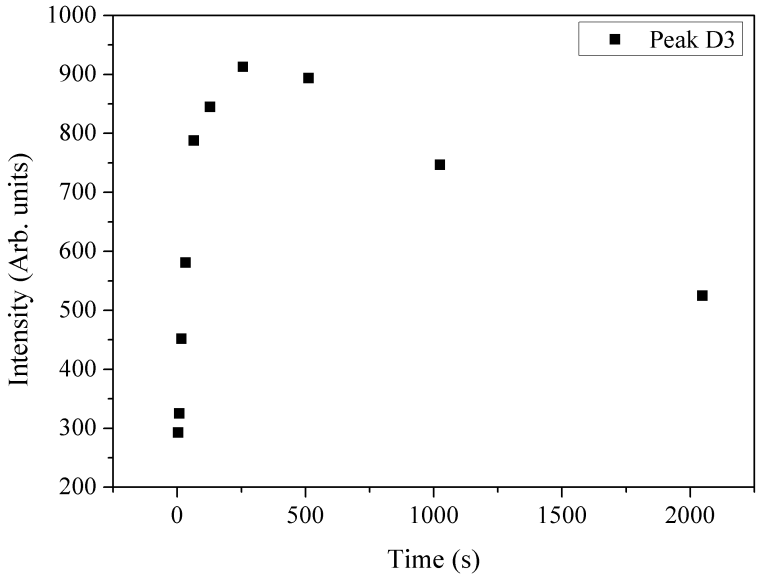

Figure 9.21: Dependence of PTTL intensity on illumination time after preheating to 350 °C for peak D3.

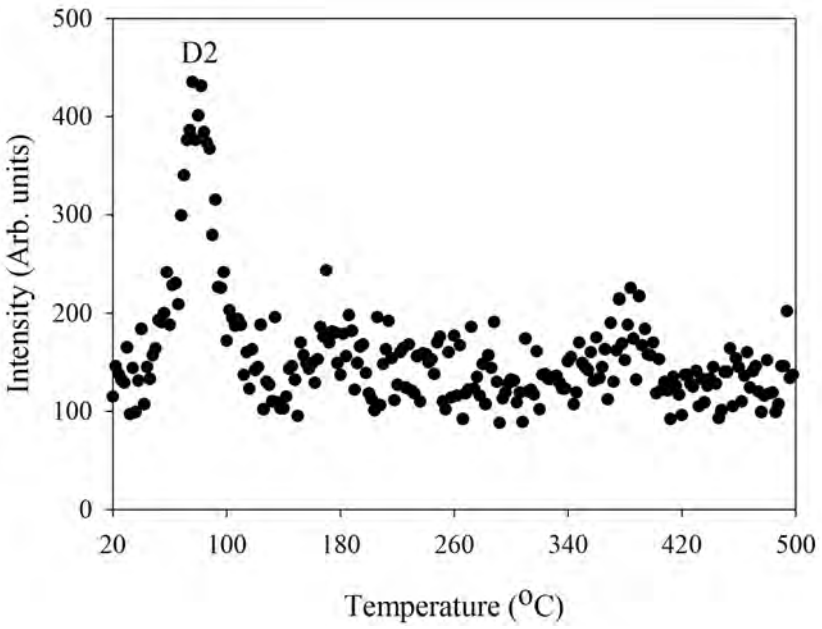

Figure 9.22: A glow curve of sample D measured at 1°C/s after irradiation to 0.2 Gy, preheating to 400°C and illumination for 10 s. Peak D2 is the PTTL peak corresponding to peak II.

9.4 Mathematical analysis of PTTL time-profiles

This section deals with a mathematical analysis of PTTL time-response profiles of sample D. The observed TL and PTTL peaks of sample D are listed in Table 9.2. The electron traps listed as 'possible donors' are the theoretically expected ones. The main donors suggested by the partial heating experiment (section 9.2) and as reflected by PTTL time-profiles (section 9.3) are listed separately. The analysis will be based on the latter two lists rather than the ideal theoretical list. N_i will denote the concentration of trapped electrons at the ith electron trap and, s_i the optical stimulation probability. The equations describing the change in the concentration of trapped electrons will be written for the illumination step only. For each PTTL peak, these equations describe the transfer of optically stimulated electrons from donors to the corresponding acceptor. As stated earlier, the number of donors depends on the preheating temperature. The solution of this set of equations is then applied to the PTTL-time response profile of the given peak. This method was developed by Chithambo et al. (2017a). As stated in chapters 7 and 8, it has been used to quantitatively describe the PTTL-time response profiles of quartz (Chithambo et al., 2018, 2019; Chithambo and Dawam, 2020), α-Al_2O_3:C (Chithambo et al., 2017a) and of unannealed α-Al_2O_3:C,Mg (Sob et al., 2021). One of the main assumptions of this method is that only a portion of electrons stimulated from donor traps are transferred to the acceptor trap to produce PTTL. The other assumption is that of negligible retrapping because the sample has first-order peaks.

Table 9.2: A summary of TL peaks, their corresponding PTTL peaks, donors and photoionization cross-section for sample D

	TL	PTTL					P. cross-section (cm^2)		
Peak label	T_m (°C)	Peak label	Preheating temp (°C)	Possible donors	Main donor[a]	Main donor[b]	Acceptor	Donor	Donor
I	52	D1	120	III IV V VII	III	III IV	3.53e-20	3.81e-18	
			200	IV V VII	IV	IV			
			260	V VII		V			
			350	VII		VII			
II	82	D2	120	III IV V VII	III	III IV	4.11e-21	3.57e-19	
			200	IV V VII	IV	IV	4.70e-21	9.58e-20	
			260	V VII		V	4.70e-21	9.82e-20	
			350	VII		VII	2.35e-21	7.82e-20	
IIa	102	D2a	120	III IV V VII	III	III IV	4.70e-21	1.37e-19	
			200	IV V VII	IV	IV	4.70e-21	1.35e-19	
			260	V VII		V	2.35e-21	1.06e-19	
			350	VII		VII			
IIb	∼140	D2b	200	IV V VII	IV	IV	5.41e-20	3.14e-18	
			260	V VII		V	3.17e-20	3.00e-18	
			350	VII		VII			
III	174	D3	200	IV V VII	IV	IV	4.11e-21	5.36e-18	
			260	V VII		V	4.11e-21	1.82e-19	
			350	VII		VII	1.17e-21	2.42e-19	
IV	234	D4	260	V VII		V	7.05e-21	1.49e-18	
			350	VII		VII	4.70e-21	1.58e-19	
V	288								
VII	384								

[a] ✓ From pulse annealing study.
[b] ✓✓ From time-response study.

9.4.1 PTTL following preheating to 120°C

For sample D, the first PTTL peak is only measured after preheating to 120°C as described in section 9.3. The observed PTTL peaks after preheating to 120°C are peaks D1, D2 and D2a. The possible donors for each of these peaks are the traps associated with peaks III, IV, V and VII. The main donor from pulse annealing is the trap associated with peak III whereas the electron traps suggested from the time-response study are the traps of peaks III and IV. By considering only the dominant donor, the PTTL profile for peaks D1, D2 or D2a can each be described as a system of one acceptor and one donor with rate equations as follows:

$$\frac{dN_3}{dt} = -s_3 N_3 \tag{9.1}$$

$$\frac{dN_j}{dt} = -s_j N_j + \alpha_3 s_3 N_3 \tag{9.2}$$

where j is either 1, 2 or 2a, depending on which of peaks D1, D2 or D2a is considered; s_j is the corresponding probability of optical stimulation and α_3 is a proportionality constant. Equation (9.1) describes the loss of electrons from the donor whereas equation (9.2) describes not only the transfer of electrons from the donor but also the loss due to illumination at the acceptor. The solution of the coupled sets of equations (9.1) and (9.2) is

$$N_j = A(e^{-s_3 t} - e^{-s_j t}) \tag{9.3}$$

where $A = \alpha_3 s_3 N_{3i}/(s_3 - s_j)$ and, N_{3i} is the initial concentration of trapped electrons at the donor trap at the start of illumination.

Increasing the number of donors to two by considering the other donor (peak IV) did not yield any improvement in the fit of D1, D2 or D2a. The fits obtained from equation (9.3) for the time-response profiles of peaks D1 and D2 are shown in Figure 9.23 in section 9.5. Fits for the time-response profiles of PTTL peaks following preheating to 200, 260 and 350°C are also shown in section 9.5.

9.4.2 PTTL following preheating to 200°C

Preheating to 200°C removes peaks I-III of sample of D and the PTTL peaks found are D1, D2, D2a, D2b and D3 respectively. The possible donors are the traps corresponding to peaks IV, V and VII however, from pulse annealing the electron trap of peak IV is the main donor. The TL time-response study also suggests

that the electron trap of peak IV is the main donor. The lesser contribution from peak V is negligible. The PTTL-time response profiles of peaks D2, D2a, D2b and D3 were best fitted by Equation (9.3) which considers a single donor.

9.4.3 PTTL following preheating to 260°C

Preheating to 260°C removes peaks I-IV of sample D. PTTL peaks D2, D2b, D3 and D4 are found. The possible donors of electron traps for these PTTL peaks are those of peaks V and VII. From the TL time-response study, we found that the significant contribution is from the electron trap of peak V. For each of these samples, an expression with the same form as equation (9.3) is sufficient to fit the experimental PTTL-time response profiles.

9.4.4 PTTL following preheating to 350°C

Preheating to 350°C removes peaks I-V. Peak VII which is only partially removed is the only donor. The observed PTTL peaks are D1, D3 and D4 respectively. For each of these peaks, a system consisting of one donor trap and one acceptor yielded a satisfactory fit.

9.5 Applications of the mathematical model

Figures 9.23-9.27 show the application of models from equation (9.3) to experimental data for each of the preheating temperatures used. The fits obtained from equation (9.3) following preheating to 120°C are shown in Figure 9.23a for peak D1 and in Figure 9.23b for peak D2 respectively. The PTTL time-response profiles from the same analysis are shown in Figures 9.24a-9.24d for peaks D2, D2a, D2b and D3 respectively after preheating to 200°C.

Figures 9.25a-9.25d show the PTTL time-response profiles of peaks D2a, D2b, D3 and D4 obtained after preheating to 260°C and fitted using expressions of the same form as equation (9.3).

Following preheating to 350°C, the PTTL time-response profiles of peaks D1 and D3 fitted using expressions of the form as equation (9.3) are shown in Figures 9.26a and 9.26b.

Figure 9.27 shows the PTTL time-response profile of peak D4, after preheating to 350°C, fitted with an expression of the same form as equation (9.3).

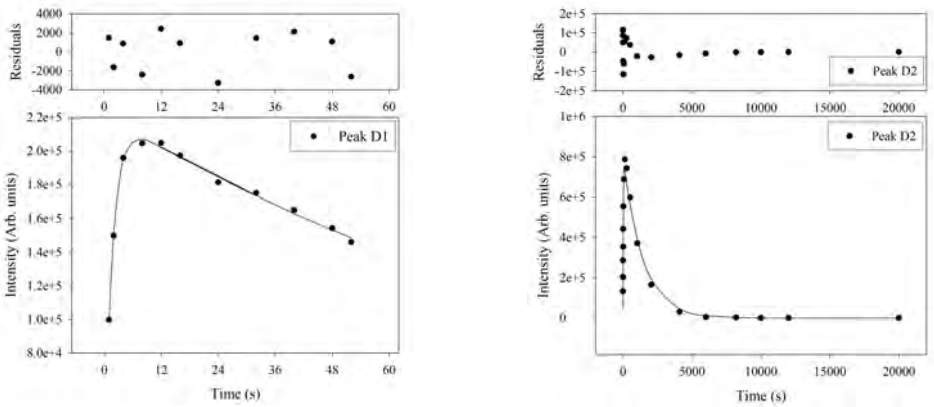

a b

Figure 9.23: PTTL time-response profiles of peaks D1 (a) and D2 (b) after preheating to 120 °C.

The optical stimulation rate $s = \Phi\sigma$ which is obtained from fitting can be used to evaluate the photoionization cross-section σ (Bøtter-Jensen et al., 2003). In this study, the incident photon flux $\Phi = 1.70 \times 10^{17}$ cm^{-2} s^{-1}. The photoionization cross section for the various peaks are included in Table 9.2 and range between 10^{-21}-10^{-18} cm^2.

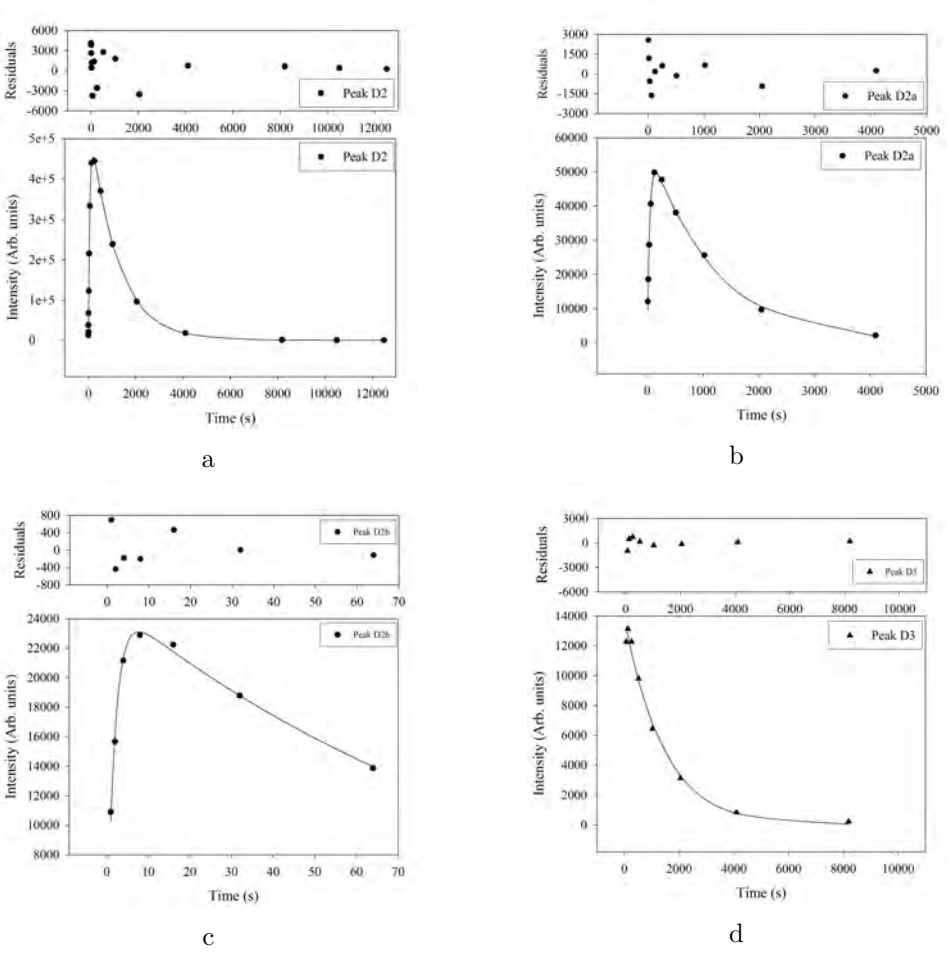

Figure 9.24: PTTL intensity against duration of illumination for peaks D2 (a), D2a (b), D2b (c) and D3 (d) after preheating to 200°C.

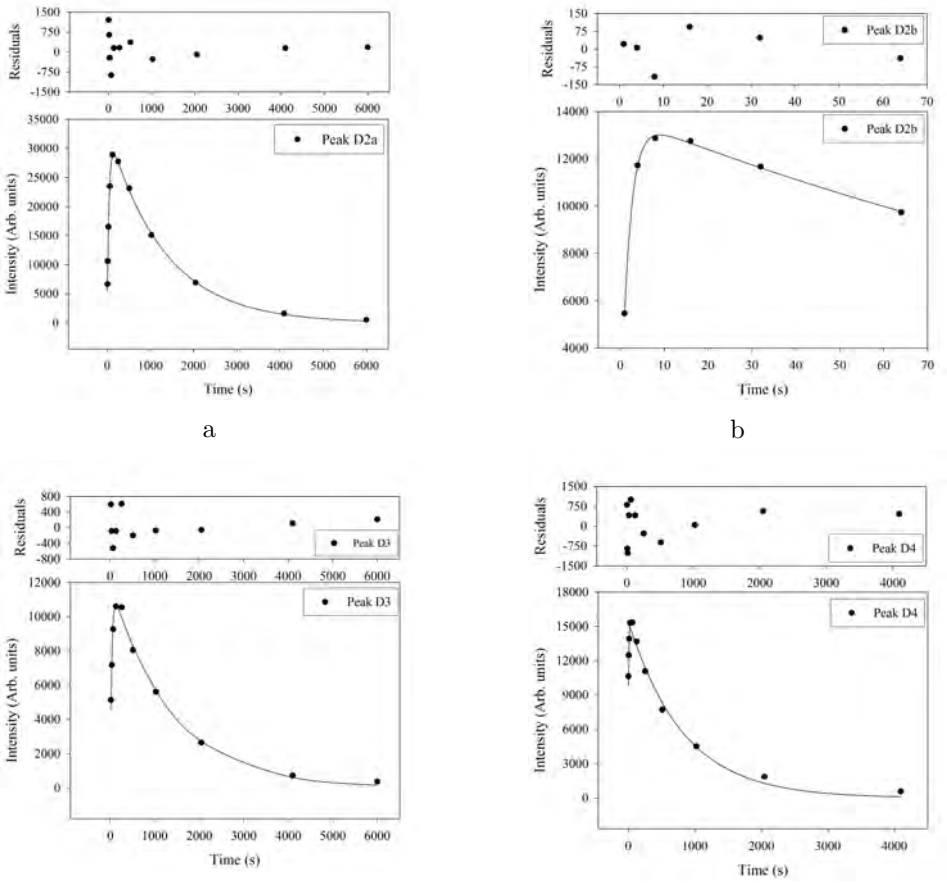

Figure 9.25: PTTL intensity against duration of illumination of peaks D2a (a), D2b (b), D3 (c) and D4 (d) after preheating to 260 °C.

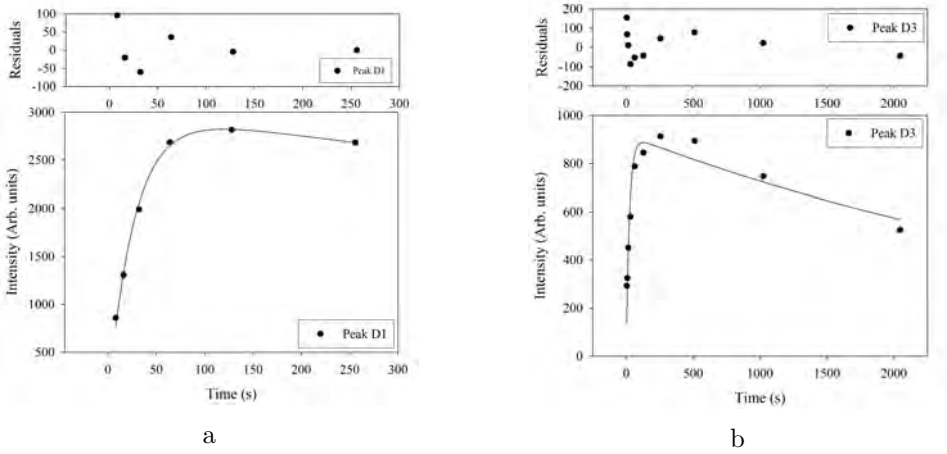

Figure 9.26: PTTL intensity against duration of illumination for peaks D1 (a) and D3 (b) after preheating to 350 °C.

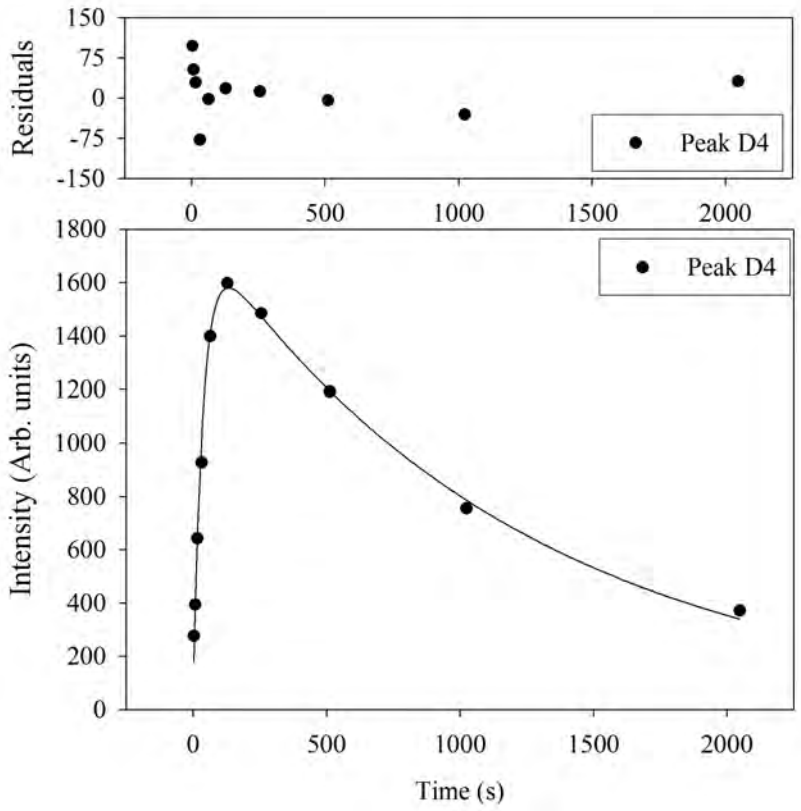

Figure 9.27: PTTL-time profile of peak D4 after preheating to 350°C.

9.6 Regarding the nature of electron traps in α-Al_2O_3:C,Mg

PTTL has been described in terms of inter-electron movement between the different traps. Some of these traps especially those below 200°C act as acceptors whereas others act as donors. The main trap (corresponding to peak III) acts both as an acceptor or a donor depending on the preheating temperature. The nature of these electron traps is not well understood. Although α-Al_2O_3 contains many impurities (McKeever et al., 1995), it is well known that the high sensitivity of this material is due to the formation of F and F^+ centres during the synthesis of α-Al_2O_3:C from Al_2O_3 in the reducing environment of carbon (Akselrod et al., 1990; McKeever et al., 1995; Yukihara and McKeever, 2011). Charge compensators are required for the F^+ centres. Akselrod et al. (1990) suggested that a C^{2+} ion acts as charge compensator to a F^+ centre by substituting an Al^{3+} ion. However, Yang et al. (2008) proposed that F^+ centres could also be charge compensated for when O^{2-} ions are replaced with C^{4-} ions. In a study on the electronic properties of carbon in α-Al_2O_3, Zhu et al. (2014) showed that under Al-rich conditions, C preferentially occupies the O site (C_O) whereas under O-rich conditions, the Al site (C_{Al}) is favoured. The kinetic analysis of α-Al_2O_3:C has shown a shallow trap near 0.72 eV (Chithambo et al., 2014). Zhu et al. (2014) deduced that this electron trap was consistent with the C_{Al} close to the conduction band minimum. Ao et al. (2017) equally showed that C_O has the lowest defect formation energy under Al-rich conditions. Ao et al. (2017) also suggested that C_O defects influence the sensitivity of α-Al_2O_3:C by inducing deep electron traps in the host band gap. In α-Al_2O_3:C,Mg, the shallowest trap has a depth of $\sim$ 0.85 eV. As suggested by Kalita and Chithambo (2017f), this electron trap near 0.85 eV is of the same origin as the corresponding trap in α-Al_2O_3:C but the difference in the two energy values (0.72 and 0.85 eV) is due to lattice stressing caused by the difference in atomic radii. In α-Al_2O_3:C,Mg, some Al sites occupied by C whereas others are occupied by Mg. The transition from the ^3P excited to the ^1S state at the F centre is characterised by emission at 420 nm (McKeever et al., 1995). The F centre is subjected to thermal quenching (Chithambo et al., 2020). In our study of TA-OSL, the activation energy of thermal quenching was evaluated as 1.043 $\pm$ 0.001 eV. Values for the activation energy of thermal quenching such as 1.08 $\pm$ 0.03 eV (Akselrod et al., 1998) and 1.025 $\pm$ 0.002 eV (Chithambo et al., 2015) have been reported for α-Al_2O_3:C. For α-Al_2O_3:C,Mg, values such as 0.90 $\pm$ 0.02 eV (Chithambo et al., 2020), and 0.96 $\pm$ 0.03 eV (Kalita and Chithambo, 2017f) have been reported. This suggests an electron trap at $\sim$ 1.00 eV near the bottom

of the conduction band. An activation energy of 1.26 ± 0.08 has been ascribed to thermal quenching at the F^+-centre (Kalita and Chithambo, 2017f). The use of a Hoya U-340 detection filter (transmission 250-390 nm FWHM) for measurements implies that recorded signal is mainly from luminescence recombination at F^+ and F centres. The presence of Mg also induced with new Mg-aggregate defect such as the F_2^{2+}(2Mg)-centre.

We speculate that the shallow electron trap in α-Al_2O_3:C,Mg is of the same nature as that of α-Al_2O_3:C. The annealing induced peak at 100°C is associated with a new Mg-aggregrate defect which is created after annealing at or above 700°C. We also speculate that electron traps associated with the other peaks could be due to charged states of C_{Al} or C_{Mg} defects. The investigation of the nature of these traps is beyond the scope of the current work and requires further studies.

9.7 Summary

A glow curve of α-Al_2O_3:C,Mg annealed at 1200°C for 15 minutes (sample D) has peaks at 52, 82, 102, 174, 234, 288 and 384°C when measured at 1°C/s after irradiation to 0.2 Gy. These peaks are labelled I, II, IIa, III, IV, V and VII respectively. The peak at 102°C is referred to as peak IIa. A peak, labelled here as IIb, is also observed at ∼140°C in a glow curve measured at 1°C/s after preheating to 120°C. Peaks IIa and IIb are induced by annealing. Peaks I, II, IIa, IIb, III and IV are reproduced as phototransferred peaks D1, D2, D2a, D2b, D3 and D4 for preheating temperatures between 120 and 350°C. After preheating to 200°C, we observed that peak D3 could only be observed from 60 s of illumination time when peak D2b, the PTTL peak corresponding to peak IIb, could no longer be observed. This result and the pulse annealing profile of peak D3 suggest that there is competition for electrons between the traps of peaks IIb and III. The electron trap corresponding to peak III can act as a donor or an acceptor depending on the preheat temperature. It acts as a donor to electron traps of peaks D1, D2 and D2a for preheating below 180°C. For preheating at or above 200°C, the trap accepts electrons from higher temperature traps. In contrast to the unannealed sample or the samples annealed at 700 and 900°C respectively, peak I of this sample is only reproduced under phototransfer after removal of peak II. For this sample and the samples annealed at 700 or 900°C, no PTTL peak found after preheating to 400°C was suitable for analysis unlike for the unannealed sample. The PTTL time-response profiles of sample D have been described as separate systems of an acceptor and a donor for the preheating temperature used.

Chapter 10

Thermally Assisted Optically Stimulated Luminescence of α-Al_2O_3:C,Mg

This chapter reports the studies of optically stimulated luminescence (OSL) from α-Al_2O_3:C,Mg. Section 10.1 deals with preparatory analysis of continuous-wave optically stimulated (CW-OSL) decay curves measured at temperatures between 20 and 200°C from the unannealed sample and the samples annealed at 700, 900 and 1200°C for 15 minutes respectively. Each CW-OSL decay curve is described as a sum of three decay components namely; the fast, the medium, and the slow components. The influence of measurement temperature, irradiation dose, and optical power density on the luminescence intensity are reported. This study of CW-OSL provides a means of investigating the role played by the shallow, intermediates and main electron traps in the luminescence of this sample. The investigation of thermally assisted OSL (TA-OSL) from deep traps is presented in section 10.2 and the kinetics parameters associated with thermal assistance and thermal quenching are also evaluated. The TA-OSL from deep traps are then compared with the CW-OSL from the shallower traps. Section 10.3 summarises the results of this chapter.

10.1 Analysis of continuous-wave optically stimulated luminescence from α-Al_2O_3:C,Mg

10.1.1 General features of OSL

CW-optical stimulation was used to investigate the luminescence properties of α-Al_2O_3:C,Mg. In CW-OSL the luminescence signal is recorded during optical exposure (Bøtter-Jensen et al., 2003). The study was carried on the unannealed sample and on the samples annealed at 700, 900 and 1200°C for 15 minutes respectively. The samples all had a mass of $\sim$ 0.060 g. A heating rate of 1°C/s was used for CW-OSL and TA-OSL measurements. CW-OSL were measured at temperatures between 20 and 200°C. In order to measure CW-OSL, the following sequence (Sequence A) was executed:

1. Heating to 500°C at 1°C/s to measure background signal
2. Irradiation to 1.0 Gy at room temperature to populate the various electron traps
3. Exposure to 470 nm blue light of power density 72 mW/cm^2 at sample position for 1000 s at temperature T_i to measure CW-OSL
4. Heating to 500°C at 1°C/s to measure the residual TL

Steps 2 - 4 of Sequence A were carried out for measurement temperatures T_i from 20 to 200°C at intervals of 20°C. Figure 10.1 shows semi-logarithmic plots of CW-OSL decay curves measured at 20, 100 and 200°C for the unannealed sample and the samples annealed at 700, 900 and 1200°C respectively.

Irrespective of annealing, Figure 10.1 shows that the OSL intensity initially decreases rapidly with measurement temperature. In particular, for CW-OSL curves measured at 100 and 200°C, the OSL intensity of each sample drops below 0.1% of its initial value after the first 100 s of stimulation. The CW-OSL curves measured at 20°C on the other hand do not decrease as much within the same interval. TL glow curves of these samples have a main peak within 150 - 200°C and secondary peaks below 150°C for a heating rate of 1°C/s. The traps associated with the shallow peaks are depleted when the sample is heated to 100°C. Similarly, the traps corresponding to these secondary peaks and the main peak are depleted by heating to 200°C. After the first 100 s of stimulation time, the CW-OSL curves then decrease slowly to a steady value. The semi-logarithmic scale was used to better

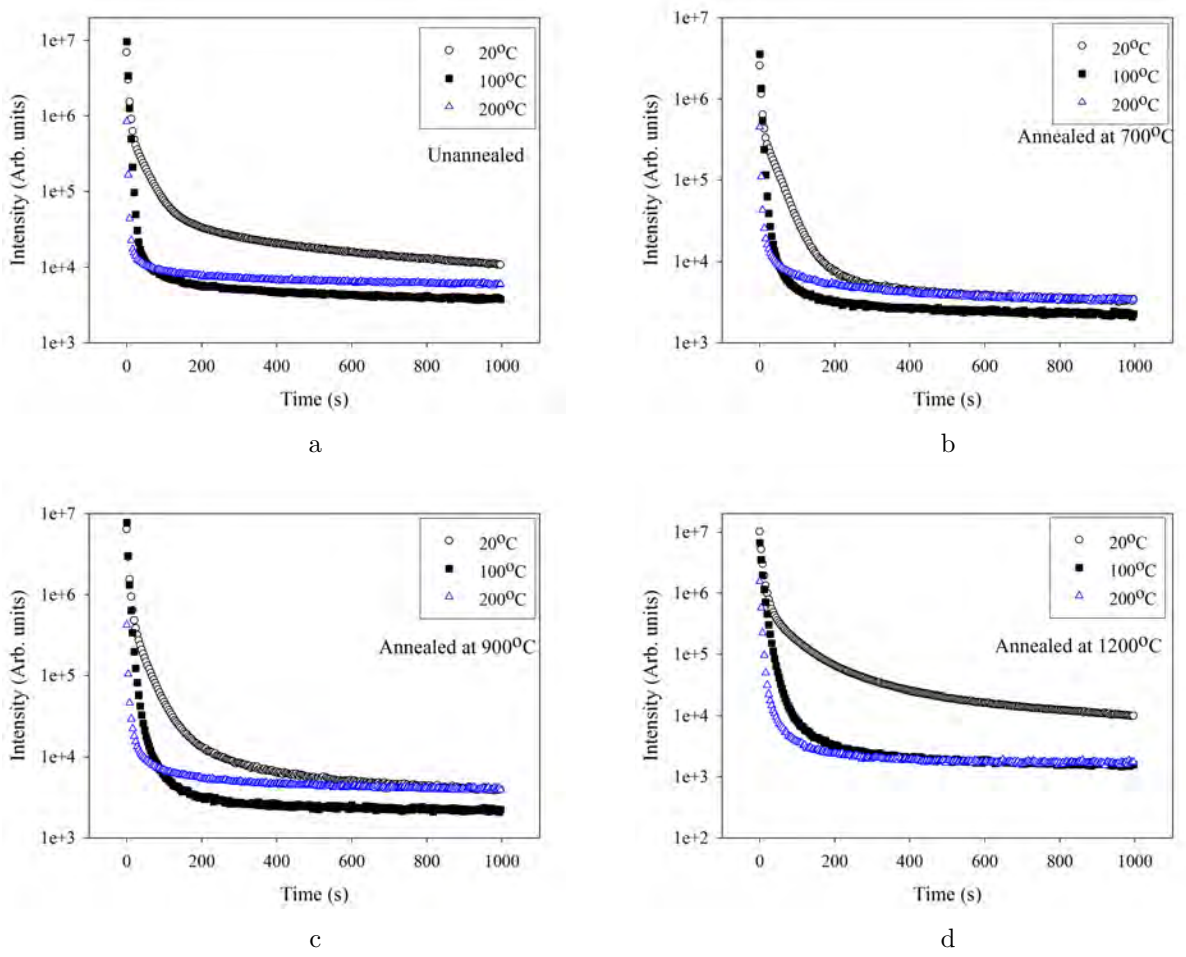

Figure 10.1: CW-OSL decay curves measured at 20, 100 and 200°C respectively after irradiation to 1.0 Gy and during 470 nm blue light illumination for 1000 s for (a) the unannealed sample, (b) the sample annealed at 700°C, (c) the sample annealed at 900°C, and (d) the sample annealed at 1200°C.

highlight the difference between the three decay curves of each sample especially at smaller stimulation times.

CW-OSL curves measured at room temperature during illumination sometimes increase initially before decreasing monotonically thereafter. This behaviour was observed clearly when short stimulation times such as 10 s and doses between 0.2 and 2.8 Gy were used. Figure 10.2 shows the CW-OSL curves measured at room temperature after irradiation to 0.2 Gy and preheating to 120°C for (a) the unannealed sample, (b) the sample annealed at 700°C, (c) the sample annealed at 900°C, and (d) the sample annealed at 1200°C respectively.

Nyirenda and Chithambo (2017) reported that under certain experimental conditions, CW-OSL curves of α-Al_2O_3:C also increase initially before decreasing mono-

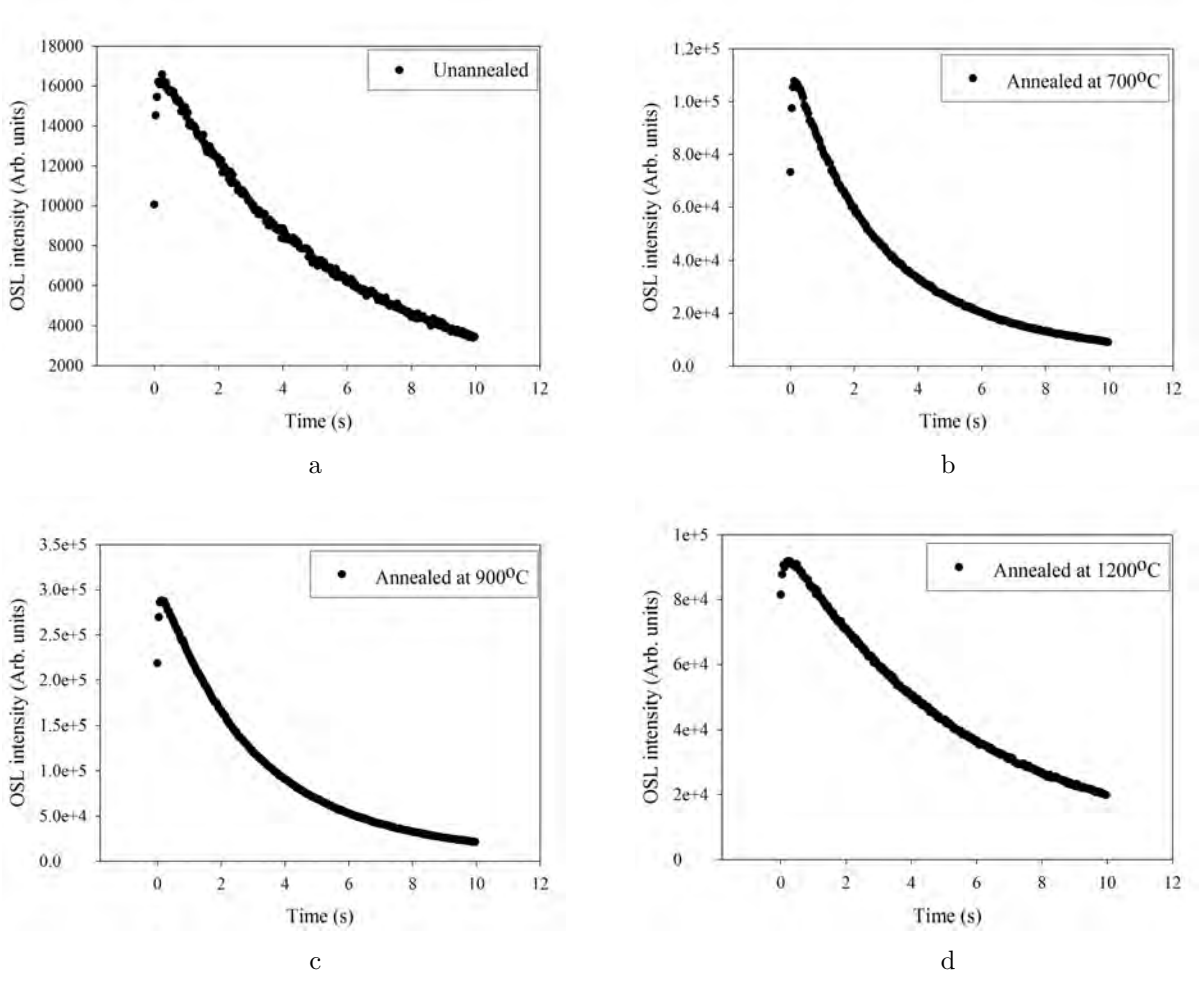

Figure 10.2: CW-OSL curves measured at room temperature after irradiation to 0.2 Gy, preheating to 120°C and during exposure to 470 nm blue light for 10 s for (a) the unannealed sample, (b) the sample annealed at 700°C, (c) the sample annealed at 900°C and (d) the sample annealed at 1200°C respectively.

tonically thereafter. Nyirenda and Chithambo (2017) showed that the initial increase of luminescence intensity with stimulation time was due to various effects such as significant charge retrapping and charge competition at electron traps and recombination centres. Kalita and Chithambo (2017h) reported CW-OSL curves of α-Al_2O_3:C,Mg measured using blue light of different optical stimulation power densities after irradiation to 1.0 Gy which only decrease monotonically with stimulation time.

The CW-OSL curves showing monotonic decay were satisfactorily fitted with the sum of three exponential functions; namely,

$$I(t) = I_1 \exp(-\lambda_1 t) + I_2 \exp(-\lambda_2 t) + I_3 \exp(-\lambda_3 t) \tag{10.1}$$

where $I(t)$ is the luminescence intensity at time t; I_1, I_2 and I_3 are scaling para-

meters and λ_1, λ_2 and λ_3 are the decay constants. These decay parameters are known as the fast (λ_1), medium (λ_2), and slow (λ_3) decay constants respectively. They have units of s^{-1} and are defined such that $\lambda_1 > \lambda_2 > \lambda_3$. The use of fitting the sum of three exponential functions to the CW-OSL curves was investigated for quartz by Smith and Rhodes (1994), Bailey et al. (1997) and Bailey (2000). The three exponential terms associated with the fast, medium, and slow decay constants do not necessarily represent separable physical mechanisms as pointed out by Chithambo and Galloway (2001) and Chithambo (2018).

Figure 10.3 shows the CW-OSL decay curves measured at 100°C after irradiation to 1.0 Gy for the unannealed sample and the samples annealed at 700, 900 and 1200°C for 15 minutes respectively. The line through the data points of each sample is the fit obtained from an equation of the same form as equation (10.1).

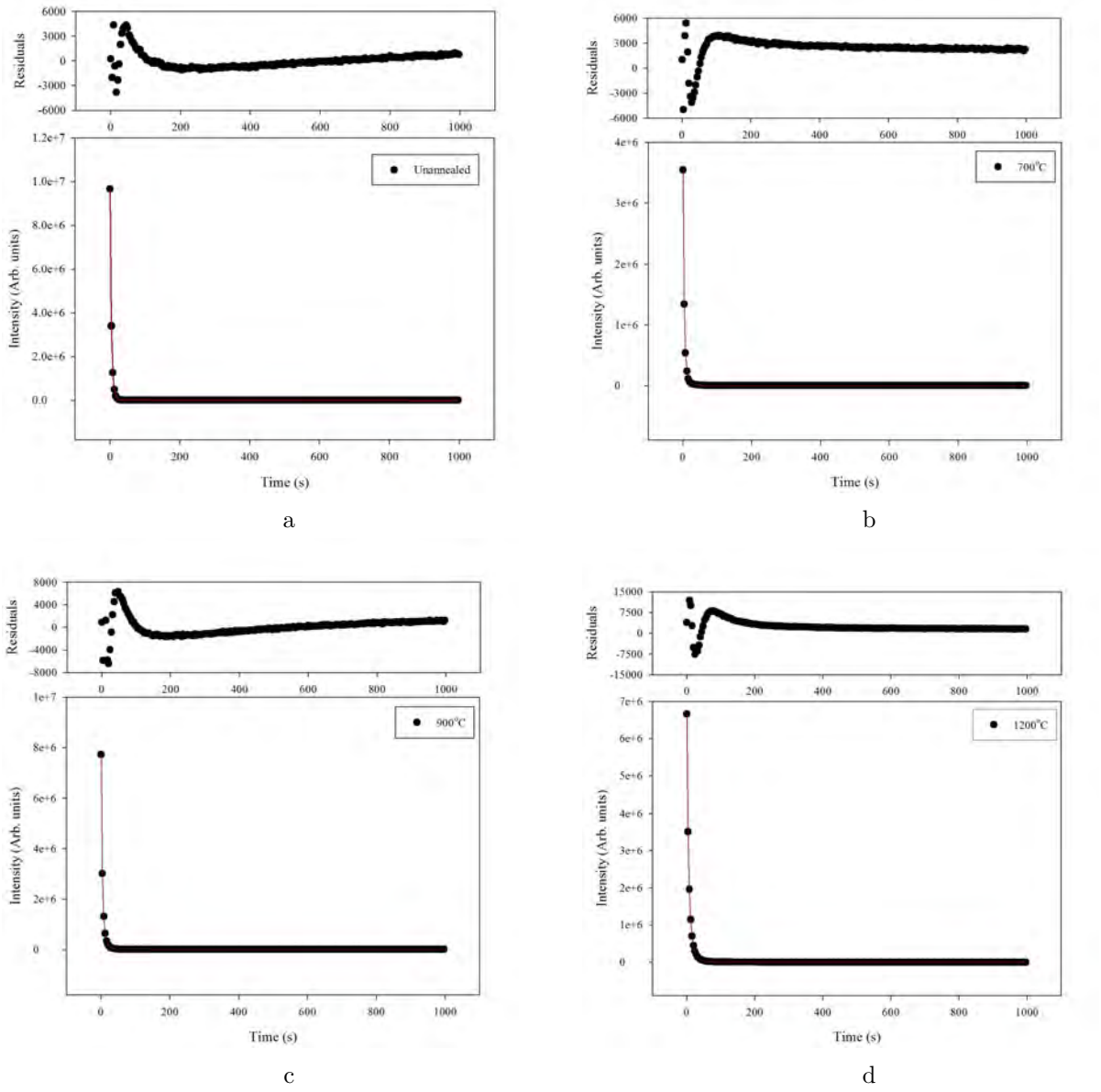

Figure 10.3: CW-OSL decay curves measured at 100 °C for (a) the unannealed sample, (b) the sample annealed at 700 °C, (c) the sample annealed at 900 °C, and (d) the sample annealed at 1200 °C. The line through the data points of each sample is the fit obtained from equation (10.1).

10.1.2 OSL component analysis

The decay constants obtained from the analysis of CW-OSL decay curves such as those shown in Figure 10.3 allow one to compute the relative contribution of each term of equation (10.1) towards the luminescence intensity. The relative contribution associated with each decay constant is expressed as

$$R_n = \frac{C_n}{C_1 + C_2 + C_3} \tag{10.2}$$

where $C_n = I_n \exp(-\lambda_n t)$ with the index n taking values 1, 2 or 3 depending on whether the fast, medium or slow term of the OSL decay is been considered (Chithambo and Galloway, 2001).

Figure 10.4 shows the relative importance of each decay component for the OSL decay curves measured at 100°C; for the unannealed sample and the samples each annealed at 700, 900 and 1200°C for 15 minutes.

For the unannealed sample, up to 82% of the luminescence intensity is initially due to the fast component with the other two components contributing less than 20%. The fast component then decreases rapidly as the illumination time increases. It decreases to a minimal level within the first 50 s of illumination time while the relative importance of the medium component increases from about 18% to 62% after 25 s of stimulation time before decreasing to a minimal level thereafter. The slow component on the other hand increases with stimulation time as the fast and medium component decrease and accounts for most of the luminescence intensity after 50 s of illumination time. These results imply that short stimulation times of say 10 or 50 s are sufficient to measure most of the fast and medium components.

For the sample annealed at 700°C, the fast component initially accounts for about 96% of the luminescence intensity whereas the medium and slow components only account for 4%. The fast component decreases with stimulation time as the contribution of the medium and slow components become more significant. The contribution of the medium component increases to about 78% after 28 s of stimulation time while that of the slow component increases to about 11% within the same time. In contrast to the medium component of the unannealed sample which decreases to a minimal level after 50 s of stimulation time, that of the sample annealed at 700°C requires up to 100 s to decrease to a similar level. The slow component of the sample annealed at 700°C becomes the most significant contributing more than 99% of the luminescence intensity after the first 100 s of stimulation time when the contribution of the fast and medium components has been reduced to a minimal level.

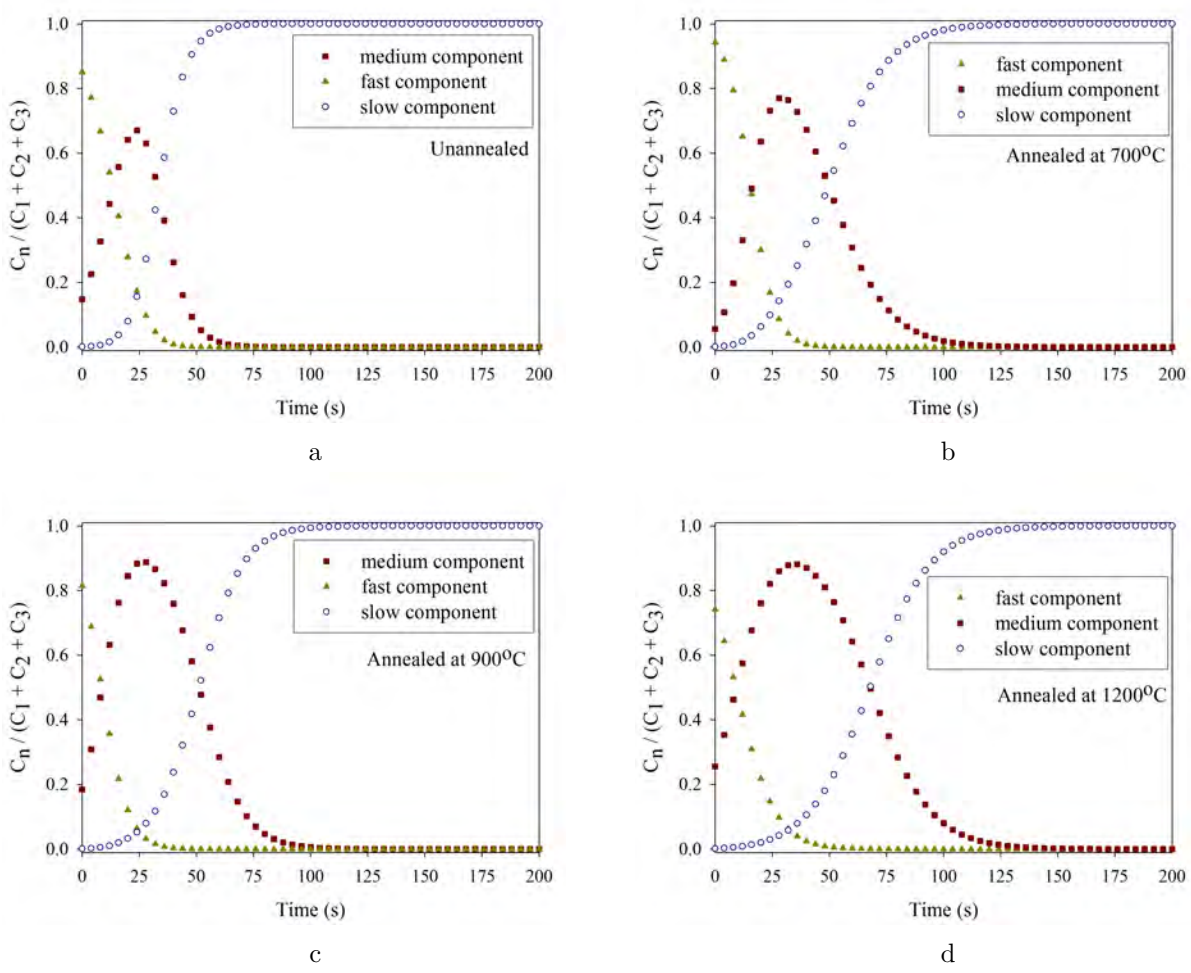

Figure 10.4: Relative importance of each component C_n of the decay curve as a function of stimulating time for (a) the unannealed sample, (b) the sample annealed at 700°C, (c) the sample annealed at 900°C, and (d) the sample annealed at 1200°C. The example shown here is for the decay curves measured at 100°C. The relative importance of each component is only shown for the first 200 s of illumination time because the important aspect of each component is captured within this timeframe.

Figure 10.4c shows that for the sample annealed at 900°C, the fast component initially contributes 80% of the luminescence intensity while the medium component contributes about 19% and the slow component the remaining 1%. The fast component then decreases to a minimal level within the first 30 s of illumination time as the medium and slow components increase. The relative importance of the medium component reaches up to 87% after the first 30 s of stimulation time while the slow component reaches about 12% within the same time. As for the sample annealed at 700°C, the medium component takes up to 100 s of stimulation time to decrease to a minimal level. The slow component of this sample contributes most of the luminescence intensity after the first 100 s of stimulation time.

The plots of Figure 10.4d show that for the sample annealed at 1200°C, the fast component initially contributes about 77% of the luminescence intensity while the medium and the slow components contribute the remaining 23%. The relative contribution of the medium component then increases to about 85% after 30 s of stimulation time while that of the fast component decreases to a minimal level. Within the same time period, the contribution of the slow component increases to about 14%. The contribution of the medium component then decreases significantly from 30 s upwards reaching a minimal level at 125 s of stimulation time. As the medium component decreases, the slow component increases and becomes the most significant after the first 125 s of stimulation time.

The results of Figure 10.4 suggest that annealing influences the relative importance of the OSL components. For instance the time taken for the medium component to decrease to a minimal level increases with annealing temperature.

10.1.3 Light induced fading of TL peaks

In order to study the role of various electron traps in OSL and the correlation with TL, the effect of illumination on TL peaks was investigated. The sample, irradiated to 3.0 Gy, was exposed to 470 nm blue light of 72 mW/cm^2 optical power density for a specific time before heating at 1°C/s to measure TL. Measurements were repeated for exposure times between 0 and 300 s in steps of 10 s. The TL intensity of each peak (peak height) was monitored with exposure time.

Figure 10.5 shows plots of normalised TL intensity against duration of illumination for peaks I-III of the unannealed sample and of the samples annealed at 700, 900 and 1200°C respectively. The dependence of normalised TL intensity on exposure time is also shown for peak IV of the sample annealed at 1200°C. the TL intensity of peaks I and III of the unannealed sample each decrease continuously with illumination as shown in Figure 10.5a. For peak II, the intensity rises initially be-

fore decreasing with further illumination. A similar observation on the behaviour of peak II was made while studying the PTTL of this sample after preheating to 60°C (Sob et al., 2021). Regarding peak A2, the PTTL peak corresponding to peak II of the same sample, it was also found that the intensity increased initially before decreasing thereafter with storage time up to 5000 s (Chapter 6). Based on this observation, we suggested that the trap corresponding to peak II is an effective competitor for the electrons evicted from other traps. The intensity of peak III is reduced to less than 10% of its initial intensity within 50 s of exposure whereas that of peak I reaches a similar level at 80 s of illumination. The slowest decrease is observed for peak II. Similar observations on the influence of light exposure were made for peaks I-III when a maximum exposure time to 2500 s was used.

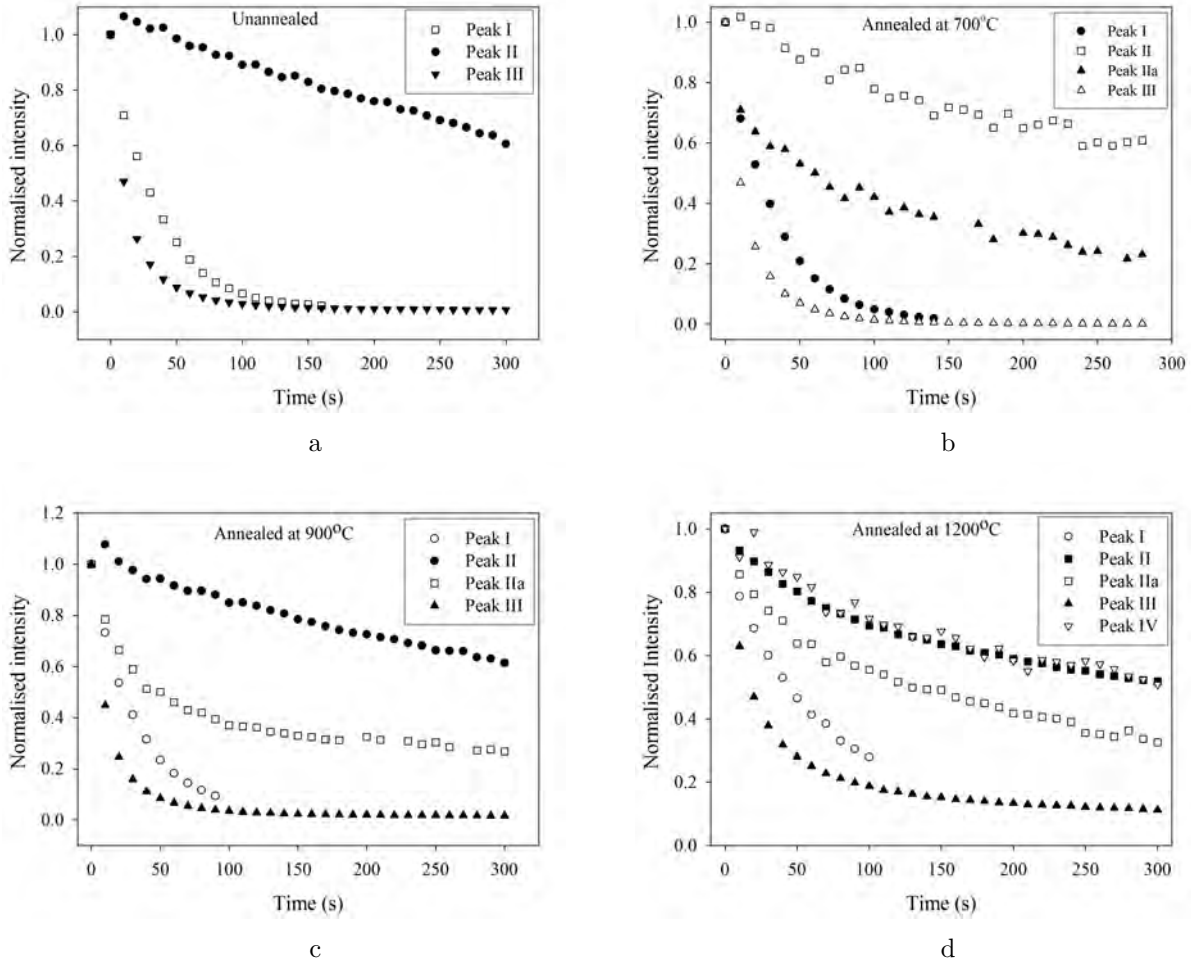

Figure 10.5: Dependence of TL intensity on illumination time for (a) peaks I-III of the unannealed sample; (b) peaks I-III of the sample annealed at 700 °C; (c) peaks I-III of the sample annealed at 900 °C and (d) peaks I-IV of the sample annealed at 1200 °C.

For the samples annealed at 700 and 900°C (Figures 10.5b and 10.5c), the intensity of peaks I-III of each sample decrease with exposure time. For peak II of the sample annealed at 900°C, the intensity also increases before decreasing thereafter. Peak III of each samples is the most sensitive to optical stimulation. Its intensity decreases rapidly within the first 50 s of illumination. Similar observations were made for the sample annealed at 1200°C as shown in Figure 10.5d.

The time taken by the intensity of peak III of each sample to reach a minimal level is consistent with the time needed to measure most of the fast and medium components of the OSL decay curves presented earlier. By extending the exposure time to 2500 s, the intensity of peak III could be reduced below 0.1% of its initial intensity. In all samples, peak I of the unannealed sample and of the sample annealed at 700°C fade to background level after 150 s of exposure. This is consistent with our earlier study of the fading of this peak (Chapter 6) and with results reported elsewhere (Kalita and Chithambo, 2017f,g). For the samples annealed at 900 and 1200°C, peak I could no longer be measured after 100 s of illumination because it was indistinct from peak II. The relatively slow decrease rate of peak II is consistent with the electron trap of peak II being an effective competitor as suggested earlier. Trindade et al. (2019) showed the correlation between the OSL active trap and the trap associated with the main TL peak (peak III) of α-Al_2O_3:C,Mg.

The light induced fading of all peaks justifies the conclusion under PTTL that all peaks are associated with acceptors or donors.

10.1.4 Effect of dose on temperature dependent OSL intensity

To study the influence of dose on OSL intensity, a modified version of Sequence A was used for measurements. The only modification was the irradiation dose. The modified sequence was executed for doses of 1.0, 3.0, and 5.0 Gy respectively for each sample. The luminescence intensity is calculated as the area under the CW-OSL curve. Figure 10.6 shows the temperature-dependence of luminescence intensity for irradiation doses of 1.0, 3.0, and 5.0 Gy respectively for the unannealed sample and the samples annealed at 700, 900, and 1200°C. Figure 10.6a shows the effect of dose on luminescence intensity of the unannealed sample for measurement temperatures between 20 and 200°C. The luminescence intensity of the unannealed sample decreases from 20 to 60°C then increases from 60 to 120°C and decreases thereafter with measurement temperature up to 200°C. This pattern is observed irrespective of the irradiation dose. The luminescence intensity is also found to increase with irradiation dose. For measurement at say 20°C for example, the

intensity value corresponding to 5.0 Gy is higher than that corresponding to 3.0 Gy and 1.0 Gy.

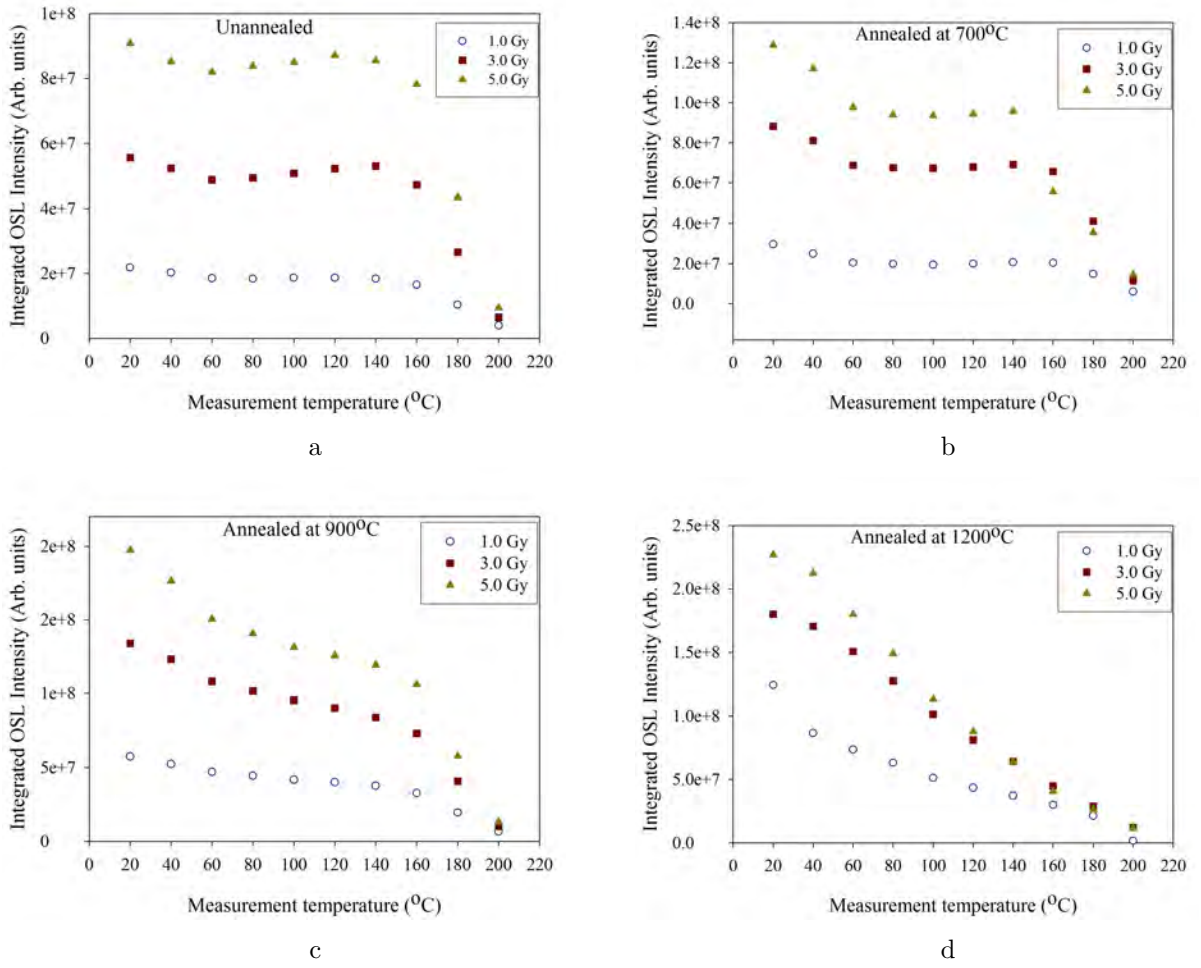

Figure 10.6: Temperature-dependence of luminescence intensity for irradiation doses of 1.0, 3.0, and 5.0 Gy for (a) the unannealed sample, (b) the sample annealed at 700°C, (c) the sample annealed at 900°C and (d) the sample annealed at 1200°C respectively.

Figure 10.6b shows the temperature-dependence of luminescence intensity for irradiation doses of 1.0, 3.0, and 5.0 Gy for the sample annealed at 700°C. The luminescence intensity of this sample decreases with measurement temperature from 20 to 60°C; increases from 60 to 140°C and then decreases thereafter with measurement temperature up to 200°C. This pattern is observed for each irradiation dose. The luminescence intensity measured at a given temperature is also found to increase with irradiation dose. The initial decrease in luminescence intensity is due to optical stimulation being dominant. The growth from 60 to 140°C is due to thermal assistance whereas as the subsequent decrease up to 200°C is

due to thermal quenching. For the samples annealed at 900 and 1200°C, the luminescence intensity decreases consistently with measurement temperature because thermal assistance is insufficient to overcome OSL or thermal quenching. The behaviour is observed irrespective of irradiation dose. For the sample annealed at 900°C, the luminescence intensity also increases with irradiation dose irrespective of measurement temperature as shown in Figure 10.6c. For the sample annealed at 1200°C, the luminescence intensity increases with irradiation dose for measurement temperature between 20 and 140°C. Studies(e.g. Kalita and Chithambo (2018b); Trindade and Jacobsohn (2018); Chithambo et al. (2020)) have shown that α-Al_2O_3:C,Mg is affected by thermal quenching and that this phenomenon is prominent for measurement temperatures above 120°C. As in α-Al_2O_3:C (Akselrod et al., 1998; Pagonis et al., 2011; Chithambo et al., 2014, 2015), the main luminescence centres in α-Al_2O_3:C,Mg (F and F^+ centres) are subject to thermal quenching (Chithambo et al., 2020). However, the decrease of luminescence intensity with measurement temperature up to 100°C for the sample annealed at 1200°C is atypical since thermal quenching is not expected to be dominant at such temperatures. It has been reported that F^+ and F centres are stable up to 1200°C (Akselrod et al., 2003b) so this behaviour cannot be directly ascribed to annealing either.

10.1.5 Dependence of luminescence intensity on optical power density

In order to study the dependence of OSL intensity on the power of the stimulating light, the following sequence (Sequence B) was executed:

1. Heating to 500°C at 1°C/s to measure background signal
2. Irradiation to 1.0 Gy at room temperature to populate the various electron traps
3. Exposure to 470 nm blue light of optical power density P_i for 10 s at 20°C
4. Heating to 500°C at 1°C/s to measure the residual TL

Sequence B was repeated for values of optical power density between 8 and 80 mW/cm^2.

Figure 10.7 shows the normalised CW-OSL curves of the unannealed and annealed samples of α-Al_2O_3:C,Mg measured during 470 nm blue light illumination of optical power densities 8, 16, 24, 64, 72, and 80 mW/cm^2 after irradiation to 1.0 Gy. The

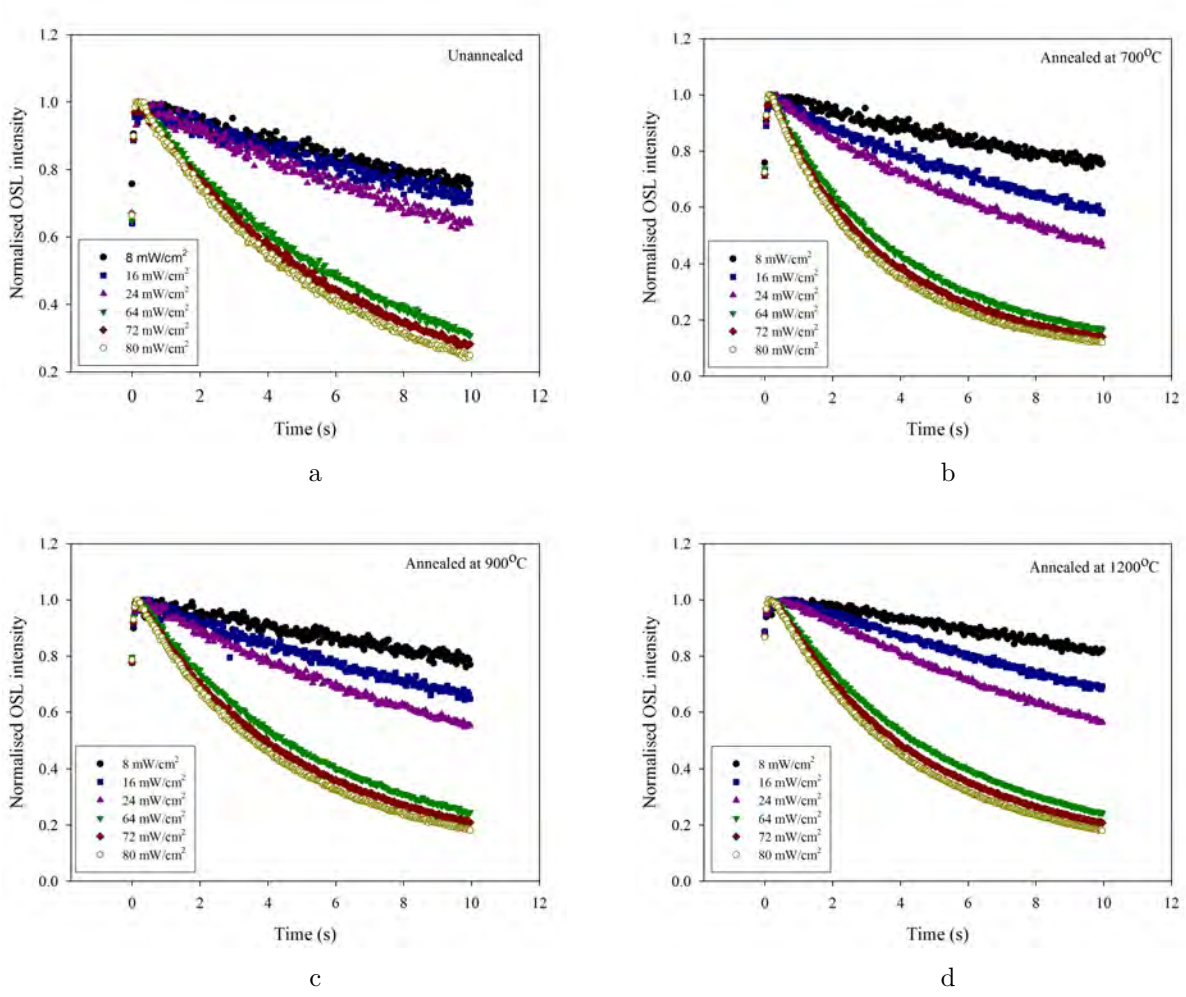

Figure 10.7: CW-OSL curves of α-Al_2O_3:C,Mg measured during 470 nm blue light stimulation of optical power densities 8, 16, 24, 64, 72, and 80 mW/cm^2 after irradiation to 1.0 Gy for (a) the unannealed sample, (b) the sample annealed at 700°C, (c) the sample annealed at 900°C and (d) the sample annealed at 1200°C respectively.

OSL curves of Figure 10.7 are characterised by the initial increase in luminescence intensity. This initial increase in luminescence intensity is noticeable for power densities within 8 - 80 mW/cm^2. Irrespective of annealing temperature, It is also found that the luminescence intensity decreases much faster with illumination time as the stimulation power increases. This faster decay with optical power density results from more electrons being stimulated in a short time as reported by Kalita and Chithambo (2017h). The OSL decay curves of α-Al_2O_3:C,Mg reported by Kalita and Chithambo (2017h) for different optical stimulation power densities behaved as those shown in Figure 10.7. The main differences between the CW-OSL curves of Figure 10.7 and those reported by Kalita and Chithambo (2017h) are the choice of stimulation time and the initial rise in luminescence intensity with stimulation time. In Figure 10.1, we showed OSL curves measured for a much longer stimulation time namely, 1000 s and at a stimulation power density of 72 mW/cm^2 which also did not rise initially with stimulation time.

Figure 10.8 shows the dependence of integrated OSL intensity on the power of the stimulating light for the unannealed sample and the samples annealed at 700, 900, and 1200°C respectively. The integrated OSL intensity, which is computed as the area under each OSL curve, increases with the power of the stimulating light for each sample. The results of Figure 10.8 follow naturally from our discussion of the influence of optical power density on stimulated electrons. Figure 10.8 also shows that the integrated OSL intensity increases with annealing temperature. Independent of the choice of stimulating light, annealing and re-use also affect the TL and OSL sensitivity in α-Al_2O_3:C,Mg (Kalita and Chithambo, 2017d).

10.2 Thermally assisted optically stimulated luminescence from deep traps

Deep traps refer to traps that are not accessible in conventional TL measurements where the sample is usually heated to 500°C e.g. (Nyirenda and Chithambo, 2017). In practise the maximum measurement temperature needs not be 500°C but can be extended somewhat beyond this depending on sample characteristics. In our context, deep traps are thermally stable but optically sensitive and lie at temperatures above 500°C. Thermally assisted OSL (TA-OSL) refers to CW-OSL measured above room temperature. For a TA-OSL measurement, the sample is usually irradiated to a much higher dose compared with doses used in conventional TL measurements. For example in their study of TA-OSL from deep electrons traps in α-Al_2O_3:C,Mg, Kalita et al. (2017a) irradiated their sample to doses such as 100 and 1000 Gy. The use of a high dose is to achieve a large concentration of electrons

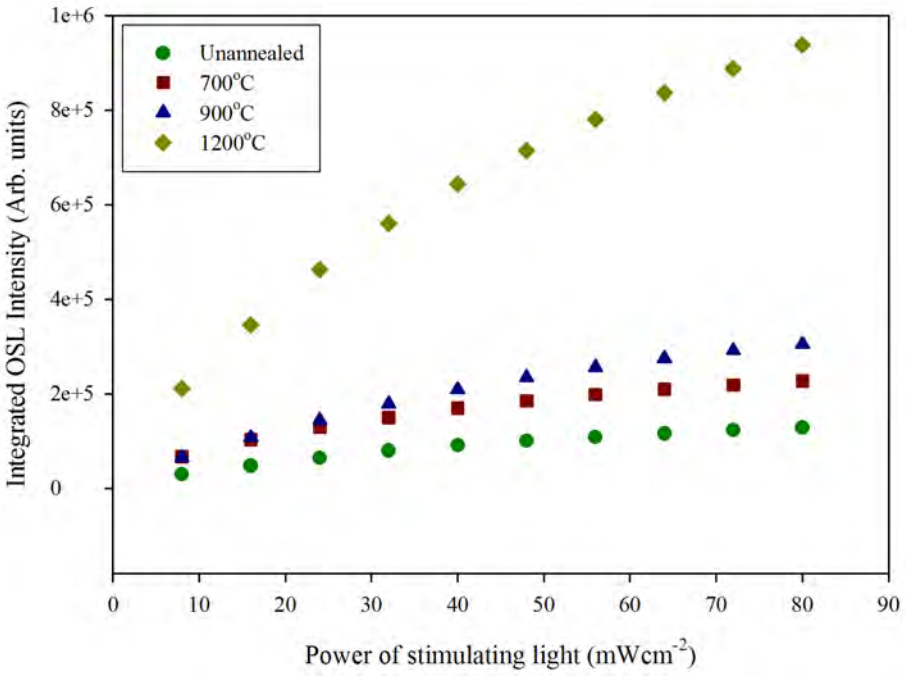

Figure 10.8: Dependence of integrated OSL intensity on the power of the stimulating light for the unannealed sample and the samples annealed at 700, 900 and 1200°C respectively.

in deep traps prior to heating. The irradiated sample is then preheated to empty the shallow, intermediate and main traps before being optically stimulated. Any ensuing luminescence is referred to as TA-OSL and is due to electrons stimulated from deep traps with the optical stimulation being made above room temperature. TA-OSL therefore provides a means to investigate the presence of deep traps in a given sample. Some of the luminescent materials for which TA-OSL has been used to investigate the presence of deep traps include quartz (Huntley et al., 1996; Chithambo and Galloway, 2001; Kitis et al., 2010; Polymeris et al., 2015a,b; Polymeris, 2016), Al_2O_3:C (Polymeris et al., 2010; Soni et al., 2012; Polymeris and Kitis, 2012; Soni et al., 2013; Meriç et al., 2016; Nyirenda and Chithambo, 2017), Al_2O_3:C,Mg (Kalita and Chithambo, 2017h; Kalita et al., 2017a; Kalita and Chithambo, 2019) and $Sr_4Al_{14}O_{25}$:Eu^{2+},Dy^{3+} (Chithambo, 2021b).

10.2.1 Influence of repetitive measurement on OSL intensity

The influence of repetitive measurement on luminescence intensity from the deep traps was investigated for the unannealed sample and the samples annealed at 700, 900, and 1200°C respectively. To access the signal from the deep traps, the sample

under investigation was irradiated to 1000 Gy at room temperature and then heated in a separate oven to 500°C to empty the shallow and main traps. Irradiation to high doses such as 1000 Gy is intended to fill the deep traps prior to heating. Once the sample had cooled to room temperature, it was then repeatedly exposed to 470 nm blue light of optical power density 72 mW/cm^2 for 10 s without being re-irradiated again between measurements. The OSL measured during exposure to blue light results from deep trap electrons since the shallow and main traps are empty after the heating step. For each TA-OSL measurement, the heating step after irradiation was carried out in a separate oven to prevent damage to the photomultiplier tube.

Figure 10.9 shows the first TA-OSL curve measured immediately after heating for the unannealed sample.

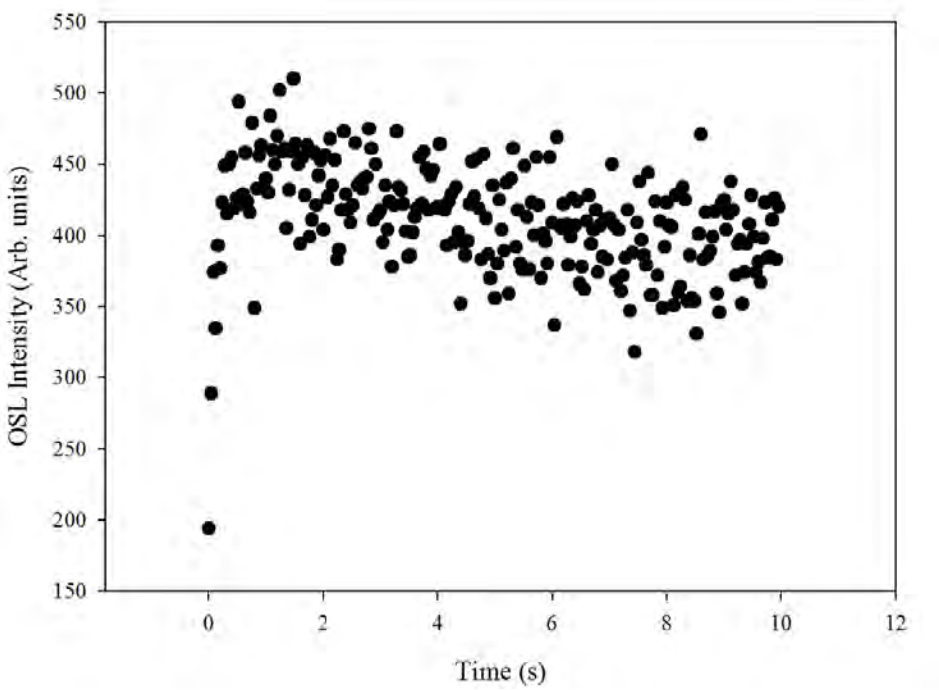

Figure 10.9: The first TA-OSL curve measured on the unannealed sample after irradiation to 1000 Gy and heating to 500°C at 1°C/s.

Figure 10.9 shows that the TA-OSL intensity initially increases before decreasing thereafter. This is not always the case, some of the time-dependence on OSL measured for the same sample but for longer stimulation time only consists of the decaying part. Given the repetitive TA-OSL curves recorded for each sample, we computed the integrated OSL intensity as the area under the TA-OSL curve for each measurement. Figure 10.10 shows the effect of repeated runs on the integrated

OSL intensity for the unannealed sample and the samples annealed at 700, 900, and 1200°C respectively.

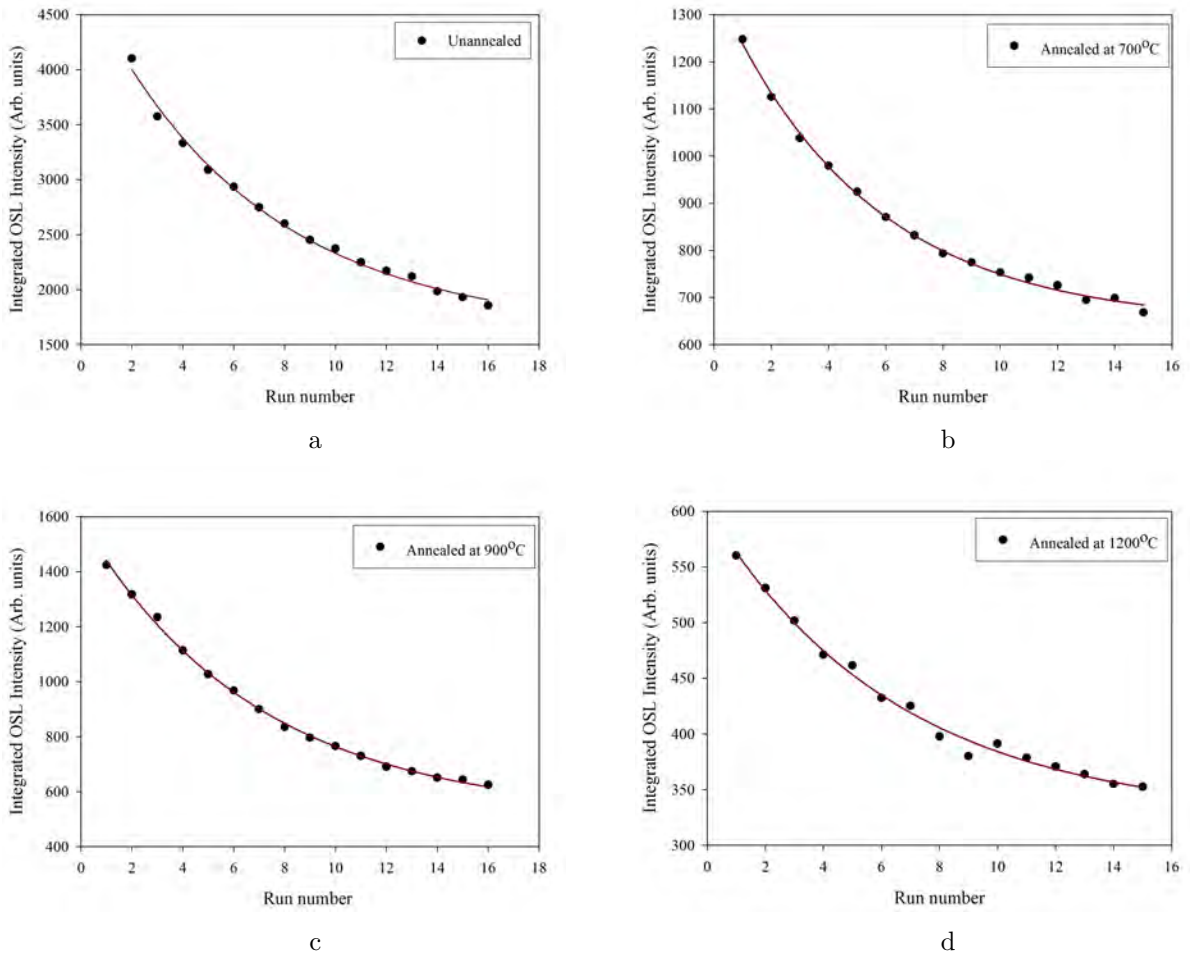

Figure 10.10: Integrated OSL intensity as a function of run number for (a) the unannealed sample, (b) the sample annealed at 700°C, (c) the sample annealed at 900°C, and (d) the sample annealed at 1200°C. The solid line through the data points of each sample is given by an exponential decreasing function.

The plots of Figure 10.10 show that the integrated OSL intensity of each sample decreases continuously with repetitive measurements. The solid line describing this decrease for each sample is given by a single exponential function. The decrease in intensity with repetitive readout can be attributed to the reduction in the concentration of electrons from deep traps with each exposure to the stimulating light. It is worth noting that the integrated OSL intensity values of the unannealed sample are the highest. Those of the samples annealed at 700 and 900°C are similar while those of the 1200°C annealed sample are the smallest. In the case of α-Al_2O_3:C, it has been shown that the population of deep traps is depleted

after annealing at 900°C (Chithambo, 2004; Yukihara et al., 2004; Yukihara and McKeever, 2006). The results in Figure 10.10 suggest that the concentration of deep traps in α-Al_2O_3:C,Mg is also affected by annealing temperature.

10.2.2 Evaluation of kinetics parameters associated with thermal assistance and thermal quenching

In order to further our study of luminescence from deep traps, CW-OSL measurements were carried out at different temperatures between 50 and 200°C. The following sequence was followed:

1. Irradiation of the sample to 1000 Gy at room temperature to populate the shallow, main and deep electron traps
2. Heating to 500°C to empty shallow and main traps
3. CW-OSL measurement at T_i from 50 to 200°C in steps of 10°C by exposure to 470 nm blue light of optical power density 40 mW/cm^2 for 5 s

The lower optical power density of 40 mW/cm^2 and a stimulation time of 5 s were used to allow for the CW-OSL measurement to be carried out at different temperatures between 50 and 200°C without further re-irradiating the sample at each step. Figure 10.11 shows TA-OSL curves measured at 50, 100, 150, and 200°C respectively for the unannealed sample after irradiation to 1000 Gy and heating to 500°C.

For each of the samples, the integrated OSL intensity was computed as the area under the given TA-OSL curve. Figure 10.12 shows the dependence of the integrated OSL intensity on measurement temperature for the unannealed sample and the samples annealed at 700, 900, and 1200°C respectively. The plots of Figure 10.12 shows that the integrated OSL intensity of each sample first increases with measurement temperature and then decreases thereafter.

The study of TA-OSL provides a means to evaluate kinetic parameters such as the activation energy for thermal assistance, E_a, the activation energy for thermal quenching, W, and the constant factor C which is related to non-radiative transitions (Chithambo, 2007a; Chithambo and Costin, 2017). This initial increase with measurement temperature is ascribed to thermal assistance whereas the subsequent decrease is ascribed to thermal quenching (Chithambo and Galloway, 2001). The

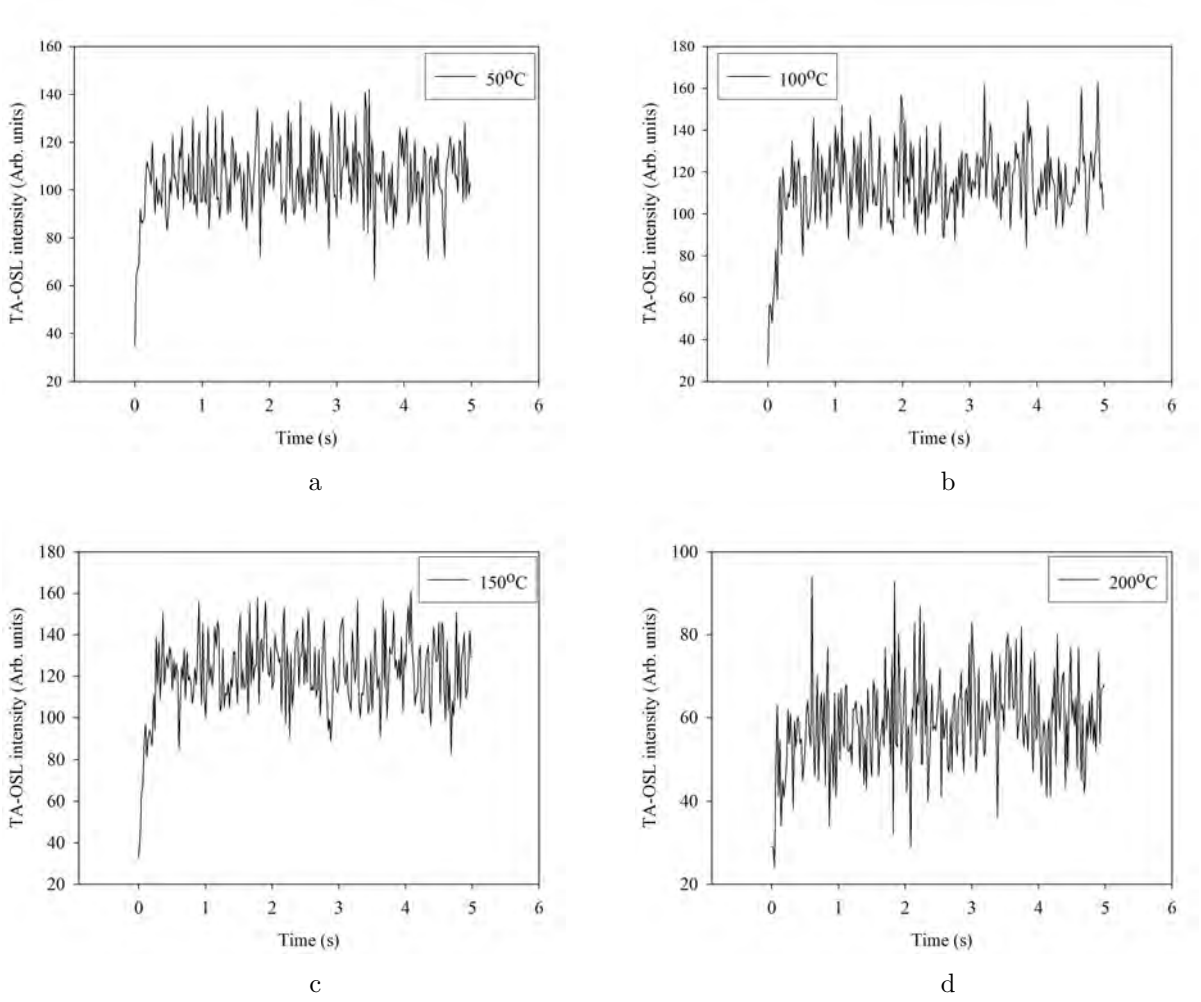

Figure 10.11: TA-OSL curves measured at (a) 50°C, (b) 100°C, (c) 150°C and (d) 200°C from the unannealed sample after irradiation to 1000 Gy and heating to 500°C at 1°C/s.

temperature-dependence of integrated OSL intensity can be expressed as

$$I_T = \frac{I_0 \prod_i^n \exp(-E_{ai}/kT)}{1 + C\exp(-W/kT)} \tag{10.3}$$

where I_0 is the initial intensity, E_{ai} is the activation energy for thermal assistance of the ith electron trap, W is the activation energy for thermal quenching, n is the number of deep traps and k is the Boltzmann constant (Chithambo and Costin, 2017). The constant $C = \nu\tau_{rad}$ where ν is the frequency factor for non-radiative transition and τ_{rad} is the luminescence lifetime for radiative recombination (Chithambo, 2007d). The number n of deep traps cannot be determined from

these measurements. By assuming a single deep trap, equation (10.3) becomes

$$I_T = \frac{I_0 \exp(-E_a/kT)}{1 + C\exp(-W/kT)}. \tag{10.4}$$

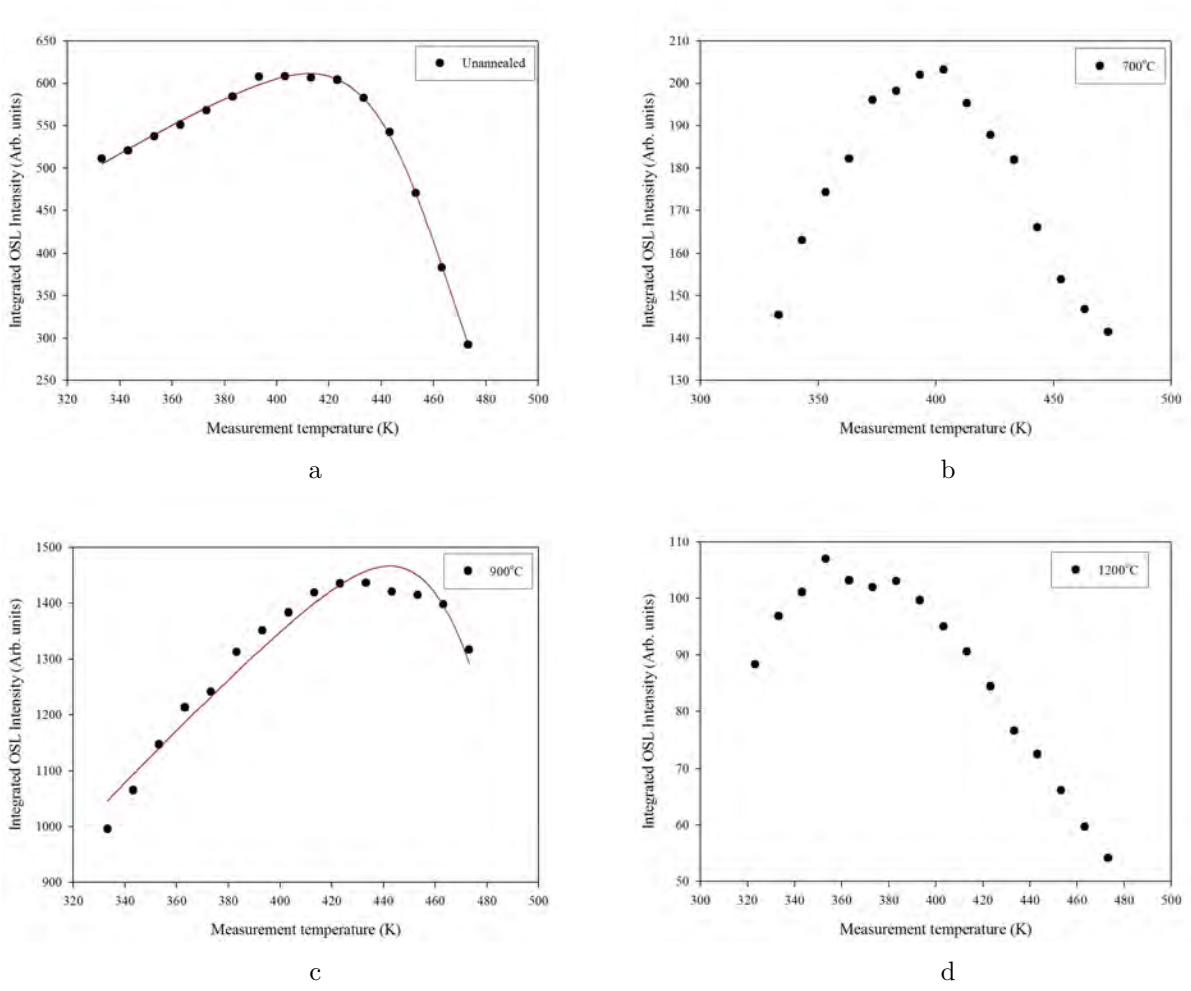

Figure 10.12: Dependence of integrated OSL intensity on measurement temperature for (a) the unannealed sample, (b) the sample annealed at 700°C, (c) the sample annealed at 900°C, and (d) the sample annealed at 1200°C.

The line through the data points of Figure 10.12a is the best fit obtained from equation (10.4) for the unannealed sample. The resulting kinetic parameters are E_a = 0.0334 ± 0.0011 eV, W = 1.0433 ± 0.0010 eV and C = 1.85 x 10^{11}. For the sample annealed at 900°C, fitting with equation (10.3) led to E_a = 0.0440 ± 0.0030 eV, W = 1.1106 ± 0.0061 eV and C = 1.85 x 10^{11} respectively. For the samples annealed at 700 and 1200°C, satisfactory fit could not be obtained. During the fitting process only a single deep electron trap was assumed because the exact number of deep traps is not known. In their study of TA-OSL from deep traps in

α-Al_2O_3:C,Mg, Kalita et al. (2017a) found the activation energy for thermal assistance associated with a deep electron trap in an unannealed sample of α-Al_2O_3:C,Mg to be 0.66 ± 0.02 eV and that of thermal quenching to be 0.90 ± 0.04 eV. For a sample annealed at 1200°C, Kalita and Chithambo (2019) reported the value of E_a as 0.21 ± 0.02 eV. The values of activation energy for thermal assistance obtained in this study for the unannealed sample and the sample annealed at 900°C are relatively smaller than the value reported by Kalita et al. (2017a) and Kalita and Chithambo (2019). Only the activation energy for thermal quenching obtained for these two samples is somewhat comparable to the value of 0.90 ± 0.04 eV reported by Kalita et al. (2017a). The discrepancies in the values found merit further investigation. Kalita and Chithambo (2019) noted that the activation energy for thermal assistance of the deep trap in a sample annealed at 1200°C was smaller than that of an unannealed sample and that a sample annealed at 1200°C produced better PTTL and TA-OSL. These results led them(Kalita and Chithambo, 2019) to the conclusion that annealing at 1200°C increases the concentration of deep traps in α-Al_2O_3:C,Mg.

10.2.3 Phototransferred thermoluminescence from deep traps

In order to monitor phototransferred thermoluminescence (PTTL) from deep traps, the following sequence was executed:

1. Heating to 500°C at 1°C/s to measure background signal
2. Irradiation to 50 Gy at room temperature to populate the deep electron traps
3. Heating to 500°C to clear shallow and main traps
4. CW-OSL measurement at temperature T_i from 20 to 240°C in steps of 20°C by exposure to 470 nm blue light of power density 72 mW/cm^2 for 20 s
5. Heating to 500°C at 1°C/s to monitor any TL signal induced by phototransfer

Figures 10.13 and 10.14 show PTTL glow curves of the unannealed sample measured at 1°C/s after TA-OSL at 20, 40, 60, 80 and at 120, 140, 160, and 180°C respectively. The glow curve measured after the TA-OSL measurement at 20°C shows two PTTL induced peaks at 50 and 190°C respectively. In addition to the PTTL peak at 190°C, the glow curve measured after the TA-OSL measurement at 40°C also has a much weaker PTTL peak near 50°C. The other glow curves measured after TA-OSL at 60°C or above only show the PTTL peak at 190°C.

PTTL was also observed after TA-OSL measurements for the samples annealed at 700, 900, and 1200°C respectively. These measurements of TA-OSL and PTTL after heating to 500°C provide additional evidence for the presence of deep traps in α-Al_2O_3:C,Mg as reported in our investigation on the analysis of PTTL-time profiles of unannealed α-Al_2O_3:C,Mg (Sob et al., 2021).

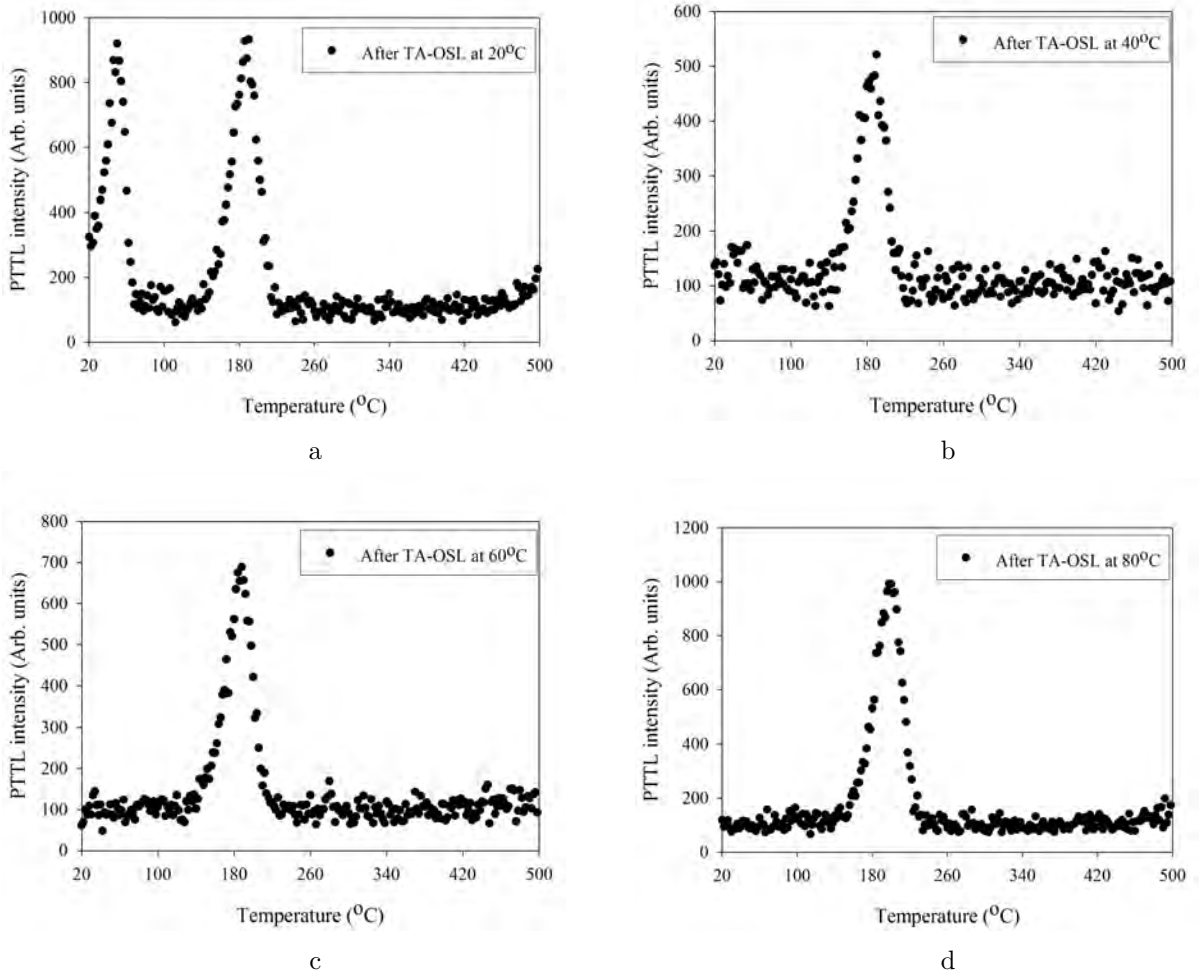

Figure 10.13: PTTL glow curves measured after TA-OSL at 20, 40, 60 and 80°C from the unannealed sample after irradiation to 50 Gy.

10.3 Summary

The luminescence properties of α-Al_2O_3:C,Mg have been investigated with optical stimulation. We observed that the luminescence properties of this sample are influenced by annealing. The presence of deep traps has been studied with TA-OSL

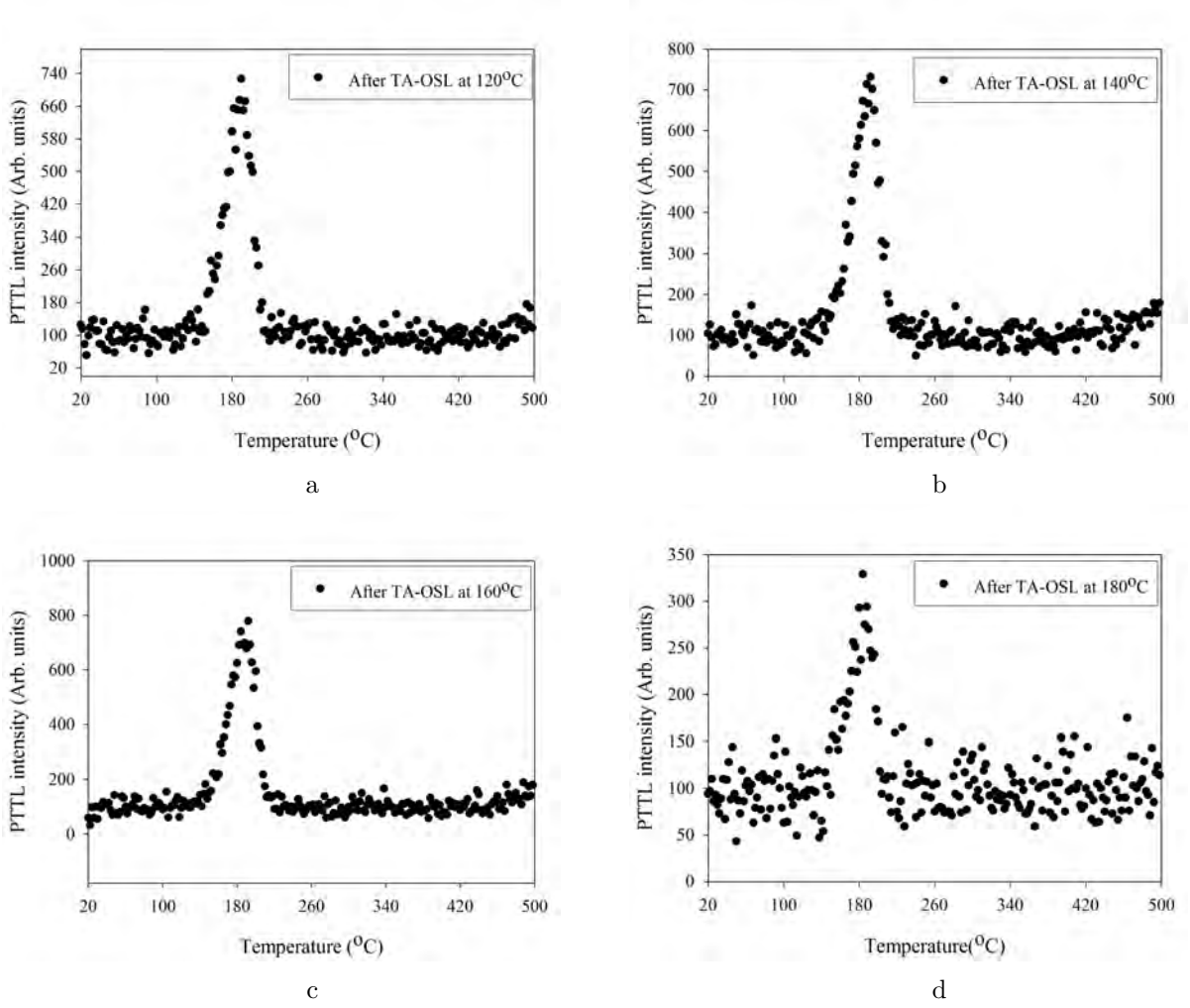

Figure 10.14: PTTL glow curves measured after TA-OSL at 120, 140, 160, and 180°C from the unannealed sample after irradiation to 50 Gy.

and we found that PTTL peaks are observed following stimulation of electrons from deep traps.

Chapter 11

Conclusion

The goals of this thesis were the investigation of the dosimetric features of α-Al_2O_3:C,Mg, the study of its phototransfer and the investigation of deep traps by means of thermally assisted optically stimulated luminescence. In addition to an unannealed sample of α-Al_2O_3:C,Mg, samples annealed at 700, 900 and 1200°C for 15 minutes each were also used. A beta source was used for irradiation. For OSL measurements, each sample was exposed to 470 nm blue LEDS. For the dose response study, a 1% absorptive neutral density filter was used in combination with a 7.5 mm thick U-340 filter to attenuate the luminescence intensity and to prevent damage to the photomultiplier tube.

A glow curve of unannealed α-Al_2O_3:C,Mg measured at 1°C/s after irradiation to 2.0 Gy consists of peaks at 43, 73, 164, 195, 246, 284, 336 and 374°C respectively. For the sample annealed at 700°C, a glow curve measured at 1°C/s after irradiation to 3.0 Gy has peaks at 46, 76, 100, 170, 199, 290, 330 and 375°C. In comparison, a glow curve of the sample annealed at 900°C and measured at 1°C/s after irradiation to 3.0 Gy consists of peaks at 49, 80, 100, 174, 206, 235, 290, 335 and 375°C/s respectively. For the sample annealed at 1200°C, which is more sensitive than the others, a glow curve measured at 1°C/s after irradiation to 0.2 Gy has peaks at 52, 82, ∼102, 174, 234, 288 and 384°C respectively. The dose response of peaks of each sample was studied for doses within 0.1 - 8.2 Gy. A shift in peak position was observed with the use of the neutral density filter. The dose response of the phototransferred peaks of each sample was also investigated.

A comprehensive study of PTTL in unannealed and annealed α-Al_2O_3:C,Mg was carried out and a mathematical analysis of the observed PTTL dependence on illumination time was developed. The PTTL time-response profile was described as separate systems of an acceptor an, donors the number of which depends on preheating and illumination. This study revealed the presence and role of deep

traps beyond 500°C which contribute to the PTTL.

Continuous-wave optical stimulation was used to investigate the role of shallow, intermediate and main traps in the luminescence process of α-Al_2O_3:C,Mg. The influence of irradiation dose on the OSL decay curves was studied. The effect of the power of the stimulating light on OSL intensity was also investigated. Thermally assisted OSL was used as a means to investigate luminescence from the deep traps. Glow curves measured immediately after thermally assisted OSL show glow peaks for each of the sample. This is additional evidence for the presence of deep traps in these samples.

11.1 Future work

In this work, a beta source was used for irradiation and 470 nm blue LEDs were used for optical stimulation. It will be interesting to study the effect of different excitation source on the luminescence centres. A study on the effect of wavelength of optical stimulation on the observed phototransferred peaks could shed more light on the role played by traps; including deep electron traps and deep holes during phototransfer. Time-resolved optical stimulation could also be used to investigate the luminescence lifetimes of α-Al_2O_3:C,Mg and the influence of irradiation dose, measurement temperature and annealing on these. Other techniques such as radioluminescence and linear-modulated optical stimulation could also be used to further the study of mechanisms of luminescence in α-Al_2O_3:C,Mg. An investigation of the origin and nature of traps in α-Al_2O_3:C,Mg is still of interest.

Appendix A

Appendix

Journal of Luminescence 230 (2021) 117721

Contents lists available at ScienceDirect

Journal of Luminescence

journal homepage: http://www.elsevier.com/locate/jlumin

Full Length Article

Analysis of illumination-time-dependent profiles of phototransferred thermoluminescence of Al_2O_3:C,Mg

A.J. Lontsi Sob [a], M.L. Chithambo [a,*], J.M. Kalita [b]

[a] Department of Physics and Electronics, Rhodes University, P O BOX 94, Grahamstown, 6140, South Africa
[b] Department of Physics, Cotton University, Guwahati, 781001, India

ARTICLE INFO

Keywords:
Phototransferred thermoluminescence
Al_2O_3:C,Mg
Electron traps
Deep-hole traps
Differential equations
Competition effects

ABSTRACT

Time-dependent profiles of phototransferred thermoluminescence (PTTL) of Al_2O_3:C, Mg are presented and analysed. Whereas qualitative discussions consider theoretical predictions, mathematical analysis of the profiles is based on experimental results. The thermoluminescence glow curve of unannealed Al_2O_3:C, Mg measured at 1 °C/s following irradiation to 2 Gy consists of at least eight peaks. There is a prominent peak at 165 °C and 7 secondary peaks at 43, 73, 195, ~246, 284, ~336 and 374 °C respectively. These are labelled I through VIII in order of appearance. Of these, only peaks I-IV are reproduced under phototransfer. The role of various electron traps as donors was determined using pulse annealing as well as by monitoring the dependence of peak intensity on duration of illumination used in the phototransfer. In particular, this shows that the electron trap for peak III at 165 °C, the main one, is the dominant donor to the electron traps responsible for PTTL at peaks I and II. There is also evidence of deep electron traps and deep hole traps beyond 500 °C which contribute to phototransferred thermoluminescence associated with peak III. The dependence of PTTL intensity on illumination time has been analysed using sets of coupled first order linear differential equations which describe the charge transfer at the electron traps involved. Particular solutions to the family of equations set up have been applied on experimental data successfully as evident in residuals associated with each fit.

1. Introduction

This report is concerned with phototransferred thermoluminescence (PTTL) from unannealed aluminium oxide doped with carbon and magnesium (Al_2O_3:C,Mg). In conventional thermoluminescence (TL), the signal is stimulated by controlled heating of a sample immediately after irradiation [1,2]. The luminescence ensues directly from the recombination with holes of electrons thermally stimulated from electron traps which are populated during the irradiation. On the other hand, in PTTL the irradiated sample is first preheated to a specific temperature and, after cooling, exposed to light of a specific wavelength before being heated again to monitor any luminescence [3,4]. The temperature the sample is preheated to is chosen so that one or several peaks in a glow curve are removed during the preheating. Any peak which appears at a temperature below the preheating temperature following illumination and subsequent heating is a PTTL peak since it is induced by optical transfer of electrons from electron traps (donors) not emptied during preheating. For convenience we refer to the deep electron source traps as donors and the lower temperature electron traps where electrons are phototransferred to as acceptors. Although this generic description assumes that higher-temperature lying electron traps will act as donors and the lowe-temperature ones as acceptors during PTTL, it has been shown that this is not always the case [3,4]. As a case in point, studies of PTTL in annealed synthetic quartz [3] as well as in natural quartz annealed at 1000 °C [4] have shown that some supposed donors can act as acceptors for certain combinations of preheating temperature and duration of optical exposure.

Al_2O_3:C,Mg, the subject of this study, is a sensitive luminescent material developed for optical data storage [5], used for fluorescence nuclear track detection [6] and investigated for various applications including 2D dosimetry in magnetic resonance guided radiotherapy [7]. In addition to its high concentration of oxygen vacancies (F and F^+ centres) owing to doping by carbon [8], co-doping with Mg is thought to generate additional colour centres such as F^+(Mg), F_2, $F^{2+}{}_2$(2 Mg) and $F^+{}_2$(2 Mg) types [9]. An F^+(Mg) electron centre is deduced to be formed when Mg replaces Al in the Al_2O_3:C, Mg matrix. In the same way, an F_2^{2+} (2 Mg) defect is concluded to arise when two F^+(Mg) centres are inter-linked. On this basis, if an F_2^{2+} (2 Mg) centre captures an electron,

* Corresponding author.
E-mail address: m.chithambo@ru.ac.za (M.L. Chithambo).

https://doi.org/10.1016/j.jlumin.2020.117721
Received 27 July 2020; Received in revised form 5 October 2020; Accepted 22 October 2020
Available online 6 November 2020

an F_2^+(2 Mg) centre is formed. On the other hand, if an electron is trapped at the F_2^+(2 Mg) aggregate, a neutral F_2(2 Mg) centre results. Owing to the presence of such electron centres, various luminescence emission bands are generated between 300 and 750 nm in Al_2O_3:C, Mg [10–12]. In particular, photoluminescence (PL) measurements have shown that Al_2O_3:C, Mg has four emission bands at 325, 500, 510 and 750 nm. These bands are attributed to F^+(Mg), F_2, F_2^{2+}(2 Mg) and F_2^+(2 Mg) centres respectively [9]. Measurements using continuous-wave and time-resolved optically stimulated luminescence as well as radioluminescence also show two prominent emission bands at 330 and 415 nm due to F^+ and F-centres respectively [12–15]. The signal discussed in this report is associated with the emission at the F centre.

A number of studies using thermoluminescence (TL) and optically stimulated luminescence (OSL) have shown the potential of use of Al_2O_3:C, Mg as a TL and OSL dosimeter [16–18]. The dose response of the main TL peak of Al_2O_3:C, Mg under beta irradiation is superlinear within 0.1–30 Gy becoming sublinearity thereafter up to 100 Gy [16]. However, a major drawback in the possible use of Al_2O_3:C, Mg as a TL or OSL dosimeter is that its luminescence fades much faster than desired for a dosimeter. Kalita and Chithambo [17] studied this issue and attributed the fading to charge hopping of electrons between the electron traps.

The luminescence properties of Al_2O_3:C, Mg have previously been studied using a combination of techniques such as TL [11,16,19–21], OSL [18,22], radioluminescence [22,23] and photoluminescence [9], Kalita and Chithambo [24], studied the PTTL of Al_2O_3:C, Mg and reported the presence of three PTTL peaks at 45, 74 and 163 °C respectively using illumination by 470 nm blue light. From that study, Kalita and Chithambo [24] concluded that the induced PTTL peaks follow the same order of kinetics as the corresponding peaks in the conventional TL glow curve. In terms of applications, previous studies examined the use of PTTL for dosimetry [25,26] or for absorption spectra of minerals as cited elsewhere [27].

This work follows in the same vein as that of Chithambo et al. [28] which reported on a systematic analysis of PTTL in α-Al_2O_3:C by relating each PTTL peak to sets of donors the number of which was determined by experiment. The mathematical formulation here is completely based on experimental results. As reported by Chithambo et al. [28], theoretical models of systems of one or two electron traps and one recombination centre are not directly applicable to α-Al_2O_3:C, and by extension to Al_2O_3:C,Mg, where the number of glow peaks and so electron traps far exceeds this [11,16,21,22]. Previously the PTTL of Al_2O_3:C, Mg was described only in qualitative terms [24,29]. It is therefore instructive to develop, examine and apply mathematical models to explain the PTTL in this material.

The aim of this work is to describe the PTTL of Al_2O_3:C, Mg both qualitatively and mathematically by relating the PTTL to a system of donor electron traps. The PTTL time-response profiles are described using systems of an acceptor and, donors the number of which depends on the preheating temperature.

2. Experimental methods

Samples used were trapezoidal shaped Al_2O_3:C, Mg of thickness 0.5 mm and side lengths 8 × 4 mm (Landauer, Inc; Oklahoma, USA) greenish in hue prior to any heat treatment with mass 0.060 g. The sample size was mistakenly reported as being 5 mm length, 2.5 mm breadth and 1 mm thickness in some of our earlier studies e.g. Refs. [11, 16,19–21,29]. The RISØ TL/OSL DA-20 Luminescence Reader was used in the measurements. The sample was irradiated *in-situ* with a $^{90}Sr/^{90}Y$ beta-source at a dose rate of 0.10 Gy/s. Luminescence was detected by a bialkali EMI 9235QB photomultiplier tube through a 7.5 mm thick Hoya U-340 filter (transmission band 250–390 nm). Measurements were made in a nitrogen atmosphere to properly thermally anchor the sample to its holder. In order to measure PTTL, a previously irradiated sample was preheated to remove certain peaks and cooled down immediately thereafter. The sample was then exposed to 470 nm blue light of optical power density 72 mW/cm^2 for a time during which some electrons were transferred from deeper electron traps to emptied shallower ones. All illuminations were made at 20 °C. Unless otherwise stated, all measurements were made at 1 °C/s and correspond to irradiation to 2 Gy.

3. Glow curve characteristics

Fig. 1 shows a glow curve measured after irradiation to 2 Gy (solid symbols). As determined by thermal cleaning, the glow curve has eight peaks at 43.3 ± 0.1, 73.0 ± 1.4, 164.7 ± 1.3, 195.3 ± 1.7, ~246, 284 ± 1.9, ~336 and 374.4 ± 3.0 °C. The peaks are referred to hereafter as I through VIII respectively. These are identified in Fig. 1 except peaks V and VII which are indistinct here. A glow curve measured after preheating to 60 °C, intended to remove peak I, and illumination for 10 s is shown for comparison. Peak I is reproduced under phototransfer as indicated.

4. Determining the role of electron traps as acceptors or donors using partial heating

The role of each electron trap either as an acceptor or a donor in the observed PTTL was investigated by partially heating and illuminating an irradiated sample. The technique was to progressively increment the preheating temperature used prior to illumination and monitoring the intensity (as peak heights) of any peaks present after the preheat. In the measurements, the sample was preheated from 60 to 600 °C at 20 °C intervals after irradiation and illuminated for 10 s each time. Each such pulse annealing measurement was repeated three times and the intensities plotted are averages from these measurements. For ease of reference, any PTTL peaks corresponding to peaks I-VIII will be referred to as A1,A2, A3 ….

4.1. Effect of partial heating on peaks I and II

Fig. 2(a) shows the dependence of the PTTL intensity on the preheating temperature for peaks AI and A2. The intensity of peak AI increases with preheating temperature between 80 and 140 °C. Peak A1

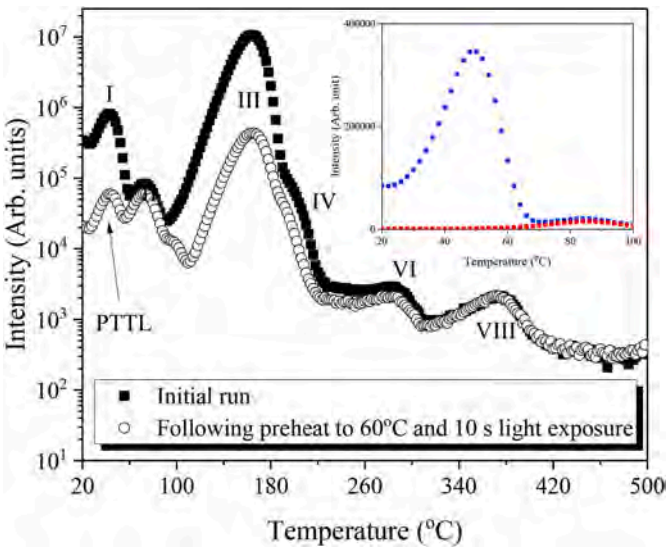

Fig. 1. Glow curves of Al_2O_3:C, Mg measured at 1 °C/s following irradiation to 2 Gy (solid symbols) and another obtained after preheating to 60 °C and subsequent illumination for 10 s (open symbols). The positions of clear peaks, except peaks V and VII which are not obvious here, are shown for reference. The inset shows, for comparison, separate glow curves measured with and without preheating where the one with preheating omitted the light exposure step. This is intended to emphasize the nature of the reproduced peak (open circles) as being due to PTTL only.

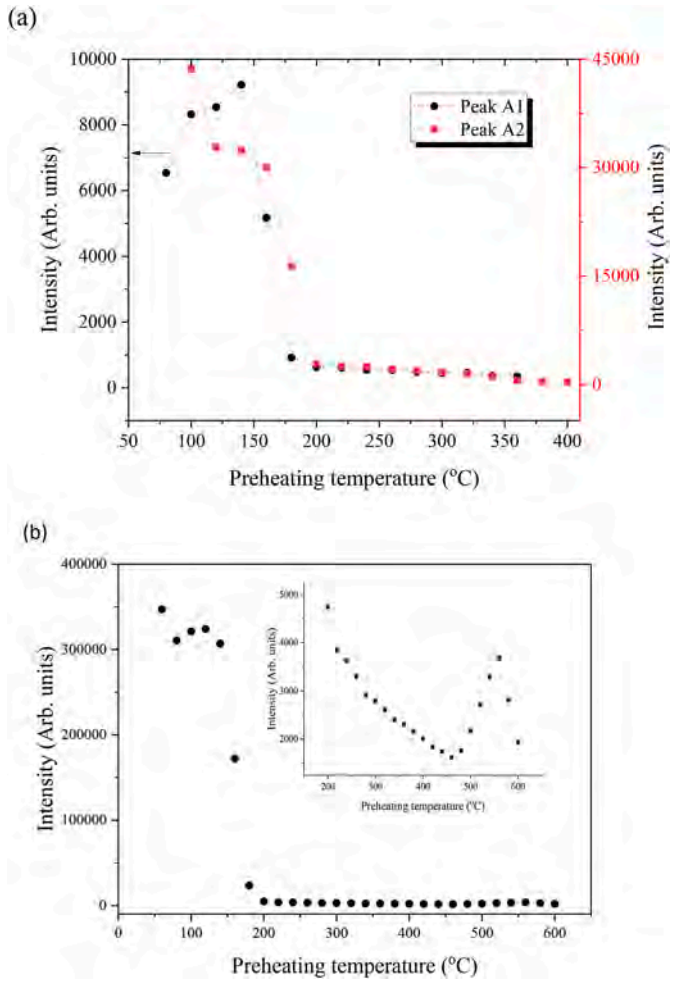

Fig. 2. Dependence of PTTL intensity on preheating temperature for peaks A1 and A2 (a) and peak III (b). The dotted lines in (a) are only visual guides. The sudden increase in signal beyond 500 °C in (b) is ascribed to the effect of deep hole traps.

then decreases rapidly in intensity thereafter from 140 to 200 °C. Notably, peak A2 decreases in intensity over the same preheating temperatures. Beyond 200 °C, the intensity of both peaks continues to decrease but do so very slowly. For preheating temperatures beyond 400 °C, it is no longer possible to measure peaks A1 and A2.

The behaviour of peak A1 between 80 and 140 °C requires comment. The intensity of an acceptor peak should remain stable as long as donors are not significantly depleted or decrease if they are. In that sense, the possible donors for peak A1 correspond to electron traps for peaks II-VIII. Preheating to 140 °C only affects the electron trap for peak II at 73 °C. Since the intensity of peak A1 increases as peak II is removed, the change must be due to a decreased role of the electron trap for peak II as a competitor for electrons that should otherwise produce peak A1. Examples of such competition effects have been observed and discussed for PTTL in synthetic and natural quartz [3,4].

Peak II (at 73 °C) decreases in intensity between 80 and 120 °C. This implies that peak II acts as a donor for peak A1 over these temperatures. What then follows, that is, the decrease in intensity of PTTL peaks A1 and A2 up to 180 °C must be due to the progressive depletion of charge from the electron trap of peak III. Increasing the preheating temperature from 200 °C onwards has little effect on the PTTL intensity of peaks A1 and A2. Thus although the putative donors for PTTL peaks A1 and A2 are the electron traps for peak III-VIII, the main donor is evidently the electron trap for peak III.

4.2. Effect of partial heating on peak III

Fig. 2(b) shows the influence of preheating on peak III. This peak appears at 165 °C but is only removed and reproduced under PTTL following preheating beyond 180 °C. The possible donors for its PTTL are the electron traps for peaks IV-VIII. Although this peak is not a PTTL peak until after preheating beyond 180 °C, its intensity slightly increases with preheating initially. Such an increase is counter-intuitive for a supposed donor for PTTL recorded at peaks A1 and A2. This means one of two things. Either the electron trap for peak III is itself a competitor or the change also reflects the decreased role of another competitor trap which in this case is the electron trap for peak A2. Beyond 180 °C, where peak III is reproduced as PTTL, that is, as A3, there is a sharp decrease in intensity. This decrease is likely caused by depletion of charge at supposed donors IV-VII.

The inset to Fig. 2(b) shows the region from 200 to 500 °C whose fine detail is obscured by the high intensity signals in the main graph. The PTTL intensity decreases monotonically from 200 to 460 °C. Peak A3 then becomes more intense reaching maximum emission at 560 °C before decreasing with further preheating up to 600 °C. Although PTTL observed beyond 500 °C can be associated with deep electron traps, it is unlikely that this would cause a sudden and significant increase in signal as shown in Fig. 2(b)inset. We will explain later how the result is associated with a deep hole trap.

4.3. Effect of partial heating on peaks IV

Peak IV, which is on the falling edge of peak III, is reproduced under phototransfer for certain combinations of preheating temperature and duration of illumination. However, the peak was found unsuitable for analysis because it could not be clearly isolated.

4.4. Effect of partial heating on peaks V-VIII

Peaks V-VIII are not reproduced under phototransfer.

5. Qualitative description of the dependence of PTTL intensity on illumination time

The dependence of PTTL intensity on illumination time is discussed for peaks A1, A2 and A3. Although peak IV is also reproduced under phototransfer, the resultant peak (A4) could not be properly isolated for such a study. For completeness and to help explain the PTTL, the influence of illumination on the intensity of the supposed donor peaks that is, any peaks not removed by preheating is also reported. The purpose of this is to confirm whether any assumed donors act as such and how important their involvement in the process is. In the measurements, an irradiated and subsequently preheated sample was illuminated by 470 nm blue light to different durations.

5.1. PTTL of peak I after preheating to 60 °C

In the first test to measure the illumination-time dependence of peak A1, the sample was preheated to 60 °C. Fig. 3 shows the dependence of PTTL intensity on illumination time for peak A1. The intensity of peak A1 goes through a maximum at 26 s with illumination time up to 26 s. For longer illumination periods than this, peak A1 can no longer be distinguished from peak II at 73 °C.

The possible donors for the PTTL of peak A1 are electron traps for peaks II-VIII since these are not removed by preheating to 60 °C. For comparison, the behaviour for peak II is also shown in Fig. 3. The intensity of this peak increases with illumination time up to 6 s before decreasing thereafter. This profile suggests that at the start of illumination the electron trap responsible for peak II acts as an acceptor but with further illumination this trap serves as a donor for peak A1.

Fig. 4 shows the dependence of TL intensity on illumination time for

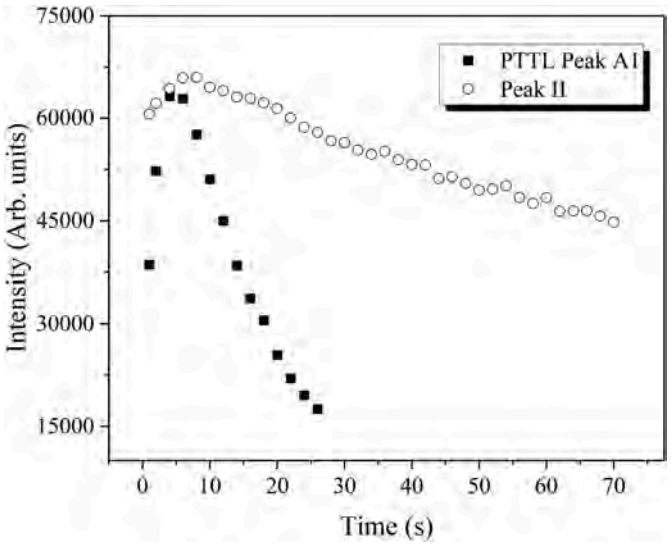

Fig. 3. Dependence of intensity on duration of illumination for peaks A1 and II.

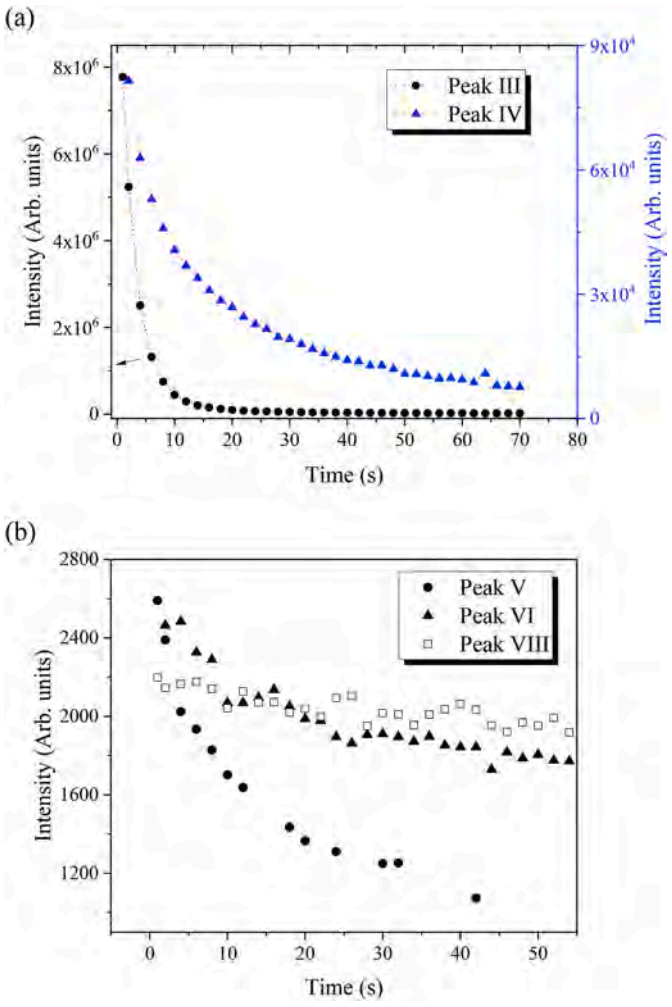

Fig. 4. The change of TL intensity with illumination time for peaks III and IV (a) and for peaks V, VI and VIII (b). The dashed lines are only visual guides.

the other donor peaks, namely, III and IV, and in Fig. 4(b) for donors V, VI and VIII. The intensity of all these peaks decreases with illumination time. Of all these peaks, the most intense one is peak III. To illustrate this point, for 2 s illumination, the intensity of peaks II and IV is only 2% that of peak III. The intensities of peaks V, VI and VIII are even lower at only about 0.05% that of peak III. Thus the main donor for peaks A1 and A2 is the electron trap for peak III. The contribution of the donor peaks as identified (and possibly of VII as well) to the PTTL of peak A1 is negligible.

5.2. PTTL from peaks I and II after preheating to 100 °C

Preheating to 100 °C removes peaks I and II at 43 and 73 °C respectively. These two peaks are reproduced by phototransfer (as A1 and A2) at the same positions. Fig. 5(a) shows that the intensity of peaks A1 and A2 both initially increase with illumination and then decrease thereafter.

Fig. 5(b) shows the dependence of TL intensity on illumination time for peaks III and IV and in the inset, for peaks VI and VIII. Peak VII is indistinct, could not be monitored, and so is not discussed. The intensity of all peaks shown in Fig. 5(b) decrease with illumination time confirming their role as possible donors for the PTTL at peaks A1 and A2. Comparing intensities, one finds that the main contributor electron traps

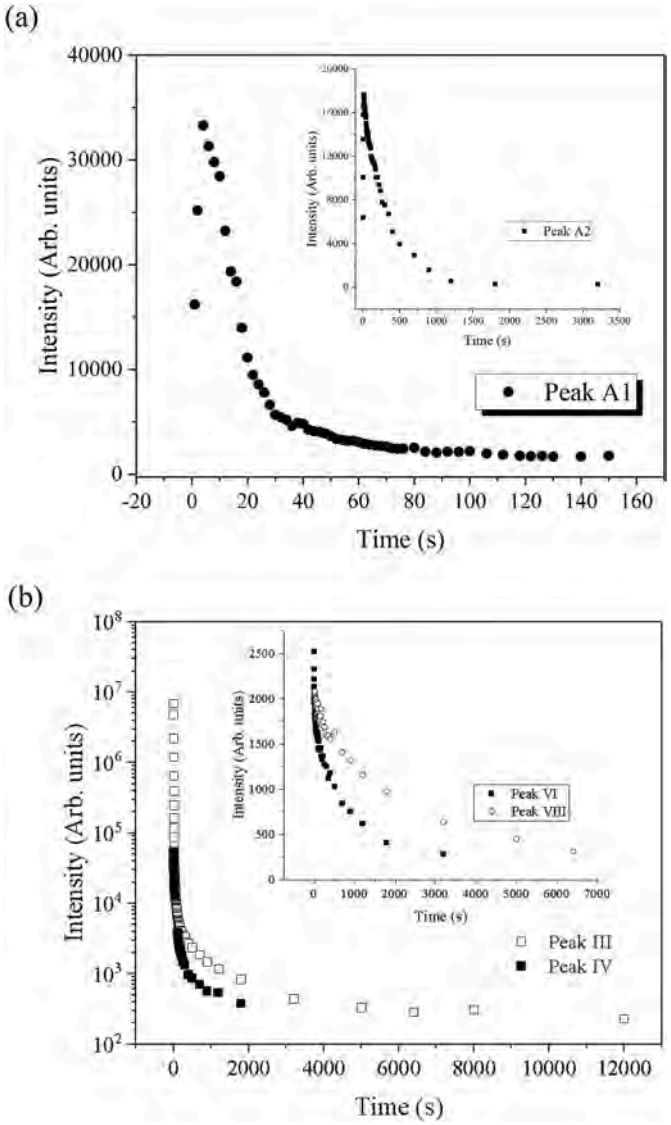

Fig. 5. The change of TL intensity with illumination time for peak A1 following preheating to 100 °C and in the inset, for peak A2 (a) The same feature for peaks III and IV, and in the inset for peaks VI and VIII (b). Peak V was indistinct and could not be monitored.

for PTLL peaks A1 and A2 correspond to peaks III and IV with peak III being dominant.

5.3. PTTL after preheating to 300 °C

When the sample is preheated to 300 °C, peaks I-VI are removed by preheating. However, only peaks I, II, III and IV are reproduced by phototransfer. This occurs for various combinations of preheating temperature and duration of illumination as shown in Fig. 6. Peak IV, which appears on the falling edge of peak III, is also reproduced for certain illumination times above 40 s but is otherwise indistinct and could not be analysed. Likewise, although peak I is reproduced by phototransfer, its intensity was too low to allow for a proper analysis of the dependence of its intensity on illumination time. Peaks V and VI are not reproduced by phototransfer.

Fig. 7 shows the dependence of PTTL intensity on duration of illumination for peaks A2 and A3. Whereas the intensity of peak A2 displays the archetypal shape, that of peak III decreases monotonically. The possible donors for this PTTL are electron traps corresponding to peaks VII and VIII. Of these only peaks VIII could be monitored (see Fig. 6) and its intensity decreases consistently with illumination time (Fig. 7, inset).

5.4. PTTL after preheating to 400 °C

Preheating to 400 °C removes all peaks in the TL glow curve. Peaks I, II and III are regenerated by phototransfer (as A1, A2 and A3). However, except for peak A3, the intensities of the two other acceptor peaks were too low for analysis. The intensity of peak A3 goes through a maximum before decreasing at longer illumination times. The supposed donor in

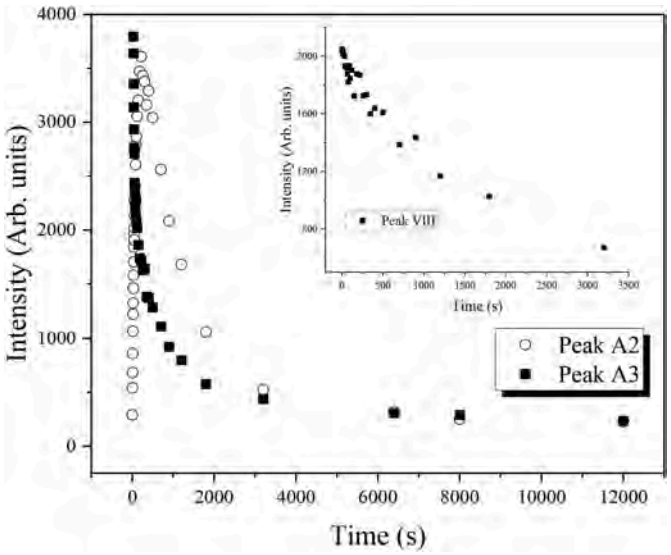

Fig. 7. PTTL intensity against duration of illumination for peaks A1 and A2 following preheating to 300 °C, and in the inset, the change in TL intensity with illumination time for peak VIII.

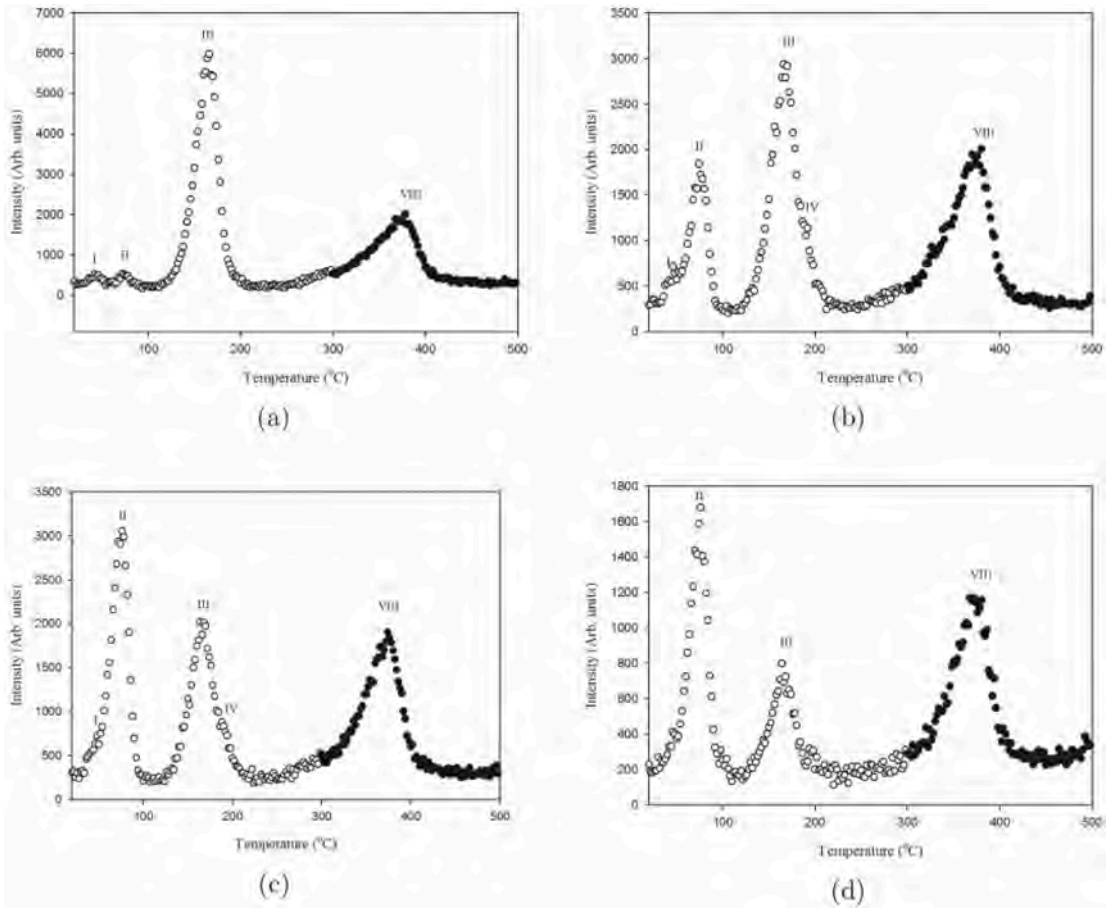

Fig. 6. Glow curves of Al_2O_3:C, Mg measured at 1 °C/s following irradiation to 2.0 Gy, preheating to 300 °C and illumination for 4 s (a) 40 s (b) 120 s (c) and 1200 s (d). The position of the otherwise indistinct peak IV is only included in (b) and (c) for reference.

this case is the deep trap(s). The plot for the time-dependence of peak A3 will be shown later in the text.

6. Mathematical analysis of PTTL time-response profiles

The dependence of PTTL intensity on duration of illumination used for phototransfer was discussed qualitatively in the preceding section. We will proceed to analyse the same mathematically. The analysis will be informed by experimental results presented in sections 4 and 5.

To aid the discussion, Table 1 lists the observed TL and PTTL peaks. Conventional TL peaks are labelled I-VIII. The PTTL peaks corresponding to these peaks are referred to as A1, A2,…These are the same labels used thus far. The electron traps listed as 'possible donors' are the theoretically expected ones. This is because, in theory, the electron trap of any peak at temperatures beyond that of one that has been removed by preheating, can serve as a donor in the PTTL process. The main donors suggested by the partial heating experiment (section 4) and as reflected by PTTL time-response profiles (section 5) are listed separately in Table 1. The analysis will be based on the latter two lists rather than the ideal theoretical list.

The concentration of trapped electrons at the ith electron trap will be denoted by N_i and the optical stimulation probabilities as s_i. The equations describing the change in the concentration of trapped electrons are written for the illumination step only. Retrapping is neglected because, as has been shown several times previously, the peaks follow first-order kinetics [16,19–21]. Each family of equations is unique to each system and has a particular solution. This solution is applied to the experimental data for that particular system. The main assumption as before [3,4] is that only a portion of electrons released from a donor trap end up at the acceptor electron trap to produce PTTL. The method used here is the same one developed by Chithambo et al. [28] and applied previously on quartz [3,4,30].

The method used here and elsewhere [3,4,28,30] should be distinguished from the kinetics-based method of say, Alexander and McKeever [27] where non-linear rate equations are used to relate the concentration of holes at a recombination centre to the concentration of electrons at electron traps and in the conduction band. Here, the transport of electrons involved in the PTTL process is described at the irradiation, preheating, illumination and heating stages. The coupled non-linear differential equations developed this way do not have analytical solutions and thus require numerical approximations to solutions. These numerical solutions are then used to generate plots of PTTL intensity as a function of illumination time by considering various assumptions such as, say, negligible retrapping or the number of electron traps involved in the process. Our approach differs from this method in several respects. We formulate differential equations only at the illumination stage. These equations describe the transfer, to an acceptor, of a proportion of electrons optically stimulated from a donor. The number of donors for any acceptor peak is determined by experiment. The sets of these equations have analytical solutions which are then applied directly to experimental data.

6.1. Time-dependence of PTTL after preheating to 60 °C

Preheating to 60 °C followed by illumination produces only peak A1. As shown in Table 1, there is only one dominant donor for the PTTL, the electron trap for peak III. Therefore, the PTTL time-response profile for peak A1 can be described in terms of a system of one acceptor and one donor with rate equations as follows:

$$\frac{dN_3}{dt} = s_3 N_3 \tag{1}$$

$$\frac{dN_1}{dt} = -s_1 N_1 + \alpha_3 s_3 N_3 \tag{2}$$

where α_3 is a constant of proportionality and all other parameters are as defined before. Equation (1) describes the loss of electrons from the donor. Equation (2) takes into account not only the transfer of electrons from the donor but the possibility of loss due to illumination at the acceptor. The solution of the coupled set Eqs. (1) and (2) is

$$N_1(t) = A(e^{-s_3 t} - e^{-s_1 t}) \tag{3}$$

where $A = (\alpha_3 s_3 N_{3i}/(s_1 - s_3)$ where N_{3i} is the initial concentration of trapped electrons at the donor trap at the start of illumination. Increasing the number of donors to two by considering both peaks III and IV as contributors did not produce any improvement in the fit. This supports the qualitative conclusion that although in theory there are 7 donors, the main contributor to the PTTL is the electron trap for peak III.

6.2. PTTL following preheating to 100 °C

When the sample is preheated to 100 °C, only peaks A1 and A2 are reproduced under phototransfer. The main contributors to the PTTL correspond to electron traps for peaks III and IV. Thus in this case we have two separate systems of one acceptor and two donors. Therefore the rate equations describing charge transfer responsible for peak A1 or A2 are

$$\frac{dN_3}{dt} = S_3 N_3 \tag{3}$$

Table 1
A summary of TL peaks, their corresponding PTTL peaks, donors and photoionization cross-section. In the study corresponding to 300 °C, only peak III could be monitored as a donor.

	TL	PTTL					P. cross-section (cm-2)		
Peak label	Tm (oC)	Peak label	Preheating temp (oC)	Possible donors	Main donor √	Main donor √√	Acceptor	Donor	Donor
I	43	A1	60	II III IV V VI VII VIII	III	III	3.26E-18	3.92E-19	
			100	II III IV V VI VII VIII	III	III IV	1.95E-18	6.93E-19	4.82E-20
			300						
II	73	A2	100	III IV V VI VII VIII	III	III IV	2.17E-18	2.17E-19	1.53E-20
			300			VII and VIII	4.70E-21	8.52E-20	
III	165	A3	300	IV V VI VII VIII	IV V VI	VII and VIII	5.25E-18	2.42E-19	4.70E-21
			400	DT	DT	DT	5.44E-18	3.10E-19	4.70E-21
IV	195	A4	300	N/A	N/A	N/A			
V	246	N/A			N/A	N/A			
VI	284	N/A			N/A	N/A			
VII	336	N/A			N/A	N/A			
VIII	374	N/A			N/A	N/A			

√ From pulse annealing study.
√√ From time-response study.

$$\frac{dN_4}{dt} = s_4 N_4 \tag{4}$$

$$\frac{dN_j}{dt} = s_j N_j + \gamma_3 s_3 N_3 + \gamma_4 s_4 N_4 \tag{5}$$

where γ_3 and γ_4 are proportionality constants. (s_j ,N_j) is either (s_1 , N_1) or (s_2, N_2) depending on which one of the two PTTL peaks is considered. The solution to the coupled first order linear differential Eqs. set (3–5) is

$$N_j(t) = A_1(e^{-s_3 t} - e^{-s_j t}) + A_2(e^{-s_4 t} - e^{-s_j t}) \tag{7}$$

where $A_1 = (\gamma_3 s_3 N_{3i}/(s_1 - s_3)$and. $A_2 = (\gamma_4 s_4 N_{4i}/(s_1 - s_4)$.

6.3. PTTL after preheating to 300 °C

Preheating to 300 °C removes peaks I to VI. Peaks A1, A2, A3 and A4 are reproduced by phototransfer. However, only peaks A2 and A3 were sufficiently intense and distinct for analysis. The only possible donors in this case are the electron traps for peaks VII and VIII (see Table 1) although in practise peak VII could not be monitored. Experimental tests (see section 5.3) suggest that the electron trap for peak VIII is the only dominant donor. On this basis, the time-response profile of the PTTL of peaks A2 and A3 were analysed using the two options of one acceptor and one donor (Eq. (3)) or one acceptor and two donors (Eq. (7)). It was found that only the second option could properly describe the result. In this particular case, the PTTL of either peak A2 or A3 cannot result from a single donor.

6.4. PTTL following preheating to 400 °C

Preheating to 400 °C removes all peaks in the conventional TL glow curve. Although peaks I, II and III are reproduced by phototransfer, only peak A3 was found suitable for further analysis. In theory, its PTTL corresponds to a simple system of one acceptor and one donor, a deep

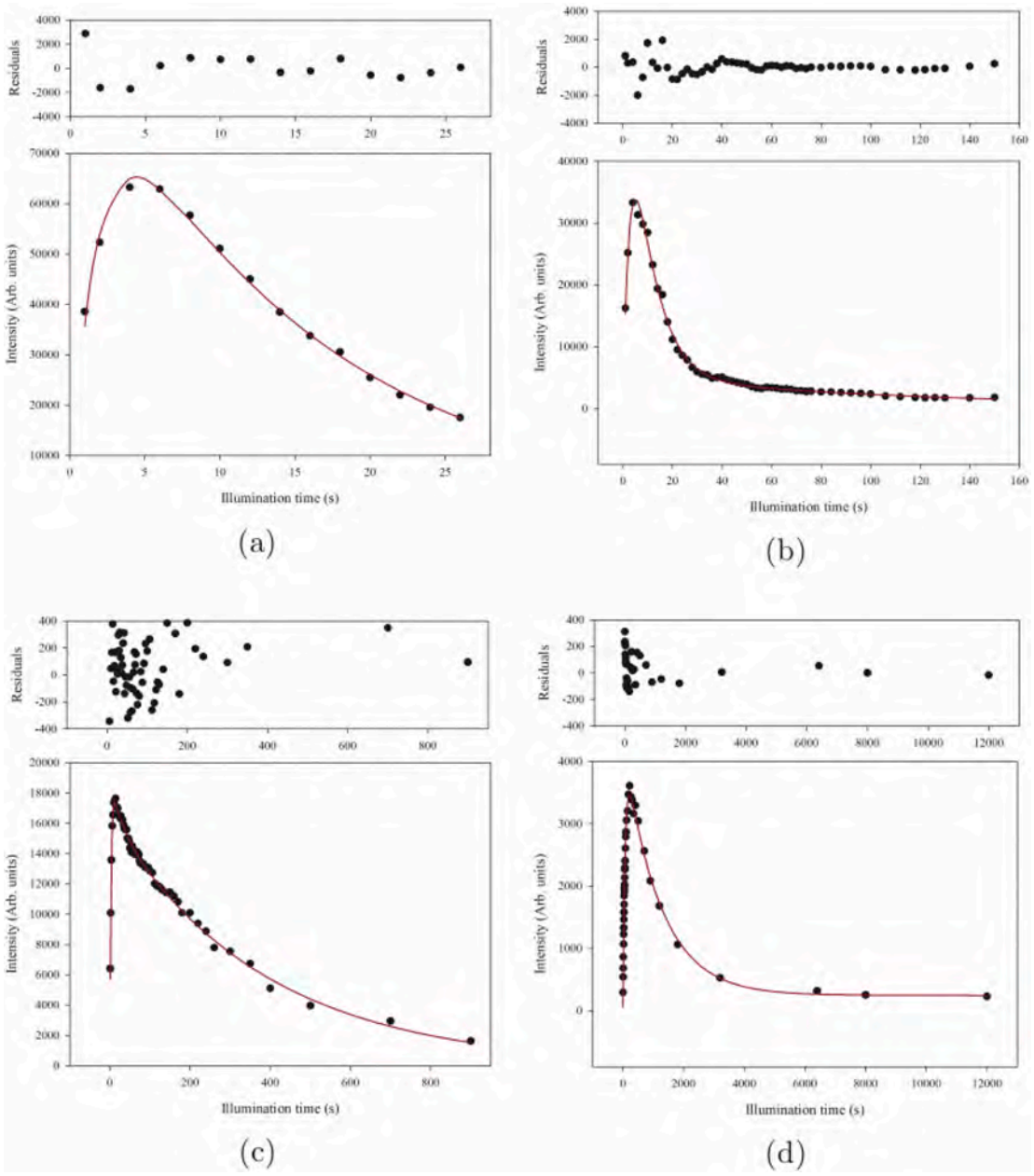

Fig. 8. PTTL intensity against duration of illumination of peak A1 following preheating to 60 °C (a) and to 100 °C (b) the change for peak A2 following preheating to 100 °C (c) and to 300 °C (d). All data is shown fitted with Eq. (7)except for (a) which is fitted with Eq. (3).

electron trap, and should be described by an expression similar to Eq. (3). However, we could not obtain a satisfactory fit by considering a system consisting of one acceptor and one donor. The lowest possible number of donors which yielded a satisfactory fit was two using an expression of the same form as Eq. (7). We therefore assume that the PTTL following preheating to 400 °C can be ascribed to the contribution of at least two deep electron donor traps.

7. Applications

Figs. 8 and 9 show applications of the models to experimental data. Fig. 8(a) shows the PTTL time-response profile of peak A1 after preheating to 60 °C. The solid line through data is the best fit of Eq, (3). Fig. 8(b) shows the result for peak A1 after preheating to 100 °C fitted with Eq. (7). The best fit of the same expression on peak A2 after preheating to 100 °C and to 300 °C are shown in Fig. 8(c) and (d). The PTTL time-response profile of peak A3 after preheating to 300 °C and 400 °C are shown in Fig. 9(a) and (b) respectively. Both are shown fitted with Eq. (7). In all cases, except perhaps for Fig. 9(a), the experimental data is satisfactory described by the models as evident in the residuals fluctuating about zero. For completeness, we have provided as *Supplementary Information*, plots of tests which though theoretically possible, were found unsuitable in practise. Since the stimulation rate $s = \Phi\sigma$ where Φ is the incident photon flux and σ the photoionization cross-section, this provided a means to determine the latter. In this study, we had $\Phi = 1.70 \times 10^{17}$ cm^{-2} s^{-1}. Examples of values of s are $s_1 = 0.5547 \pm 0.0253$ and $s_3 = 0.0667 \pm 0.0021$ in the fit for peak A1 after preheating to 60 °C. The photoionization cross-section calculated for the various peaks are included in Table 1 and range between.

10^{-21} -10^{-18} cm^{-2}.

Fig. 2(b) inset showed a notable response of PTTL to preheating. Peak A3 increases with preheating up to 560 °C before decreasing with further preheating up to 600 °C. As stated, this sudden and significant increase in signal is unlikely to be associated with deep electron traps. Yukihara et al. [31] suggested that deep hole traps become unstable between ~530 and 600 °C in Al_2O_3:C. We conclude that the same process is responsible for the result observed in Fig. 2(b) inset. A similar type of generation of holes was used by Chithambo [32] to explain the dose response in Al_2O_3:C. Heating in this temperature region produces a large number of holes. Some of these holes are captured at F centres converting them to F^+ centres. As known, the recombination of an electron with an F^+ centre produces an excited F centre. Luminescence, including TL, at 420 nm results following relaxation of the electron from an excited 3P to the 1S ground state at the F-centre [8]. Therefore the TL or PTTL intensity in this case reflects changes in the concentration of holes owing to preheating between 500 and 600 °C as observed. To our knowledge, this is the first demonstration of involvement of deep hole traps in the PTTL of Al_2O_3:C,Mg.

As a final point, we note the behaviour of peak II in Fig. 3. The intensity of this peak does not decrease consistently with illumination as expected of a donor but instead increases for the first 6 s before the expected decrease appears. This behaviour is classified as a competition effect. This is defined as processes that enhance or depress the capture of charge at electron traps during illumination and how this affects the output from acceptors or contribution of donors [3,4]. The conventional interpretation of PTTL assumes that when electrons are released from donor traps during illumination, they can move to a recombination centre, get re-trapped or transit to acceptors. Although this idealized description aids the formulation of mathematical expressions to describe phototransfer, the real effects are far more complex and affected by competition effects. These have been investigated in detail in quartz [3,4] and were briefly discussed for PTTL in α-A1$_2$O$_3$:C [30]. Competition effects in Al_2O_3:C, Mg may involve not only electron traps but also hole traps and will be studied in detail elsewhere.

8. Conclusion

We have reported a comprehensive study of PTTL in Al_2O_3:C, Mg and developed a mathematical description of the observed PTTL dependence on illumination time. The PTTL has been experimentally demonstrated as separate systems of an acceptor and, donors the number of which is affected by various combinations of preheating and illumination. The systems have been analysed as coupled sets of linear first order differential equations describing the charge transfer at the illumination step. Particular solutions have been applied to experimental data. The study has also revealed the presence and role of deep hole traps beyond 500 °C which contribute to the PTTL observed. To our knowledge, this is the first time this has been reported. The study suggests that competition effects in Al_2O_3:C, Mg may involve not only electron traps but also hole traps and is a problem that requires further examination. This study has contributed to a better understanding of the processes and analysis of PTTL in Al_2O_3:C, Mg and may be of interest to readers interested in

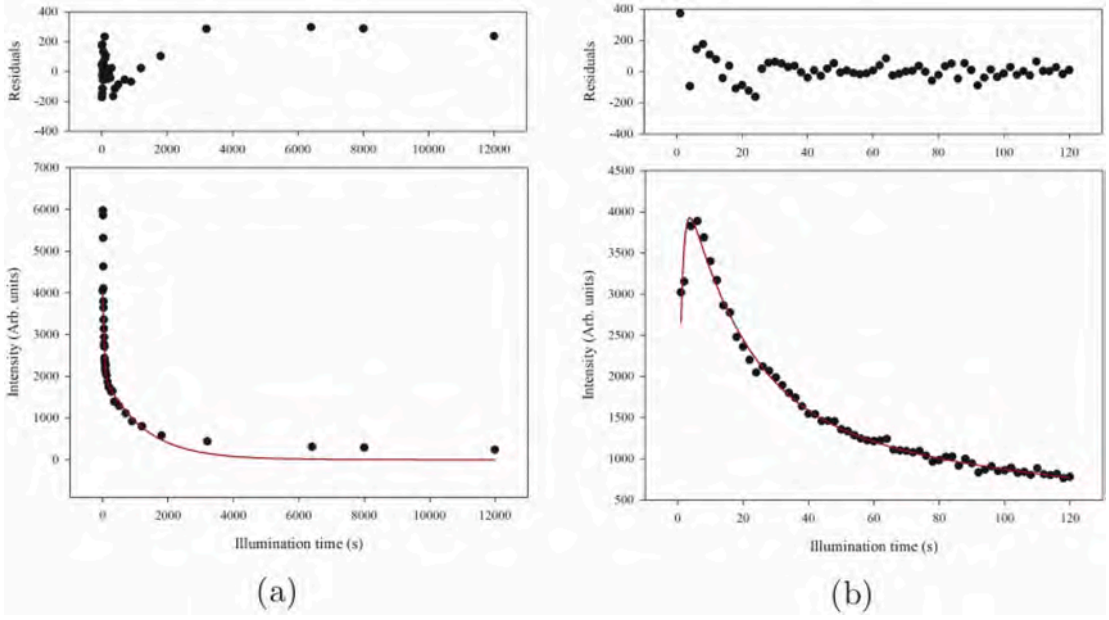

Fig. 9. PTTL intensity against duration of illumination of peak A3 following preheating to 300 °C (a) and to 400 °C (b).

dosimetry and solid state defect research.

CRediT author statement

A.J. Lontsi Sob, Investigation, Validation, Writing - original draft, Formal analysis. M.L. Chithambo, Conceptualization, Methodology, Validation, Writing - review & editing, Visualization, Project administration, Funding acquisition, Supervision. J.M. Kalita, Writing – Editing, Validation

Declaration of competing interest

The authors declare that they have no known competing financial interests or personal relationships that could have appeared to influence the work reported in this paper.

Acknowledgement

We acknowledge with gratitude funding from Rhodes University and the National Research Foundation of South Africa.

Appendix A. Supplementary data

Supplementary data to this article can be found online at https://doi.org/10.1016/j.jlumin.2020.117721.

References

[1] S.W.S. McKeever, Thermoluminescence of Solids, Cambridge University Press, Cambridge, 1985.
[2] R. Chen, S.W.S. McKeever, Theory of Thermoluminescence and Related Phenomena, World Scientific, Singapore, 1997.
[3] M.L. Chithambo, R.R. Dawam, Phototransferred thermoluminescence of annealed synthetic quartz: analysis of illumination-time profiles, kinetics and competition effects, Radiat. Meas. 131 (2020) 106236.
[4] M.L. Chithambo, D.E. Folley, S. Chikwembani, Phototransferred thermoluminescence from natural quartz annealed at 1000°C : analysis of time-dependent evolution of intensity and competition effects, J. Lumin. 216 (2019) 116730.
[5] M.S. Akselrod, A.E. Akselrod, S.S. Orlov, S. Sanyal, T.H. Underwood, New aluminum oxide single crystals for volumetric optical data storage 5069 (2003) 244–251.
[6] M.S. Akselrod, G.J. Sykora, Fluorescent nuclear track detector technology a new way to do passive solid state dosimetry, Radiat. Meas. 46 (2011) 1671–1679.
[7] N. Shrestha, E.G. Yukihara, Davide Cusumano, Lorenzo Placidi Al2O3:C and Al2O3:C,Mg optically stimulated luminescence 2D dosimetry applied to magnetic resonance guided radiotherapy, Radiat. Meas. 138 (2020) 106439.
[8] S.W.S. McKeever, M. Moscovitch, P.D. Townsend, Thermoluminescence Dosimetry Materials: Properties and Uses, Nuclear Technology Publishing, United Kingdom, 1995.
[9] G.J. Sykora, M.S. Akselrod, Photoluminescence study of photochromically and radiochromically transformed Al_2O_3:C,Mg crystals used for fluorescent nuclear track detectors, Radiat. Meas. 45 (2010) 631–634.
[10] M.S. Akselrod, A.E. Akselrod, S.S. Orlov, S. Sanyal, T.H. Underwood, Fluorescent Aluminum oxide crystals for volumetric optical data storage and imaging application, J. Fluoresc. 13 (2003) 503–511.
[11] J.M. Kalita, M.L. Chithambo, The effect of annealing and beta irradiation on thermoluminescence spectra of α-Al_2O_3:C,Mg, J. Lumin. 196 (2018) 195–200.
[12] M.L. Chithambo, J.M. Kalita, A. Finch, F- and F+-band radioluminescence and the influence of annealing on its emission spectra in Al_2O_3:C,Mg, Radiat. Meas. 134 (2020) 106306.
[13] S. Sanyal, M.S. Akselrod, Anisotropy of optical absorption and fluorescence in Al_2O_3:C, Mg crystals, J. Appl. Phys. 98 (2005), 033518.
[14] G. Denis, M.G. Rodriguez, M.S. Akselrod, T.H. Underwood, E.G. Yukihara, Time-resolved measurements of optically stimulated luminescence of Al_2O_3:C and Al_2O_3:C,Mg, Radiat. Meas. 46 (2011) 1457–1461.
[15] E.G. Yukihara, S.W.S. McKeever, Optically Stimulated Luminescence: Fundamentals and Applications, Wiley, 2011.
[16] J.M. Kalita, M.L. Chithambo, The influence of dose on the kinetic parameters and dosimetric features of the main thermoluminescence glow peak in α-Al_2O_3:C,Mg, Nuclear Instrum. Meth. Res. B 394 (2017) 12–19.
[17] Kalita, J. Chithambo Kalita, M.L. Chithambo, A comparative study of the dosimetric features of α-Al_2O_3:C,Mg and α-Al_2O_3, C. Radiat. Prot. Dosim. 177 (2017) 261–271, 2017.
[18] J.M. Kalita, M.L. Chithambo, On the sensitivity of thermally and optically stimulated luminescence of α-Al_2O_3:C and α-Al_2O_3:C,Mg, Radiat. Meas. 99 (2017) 18–24.
[19] J.M. Kalita, M.L. Chithambo, Features of an annealing-induced thermoluminescence peak in α-Al_2O_3:C,Mg, Opt. Mater. 70 (2017) 158–164.
[20] J.M. Kalita, M.L. Chithambo, Thermoluminescence of α-Al_2O_3:C,Mg: kinetic analysis of the main glow peak, J. Lumin. 182 (2017) 177–182.
[21] J.M. Kalita, M.L. Chithambo, Comprehensive kinetic analysis of thermoluminescence peaks of α-Al_2O_3:C,Mg, J. Lumin. 185 (2017) 72–82.
[22] M.G. Rodriguez, G. Denis, M.S. Akselrod, T.H. Underwood, E.G. Yukihara, Thermoluminescence, optically stimulated luminescence and radioluminescence properties of Al_2O_3:C,Mg, Radiat. Meas. 46 (2011) 1469–1473.
[23] M.L. Chithambo, J.M. Kalita, A. Finch, F- and F^+-band radioluminescence and the influence of annealing on its emission spectra in Al_2O_3:C,Mg, Radiat. Meas. 134 (2020) 106306.
[24] J.M. Kalita, M.L. Chithambo, Phototransferred thermoluminescence in α-Al_2O_3:C, Mg under 470 nm blue light stimulation, J. Lumin. 188 (2017) 371–377.
[25] I.K. Bailiff, N.R.J. Poolton, Studies of charge transfer mechanisms in feldspars, Nucl. Tracks Radiat. Meas. 18 (1991) 111–118.
[26] L. Bossin, I.K. Bailiff, I. Terry, Phototransferred TL properties of alumina substrates, Radiat. Meas. 120 (2018) 41–46.
[27] C.S. Alexander, S.W.S. McKeever, Phototransferred thermoluminescence, J. Phys. D Appl. Phys. 31 (1998) 2908–2920.
[28] M.L. Chithambo, C. Seneza, J.M. Kalita, Phototransferred thermoluminescence of Al_2O_3:C: experimental results and empirical models, Radiat. Meas. 105 (2017) 7–16.
[29] J. Kalita, M.L. Chithambo, Phototransferred thermoluminescence and thermally-assisted optically stimulated luminescence dosimetry using α-Al_2O_3:C,Mg annealed at 1200 °C, J. Lumin. 205 (2019) 1–6.
[30] M.L. Chithambo, P. Niyonzima, J.M. Kalita, Phototransferred thermoluminescence of synthetic quartz: analysis of illumination-time response curves, J. Lumin. 198 (2018) 146–154.
[31] E.G. Yukihara, V.H. Whitley, J.C. Polf, D.M. Klein, S.W.S. McKeever, A.E. Akselrod, M.S. Akselrod, The effects of deep trap population on the thermoluminescence of Al_2O_3:C, Radiat, Meas 37 (2003) 627–638.
[32] M.L. Chithambo, Concerning secondary thermoluminescence peaks in α-Al_2O_3:C, South Africa, J. Sci. 100 (2004) 524–527.

Physica B 624 (2022) 413438

Contents lists available at ScienceDirect

Physica B: Physics of Condensed Matter

journal homepage: www.elsevier.com/locate/physb

Light-induced inter-electron-trap charge movement in annealed Al_2O_3:C, Mg

M.L. Chithambo [a,*], A.J. Lontsi Sob [a], J.M. Kalita [b]

[a] Department of Physics and Electronics, Rhodes University, P O BOX 94, Makhanda, 6140, South Africa
[b] Department of Physics, Cotton University, Guwahati, 781001, India

ARTICLE INFO

Keywords:
Phototransferred thermoluminescence
Al_2O_3:C,Mg
Electron traps
Annealing
Point-defects

ABSTRACT

Inter-electron-trap charge movement induced under phototransferred thermoluminescence (PTTL) in Al_2O_3:C, Mg annealed at 700 and 900 °C is reported. Such annealing modifies the emission spectrum and electron trapping states in Al_2O_3:C,Mg. The glow curve of Al_2O_3:C,Mg annealed at 700 °C has eight peaks at 46, 76, 100, 170, 199, 290, 330 and 375 °C respectively. In comparison, that of the sample annealed at 900 °C has nine at 49, 80, 100, 174, 206, 235, 290, 335 and 375 °C. The peaks are labelled I, II, III … in that order. Only peaks I-IV re-appear under phototransfer. The PTTL is analysed qualitatively as well as by computational and phenomenological models as systems of an acceptor and multiple donors. Point defects that likely contribute to emergence of PTTL are discussed and are deduced to lie mostly in the oxygen sub-lattice.

1. Introduction

Alumina (Al_2O_3) is a well-known wide band-gap insulator with a diverse range of point defects [1,2] some of which produce luminescence under optical or thermal stimulation [3–5]. Although various types are intrinsic, some of the defects in question are generated by thermal reduction, irradiation by energetic neutrons, electrons or ions as well as by addition of impurities to the Al_2O_3 lattice [1]. The imperfections mostly reside in the oxygen sub-lattice. The quintessence of these are the F^+ and F electron centres consisting of one or two electrons trapped at an oxygen vacancy [1]. Alternatives, whose existence is rationalized, include the F_2, F_2^+, F_2^{2+} and F_3^+ aggregates [6–8] and others like the α centre whose presence is moot.

The doping of Al_2O_3 with C and Mg is thought to modify the balance of F and F^+ centres within it to the extent that the concentration of F^+ centres exceeds that in Al_2O_3 when doped with C alone [6]. This is evident by the comparative increase in intensity of the 325 nm emission band attributed to the F^+ centre [7]. The luminescence lifetime of the F^+ centre emission, at 7 ns, is much faster than the 35 ms of the F colour centre [3]. This dynamic has been exploited to see to Al_2O_3:C,Mg as a fluorescent nuclear track detector in neutron-based dosimetry [6–8]. Besides the 325 nm one, a large number of other bands span the emission spectrum of Al_2O_3:C,Mg between 300 and 800 nm. Examples at 410, 500, 510 and 750 nm are linked to F, F_2, F_2^{2+}(2 Mg) and F_2^+(Mg) colour centres respectively [6,9,10]. With specific reference to Al_2O_3:C,Mg, the F^+(Mg) is a single oxygen vacancy charge compensated for by Mg. An inter-link of a pair of F^+(Mg) centres is thought to produce the F_2^{2+}(2 Mg) mentioned earlier. If the latter captures an electron in a radiolytic reaction, the product is the F_2^+(2 Mg) centre.

The diversity displayed in emission characteristics is mirrored under electron trapping states. The thermoluminescence glow curve of Al_2O_3:C,Mg has a dominant peak near 161°*C* and a motley of no less than six secondary glow peaks [11–13]. All peaks follow first order kinetics. When Al_2O_3:C,Mg is annealed at elevated temperature, significant changes occur in its emission and glow curve features. Whereas emission bands at 325, 420 and 485 nm stand out [11,12], the intensity of the 485 nm band decreases and more glow peaks appear when the material is annealed at 900 °C [12]. The drop in the 485 nm emission is singled out here because it exemplifies the influence of annealing on complex defects. The decrease of the 485 nm band is ascribed to the dissociation of F_2^{2+}(2 Mg) electron centres responsible for this band [12]. Of relevance to this work is that Al_2O_3:C,Mg, whether annealed or not, is sensitive to optical stimulation over a wide range of measurement temperature.

Thermoluminescence, the method used here, is a sensitive technique for monitoring changes in defect concentration in insulators and semiconductors. Certain type of imperfections within these materials can trap and retain free electrons or holes. The release of the trapped charges

* Corresponding author.
E-mail address: m.chithambo@ru.ac.za (M.L. Chithambo).

https://doi.org/10.1016/j.physb.2021.413438
Received 7 July 2021; Received in revised form 7 September 2021; Accepted 18 September 2021
Available online 25 September 2021

under heating at a linear rate can be measured as a temperature and wavelength-resolved set of signals and is called a glow curve if the signal is recorded over a fixed detection band. Each discrete peak in the glow curve reflects the presence of a particular type of electron-trapping point defect. The utility of TL for studies of wide band-gap insulators like Al_2O_3:C,Mg is that they offer a means to sense the presence of and changes in defect concentration, their complexes and influence of experimental treatment such as annealing on their stability and in general, sensitivity of various electron traps including deep ones to thermal and optical stimulation.

The presence of many colour centres and an array of electron traps that can be optically and thermally stimulated creates analytical problems that cannot always be resolved by empiricism or hindsight. Whereas some changes in defect concentration can be sensed with a degree of precision using TL by monitoring specific electron traps, the question that arises is how the optically induced transfer of electrons between a large collection of stable and unstable electron traps in Al_2O_3:C,Mg ought to be studied. Phototransferred thermoluminescence (PTTL) is one means to do so. Indeed for α-Al_2O_3:C, some previous studies [14,15] show its relevance. PTTL arises due to transfer of electrons, by light, from one electron trap to another and is conveniently investigated if the source or donor trap is more stable that the acceptor electron trap. However, a number of studies [15–20] have shown that this definition is axiomatic. It implies that the charge transfer involved is a one-way process from donor to acceptor and that PTTL will ensue as long as at least one empty electron trap is available. The reality is different and the axiom is only a fortunate experimental exception. As has been shown in Al_2O_3:C [15], quartz [16–18] and tanzanite [19], PTTL sometimes only appears when multiple peaks have been removed. Even so, PTTL appears at only some and not all peaks as also observed in unannealed Al_2O_3:C,Mg [20]. Indeed, it is not unusual for the intensity of the supposed donor peaks to counterintuitively increase with measurement or for a peak to act as an acceptor only in the presence or absence of certain supposed donor peaks.

Some studies e.g. Refs. [14,21–23] state that annealing α-Al_2O_3:C near 900 °C depletes deep electron traps. Such changes in the occupancy of the latter affects the sensitivity of α-Al_2O_3:C to thermal or optical stimulation. It is also known to affect its dose response [24]. Although similar annealing may empty deep electron traps in α-Al_2O_3:C,Mg, it causes other changes besides. Akselrod et al. [25] noted that annealing α-Al_2O_3:C,Mg above 700 °C destroyed the F_2^{2+}(2 Mg) colour centre. In related work, Kalita and Chithambo [26] observed change in sensitivity of Al_2O_3:C,Mg due to annealing at 700 °C and 900 °C. Changes in luminescence bands due to dissociation of F_2^{2+}(2 Mg) centre caused by annealing at 700 °C or beyond were confirmed in TL spectral measurements [12].

Since annealing modifies both the emission and glow curve features, this work examines PTTL of Al_2O_3:C,Mg annealed at 700 and 900 °C and is a natural progression from our previous work that investigated PTTL in unannealed Al_2O_3:C,Mg [20]. We identify and discuss the role of electron traps as acceptors or donors and analyse the PTTL time-response profiles using various mathematical models. The report also describes point defects that are likely involved in the emission of the PTTL.

2. Experimental methods

Samples used were Al_2O_3:C,Mg trapezoids of thickness 0.5 mm, side lengths 8 × 4 mm and mass 0.060 g (Landauer, Inc; Oklahoma, USA). The samples were annealed in a tube furnace (Kiln Contracts (Pty) Ltd, Cape Town) at 700 and 900 °C for 15 min prior to use. For ease of reference, the sample annealed at 700 °C will be called sample S and the one annealed at 900 °C; sample N. Measurements were made on the RISØ TL/OSL DA-20 Luminescence Reader. Samples were irradiated *in-situ* with a $^{90}Sr/^{90}Y$ beta-source at a rate of 0.10 Gy s^{-1}. Luminescence was detected by an EMI 9235QB photomultiplier tube through a 7.5 mm thick Hoya U-340 filter (transmission band 250–390 nm). PTTL was measured as typical starting with the preheating of a previously irradiated sample to remove certain peaks. The sample was then exposed to 470 nm blue light for a time to transfer electrons from deeper electron traps to shallower ones purposely emptied by the preheating. All illumination was done at room temperature with the LEDs set at an optical power density of 72 mW cm^{-2} at sample position. Unless otherwise stated, all measurements were made at 1 °C s^{-1} and correspond to irradiation to 2 Gy.

3. Glow curve characteristics

Fig. 1 shows glow curves of samples S (solid symbols) and N (open symbols). Sample S has eight peaks, and sample N; nine. The peaks for sample S are at 46, 76, 100, 170, 199, 290, 330 and 375 °C whereas those of sample N appear at 49, 80, 100, 174, 206, 235, 290, 335 and 375 °C. These peaks are referred to hereafter as I through IX. Only some stand out in Fig. 1. The complete set in each case was determined by thermal cleaning. There are other differences between the glow curves besides their number of glow peaks. When the annealing temperature is increased from 700 to 900 °C, the intensity of TL beyond 260 °C in sample N drops below that in sample S. It is also clear that although both samples have peaks near 290 and 330 °C, sample N has an additional one interposed between the two.

Once an irradiated sample has been preheated, there is an expectation that subsequent illumination will induce PTTL. The inset to Fig. 1 compares measurements on samples S and N made without and with preheating (to 375 and 300 °C respectively) and no exposure to light. There are no peaks at the position of removed peaks on re-measurement.

Results of tests preparatory to measurement of PTTL from samples S and N are shown in Fig. 2. The glow curves were obtained after preheating to 260 °C and illumination for 12 s. Both samples produce PTTL. In this example, only peaks II and III reappear under phototransfer in both samples as does peak I in sample N. Thus, not all peaks I–V or I-VI removed by the preheating in samples S and N respectively are reproduced as a result of phototransfer.

The reproducibility of the peak position was assessed by using the best estimate of the position as the average and the uncertainty as the standard deviation for five consecutive measurements. Each of peaks I-IX was found to be within 1.0% of the average for sample S except peak II

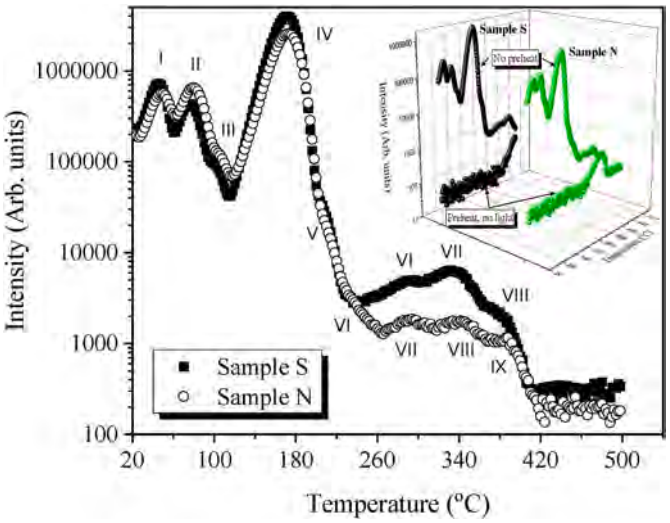

Fig. 1. Glow curves of Al_2O_3:C,Mg annealed at 700 and 900 °C measured at 1 °C s^{-1} following irradiation to 2 Gy. Annealing modifies the number of peaks and to some extent, their intensity. The sample annealed at 700 °C is labelled S and that at 900 °C, N. The approximate peak positions are indicated. When the glow curves are measured after preheating but without any illumination, no peaks are observed at the position of the removed peaks (inset).

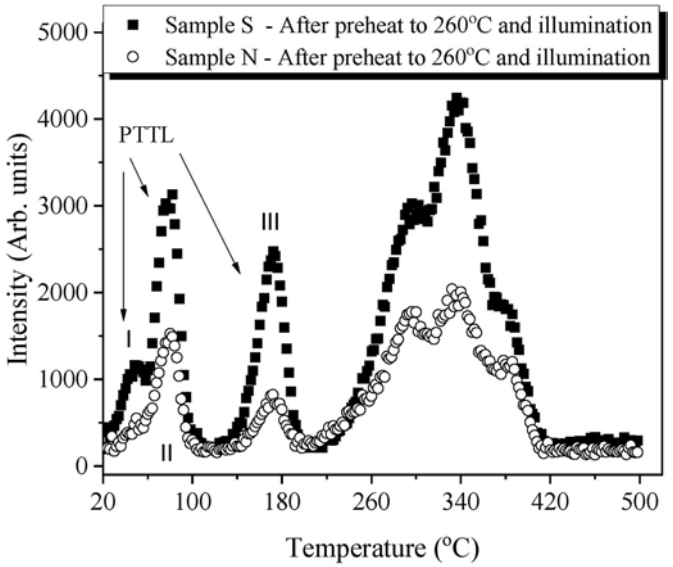

Fig. 2. Glow curves of samples S and N recorded following irradiation to 2 Gy, preheating to 260 °C and illumination for 12 s. Both samples produce PTTL.

which was within 1.6%. In comparison, for sample N, peak III has a fractional uncertainty of 2% and all else, no more than 1%. Thus all peaks are properly reproducible.

4. Identifying electron traps as acceptors or donors using step-annealing

The sequential experimental steps of partial heating followed by illumination collectively known as step- or pulse-annealing were used to determine the role of each electron trap as an acceptor or a donor in the PTTL. Preheating temperatures preceding each illumination were incremented at intervals and the intensity of any peaks present after the preheat monitored. Thus, samples S and N were preheated from 60 to 500 °C at 10 °C intervals after irradiation and illuminated for 12 s after each preheat. Any PTTL peaks corresponding to conventional TL peaks of sample S will be referred to as S1, S2, …whereas for sample N, the shorthand will be N1, N2 …

4.1. Effect of step-annealing on peaks I, II and III

Fig. 3(a) shows the dependence of the PTTL intensity on preheating temperature for peaks S1, S2 and S3. Peak I is independent of preheating between 80 and 150 °C. Since peak I occurs at 46 °C, any other peaks in this region, namely, peaks II and III may be expected to serve as donors for its corresponding PTTL peak, namely, peak S1. For this reason, the sharp decrease in intensity of peak S1 between 150 and 200 °C reflects the removal of a donor electron trap. Beyond 190 °C, the peak continues to fade in intensity with preheating but does so slowly. The change for peaks S2 and S3 can, in outline, be accounted for in the same way. Peak IV, the prominent one in the conventional glow curve, appears within the interval 150–200 °C where the intensity of each PTTL peak decreases rapidly. Beyond 200 °C, the decrease of S1 coincides with the removal of peaks V-VIII. There are therefore at least five possible donors for the PTTL measured at peaks S1, S2 and S3. These are the electron traps of peaks IV-VIII, the dominant one of which corresponds to peak IV.

Fig. 3(b) shows the influence of preheating temperature on peaks N1, N2 and N3. The rapid decrease in intensity of these peaks from 60 to 200 °C over which peak IV is removed, implies that the latter is a putative main donor. Beyond 200 °C, only peak N2 could be monitored and, its intensity continues to decrease gradually. This suggests that the electron traps of peaks V-VIII also serve as donors although as weak ones. Peaks N1 and N3 become obscured by brighter adjacent peaks as the preheating temperature is increased. This is why the preheating temperatures, following which they could be monitored, were limited. Nevertheless, we can deduce that the main donor for their PTTL corresponds to peak IV.

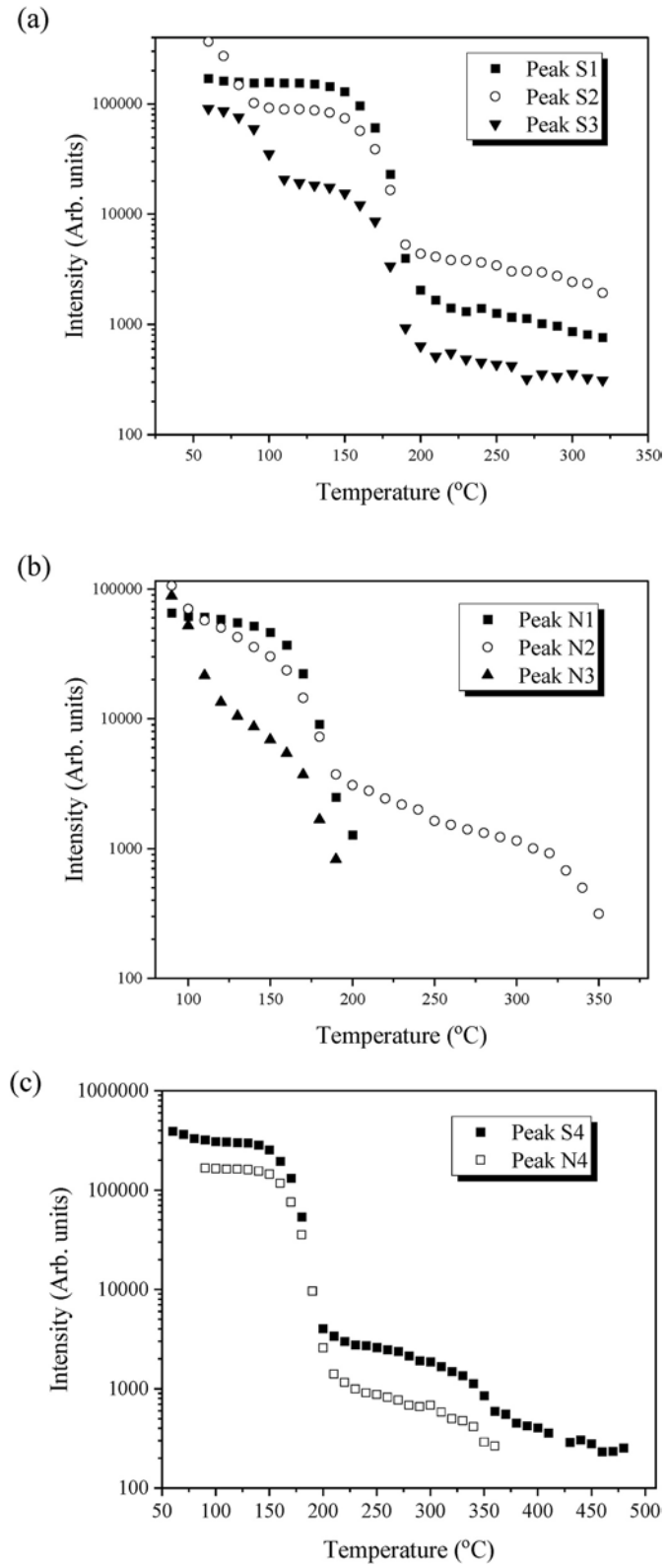

Fig. 3. Influence of preheating on the intensity of peaks S1, S2 and S3 (a) and of peaks N1, N2 and N3 (b) the effect of preheating on peak IV, the dominant one in both samples S and N. This appears under PTTL as S4 (c).

4.2. Effect of partial heating on peak IV

Fig. 3(c) shows the effect of preheating on peak IV, the dominant one that occurs at 170 °C in sample S and at 174 °C in sample N. In both cases, the peak re-appears under PTTL where it is labelled S4 or N4. The peak becomes fainter as preheating extends beyond 200 °C in a manner consistent with the decreasing role of its source traps. The possible donors for the PTTL observed are therefore electron traps for peak V onwards.

4.3. Effect of partial heating on peak V

Peak V, which is collocated with peak IV at the latter's falling edge, is only reproduced for certain combinations of preheating temperature and duration of illumination. The peak could not be properly isolated and was hence deemed unsuitable for study. None of the other peaks are reproduced under phototransfer in either sample.

5. Qualitative analysis of PTTL time-response profiles

The preceding study has shown that in principle every acceptor is linked with multiple donors. It is also apparent that the contribution of some of the supposed donors is inconsequential. The dependence of PTTL intensity on duration of illumination used to induce it is useful in understanding the effectiveness of the phototransfer and helps determine the extent to which presumed donor electron traps influence the process. In the measurements, an irradiated and subsequently preheated sample was illuminated for various duration. The intensity of both acceptor and donor peaks were monitored.

5.1. PTTL of peaks I and II after preheating to 100 °C

Fig. 4(a) shows the dependence of PTTL intensity on duration of illumination for peaks S1 and N1 following preheating to 100 °C. The intensities both go through a maximum with illumination time. Peak S1 is consistently higher in intensity than N1 (for the 2 Gy used in this study). This is because the supposed donor peaks of peak N1, namely IV onwards are all weaker in intensity than those of peak S1 as is shown in Fig. 1.

Fig. 4(b) shows the PTTL time-response profile for peaks S2 and N2. The intensities also go through a peak with duration of illumination. Unlike the earlier result for S1 and N1, the intensity of peak N2 exceeds that of S2 although the reverse is true under conventional TL. The reason for this may be that most electrons released from donor electron traps in sample S transit to the electron trap of peak I rather than that of peak II.

The discussion thus far has reasoned that peaks IV-VII are associated with electron traps that serve as donors for the PTTL recorded. This is because any peak not removed by preheating may be expected to contribute to the PTTL as a donor. The step-annealing findings of Figs. 3 (a) and 3(b), although consistent with this notion, also suggest that of the many donor peaks available, the ones that make a material contribution are few. To demonstrate this further, Fig. 4(c) shows the influence of illumination on intensity of supposed donor peaks for peaks S1 and S2, namely, peaks III-VII. All peaks undergo light-induced fading as might be expected of a donor peak. Of these, the most intense are peaks IV and V which decrease more rapidly than all else. The initial intensity of each of peaks V-VII is 1.3, 0.1, 0.1 and 0.07% that of peak IV. Thus, although peaks V-VII are donors, in practise their contribution is negligible. The PTTL observed at peaks S1 can hence be described as of a system of one acceptor and one donor.

5.2. PTTL following preheating to 120 °C

Peaks I, II and III of each sample are removed after preheating to 120 °C. The resulting phototransferred peaks are transient and could only be monitored for illumination times not exceeding 100 s. Fig. 5 shows the dependence of PTTL intensity on illumination time for peaks S1 and N1. The intensity goes through a maximum in both cases. In comparison, PTTL peak S2 has a similar profile but extends to 10,000 s. The change for peaks S3 and N3 is similar (supplementary information). The possible donors for PTTL in sample S are electron traps of peaks IV-VII, and for sample N, those of peaks IV-VIII. For both samples, these peaks decrease in intensity as would be expected of a donor. Analysis to quantify the contribution of these donors to the PTTL will be shown later.

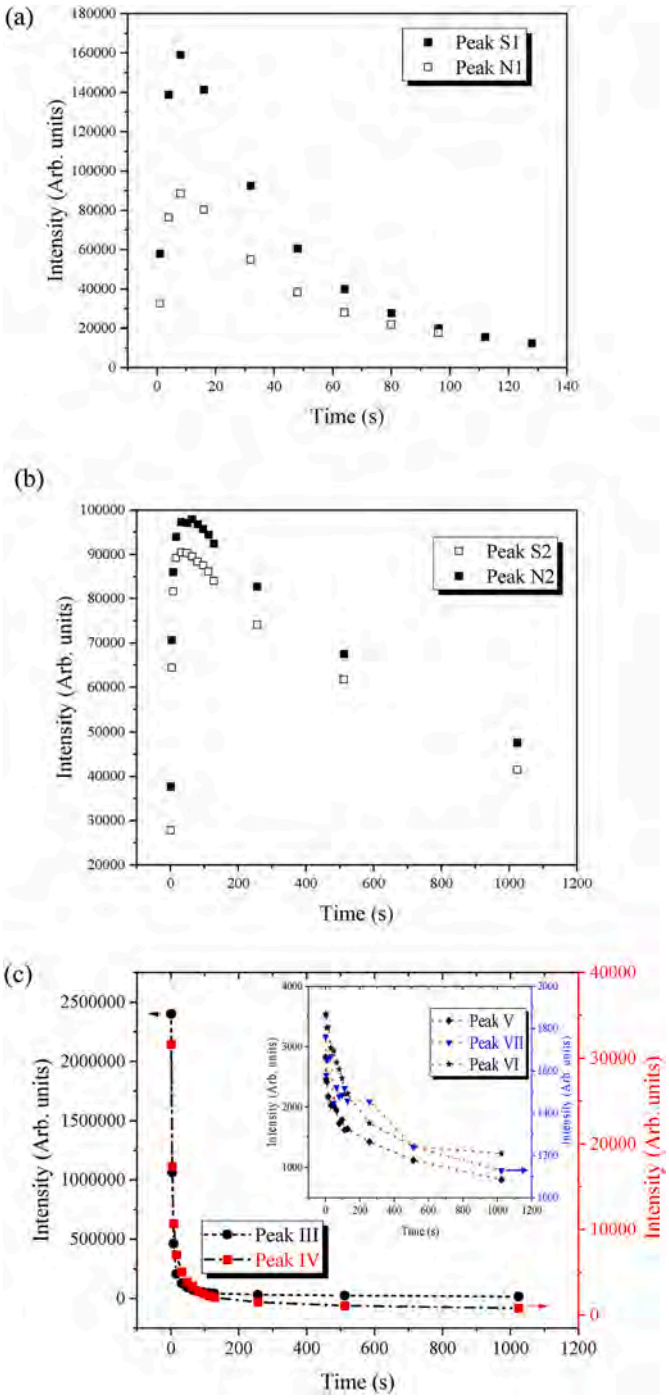

Fig. 4. Dependence of PTTL intensity on duration of illumination for peaks S1 and N1 (a) PTTL time-response profiles for peaks S2 and N2 (b) influence of illumination on intensity of peaks IV-VII, the supposed donor peaks for peaks S1 and S2 (c). The lines through data are only visual guides.

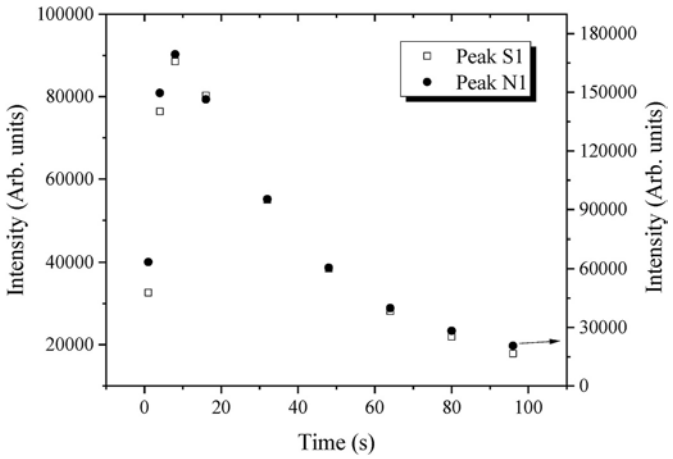

Fig. 5. Dependence of PTTL intensity on illumination time for peaks S1 and N1 after preheating to 120 °C. The measurements correspond to preheating to 120 °C.

5.3. PTTL following preheating to 200 °C

Preheating to 200 °C removes peaks I-IV of each sample. All four peaks are reproduced under phototransfer. Interestingly, an additional PTTL peak near 140 °C here denoted N3b appears in sample N. This is shown in Fig. 6(a) which compares two glow curves, one measured immediately after irradiation (open symbols) and the second (solid symbols) measured after preheating to 200 °C and illumination for 12 s. The appearance of the new peak for sample N may be due to dissociation of F_2^{2+}(2 Mg) electron centre as discussed previously [11].

Fig. 6(b) is a plot of the PTTL intensity against illumination time for peaks S1 and S2 following preheating to 200 °C. These peaks display an interesting contrast. Although they both initially increase in intensity with illumination, the domain of S1 is limited. This is evident by examining the ratio of S1 to S2 (open circles) which show that the intensity of S1 never exceeds 50% that of S2 and decreases steadily in comparison to S2 within the first 64 s. In comparison, a plot of peak S2 displays the archetypal shape (inset). The latter feature was also shown by peaks N1 and N2 as well as by peaks S3, N3, N3b, S4 and N4. Their supposed donor peaks all decrease with illumination as might be expected.

5.4. PTTL following preheating to 260 °C

When the sample is preheated to 260 °C to remove peaks I-IV, these four peaks I-IV re-appear under phototransfer. The illumination-time dependence of peaks S1 and N1 is instructive. These peaks exemplify a problem of monitoring the change in PTTL for a weak-intensity peak that lies adjacent to a particularly bright one. As the duration of illumination is increased, the pair increases in intensity but the prominent one tends to obscure the fainter peak of interest to the extent that the latter becomes indistinct and cannot be reliably monitored. The PTTL peak therefore appears to be transient. Such behaviour is shown in Fig. 7 (a) for peaks S1 and N1. This means that one cannot go beyond a guess as to their future trend and predictive models may be necessary. The change for peaks S2, S3, S4 and N2, N3 and N4 have been omitted to avoid repetition as they show the typical increase followed by a decrease.

5.5. PTTL following preheating to 360 °C

Following preheating to 360 °C, all but the last peak are removed in each sample. Unlike before, only the first three peaks (S1, S2 and S3) are seen in sample S. On the other hand, the first peak (N1) does not re-appear in sample N where the PTTL is only observed at peaks N2 and

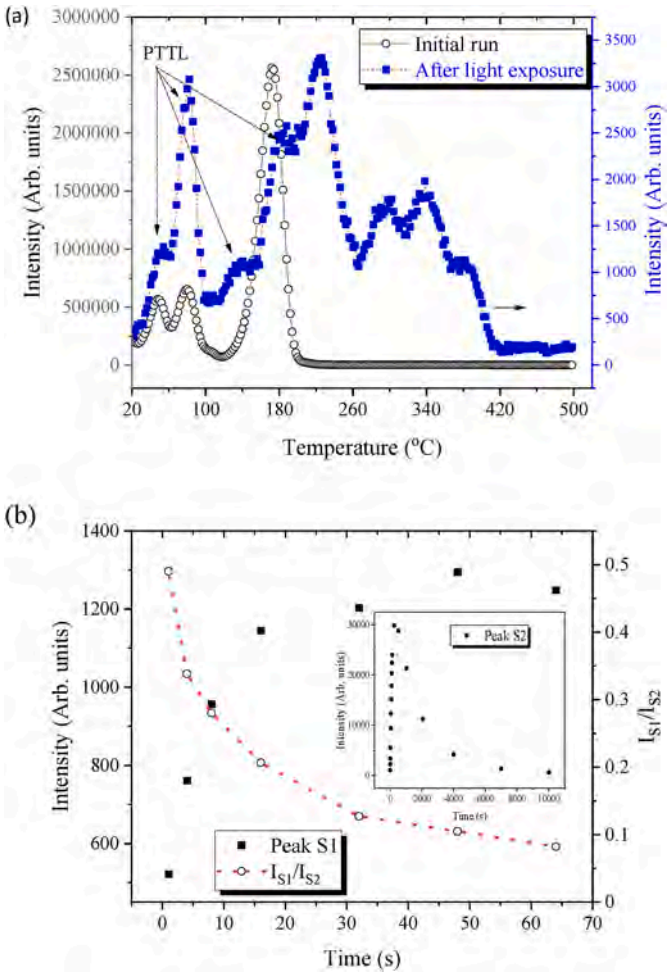

Fig. 6. A comparison of two glow curves, one measured immediately after irradiation (open symbols) and the second (solid symbols) measured after preheating to 200 °C and illumination for 12 s. An additional peak near 140 °C comes up (a) The PTTL time-response profiles of peak S1 and in the inset, the profile of peak S2. The ratio of intensities of peak S1 to S2 (I_{S1}/I_{S2}) emphasize that peak S1 is not only transient but also of low intensity (b). The dotted lines are visual guides.

N3. PTTL is also not produced at the dominant peak IV in both cases. The lack of any PTTL at peak N1 suggests strong competitive retrapping at the electron traps for peaks II and III. For either sample, the acceptor electron trap can be associated with one donor, that is, peak VIII in sample S and, IX in sample N. Since as discussed before, peaks above 260 °C in sample N are weaker than those in sample S, we would expect PTTL peaks N2 and N3 to be weaker in intensity than peaks S2 and S3. This is shown to be the case in Fig. 7(b) for peaks S2 and N2. Both systems are of one acceptor and one donor.

5.6. PTTL following preheating to 400 °C

There was no PTTL induced after preheating to 400 °C. There is thus no contribution to the PTTL from deep electron traps in annealed Al_2O_3:C,Mg for the 2 Gy dose used. Since similar measurements on an unannealed sample did show PTTL [20], annealing must have reduced the concentration of deep electron traps.

5.7. Influence of illumination on donor peaks

For completeness, the intensity of donor peaks for each preheating were monitored to determine to what extent the peaks act as such. Fig. 7

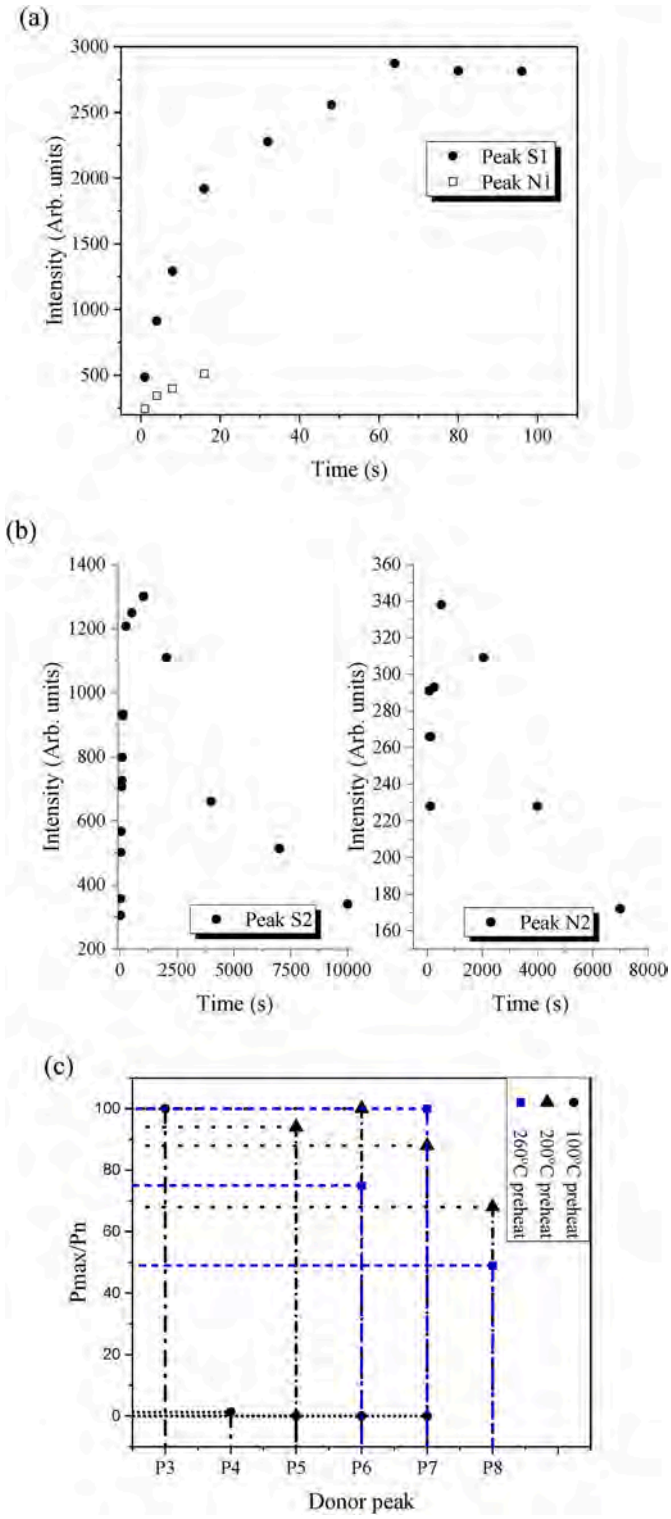

Fig. 7. The PTTL profiles of peaks S1 and N1. The peaks could be monitored for only brief periods before they became obscured by brighter adjacent peaks (a) A comparison of time-dependent profiles of peaks S2 and N2. The intensity of peak S2 exceeds that of N2 throughout measurement (b) Ratios of the most prominent peak to all others in the set of donors for a particular acceptor (c). The drop lines are visual guides.

(c) shows, for each preheating temperature, ratios of the most prominent peak to all others in the set of donors for a particular acceptor for sample S. For example, the plot shows that although PTTL corresponding to preheating to 100 °C is associated with five possible donors, the contribution of four, at ~1%, is negligible and the system is essentially one of one acceptor and one donor. In the same way, the PTTL following preheating to 260 °C can be associated with three donors. However, as found by experiment, all three are weak donors and the third can be neglected which reduces the system to one of one acceptor and two donors. The data for preheating to 200 °C shows that all four donors ought to be included in any analysis. Figs. 1 and 3(a) suggest that the contribution of the fourth can be neglected and the system can be analysed as a system of one acceptor and three donors.

6. Analysis of PTTL time-response profiles

6.1. Phenomenological model

The PTTL time-response profiles (dependence of PTTL intensity on duration of illumination) were described qualitatively in the preceding section by linking each acceptor to presumed donors using the effect of illumination on the intensity of the latter. In the study preceding that, step-annealing was used to demonstrate which donor peaks, when depleted, cause the most reduction in acceptor intensity. We now use that body of evidence to mathematically describe the PTTL time-response profiles.

When an irradiated and preheated sample is illuminated, the electrons stimulated to the conduction band can undergo a direct route to recombination, suffer a back reaction to the source trap or scatter into an empty shallower-energy electron trap. Thus only a portion of electrons released from donor electron traps transit to the acceptor to produce PTTL. The time-response of this PTTL can be modelled using a system of one acceptor and one or more donors. During illumination, electrons are stimulated from a donor electron trap at a rate $f = \Phi\sigma$ (where Φ is the incident photon flux and σ the photoionization cross-section). In this way, one can quantify the fraction of electrons released from a specific donor that is captured at the acceptor trap. For example, if $f_i N_i$ is the number of electrons stimulated from the i^{th} donor, the portion that ends up at an acceptor is $\alpha_i f_i N_i$ where α_i is a proportionality constant. Thus, one generates a set of rate equations describing the change in the concentration of trapped electrons in the acceptor and donor electron traps at the illumination step. The thermoluminescence intensity is proportional to the time-dependent concentration of electrons at the acceptor electron trap. A number of studies [11,27,28] have shown that TL peaks in Al_2O_3:C,Mg follow first order kinetics. As such, each system of coupled differential equations is linear and has a particular solution. This solution is applied to the experimental data for that particular system. This is the same method used to explain PTTL time profiles in α-Al_2O_3:C [15], synthetic quartz [16,18], natural quartz [17,29], Al_2O_3:C,Mg [20] and tanzanite [19].

For a general system of one acceptor and n donors, the light-induced inter-electron-trap transport of charge to the acceptor from n donors each with electron concentration N_j where $j = 1 \ldots n \ldots$, is

$$N' = \begin{pmatrix} N_n' \\ N_{n-1}' \\ . \\ . \\ . \\ N_k' \end{pmatrix} = AN \equiv \begin{pmatrix} -f_n & 0 & 0 & \ldots & . \\ 0 & -f_{n-1} & 0 & \ldots & . \\ 0 & 0 & . & \ldots & . \\ . & . & . & \ldots & . \\ . & . & . & \ldots & . \\ \alpha_n f_n & \alpha_{n-1} f_{n-1} & . & \ldots & -f_k \end{pmatrix} \begin{pmatrix} N_n \\ N_{n-1} \\ . \\ . \\ N_k \end{pmatrix} \quad (1)$$

where N_k is the concentration of electrons at the acceptor. The terms f_n … $\alpha_n f_n$… are as defined earlier. Equation (1) has the general form

$$N' = [N_{ij}]N = AN$$

A is the matrix of coefficients, the elements in the ith row and jth column are as specified, and N are eigenvectors.

Measurements made after preheating to certain temperatures presume that any peak not removed by preheating may act as a donor. However, as seen earlier, not all supposed donors make a meaningful contribution. Therefore, systems of acceptor and donors ought to be analysed as informed by experimental results. In this way, the PTTL at peaks S1, S2 or N1, N2 following preheating to 260 and 200 °C can respectively be described as systems of one acceptor and two or three donors. In comparison, the PTTL at peak S1 can be analysed as a system of one acceptor and one donor for preheating to 100 or 360 °C.

The transport of electrons to an acceptor from, say, two donors can be expressed as

$$\boldsymbol{N}' = \begin{pmatrix} -f_a & 0 & 0 \\ 0 & -f_b & 0 \\ \alpha_a f_a & \alpha_b f_b & -f_l \end{pmatrix} \begin{pmatrix} N_a \\ N_b \\ N_k \end{pmatrix} \tag{2}$$

where all symbols retain meanings as defined earlier. The eigenvectors of the three equations in Eq. (2) can be abstracted by solving the characteristic equation found by setting the determinants of coefficients to zero, namely,

$$|A - m\boldsymbol{I}| = 0 \tag{3}$$

where m are the eigenvalues and $\boldsymbol{I}$ is the unit matrix. Using this method (see also [19]), it is found that $m = -f_a, -f_b$ and $-f_k$. Therefore the general solution of the 3×3 matrix of Eq. (2) is

$$\boldsymbol{N} = \begin{pmatrix} N_1 \\ N_2 \\ N_k \end{pmatrix} = c_1 \begin{pmatrix} f_k - f_a \\ 0 \\ \alpha_a f_a \end{pmatrix} e^{-f_a t} + c_2 \begin{pmatrix} 0 \\ f_k - f_b \\ \alpha_b f_b \end{pmatrix} e^{-f_b t} + c_3 \begin{pmatrix} 0 \\ 0 \\ 1 \end{pmatrix} e^{-f_k t} \tag{4}$$

where c_1, c_2 and c_3 are integration constants. Equation (4) is an initial-value problem, whose integration constants can readily be found. The particular solution describing the time dependence of the PTTL at the acceptor N_k is then

$$N_k = B_1\left(e^{-f_k t} - e^{-f_a t}\right) + B_2\left(e^{-f_k t} - e^{-f_b t}\right) \tag{5}$$

where $B_1 = (\alpha_a f_a N_{1i})/(f_a - f_k)$, $B_2 = (\alpha_b f_b N_{2i})/(f_b - f_k)$, where N_{1i} and N_{2i} are the initial concentration of electrons at the donor electron traps. It is helpful to mention that in data fitting, the form written as Eq. (5) is used because the coefficients B_1 and B_2, being themselves products of constants are also just constants. In the same way, the time dependence of the PTTL for a system of one acceptor and three donors is

$$N_k = C_1\left(e^{-f_2 t} - e^{f_k t}\right) + C_2\left(e^{-f_3 t} - e^{f_k t}\right) + C_3\left(e^{-f_4 t} - e^{f_k t}\right) \tag{6}$$

where $C_1 = \alpha_2 f_2 N_{2i}/(f_k - f_2)$, $C_2 = \alpha_3 f_3 N_{3i}/(f_k - f_3)$ and $C_3 = \alpha_4 f_4 N_{4i}/(f_1 - f_4)$ and all other parameters have the same meanings as defined before. The particular solution for a system of one acceptor and one donor is

$$N_k = D\left(e^{-f_2 t} - e^{f_k t}\right) \tag{7}$$

where $D = \alpha f_2 N_i/(f_k - f_2)$ and all other symbols are as defined earlier.

For illustrative purposes, we consider the PTTL at peak S1, S2 and S3 following preheating to 100, 260 and 200 °C in that order. Here the PTTL can respectively be described as systems of one acceptor and one, two or three donors. Fig. 8(a) shows the plot of PTTL intensity against illumination time for peak S1 following preheating to 100 °C fitted by Eq. (7). On the other hand, Fig. 8(b) and (c) show the time-response profiles of peaks S2 and S3 fitted by Eqs. (6) and (5). These correspond to preheating to 260 and 200 °C respectively. In all cases, the models satisfactorily describe the time-response profiles.

6.2. A kinetics-based description of PTTL

The discussion thus far has presented PTTL in terms of transfer of a portion of electrons from a donor to an acceptor as a first-order process

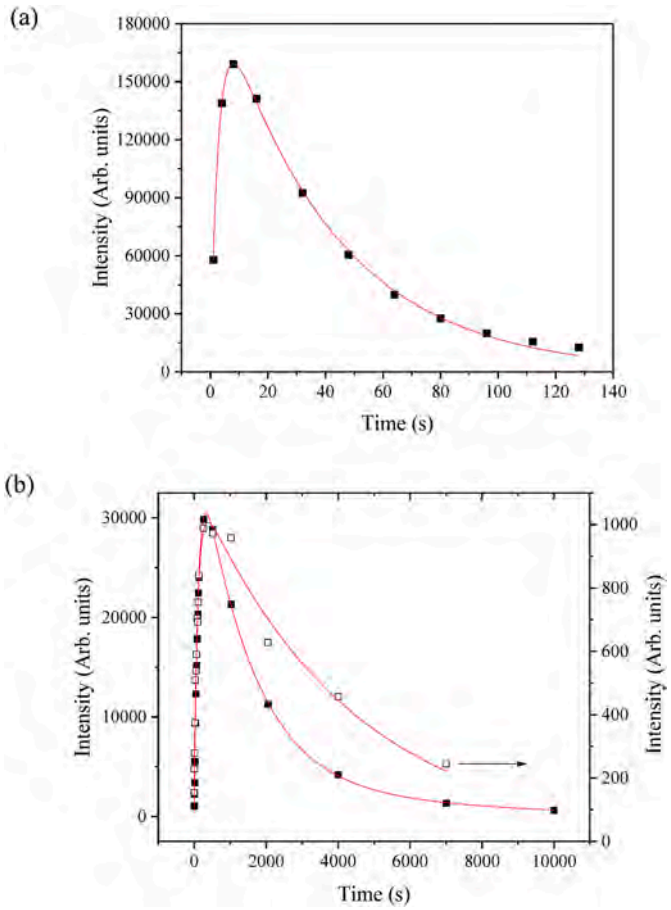

Fig. 8. PTTL intensity against duration of illumination of peak S1 following preheating to 100 °C (a) and for peaks S2 and S3 after preheating to 260 and 200 °C respectively (b). The data are shown fitted by Eqs. (4)–(6) respectively.

based on experimental evidence. The results may also be analysed using sets of kinetics rate equations where the change of electron concentration at the acceptor and donor traps considers the rate of electron transport through the conduction band. Any retrapping is now taken into account.

As an example, the transport of electrons for a system of, say, one acceptor and three donors can be written as

$$\frac{dn_{d1}}{dt} = -f_{d1} n_{d1} + n_c(N_{d1} - n_{d1})A_{d1} \tag{8}$$

$$\frac{dn_{d2}}{dt} = -f_{d2} n_{d2} + n_c(N_{d2} - n_{d2})A_{d2} \tag{9}$$

$$\frac{dn_{d3}}{dt} = -f_{d3} n_{d3} + n_c(N_{d3} - n_{d3})A_{d3} \tag{10}$$

$$\frac{dn_c}{dt} = -A_m m n_c + \sum f_{di} n_{di} - n_{di}(N_{di} - n_{di})A_{di} \tag{11}$$

$$I_{PTTL} = \frac{dm}{dt} = -A_m m n_c \tag{12}$$

where N_{di} is the concentration of the ith electron trap, n_{di} the electron concentration at the ith electron trap, A_{di} the corresponding recombination probability and A_m the recombination probability at the recombination centre and all other symbols have their usual meanings. Equations (8)–(12) describe the optical stimulation and, retrapping of electrons at donor electron traps. Equation (11) describes the electron flow through the conduction band and Eq. (12), the PTTL intensity. This

is a family of non-linear coupled first order differential equations. This set of equations does not have analytical solutions and require computational simulation to generate an approximation to a numerical solution. The values of the various parameters that are retained are ones that produce a good match between model and experimental data.

Fig. 9 compares the simulated curve (solid line) with experimental data (solid symbols) for the time-dependent plot for peak S2 following preheating to 200 °C. This is a system of one acceptor and three donors. The final set of parameters in the simulation are $f_{d1} = 9.0x10^{-3}$ s^{-1}, $f_{d2} = 6.8x10^{-4}$ s^{-1}, $f_{d3} = 9.7x10^{-4}$ s^{-1}, $N_{d1} = 10^{10}$ cm^{-3}, $N_{d2} = 10^{14}$ cm^{-3}, $N_{d3} = 10^{12}$ cm^{-3}, $A_{d1} = A_{d2} = A_{d3} = 10^{-15}$ cm^3 s^{-1}, $A_m = 10^{-6}$ cm^3 s^{-1}. The initial conditions were taken as $N_{d1}(0) = N_{d2}(0) = N_{d3}(0) = 10^{10}$ cm^{-3}; $n_c = 0$ cm^{-3}. Using this set of parameters, the simulated curve reproduces the correct shape of the time-response profile and gives a reasonably good agreement between simulation and experimental data. Including retrapping in the model does not necessarily improve the fit so the peak is really consistent with first order kinetics as reported elsewhere [11].

7. Discussion

Studies on the TL of Al_2O_3:C,Mg [11–13] and its TL spectra [12,13] have shown that its glow curve contains a large number of glow peaks. The luminescence corresponding to these peaks is emitted over several emission bands as also demonstrated using photoluminescence, optically stimulated luminescence and radioluminescence [6,7,9,13,30]. In '*as received*' samples, the TL spectrum has obvious bands centered at 325, 410 and 485 nm attributed to F^+, F and F_2^{2+} electron centres.

When Al_2O_3:C,Mg is annealed at 700 and 900 °C, the number of peaks in its glow curve increases with the most notable addition being the appearance of a new peak at 100 °C. The emission bands remain unchanged with annealing except for a decrease in the intensity of the 485 nm band. The intensity of the 330 nm band exceeds that of the 485 nm band. These bands are present in Al_2O_3:C, the widely studied precursor of Al_2O_3:C,Mg. When Al_2O_3:C is doubly doped with C and Mg to produce Al_2O_3:C,Mg, various additional bands appear including the 500, 510, and 750 nm ones ascribed to aggregate F_2, F_2^{2+}, and F_2^{+} electron centres.

There is some certainty borne of rationalisation about the identity of point defects responsible for a range of emission bands in Al_2O_3:C,Mg. In contrast, similar confidence about the nature of electron traps, which would be useful in interpreting its PTTL, is lacking. For example, Al_2O_3:C has at least five glow peaks [31] but the nature of the electron traps has been discussed properly for only two of them. The incorporation of carbon in α-Al_2O_3 during its synthesis exploits its capacity to be *reduced* so as to promote the formation of a large number of F and F^+ centres in the resulting α-Al_2O_3:C [3]. Using density functional theory, Zhu et al. [32] reported that C tends to occupy the O site when Al is in greater concentration but preferentially moves to the Al site under O-rich conditions in alumina. They concluded that carbon at an Al site (C_{Al}) induces energy states close to the conduction band minimum that can serve as electron traps.

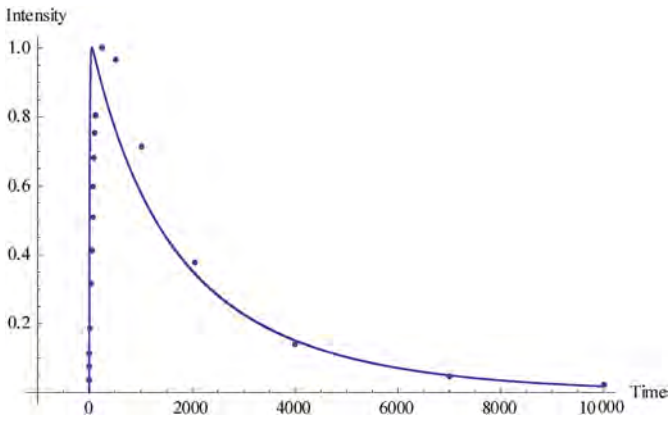

Fig. 9. A comparison of the simulated curves (solid line) with experimental data (solid symbols). The data shown is the time-dependent plot for peak S2 following preheating to 200 °C. This is a system of one acceptor and three donors.

The foregoing ideas are a useful starting point for developing a model for PTTL in Al_2O_3:C,Mg. For instructive purposes, we consider sample S which has eight peaks but whose PTTL is produced only at the first four. The question we wish to address is what the identity of electron traps involved in the PTTL are. Experimental values of the activation energy of peak I in α-Al_2O_3:C and α-Al_2O_3:C,Mg are of the order of 0.70 eV and 0.80 eV respectively [11,31]. These are consistent with the notion of C_{Al} induced electron trapping states near the conduction band minimum. We deduce that the acceptor peak I in Al_2O_3:C,Mg is an example of such electron traps.

It is our view that emission of PTTL at and involving the main peak relates to both the F^+ and F centre electron centres. This is because the introduction of Mg in Al_2O_3:C,Mg enhances the formation of F^+ centres [6]. The role of F^+ and F centres in the PTTL process is complementary. When irradiated Al_2O_3:C,Mg is preheated to remove peaks I-III, peak IV acts as the dominant donor. Owing to that irradiation, the concentration of F centres is increased by radiolytic conversion of F^+ to F centres. The TL, which is emitted mostly at 410 nm e.g. Refs. [3,30], corresponds to the relaxation of electrons from an excited 3P to the 1S ground state [3]. The F^+ luminescence precursors are produced either during growing of the crystal as pointed out earlier or by capture of holes by F-centres [3]. The holes in question arise from the same irradiation the sample is exposed to prior to measurement of PTTL. To explain the role of the F-centre in the affecting the PTTL intensity, we deduce that this centre doubles up as both a luminescence centre and a donor electron trap. The electron trap is the 1P state, which in the F centre, lies within or very close to the conduction band [3]. Any electrons in this energy state can be readily released during the illumination that precedes measurement of PTTL. Evidence of the 1P state as an electron trap is also seen in thermally stimulated currents measured from alumina [3]. The 1P state can be occupied in intrinsic F centres and even in excited F centres because the occupation of an energy state is a probabilistic not deterministic quantum event. It has also been suggested elsewhere [33,34] that some electron can transit from the 3P to state to the conduction band with increase in temperature. Therefore, some of the electrons released following optical ionization of the F centre transit to acceptor electron traps to produce PTTL. The F centre is the dominant donor because of the conversion of a high concentration of pre-existing F^+ to F centres which adds to the remanent F centres.

To understand why peak IV produces very poor intensity PTTL when the sample is preheated to 360 °C, we need to reprise the argument above for deep electron traps but at the illumination stage. The number of free electrons due to optical transfer from deep electron traps is far less than that after irradiation. As a consequence, the concentration of F centres produced due to electron capture at F^+ centres at the illumination stage is negligible, a fact reflected as poor intensity PTTL. Direct electron trapping at the F centre is unlikely since this electron centre has no charge imbalance. One could also theorise double electron trapping at α centres but this too is unlikely as any α.

7.1. Centres will be unstable and in very low concentrations

The identity of point defects responsible for the many other electron traps in Al_2O_3:C,Mg is less easy to explain. As a case in point, a pair of adjacent F^+ centres can aggregate to form F_2^{2+} complexes. One can rationalise that optical transfer of electrons from the F_2 centre would contribute to the PTTL observed at peaks I-IV. For the same reasons as before, the F_2 centre cannot be effective as acceptor electron traps. These and other processes are at this stage only a cause for speculation for

which further work is required. This is because the notions of aggregates as quoted are axiomatic. Other point defects requiring charge balance over a longer spatial range cannot be ruled out.

8. Conclusion

Phototransferred thermoluminescence (PTTL) of Al_2O_3:C,Mg annealed at 700 and 900 °C has been reported. Although the samples have no less than 8 peaks each, only the first four in both samples are reproduced under phototransfer for preheating between 100 and 360 °C. The role of various electron traps as donors was studied using pulse annealing as well as by using time-response profiles. The set of donors corresponding to each acceptor was studied both qualitatively and quantitatively. The dependence of PTTL intensity on illumination time has been analysed using sets of coupled linear differential equations for systems consisting of an acceptor and donors as informed by experiment. Point defects that likely contribute to emergence of PTTL are discussed.

Credit author statement

M L Chithambo: Conception, data analysis, model development, writing, editing. J L Sob: Experiment and data collection, data analysis, writing. J L Kalita: Editing.

Declaration of competing interest

The authors declare that they have no known competing financial interests or personal relationships that could have appeared to influence the work reported in this paper.

Acknowledgement

This work was made possible because of generous funding from Rhodes University and the National Research Foundation of South Africa.

Appendix A. Supplementary data

Supplementary data to this article can be found online at https://doi.org/10.1016/j.physb.2021.413438.

References

[1] F. Agullo-Lopez, C.R.A. Catlow, P.D. Townsend, Point Defects in Materials, Academic Press, London, 1988.
[2] N. Itoh, A.M. Stoneham, Materials Modification by Electronic Excitation, Cambridge University Press, Cambridge, 2001.
[3] S.W.S. McKeever, M. Moscovitch, P.D. Townsend, Thermoluminescence Dosimetry Materials: Properties and Uses, Nuclear Technology Publishing, United Kingdom, 1995.
[4] L. Bøtter-Jensen, S.W.S. McKeever, A.G. Wintle, Optically Stimulated Luminescence Dosimetry, Elsevier, Amsterdam, 2003.
[5] G. Solé, L.E. Bausá, D. Jaque, Optical Spectroscopy of Inorganic Solids, John Wiley, Chichester, 2005.
[6] G.J. Sykora, M.S. Akselrod, Photoluminescence study of photochromically and radiochromically transformed Al_2O_3:C,Mg crystals used for fluorescent nuclear track detectors, Radiat. Meas. 45 (2010) 631–634.
[7] G. Denis, M.G. Rodriguez, M.S. Akselrod, T.H. Underwood, E.G. Yukihara, Time-resolved measurements of optically stimulated luminescence of Al_2O_3:C and Al_2O_3:C,Mg, Radiat. Meas. 46 (2011) 1457–1461.
[8] M.S. Akselrod, G.J. Sykora, Fluorescent nuclear track detector technology a new way to do passive solid state dosimetry, Radiat. Meas. 46 (2011) 1671–1679.
[9] Marcos Trindade, Luiz Gustavo Jacobsohn, Thermoluminescence and radioluminescence of α-Al_2O_3:C,Mg at high temperature, J. Lumin. (2018) 598–602.
[10] B.D. Evans, G.J. Pogatshnik, Y. Chen, Optical properties of lattice defects in α-Al2O3, Nucl. Instrum. Methods Phys. Res. B 91 (1994) 258–262.
[11] J.M. Kalita, M.L. Chithambo, Comprehensive kinetic analysis of thermoluminescence peaks of α-Al_2O_3:C,Mg, J. Lumin. 185 (2017) 72–82.
[12] J.M. Kalita, M.L. Chithambo, The effect of annealing and beta irradiation on thermoluminescence spectra of α-Al_2O_3:C,Mg, J. Lumin. 196 (2018) 195–200.
[13] M.G. Rodriguez, G. Denis, M.S. Akselrod, T.H. Underwood, E.G. Yukihara, Thermoluminescence, optically stimulated luminescence and radioluminescence properties of Al_2O_3:C,Mg, Radiat. Meas. 46 (2011) 1469–1473.
[14] L.E. Colyott, M.S. Akselrod, S.W.S. McKeever, Phototransferred thermoluminescence in α-Al_2O_3:C, radiat, Prot. Dosim. 65 (1996) 263–266.
[15] M.L. Chithambo, C. Seneza, J.M. Kalita, Phototransferred thermoluminescence of α-Al_2O_3:C: experimental results and empirical models, Radiat. Meas. 105 (2017) 7–16.
[16] M.L. Chithambo, P. Niyonzima, J.M. Kalita, Phototransferred thermoluminescence of synthetic quartz: analysis of illumination-time response curves, J. Lumin. 198 (2018) 146–154.
[17] M.L. Chithambo, D.E. Folley, S. Chikwembani, Phototransferred thermoluminescence from natural quartz annealed at 1000°C: analysis of time-dependent evolution of intensity and competition effects, J. Lumin. 216 (2019) 116730.
[18] M.L. Chithambo, R.R. Dawam, Phototransferred thermoluminescence of annealed synthetic quartz: analysis of illumination-time profiles, kinetics and competition effects, Radiat. Meas. 131 (2020) 106236.
[19] M.L. Chithambo, Phototransferred thermoluminescence of tanzanite: a matrix-based analysis of time-response profiles and mechanisms, J. Lumin. 234 (2021) 117969.
[20] A.J. Lontsi Sob, M.L. Chithambo, J.M. Kalita, Analysis of illumination-time-dependent profiles of phototransferred thermoluminescence of Al_2O_3:C,Mg, J. Lumin. 230 (2021) 117721.
[21] E.G. Yukihara, V.H. Whitley, J.C. Polf, D.M. Klein, S.W.S. McKeever, A.E. Akselrod, M.S. Akselrod, The effects of deep trap population on the thermoluminescence of Al_2O_3, C. Radiat. Meas. 37 (2003) 627–638.
[22] M.L. Chithambo, Concerning secondary thermoluminescence peaks in α-Al2O3, C. S. Afr. J. Sci. 100 (2004) 524–527.
[23] E.G. Yukihara, S.W.S. Mckeever, Ionisation density dependence of the optically and thermally stimulated luminescence from Al2O3:C, Radiat. Protect. Dosim. 119 (2006) 206–217.
[24] D. Lo, J.L. Lawless, R. Chen, Superlinear dose dependence of high temperature thermoluminescence peaks in Al2O3:C, Radiat. Protect. Dosim. 119 (2006) 71–74.
[25] M.S. Akselrod, A.E. Akselrod, S.S. Orlov, S. Sanyal, T.H. Underwood, Fluorescent aluminum oxide crystals for volumetric optical data storage and imaging applications, J. Fluoresc. 13 (2003) 503–511.
[26] J.M. Kalita, M.L. Chithambo, On the sensitivity of thermally and optically stimulated luminescence of α-Al2O3:C and α-Al2O3:C,Mg, Radiat. Meas. 99 (2017) 18–24.
[27] J.M. Kalita, M.L. Chithambo, Thermoluminescence of α-Al_2O_3:C,Mg: kinetic analysis of the main glow peak, J. Lumin. 182 (2017) 177–182.
[28] J.M. Kalita, M.L. Chithambo, The influence of dose on the kinetic parameters and dosimetric features of the main thermoluminescence glow peak in α-Al_2O_3:C,Mg, Nucl. Instrum. Methods B. 394 (2017) 12–19.
[29] D.E. Folley, M.L. Chithambo, Analysis of thermoluminescence and phosphorescence related to phototransfer in natural quartz, J. Lumin. 238 (2021) 118217.
[30] M.L. Chithambo, J.M. Kalita, A.A. Finch, A, F- and F^+-band radioluminescence and the influence of annealing on its emission spectra in Al_2O_3:C,Mg, Radiat. Meas. 134 (2020) (2020) 106306.
[31] M.L. Chithambo, C. Seneza, F.O. Ogundare, Kinetic analysis of high temperature secondary thermoluminescence glow peaks in α-Al_2O_3, C. Radiat. Meas. 66 (2014) 21–30.
[32] J. Zhu, K.P. Muthe, R. Pandey, Stability and electronic properties of carbon in α-Al2O3, J. Phys. Chem. Solid. 75 (2014) 379–383.
[33] G. Molnar, M. Benabdesselam, J. Borossay, P. Iacconi, D. Lapraz, M. Akselrod, Influence of the irradiation temperature on the dosimetric and high temperature TL peaks of Al2O3:C, Radiat, Prot. Dosim. 100 (2002) 139–142.
[34] V.S. Kortov, I.I. Milman, S.V. Nikiforov, The effect of deep traps on the main features of thermoluminescence in dosimetric α-Al_2O_3:C, Radiat, Prot. Dosim. 84 (1999) 35–38.

Bibliography

F. Agulló-López, C. R. A. Catlow, and P. D. Townsend. *Point defects in materials*. Academic press, 1988.

M. F. Ahmed, E. Schnell, S. Ahmad, and E. G. Yukihara. Image reconstruction algorithm for optically stimulated luminescence 2D dosimetry using laser-scanned Al_2O_3:C and Al_2O_3:C,Mg films. *Phys. Med. Biol.*, 61(20):7484–7506, 2016.

M. S. Akselrod and S. W. S. McKeever. A Radiation Dosimetry Method Using Pulsed Optically Stimulated Luminescence. *Radiat. Prot. Dosim.*, 81(3):167–175, 1999.

M. S. Akselrod and G. J. Sykora. Fluorescent nuclear track detector technology - a new way to do passive solid state dosimetry. *Radiat. Meas.*, 46(12):1671–1679, 2011.

M. S. Akselrod, V. S. Kortov, D. J. Kravetsky, and V. I. Gotlib. Highly Sensitive Thermoluminescent Anion-Defective α-Al_20_3:C Single Crystal Detectors. *Radiat. Prot. Dosim.*, 32(1):15–20, 1990.

M. S. Akselrod, N. Agersnap Larsen, V. Whitley, and S. W. S. McKeever. Thermal quenching of F-center luminescence in Al_2O_3:C. *J. Appl. Phys.*, 84(6):3364–3373, 1998.

M. S. Akselrod, A. E. Akselrod, S. S. Orlov, S. Sanyal, and T. H. Underwood. Fluorescent aluminum oxide crystals for volumetric optical data storage and imaging applications. *J. Fluoresc.*, 13:503–511, 2003a.

M. S. Akselrod, A. E. Akselrod, S. S. Orlov, S. Sanyal, and T. H. Underwood. New aluminum oxide single crystals for volumetric optical data storage. volume 5069, pages 244–251, 2003b.

M. S. Akselrod, A. E. Akselrod, S. S. Orlov, S. Sanyal, and T. H. Underwood. New aluminum oxide single crystals for volumetric optical data storage. In *Optical Data Storage*, page TuC3. Optical Society of America, 2003c.

C. S. Alexander and S. W. S. McKeever. Phototransferred thermoluminescence. *J. Phys. D: Appl. Phys.*, 31:2908–2920, 1998.

C. S. Alexander, M. F. Morris, and S. W. S. McKeever. The time and wavelength response of phototransferrred thermoluminescence in natural and synthetic quartz. *Radiat. Meas.*, 27:153–159, 1997.

L. Ao, A. Pham, X. Xiang, S. Li, and X. Zu. Defect induced charge trapping in C-doped α-al_2o_3. *J. Appl. Phys.*, 122(2):025702, 2017.

R. M. Bailey. The slow component of quartz optically stimulated luminescence. *Radiat. Meas.*, 32(3):233–246, 2000.

R. M. Bailey, B. W. Smith, and E. J. Rhodes. Partial bleaching and the decay form characteristics of quartz osl. *Radiat. Meas.*, 27(2):123–136, 1997.

I. Bailiff. Characteristics of time-resolved luminescence in quartz. *Radiat. Meas.*, 32:401–405, 2000.

I. K. Bailiff and N. R. J. Poolton. Studies of charge transfer mechanisms in feldspars. *Int. J. Rad. Appl. Instrum. D*, 18(1):111–118, 1991.

M. Bertucci, I. Veronese, and M. C. Cantone. Photo-transferred thermoluminescence from deep traps in quartz. *Radiat. Meas.*, 46:588–590, 2011.

D. S. Betts, L. Couturier, A. H. Khayrat, B. J. Luff, and P. D. Townsend. Temperature distribution in thermoluminescence experiments. I. experimental results. *J. Phys. D: Appl. Phys.*, 26:843–848, 1993.

A. J. J. Bos. Theory of thermoluminescence. *Radiat. Meas.*, 41:45–56, 2006.

L. Bossin, I. K. Bailiff, and I. Terry. Phototransferred tl properties of alumina substrates. *Radiat. Meas.*, 120:41–46, 2018.

L. Bøtter-Jensen, G. A. T. Duller, A. S. Murray, and D. Banerjee. Blue light emitting diodes for optical stimulation of quartz in retrospective dosimetry and dating. 84:335–340, 1999.

L. Bøtter-Jensen, S. W. S. McKeever, and A. G. Wintle. *Optically Stimulated Luminescence Dosimetry*. Elsevier, 2003.

J. D. Brewer, B. Jeffries, and G. P. Summers. Low-temperature fluorescence in sapphire. *Phys. Rev. B*, 22(10):4900–4906, 1980.

E. Bulur. An alternative technique for optically stimulated luminescence (osl) experiment. *Radiat. Meas.*, 26(5):701–709, 1996.

E. Bulur. Photo-transferred luminescence from beo ceramics. *Radiat. Meas.*, 42 (3):334–340, 2007.

A. H. Carter. *Classical and statistical thermodynamics*. Prentice Hall, 2000.

R. Chen and S. W. S. McKeever. *Theory of Thermoluminescence and Related Phenomena*. World Scientific, 1997.

R. Chen and V. Pagonis. *Thermally and Optically Stimulated Luminescence A Simulation Approach*. John Wiley & Sons Ltd, 2011.

R. Chen, N. Kristianpoller, Z. Davidson, and R. Visocekas. Mixed first and second order kinetics in thermally stimulated processes. *J. Lumin.*, 23(3):293–303, 1981.

M. Chithambo. Phototransferred thermoluminescence of tanzanite: A matrix-based analysis of time-response profiles and competition effects. *J. Lumin.*, 234: 117969, 2021a.

M. L. Chithambo. Dependence of the thermal influence on luminescence lifetimes from quartz on the duration of optical stimulation. *Radiat. Meas.*, 37(2):167–175, 2003.

M. L. Chithambo. Concerning secondary thermoluminescence peaks in α-Al_2O_3:C. *S. Afr. J. Sci.*, 100:524–527, 2004.

M. L. Chithambo. On the correlation between annealing and variabilities in pulsed-luminescence from quartz. *Radiat. Meas.*, 41(7):862–865, 2006.

M. L. Chithambo. The analysis of time-resolved optically stimulated luminescence: II. computer simulations and experimental results. *J. Phys. D Appl.*, 40:1880–1889, 2007a.

M. L. Chithambo. The analysis of time-resolved optically stimulated luminescence: I. theoretical considerations. *J. Phys. D Appl. Phys.*, 40(7):1874–1879, 2007b.

M. L. Chithambo. The analysis of time-resolved optically stimulated luminescence: II. computer simulations and experimental results. *J. Phys. D Appl. Phys.*, 40 (7):1880–1889, 2007c.

M. L. Chithambo. The analysis of time-resolved optically stimulated luminescence: I. theoretical considerations. *J. Phys. D Appl.*, 40(7):1874–1879, 2007d.

M. L. Chithambo. A time-correlated photon counting system for measurement of pulsed optically stimulated luminescence. *J. Lumin.*, 131(1):92–98, 2011.

M. L. Chithambo. *An Introduction to Time-Resolved Optically Stimulated Luminescence*. A Morgan & Claypool Publishers, 2018.

M. L. Chithambo. Thermal assistance in the optically stimulated luminescence of superluminous $Sr_4Al_{14}O_{25}$: Eu^{2+},Dy^{3+}. *Phys. Rev. B Condens. Matter*, 603: 412722, 2021b.

M. L. Chithambo and G. Costin. Temperature-dependence of time-resolved optically stimulated luminescence and composition heterogeneity of synthetic α-Al_2O_3:C. *J. Lumin.*, 182:252–262, 2017.

M. L. Chithambo and R. R. Dawam. Phototransferred thermoluminescence of annealed synthetic quartz: Analysis of illumination-time profiles, kinetics and competition effects. *Radiat. Meas.*, 131:106236, 2020.

M. L. Chithambo and R. B. Galloway. A pulsed light-emitting-diode system for stimulation of luminescence. *Meas. Sci. Technol.*, 11(4):418–424, 2000.

M. L. Chithambo and R. B. Galloway. On the slow component of luminescence stimulated from quartz by pulsed blue light-emitting diodes. *Nucl. Instrum. Meth. B*, 183(3):358–368, 2001.

M. L. Chithambo and F. O. Ogundare. Luminescence lifetime components in quartz: Influence of irradiation and annealing. *Radiat. Meas.*, 44(5):453–457, 2009.

M. L. Chithambo, C. Seneza, and F. O. Ogundare. Kinetic analysis of high temperature secondary thermoluminescence glow peaks in α-Al_2O_3:C. *Radiat. Meas.*, 66:21–30, 2014.

M. L. Chithambo, A. N. Nyirenda, A. A. Finch, and N. S. Rawat. Time-resolved optically stimulated luminescence and spectral emission features of α-Al_2O_3:C. *Phys. Rev. B Condens. Matter*, 473:62–71, 2015.

M. L. Chithambo, C. Seneza, and J. Kalita. Phototransferred thermoluminescence of α-Al_2O_3:C: Experimental results and empirical models. *Radiat. Meas.*, 105: 7–16, 2017a.

M. L. Chithambo, A. H. Wako, and A. A. Finch. Thermoluminescence of $SrAl_2O_4$:Eu^{2+},Dy^{3+}: Kinetic analysis of a composite-peak. *Radiat. Meas.*, 97: 1–13, 2017b.

M. L. Chithambo, P. Niyonzima, and J. M. Kalita. Phototransferred thermoluminescence of synthetic quartz: Analysis of illumination-time response curves. *J. Lumin.*, 198:146–154, 2018.

M. L. Chithambo, D. E. Folley, and S. Chikwembani. Phototransferred thermoluminescence from natural quartz annealed at 1000°C: Analysis of time-dependent evolution of intensity and competition effects. *J. Lumin.*, 216:116730, 2019.

M. L. Chithambo, J. M. Kalita, and A. A. Finch. F- and F^+-band radioluminescence and the influence of annealing on its emission spectra in Al_2O_3:C,Mg. *Radiat. Meas.*, 134:106306, 2020.

G. Denis, M. Akselrod, and E. G. Yukihara. Influence of shallow traps on time-resolved optically stimulated luminescence measurements of Al_2O_3:C,Mg. *J. Appl. Phys.*, 109(10):104906, 2011a.

G. Denis, M. G. Rodriguez, M. S. Akselrod, T. H. Underwood, and E. G. Yukihara. Time-resolved measurements of optically stimulated luminescence of Al_2O_3:C and Al_2O_3:C,Mg. *Radiat. Meas.*, 46(12):1457–1461, 2011b.

R. Doremus. *Alumina*, pages 1–26. 01 2008. ISBN 978-0-387-73361-6.

S. A. Eller, M. F. Ahmed, J. A. Bartz, M. S. Akselrod, G. Denis, and E. G. Yukihara. Radiophotoluminescence properties of Al_2O_3:C,Mg crystals. *Radiat. Meas.*, 56:179–182, 2013.

B. D. Evans. A review of the optical properties of anion lattice vacancies, and electrical conduction in α-Al_2O_3: their relation to radiation-induced electrical degradation. *J. Nucl. Mater*, 219:202–223, 1995.

B. D. Evans and M. Stapelbroek. Optical properties of the F^+ center in crystalline al_2o_3. *Phys. Rev. B*, 18:7089–7098, 1978.

M. Fox. *Optical Properties of Solids*. Oxford University Press, 2001.

M. Gaft, R. Reisfeld, and G. Panczer. *Modern Luminescence Spectroscopy of Minerals and Materials*. Springer, Berlin, 2005.

R. B. Galloway. Luminescence lifetimes in quartz: dependence on annealing temperature prior to beta irradiation. *Radiat. Meas.*, 35(1):67–77, 2002.

R. B. Galloway, D. G. Hong, and H. J. Napier. A substantially improved green-light-emitting diode system for luminescence stimulation. *Meas. Sci. Technol.*, 8 (3):267–271, 1997.

G. F. J. Garlick and A. F. Gibson. The electron trap mechanism of luminescence in sulphide and silicate phosphors. *Proc. Phys. Soc.*, 60:574–589, 1948.

S. G. Gorbics, A. E. Nash, and F. H. Attix. Thermal quenching of luminescence in six thermoluminescent dosimetry phosphors—i: Quenching of x-ray-excited radioluminescence. *Int. J. Appl. Radiat. Isot.*, 20(12):829–841, 1969.

B. Henderson and G. F. Imbusch. *Optical Spectroscopy of inorganic solids (reprint)*. Oxford Science Publications, 2006.

D. J. Huntley, D. I. Godfrey-Smith, and L. W. M. Thewalt. Optical dating of sediments. *Nature*, 313:105–107, 1985.

D. J. Huntley, M. A. Short, and K. Dunphy. Deep traps in quartz and their use for optical dating. *Can. J. Phys.*, 74(3–4):81–91, 1996.

J. M. Kalita and M. L. Chithambo. The influence of dose on the kinetic parameters and dosimetric features of the main thermoluminescence glow peak in α-Al_2O_3:C,Mg. *Nucl. Instrum. Meth. B*, 394:12–19, 2017a.

J. M. Kalita and M. L. Chithambo. Features of an annealing-induced thermoluminescence peak in α-Al_2O_3:C,Mg. *Opt. Mater.*, 70:158–164, 2017b.

J. M. Kalita and M. L. Chithambo. Thermoluminescence of α-Al_2O_3:C,Mg: Kinetic analysis of the main glow peak. *J. Lumin.*, 182:177–182, 2017c.

J. M. Kalita and M. L. Chithambo. On the sensitivity of thermally and optically stimulated luminescence of α-Al_2O_3:C and α-Al_2O_3:C,Mg. *Radiat. Meas.*, 99: 18–24, 2017d.

J. M. Kalita and M. L. Chithambo. Phototransferred thermoluminescence in α-Al_2O_3:C,Mg under 470nm blue light stimulation. *J. Lumin.*, 188:371–377, 2017e.

J. M. Kalita and M. L. Chithambo. Comprehensive kinetic analysis of thermoluminescence peaks of α-Al_2O_3:C,Mg. *J. Lumin.*, 185:72–82, 2017f.

J. M. Kalita and M. L. Chithambo. A comparative study of the dosimetric features of α-Al_2O_3:C,Mg and α-Al_2O_3:C. *Radiat. Prot. Dosim.*, 177(3):261–271, 2017g.

J. M. Kalita and M. L. Chithambo. Temperature dependence of optically stimulated luminescence of α-al2o3:c,mg. *Nucl. Instrum. Meth. B*, 410:16–20, 2017h.

J. M. Kalita and M. L. Chithambo. The effect of annealing and beta irradiation on thermoluminescence spectra of α-Al_2O_3:C,Mg. *J. Lumin.*, 196:195–200, 2018a.

J. M. Kalita and M. L. Chithambo. Thermoluminescence of α-Al_2O_3:C,Mg annealed at 1200°c. *Nucl. Instrum. Meth. B*, 422:78–84, 2018b.

J. M. Kalita and M. L. Chithambo. Phototransferred thermoluminescence and thermally-assisted optically stimulated luminescence dosimetry using α-Al_2O_3:C,Mg annealed at 1200°c. *J. Lumin.*, 205:1–6, 2019.

J. M. Kalita, M. L. Chithambo, and G. S. Polymeris. Thermally-assisted optically stimulated luminescence from deep electron traps in α-Al_2O_3:C,Mg. *Nucl. Instrum. Meth. B*, 403:28–32, 2017a.

J. M. Kalita, M. L. Chithambo, and G. S. Polymeris. Thermally-assisted optically stimulated luminescence from deep electron traps in α-Al_2O_3:C,Mg. *Nucl. Instrum. Meth. B*, 403:28–32, 2017b.

P. Kelly and P. Bräunlich. I. phenomenological theory of thermoluminescence. *Phys. Rev. B*, 1:1587–1595, 1970.

G. Kitis, N. G. Kiyak, G. S. Polymeris, and V. Pagonis. Investigation of osl signals from very deep traps in unfired and fired quartz samples. *Nucl. Instrum. Meth. B*, 268(6):592–598, 2010.

C. Kittel. *Introduction to Solid State Physics*. John Wiley & Sons, Inc, 2005.

E. Kouroukla. *Luminescence dosimetry with ceramic materials for application to radiological emergencies and other incidents*. PhD thesis, Durham theses, Durham University, http://etheses.dur.ac.uk/11362/, 2015.

J. Kouwenberg. *Fluorescent Nuclear Track Detectors for Alpha Particle Measurement*. PhD thesis, 07 2018.

B. G. Markey, L. E. Colyott, and S. W. S. Mckeever. Time-resolved optically stimulated luminescence from α-Al_2O_3:C. *Radiat. Meas.*, 24(4):457–463, 1995.

C. E. May and J. A. Partridge. Thermoluminescence kinetics of alpha irradiated alkali halides. *J. Chem. Phys.*, 40:1401–1415, 1964.

S. W. S. McKeever. *Thermoluminescence of solids*. Cambridge University Press, 1985.

S. W. S. McKeever, M. Moscovitch, and P. D. Townsend. *Thermoluminescence Dosimetry Materials: Properties and Uses*. Nuclear Technology, 1995.

N. Meriç, E. Şahiner, and G. S. Polymeris. Thermally assisted osl (ta-osl) reproducibility in Al_2O_3:C and its implication on the corresponding thermoluminescence (tl) reproducibility. *Radiat. Meas.*, 90:269–273, 2016.

Milanovich-Reichhalter and N. Vana. Phototransferred thermoluminescence in quartz. *Radiat. Prot. Dosim.*, 33:211–213, 1990.

D. R. Mishra, M. S. Kulkarni, K. P. Muthe, C. Thinaharan, M. Roy, S. K. Kulshreshtha, S. Kannan, B. C. Bhatt, S. K. Gupta, and D. N. Sharma. Luminescence properties of α-Al_2O_3:C crystal with intense low temperature tl peak. *Radiat. Meas.*, 42(2):170–176, 2007.

N. F. Mott and R. W. Gurney. *Electronic Processes in Ionic Solids, 2nd Ed.* Oxford University Press, 1948.

R. Nanjundaswamy, K. Lepper, and S. W. S. McKeever. Thermal quenching of thermoluminescence in natural quartz. *Radiat. Prot. Dosim.*, 100:305–308, 2002.

S. V. Nikiforov, I. I. Milman, and V. S. Kortov. Thermal and optical ionization of f-centers in the luminescence mechanism of anion-defective corundum crystals. *Radiat. Meas.*, 33(5):547–551, 2001.

A. N. Nyirenda and M. L. Chithambo. Factors influencing the shape of cw-osl signal obtained by stimulation of very deep traps in carbon-doped aluminium oxide: An experimental study. *J. Lumin.*, 192:436–442, 2017.

F. O. Ogundare, S. A. Ogundele, M. L. Chithambo, and M. K. Fasasi. Thermoluminescence characteristics of the main glow peak in α-Al_2O_3:C exposed to low environmental-like radiation doses. *J. Lumin.*, 139:143–148, 2013.

V. Pagonis, G. Kitis, and C. Furetta. *Numerical and Pratical Exercises in Thermoluminescence*. Springer, 2006.

V. Pagonis, S. Mian, M. L. Chithambo, E. Christensen, and C. Barnold. Experimental and modelling study of pulsed optically stimulated luminescence in quartz, marble and beta irradiated salt. *J. Phys. D Appl. Phys.*, 42:055407, 2009.

V. Pagonis, C. Ankjærgaard, A. S. Murray, M. Jain, R. Chen, J. Lawless, and S. Greilich. Modelling the thermal quenching mechanism in quartz based on time-resolved optically stimulated luminescence. *J. Lumin*, 130:902–909, 2010.

V. Pagonis, R. Chen, J. W. Maddrey, and B. Sapp. Simulations of time-resolved photoluminescence experiments in α-Al_2O_3:C. *J. Lumin.*, 131(5):1086–1094, 2011.

V. Pagonis, M. Chithambo, R. Chen, A. Chruścińska, M. Fasoli, S. H. Li, M. Martini, and K. Ramseyer. Thermal dependence of luminescence llifetime and radioluminescence. *J. Lumin*, 145:38–48, 2014.

S. A. Petrov and I. K. Bailiff. Thermal quenching and the initial rise technique of trap depth evaluation. *J. Lumin.*, 65(6):289–291, 1995.

G. S. Polymeris. Thermally assisted osl (ta-osl) from various luminescence phosphors; an overview. *Radiat. Meas.*, 90:145–152, 2016.

G. S. Polymeris and G. Kitis. Thermally assisted photo transfer osl from deep traps in Al_2O_3:C grains exhibiting different tl peak shapes. *Appl. Radiat. Isot.*, 70(10):2478–2487, 2012.

G. S. Polymeris, S. Raptis, D. Afouxenidis, N. C. Tsirliganis, and G. Kitis. Thermally assisted osl from deep traps in Al_2O_3:C. *Radiat. Meas.*, 45(3):519–522, 2010.

G. S. Polymeris, E. Şahiner, N. Meriç, and G. Kitis. Thermal assistance in ta – osl signals of feldspar and polymineral samples; comparison with the case of pure quartz. *Radiat. Meas.*, 81:270–274, 2015a.

G. S. Polymeris, E. Şahiner, N. Meriç, and G. Kitis. Experimental features of natural thermally assisted osl (nta-osl) signal in various quartz samples; preliminary results. *Nucl. Instrum. Meth. B*, 349:24–30, 2015b.

J. T. Randall and M. H. F. Wilkins. Phosphorescence and electrons traps: I. the study of trap distributions. *Proc. R. Soc. London*, A 184:366–389, 1945a.

J. T. Randall and M. H. F. Wilkins. Phosphorescence and electrons traps: II. the interpretation of long-period phosphorescence. *Proc. R. Soc. London*, A 184: 390–407, 1945b.

R. Riedel and I.-W. Chen. *Ceramics Science and Technology Volume 2: Materials and Properties*. Wiley-VCH Verlag GmbH & Co. KGaA, 2008.

M. G. Rodriguez, G. Denis, M. S. Akselrod, T. H. Underwood, and E. G. Yukihara. Thermoluminescence, optically stimulated luminescence and radioluminescence properties of Al_2O_3:C,Mg. *Radiat. Meas.*, 46(12):1469–1473, 2011.

D. C. W. Sanderson and R. J. Clark. Pulsed photostimulated luminescence of alkali feldspars. *Radiat. Meas.*, 23(2):633–639, 1994.

A. J. J. Santos, J. F. de Lima, and M. E. G. Valerio. Phototransferred thermoluminescence of quartz. *Radiat. Meas.*, 33:427–430, 2001.

S. Sanyal and M. S. Akselrod. Anisotropy of optical absorption and fluorescence in Al_2O_3:C,Mg crystals. *J. Appl. Phys.*, 98(3):033518, 2005.

N. Shrestha, E. G. Yukihara, D. Cusumano, and L. Placidi. Al_2O_3:C and Al_2O_3:C,Mg optically stimulated luminescence 2D dosimetry applied to magnetic resonance guided radiotherapy. *Radiat. Meas.*, 138:106439, 2020.

B. W. Smith and E. J. Rhodes. Charge movements in quartz and their relevance to optical dating. *Radiat. Meas.*, 23(2):329–333, 1994.

A. J. L. Sob, M. L. Chithambo, and J. M. Kalita. Analysis of illumination-time-dependent profiles of phototransferred thermoluminescence of Al_2O_3:C,Mg. *J. Lumin.*, 230:117721, 2021.

A. Soni, D. R. Mishra, B. C. Bhatt, S. K. Gupta, N. S. Rawat, M. S. Kulkarni, and D. N. Sharma. Characterization of deep energy level defects in α-al$_2$o$_3$:c using thermally assisted osl. *Radiat. Meas.*, 47(2):111–120, 2012.

A. Soni, D. R. Mishra, B. C. Bhatt, S. K. Gupta, N. S. Rawat, M. S. Kulkarni, and D. N. Sharma. Improvement in dose threshold of α-Al_2O_3:C using thermally assisted osl. *Radiat. Meas.*, 49:67–72, 2013.

N. A. Spooner. On the optical dating signal from quartz. *Radiat. Meas.*, 23(2): 593–600, 1994.

G. P. Summers. Thermoluminescence in single crystal α-Al_2O_3. *Radiat. Prot. Dosim.*, 8(1-2):69–80, 1984.

G. J. Sykora and M. S. Akselrod. Photoluminescence study of photochromically and radiochromically transformed Al_2O_3:C,Mg crystals used for fluorescent nuclear track detectors. *Radiat. Meas.*, 45(3):631–634, 2010.

Technical University of Denmark. *Guide to "The Risø TL/OSL Reader "*, 2011.

R. J. D. Tilley. *Defects in Solids*. John Wiley & Sons, Inc, 2008.

N. M. Trindade and L. G. Jacobsohn. Thermoluminescence and radioluminescence of α-Al_2O_3:C,Mg at high temperatures. *J. Lumin.*, 204:598–602, 2018.

N. M. Trindade, L. G. Jacobsohn, and E. M. Yoshimura. Correlation between thermoluminescence and optically stimulated luminescence of α-Al_2O_3:C,Mg. *J. Lumin.*, 206:298–301, 2019.

N. M. Trindade, M. G. Magalhães, M. C. S. Nunes, E. M. Yoshimura, and L. G. Jacobsohn. Thermoluminescence of uv-irradiated α-Al_2O_3:C,Mg. *J. Lumin.*, 223:117195, 2020.

F. D. Walker, L. E. Colyott, N. A. Larsen, and S. W. S. McKeever. The wavelength dependence of light-induced fading of thermoluminescence from α-Al_2O_3:C. *Radiat. Meas.*, 26:711–718, 1996.

A. G. Wintle. Thermal Quenching of Thermoluminescence in Quartz. *Geophys. J. Int.*, 41(1):107–113, 1975.

A. G. Wintle and A. S. Murray. The relationship of quartz thermoluminescence, photo-transferred thermoluminescence, and optically stimulated luminescence. *Radiat. Meas.*, 27:611–624, 1997.

X. Yang, H. Li, Q. Bi, Y. Cheng, Q. Tang, and J. Xu. Influence of carbon on the thermoluminescence and optically stimulated luminescence of α-al$_2$o$_3$:c crystals. *J. Appl. Phys.*, 104(12):123112, 2008.

E. G. Yukihara and S. W. S. McKeever. Spectroscopy and optically stimulated luminescence of Al_2O_3:C using time-resolved measurements. *J. Appl. Phys.*, 100 (8):083512, 2006.

E. G. Yukihara and S. W. S. McKeever. *Optically Stimulated Luminescence Fundamentals and Applications*. John Wiley & Sons Ltd, 2011.

E. G. Yukihara, V. H. Whitley, J. C. Polf, D. M. Klein, S. W. S. McKeever, A. E. Akselrod, and M. S. Akselrod. The effects of deep trap population on the thermoluminescence of Al_2O_3:C. *Radiat. Meas.*, 37(6):627–638, 2003.

E. G. Yukihara, V. H. Whitley, S. W. S. McKeever, A. E. Akselrod, and M. S. Akselrod. Effect of high-dose irradiation on the optically stimulated luminescence of Al_2O_3:C. *Radiat. Meas.*, 38(3):317–330, 2004.

J. Zhu, K. P. Muthe, and R. Pandey. Stability and electronic properties of carbon in α-Al_2O_3. *J. Phys. Chem. Solids*, 75(3):379–383, 2014.

Colophon

This thesis is based on a template developed by Matthew Townson and Andrew Reeves. It was typeset with LaTeX 2_ε. It was created using the *memoir* package, maintained by Lars Madsen, with the *madsen* chapter style. The font used is Latin Modern, derived from fonts designed by Donald E. Knuth.